

Dissertation zur Erlangung des Doktorgrades
der Fakultät für Chemie und Pharmazie
der Ludwig-Maximilians-Universität München

Functionalised phosphines
—
Fascinating multidentate ligands
for
luminescent Zn(II) and Cu(I) complexes

von

Sarah Maria Elisabeth Linert

aus

Augsburg, Deutschland

2020

Erklärung

Diese Dissertation wurde im Sinne von § 7 der Promotionsordnung vom 28. November 2011 von Herrn Prof. Dr. Konstantin Karaghiosoff betreut.

Eidesstattliche Versicherung

Diese Dissertation wurde eigenständig und ohne unerlaubte Hilfe erarbeitet.

München, 05.08.2020

Sarah Linert

Dissertation eingereicht am: 05.08.2020

1. Gutachter: Prof. Dr. Konstantin Karaghiosoff

2. Gutachter: Senior Lecturer Dr. Lee Higham

Mündliche Prüfung am: 26.08.2020

Acknowledgments

Many people have supported me in the process of producing this thesis. Therefore I want to thank all of them very much.

First of all I want to thank my supervisor Prof. Dr. Konstantin Karaghiosoff for the possibility to make my PhD and research on a fascinating and interesting topic. He was very supportive and encouraging and it always was a pleasure to discuss new ideas with him.

I want to thank Dr. Lee Higham for the opportunity to spend some months in his research group at Newcastle University. This interesting time gave me a new sight on my research topic. I also want to thank him for second reviewing my thesis.

I also want to thank Prof. Dr. Thomas Klapötke for welcoming me in his research group.

I want to thank the current and former members of the research groups of Prof. Karaghiosoff and Prof. Klapötke for the great working atmosphere, nice conversations and the fun we had together. Special thanks go to Dr. Marco Reichel for proofreading of this thesis and Christin Kirst for the introduction into the use of Gaussian and teaching me how to solve crystal structures. I also want to thank Dr. Christina Hettstedt for supervising me during my master thesis on P,N ligands based on picolylphosphines, which led to this thesis.

Special thanks go to Ms. Irene Scheckenbach for her help with organisational issues.

I also want to thank the research group of Dr. Higham and everyone else in the Johnston Lab for the warm welcome, the pleasant cooperation and making my time in Newcastle unforgettable. Special thanks go to Charlotte Hepples for her advice regarding the synthesis of Bodipy.

Several students have contributed to this work: Fabian Pilz (B.Sc thesis), Philipp Schmidt, Sebastian Wagner, Victoria DiBacco (F-Praktikum), Leonard Moser (M.Sc. thesis), Matthew Dean and Thomas Colgan (Erasmus students). Many thanks to all of you.

I want to thank Prof. Dr. Konstantin Karaghiosoff and Christin Kirst for the measurement of crystal structures, as well as Dr. Paul Waddell from Newcastle University for measurement and solving of crystal structures. I also want to thank Ms. Brigitte Breitenstein from the LMU for measuring low temperature NMR spectra and Dr. Corinne Wills from Newcastle University for the measurement of NMR spectra at the 500 MHz device. I want to thank Dr. Andreas Jakowetz for the measurement of photophysical data.

Finally I want to thank my family for their constant support and their patience during the time of my PhD thesis.

Table of contents

Table of contents	I
Abbreviations	VII
Colour scheme in figures of crystal structures	IX
Chapter 1: Introduction	
1.1 Organophosphorus compounds	2
1.1.1 Chlorophosphines	2
1.1.2 Primary phosphines	3
1.1.3 Tertiary phosphines	4
1.2 Luminescence.....	5
1.3 Organic Light Emitting Diodes (OLEDs)	6
1.4 Previous work on picolylphosphine based luminescent compounds.....	7
1.5 Aims of the project.....	8
1.6 References	9
Chapter 2: P,N Ligands	
2.1 Introduction	14
2.2 Results and discussion	15
2.2.1 Synthesis	15
2.2.1.1 Silyl compounds	15
2.2.1.2 Chlorophosphines	16
2.2.1.3 Picolylphosphine based compounds.....	18
2.2.1.4 Bis(picolyl)phosphine based compounds.....	19
2.2.1.5 Tris(picolyl)phosphine based compounds	20
2.2.1.6 Tris(benzoxazol-2-ylmethyl)phosphine.....	21
2.2.2 NMR data	22
2.2.2.1 2-((Trimethylsilyl)methyl)benzoxazole	22
2.2.2.2 Picolylphosphine based compounds.....	22
2.2.2.3 Bis(picolyl)phosphine based compounds.....	24
2.2.2.4 Tris(picolyl)phosphine based compounds	26
2.2.2.5 Tris(benzoxazol-2-ylmethyl)phosphine.....	26
2.2.3 Photophysical data of 2-26	27
2.2.4 Crystal structure of tris(benzoxazol-2-ylmethyl)phosphine oxide 2-27	29
2.3 Summary	30
2.4 Experimental	31
2.4.1 General.....	31
2.4.1.1 Schlenk technique	31

2.4.1.2 Preparation of NMR samples under Schlenk conditions	32
2.4.1.3 Solvents	32
2.4.1.4 Chemicals	32
2.4.1.5 NMR spectroscopy	32
2.4.1.6 Mass spectrometry	32
2.4.1.7 Elemental analysis.....	32
2.4.1.8 Single crystal X-ray diffraction	33
2.4.1.9 Data collection from the diffractometer and solving of the crystal structures	33
2.4.1.10 PL spectroscopy and TCSPC measurements	33
2.4.2 Syntheses	33
2.4.2.1 2-((Trimethylsilyl)methyl)pyridine 2-1	33
2.4.2.2 2-Methyl-6-((trimethylsilyl)methyl)pyridine 2-2	34
2.4.2.3 2,4-Dimethyl-6-((trimethylsilyl)methyl)pyridine 2-3	34
2.4.2.4 2-((Trimethylsilyl)methyl)benzoxazole 2-4	35
2.4.2.5 <i>iso</i> Propyldichlorophosphine 2-5	35
2.4.2.6 <i>tert</i> Butyldichlorophosphine 2-6	36
2.4.2.7 <i>Triisopropyl</i> phenyldichlorophosphine 2-7	36
2.4.2.8 Attempted synthesis of dichloro(4,6-dimethylpyridin-2-ylmethyl)phosphine 2-8	37
2.4.2.9 Attempted synthesis of bis(4,6-dimethylpyridin-2-ylmethyl)chlorophosphine 2-9	37
2.4.2.10 Diphenyl(pyridin-2-ylmethyl)phosphine 2-10	38
2.4.2.11 Diphenyl(6-methylpyridin-2-ylmethyl)phosphine 2-11	38
2.4.2.12 Diphenyl(4,6-dimethylpyridin-2-ylmethyl)phosphine 2-12	38
2.4.2.13 Phenyl-bis(pyridin-2-ylmethyl)phosphine 2-13	39
2.4.2.14 Phenyl-bis(6-methylpyridin-2-ylmethyl)phosphine 2-14	39
2.4.2.15 Phenyl-bis(4,6-dimethylpyridin-2-ylmethyl)phosphine 2-15	40
2.4.2.16 <i>iso</i> Propyl-bis(6-methylpyridin-2-ylmethyl)phosphine 2-16	40
2.4.2.17 <i>iso</i> Propyl-bis(4,6-dimethylpyridin-2-ylmethyl)phosphine 2-17	40
2.4.2.18 Attempted synthesis of <i>tert</i> butyl-bis(6-methylpyridin-2-ylmethyl)phosphine 2-18	41
2.4.2.19 Attempted synthesis of <i>tert</i> butyl-bis(4,6-dimethylpyridin-2-ylmethyl)phosphine 2-19	41
2.4.2.20 <i>Triisopropyl</i> phenyl-bis(6-methylpyridin-2-ylmethyl)phosphine 2-20	42
2.4.2.21 <i>Triisopropyl</i> phenyl-bis(4,6-dimethylpyridin-2-ylmethyl)phosphine 2-21	42
2.4.2.22 Tris(6-methylpyridin-2-ylmethyl)phosphine 2-24	42
2.4.2.23 Tris(4,6-dimethylpyridin-2-ylmethyl)phosphine 2-25	43
2.4.2.24 Tris(benzoxazol-2-ylmethyl)phosphine 2-26	43
2.4.3 Crystallographic data	44
2.5 References	45

Chapter 3: Synthesis, molecular and crystal structures of picolyl, lutidinyl and collidinyl phosphine hydrochlorides

3.1 Introduction	48
3.2 Results and discussion	49
3.2.1 Synthesis	49
3.2.2 NMR data	51
3.2.3 Crystal structures	53
3.2.4 DFT calculations	60
3.3 Summary	62
3.4 Experimental	63
3.4.1 DFT calculations	63
3.4.2 Syntheses	63
3.4.2.1 2-((Diphenylphosphino)methyl)pyridine-1-ium chloride 3-1	63
3.4.2.2 2-((Diphenylphosphino)methyl)-6-methylpyridine-1-ium chloride 3-2	64
3.4.2.3 2-((Diphenylphosphino)methyl)-4,6-dimethylpyridine-1-ium chloride 3-3	64
3.4.2.4 (Pyridin-2-ylmethyl)dichlorophosphine 3-4	64
3.4.2.5 2-((Dichloro-phosphino)methyl)-pyridin-1-ium chloride 3-5	65
3.4.3 Molecular Orbital Contributions	65
3.4.4 Crystallographic data	66
3.5 References	67

Chapter 4: Zinc complexes

4.1 Introduction	70
4.1.1 Coordination chemistry of zinc	70
4.1.2 Luminescent properties of Zn complexes	70
4.2 Results and discussion	71
4.2.1 Synthesis	71
4.2.2 NMR data	71
4.2.3 Photophysical data	75
4.2.4 Crystal structure of 4-1	77
4.2.5 DFT calculations	78
4.3 Summary	80
4.4 Experimental	81
4.4.1 DFT calculations	81
4.4.2 Syntheses	81
4.4.2.1 Phenyl-bis(pyridin-2-ylmethyl)phosphine zinc chloride complex 4-1	81
4.4.2.2 Phenyl-bis(6-methylpyridin-2-ylmethyl)phosphine zinc chloride complex 4-2	81

4.4.2.3 Phenyl-bis(4,6-dimethylpyridin-2-ylmethyl)phosphine zinc chloride complex 4-3	81
4.4.2.4 <i>iso</i> Propyl-bis(6-methylpyridin-2-ylmethyl)phosphine zinc chloride complex 4-4	82
4.4.2.5 <i>iso</i> Propyl-bis(4,6-dimethylpyridin-2-ylmethyl)phosphine zinc chloride complex 4-5	82
4.4.2.6 Tris(6-methylpyridin-2-ylmethyl)phosphine zinc chloride complex 4-6	82
4.4.2.7 Tris(4,6-dimethylpyridin-2-ylmethyl)phosphine zinc chloride complex 4-7	82
4.4.3 Crystallographic data	83
4.5 References	84
Chapter 5: Copper(I) complexes	
5.1 Introduction	86
5.1.1 Copper(I) complexes	86
5.1.2 Luminescent properties of Cu(I) complexes	86
5.2 Results and discussion	87
5.2.1 Synthesis	87
5.2.2 Photophysical data.....	89
5.2.3 Crystal structures	91
5.2.3.1 Crystal structure of 5-4	91
5.2.3.2 Crystal structures of 5-7 and 5-11	93
5.2.3.3 Crystal structures of 5-9 and 5-13	99
5.2.3.4 Crystal structure of 5-10	103
5.2.3.5 Crystal structures of 5-14 , 5-17 and 5-18	105
5.2.3.6 Crystal structures of 5-20 and 5-21	109
5.2.3.7 Formation and crystal structures of hydrolysis products Co_2PO_2^- Cu(II)Cl 5-23 and PhLutPO ₂ ⁻ 6-methylpicolinate Cu(II) 5-24	111
5.2.4 DFT calculations	115
5.3 Summary	117
5.4 Experimental	119
5.4.1 Phenyl-bis(6-methylpyridin-2-ylmethyl)phosphine copper(I) chloride complex 5-1	119
5.4.2 Phenyl-bis(6-methylpyridin-2-ylmethyl)phosphine copper(I) bromide complex 5-2	119
5.4.3 Phenyl-bis(6-methylpyridin-2-ylmethyl)phosphine copper(I) iodide complex 5-3	119
5.4.4 Phenyl-bis(4,6-dimethylpyridin-2-ylmethyl)phosphine copper(I) chloride complex 5-4	120
5.4.5 Phenyl-bis(4,6-dimethylpyridin-2-ylmethyl)phosphine copper(I) bromide complex 5-5	120
5.4.6 Phenyl-bis(4,6-dimethylpyridin-2-ylmethyl)phosphine copper(I) iodide complex 5-6	120
5.4.7 <i>iso</i> Propyl-bis(6-methylpyridin-2-ylmethyl)phosphine copper(I) chloride complex 5-7	120
5.4.8 <i>iso</i> Propyl-bis(6-methylpyridin-2-ylmethyl)phosphine copper(I) bromide complex 5-8	121
5.4.9 <i>iso</i> Propyl-bis(6-methylpyridin-2-ylmethyl)phosphine copper(I) iodide complex 5-9	121

5.4.10 <i>iso</i> Propyl-bis(6-methylpyridin-2-ylmethyl)phosphine copper(I) thiocyanate complex 5-10	121
5.4.11 <i>iso</i> Propyl-bis(4,6-dimethylpyridin-2-ylmethyl)phosphine copper(I) chloride complex 5-11	121
5.4.12 <i>iso</i> Propyl-bis(4,6-dimethylpyridin-2-ylmethyl)phosphine copper(I) bromide complex 5-12	122
5.4.13 <i>iso</i> Propyl-bis(4,6-dimethylpyridin-2-ylmethyl)phosphine copper(I) iodide complex 5-13	122
5.4.14 Tris(6-methylpyridin-2-ylmethyl)phosphine copper(I) chloride complex 5-14	122
5.4.15 Tris(6-methylpyridin-2-ylmethyl)phosphine copper(I) bromide complex 5-15	122
5.4.16 Tris(6-methylpyridin-2-ylmethyl)phosphine copper(I) iodide complex 5-16	123
5.4.17 Tris(4,6-dimethylpyridin-2-ylmethyl)phosphine copper(I) chloride complex 5-17	123
5.4.18 Tris(4,6-dimethylpyridin-2-ylmethyl)phosphine copper(I) bromide complex 5-18	123
5.4.19 Tris(4,6-dimethylpyridin-2-ylmethyl)phosphine copper(I) iodide complex 5-19	123
5.4.20 Phenyl-bis(pyridin-2-ylmethyl)phosphine oxide copper(I) chloride complex 5-20	123
5.4.21 Phenyl-bis(pyridin-2-ylmethyl)phosphine oxide copper(I) bromide complex 5-21	124
5.4.22 Phenyl-bis(pyridin-2-ylmethyl)phosphine oxide copper(I) iodide complex 5-22	124
5.4.23 Crystallographic data	125
5.5 References	129
Chapter 6: Transition metal complexes of fluorescent P,N ligands based on Bodipy	
6.1 Introduction	133
6.1.1 Bodipy	133
6.1.2 Metal complexes of Bodipy derivatives	134
6.2 Results and discussion	135
6.2.1 Synthesis of primary phosphine 6-5	135
6.2.2 Synthesis of the P,N ligands	137
6.2.3 Transition metal complexes	139
6.2.3.1 Manganese complexes	139
6.2.3.2 Zinc complexes	140
6.2.3.3 Copper complexes	141
6.2.4 Photophysical data	142
6.2.5 Crystal structures	143
6.2.5.1 Crystal structure of 6-13	143
6.2.5.2 Crystal structure of 6-17	145
6.3 Summary	148
6.4 Experimental	148
6.4.1 General	148
6.4.1.1 Schlenk technique	148

6.4.1.2 Solvents	148
6.4.1.3 Chemicals	149
6.4.1.4 NMR	149
6.4.1.5 IR spectroscopy	149
6.4.1.6 X-ray diffraction of single crystals.....	149
6.4.1.7 Data collection from the diffractometer and crystal structure solution	149
6.4.1.8 Absorption and Emission Spectroscopy.....	149
6.4.1.9 Quantum Yield Method	150
6.4.2 Syntheses	150
6.4.2.1 10-(4-Bromophenyl)-2,8-diethyl-5,5-difluoro-1,3,7,9-tetramethyl-5 <i>H</i> -4λ ⁴ ,5λ ⁴ -dipyrrolo-[1,2- <i>c</i> :2',1'- <i>f</i>][1,3,2]diazaborinine 6-1	150
6.4.2.2 10-(4-Bromophenyl)-2,8-diethyl-1,3,5,5,7,9-hexamethyl-5 <i>H</i> -4λ ⁴ ,5λ ⁴ -dipyrrolo[1,2- <i>c</i> :2',1'- <i>f</i>][1,3,2]diazaborinine 6-2	151
6.4.2.3 Diethyl (4-(2,8-diethyl-5,5-difluoro-1,3,7,9-tetramethyl-5 <i>H</i> -4λ ⁴ ,5λ ⁴ -dipyrrolo[1,2- <i>c</i> :2',1'- <i>f</i>][1,3,2]diazaborinin-10-yl)phenyl)phosphonate 6-3	152
6.4.2.4 Diethyl (4-(2,8-diethyl-1,3,5,5,7,9-hexamethyl-5 <i>H</i> -4λ ⁴ ,5λ ⁴ -dipyrrolo[1,2- <i>c</i> :2',1'- <i>f</i>][1,3,2]-diazaborinin-10-yl)phenyl)phosphonate 6-4	152
6.4.2.5 2,8-Diethyl-1,3,5,5,7,9-hexamethyl-10-(4-phosphanylphenyl)-5 <i>H</i> -4λ ⁴ ,5λ ⁴ -dipyrrolo[1,2- <i>c</i> :2',1'- <i>f</i>][1,3,2]diazaborinine 6-5	153
6.4.2.6 10-(4-(Bis(2-(pyridin-2-yl)ethyl)phosphanyl)phenyl)-2,8-diethyl-1,3,5,5,7,9-hexamethyl-5 <i>H</i> -4λ ⁴ ,5λ ⁴ -dipyrrolo[1,2- <i>c</i> :2',1'- <i>f</i>][1,3,2]diazaborinine 6-6	154
6.4.2.7 (4-(2,8-Diethyl-1,3,5,5,7,9-hexamethyl-5 <i>H</i> -4λ ⁴ ,5λ ⁴ -dipyrrolo[1,2- <i>c</i> :2',1'- <i>f</i>][1,3,2]diazaborinin-10-yl)phenyl)bis(2-(pyridin-2-yl)ethyl)phosphine oxide 6-7	154
6.4.2.8 10-(4-(Bis(pyridin-2-ylmethyl)phosphanyl)phenyl)-2,8-diethyl-1,3,5,5,7,9-hexamethyl-5 <i>H</i> -4λ ⁴ ,5λ ⁴ -dipyrrolo[1,2- <i>c</i> :2',1'- <i>f</i>][1,3,2]diazaborinine 6-9	155
6.4.2.9 Reaction of 6-6 with MnBr(CO) ₅ 6-10	156
6.4.2.10 Reaction of 6-9 with MnBr(CO) ₅ 6-11	156
6.4.2.11 Reaction of 6-6 with ZnBr ₂ 6-12	156
6.4.2.12 Reaction of 6-9 with ZnBr ₂ 6-13	156
6.4.2.13 Reaction of 6-6 with CuCl 6-14	157
6.4.2.14 Reaction of 6-9 with CuCl 6-15	157
6.4.2.15 Reaction of 6-6 with Cu(MeCN) ₄ PF ₆ 6-16	157
6.4.2.16 Reaction of 6-9 with Cu(MeCN) ₄ PF ₆ 6-17	157
6.4.3 Crystallographic data	158
6.5 References	159
Chapter 7: Summary	161
List of compounds	167

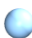








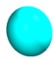


Abbreviations

Å	Angstroms
Alk	Alkyl
Ar	Aryl
ax	Axial
ABCN	1,1'-azobis(cyclohexane-carbonitrile)
Bn	Benzyl
Bodipy	4,4-difluoro-4-bora-3a,4a-diaza-s-indacene
br	Broad Signal (NMR)
°	Degrees
°C	Degrees Celsius
CC	Cluster Centred
CCDC	Cambridge Crystallographic Data Centre
CIS	Coordination Induced Shift
Col	Collidiny
d	Days; Doublet (NMR)
δ	Chemical shift (NMR)
DCM	Dichloromethane
DDQ	2,3-Dicyano-5,6-dichloroparabenzoquinone
DFT	Density Functional Theory
DIPEA	Diisopropylethylamine
DMSO	Dimethyl sulfoxide
DPPB	1,4-Bis(diphenylphosphino)butane
EML	Emissive Layer
eq	Equivalents; Equatorial
ETL	Electron Transport Layer
Et ₂ O	Diethyl ether
EtOAc	Ethyl acetate
eV	Electron Volt
(Fe(salen)) ₂ O	μ-Oxo-bis[<i>N,N'</i> -ethylene[salicylidenimino(2-)]] <i>diiron</i>
g	Grams
h	Hours
hept	septet
HOMO	Highest Occupied Molecular Orbital
HTL	Hole Transport Layer
Hz	Hertz
IC	Internal Conversion
<i>i</i> Pr	<i>iso</i> Propyl
IR	Infrared spectroscopy
ISC	Intersystem Crossing
ITO	Indium Tin Oxide
<i>J</i>	Coupling constant (NMR)
L	Ligand
LC	Ligand Centred
LDA	Lithiumdiisopropylamine
LUMO	Lowest Unoccupied Molecular Orbital

Lut	Lutidinyl
m	Multiplet (NMR); medium (IR)
M	Molar
Me	Methyl
MeCN	Acetonitrile
MeLi	Methyl lithium
MeOH	Methanol
Mes	Mesityl
mg	Milligrams
MHz	Megahertz
min	Minutes
mL	Millilitres
MLCT	Metal-to-Ligand Charge Transfer
mmol	Millimoles
μs	Microseconds
<i>n</i> BuLi	<i>n</i> Butyl lithium
nm	Nanometres
NMR	Nuclear Magnetic Resonance
OLED	Organic Light Emitting Diode
Φ _F	Quantum yield
p	Quintet (NMR)
Ph	Phenyl
Pic	Picolyl
PL	Photoluminescence
ppm	Parts per million
ps	Picoseconds
py	Pyridine
q	Quartet (NMR)
RT	Room Temperature
s	Singlet (NMR); strong (IR); seconds
S ₀	Ground State (Singlet)
S ₁	First Excited State (Singlet)
salen	2,2'-((1 <i>E</i> ,1' <i>E</i>)-(ethane-1,2-diylbis(azanylylidene))bis(methanylylidene))diphenolate
SOC	Spin-orbit Coupling
SOMO	Singly Occupied Molecular Orbital
t	Triplet (NMR)
T ₁	First Excited State (Triplet)
TADF	Thermally Activated Delayed Fluorescence
<i>t</i> Bu	<i>tert</i> Butyl
TCSPC	Time-Correlated Single Photon Counting
TD-DFT	Time-Dependent Density Functional Theory
TFA	Trifluoroacetic acid
THF	Tetrahydrofuran
TIPP	Tri <i>is</i> opropylphenyl
TLC	Thin Layer Chromatography
TMS	Trimethylsilyl
TMSCl	Trimethylsilylchloride
UV	Ultraviolet

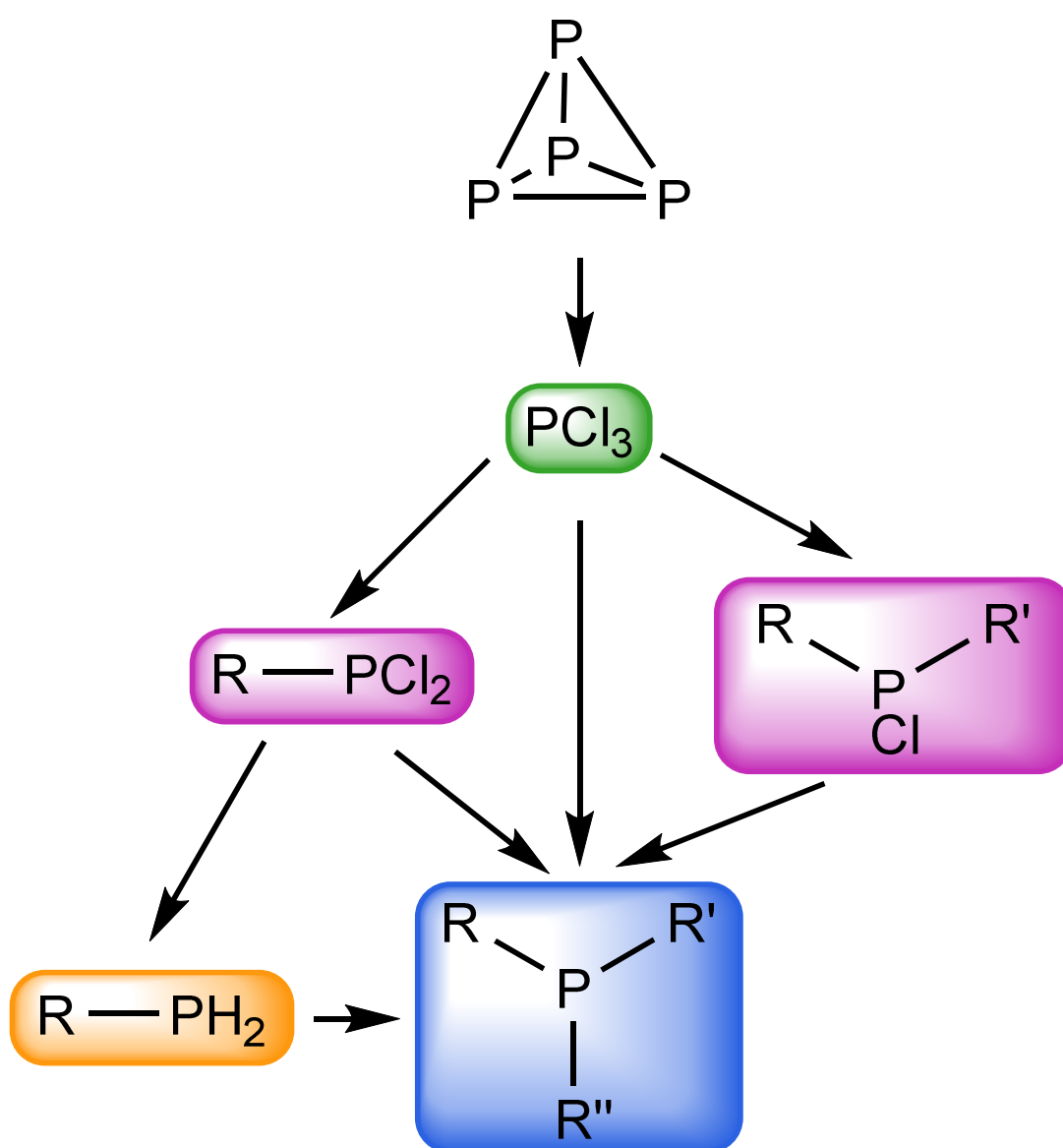
UV/Vis	Ultraviolet/visual
w	weak (IR)
XMCT	Halide-to-Metal Charge Transfer

Colour scheme in figures of crystal structures

H	B	C	N	O	Cl	P	S	Br	Cu	Zn	I
											

Chapter 1

Introduction



1.1 Organophosphorus compounds

Organophosphorus compounds are organic molecules, which contain at least one phosphorus atom. They are widely used in many fields of life, such as in catalysis,^[1] as complex ligands,^[2] in medicine,^[3] as pesticides^[4] and as flame retardants.^[5] Furthermore they are good candidates for functional materials for new applications, like luminescent devices.^[6]

As it is not the intention to give an overview on organophosphorus compounds to the full extent here, this chapter will only describe the most important aspects of the chemistry of chlorophosphines, primary phosphines and tertiary phosphines. These three classes of organophosphorus compounds are of particular importance for this work.

The organophosphorus compounds developed within this thesis will be investigated focusing on their coordination behaviour towards d¹⁰ metals and possible luminescent properties.

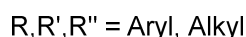
1.1.1 Chlorophosphines

Compounds with P–Cl bonds (PCl₃, RPCl₂, R₂PCl) are still a current field of research, as they are very reactive compounds and often used as starting materials to form P–C, P–N and P–O bonds.^[7]

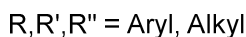
Phosphorus trichloride (trichlorophosphine, PCl₃) is an industrially very important chemical, which is used as the starting material for the synthesis of the majority of organophosphorus compounds.^[8] It is usually synthesised on a large scale by reaction of elemental phosphorus with chlorine in a volume of 700000 tonnes per year.^[8-9]

Dichlorophosphines RPCl₂ can be synthesised in many different ways, such as chlorination of primary phosphines or aminophosphines.^[10] The most common synthesis of dichlorophosphines is the reaction of organometallic reagents (with Li, Mg, Zn, etc.) with phosphorus trichloride.^[7e, 11] In particular organozinc reagents are becoming increasingly important for the synthesis of chlorophosphines, due to their high selectivity and tolerance of different functional groups.^[12] However, the development of straightforward and general protocols for formation of P–C bonds remains still a challenge in organophosphorus chemistry.

Dichlorophosphines are important starting materials for the synthesis of a variety of organophosphorus compounds (Scheme 1). They can be used to synthesise primary phosphines^[10d, 13] as well as tertiary phosphines^[7a-e] or aminophosphines.^[7f-j] It is also possible to form P–P bonds to yield diphosphenes^[11a, 14] or cyclophosphines.^[10c, 15] Other products, which can be obtained starting from dichlorophosphines, include phosphonic^[7k-n] and phosphinic acids.^[7o, 7p] They are also valuable starting materials for the synthesis of phosphalkynes.^[16]

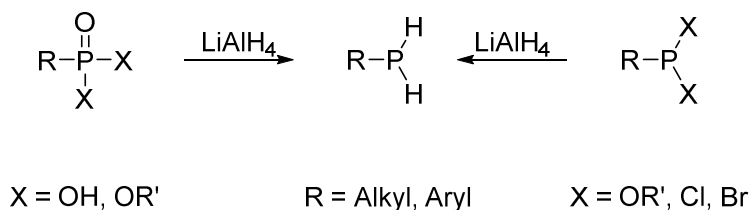


Similar to the dichlorophosphines monochlorophosphines can be synthesised by chlorination of secondary phosphines^[10b, 17] or aminophosphines.^[18] Another way to produce monochlorophosphines is the reaction of organometallic reagents (usually with Li or Mg) with PCl_3 ^[19] or – to obtain chlorophosphines with different organic substituents – with dichlorophosphines.^[7a, 20] The chemistry of monochlorophosphines R_2PCl is very similar to that of dichlorophosphines. They have been used as starting materials to replace the P–Cl bond with a P–C,^[21] P–H,^[22] P–N,^[23] P–P^[24] or P–O bond (Scheme 2).^[25]



1.1.2 Primary phosphines

Primary phosphines are usually synthesised by reduction of the corresponding phosphonic acid, phosphonate, dichlorophosphine or other suitable phosphorus derivatives (Scheme 3).^[26]

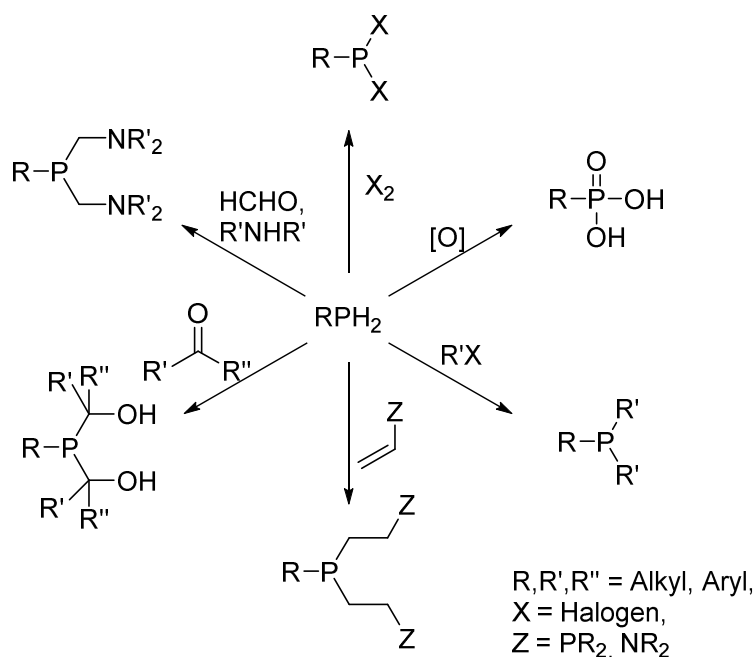


Scheme 3: Synthetic strategies to obtain primary phosphines.

Most primary phosphines are difficult to handle due to their high toxicity and high reactivity. Many primary phosphines react violently upon contact to air and often can ignite spontaneously.^[27]

In the research group of *L. Higham* some studies about the air stability of primary phosphines have been accomplished.^[27a, 27d, 28] They found that primary phosphines become air stable, if the organic substituent provides steric hindrance. In addition the organic substituent should contain conjugated π -system and/or heteroatoms, which move the localisation of the HOMO away from the phosphorus atom. It is also important that the SOMO energy of the corresponding radical cation should be higher than -10 eV.^[27a]

The high reactivity of the primary phosphines makes them a good starting material to introduce a wide variety of functional groups to the phosphorus, such as alkyl or aryl groups or halogens (Scheme 4).^[28-29]

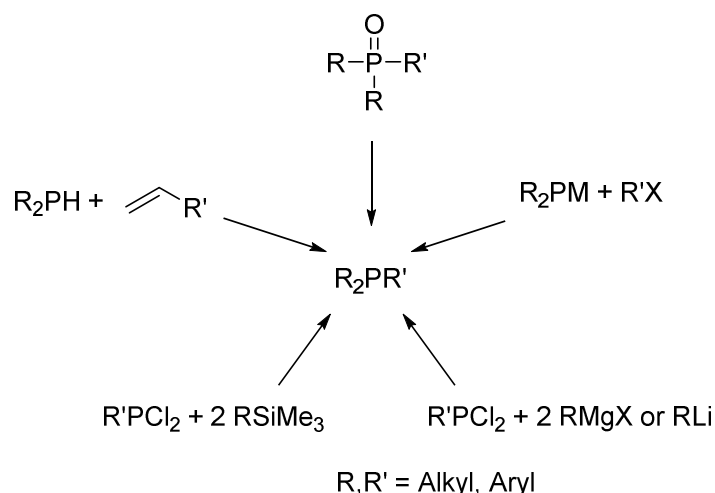


Scheme 4: Selected reactions using primary phosphines as starting material.

1.1.3 Tertiary phosphines

Organophosphorus compounds of the type R_3P , with R being alkyl or aryl groups, are called tertiary phosphines.

There are many different ways to synthesise tertiary phosphines, such as reaction of metal phosphides with alkyl or aryl halides, reaction of chlorophosphines with organometallic reagents or trimethylsilyl compounds, *Michael* additions or reduction of phosphine oxides (Scheme 5).^[7e, 30]



Scheme 5: Synthetic strategies to obtain tertiary phosphines.

Most tertiary phosphines are easily oxidised to the corresponding phosphine oxides.^[30c] The reactivity of phosphines is strongly determined by the lone pair on the phosphorus atom, meaning that phosphines usually react as nucleophiles.^[30c]

In organic chemistry tertiary phosphines are often used as reagents or as catalysts.^[31] Due to their high oxophilicity phosphines are good reducing agents, which are used in reactions, such as *Staudinger*,^[32] *Wittig*,^[33] *Mitsunobu*^[34] and *Appel* reactions.^[35] Phosphine catalysts have applications in *Morita-Baylis-Hillman* reactions,^[36] cycloaddition reactions,^[37] and other nucleophilic additions.^[38] The use of chiral phosphines also allows catalysis of asymmetric reactions.^[38a, 39]

The free electron pair also allows the coordination to metal centres, which makes the phosphines good ligands for complexes.^[30a, 30c]

Such phosphine complexes have been utilised as catalysts for reactions like hydrogenations,^[40] hydrosilylations,^[41] carbonylations^[42] and cross-coupling reactions.^[43]

Also a lot of research has been done on phosphine complexes with luminescent properties during the last decades. These complexes have potential applications e.g. as chemical sensors, for biological labelling, for photoredox catalysis and as emitter materials in organic light emitting diodes (OLEDs).^[44] The research for materials for OLEDs focuses mainly on complexes of the coinage metals, especially copper(I).^[45]

This thesis will focus on complexes with luminescent properties for possible applications in OLEDs. Therefore in the following paragraphs some information on luminescence and OLEDs is delivered.

1.2 Luminescence

Luminescence is an emission of photons from an electronically excited species. Depending on the mode of excitation there are different types of luminescence, such as radioluminescence (emission of light due to ionising radiation), thermoluminescence (emission of light due to heating), chemiluminescence (emission of light due to chemical reaction), bioluminescence (emission of light due to a biochemical process), electroluminescence (emission of light due to electric current passing through a substance) and photoluminescence (emission of light due to the absorption of light).^[46]

It is possible to distinguish between fluorescence, phosphorescence and delayed fluorescence, depending on the relaxation mode of the molecule.^[46]

Upon absorption of a photon a molecule is excited from the ground state S_0 to an excited state S_1 or S_2 respectively (Figure 1).^[46]

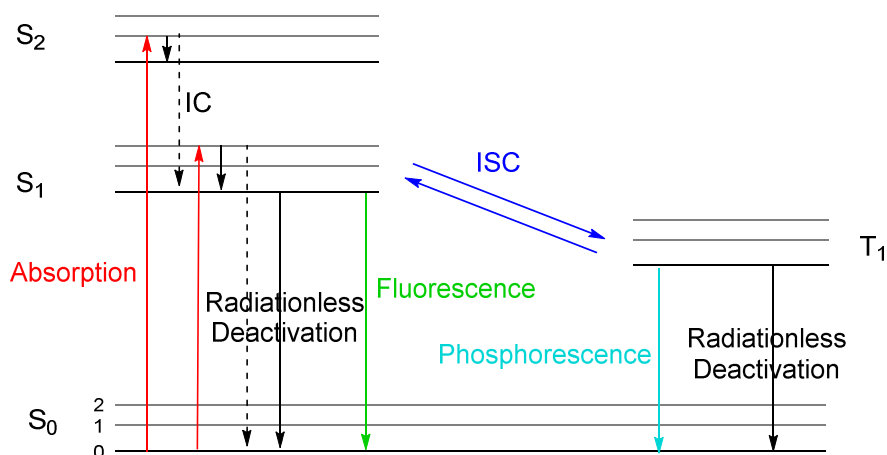


Figure 1: Jablonski diagram.

After the molecule has been excited it can return to the ground state on different pathways. Fluorescence is the emission of a photon from a molecule during the spin-allowed relaxation from the first singlet excited state (S_1) to the ground state (S_0). It is also possible that the molecule loses the energy on competing pathways without light emission (e.g. internal conversion (IC), intersystem crossing (ISC), intramolecular charge transfer, conformational change).^[46]

If the spin-orbit coupling (SOC) of a molecule is large enough, it can make the spin-forbidden transition from S_1 to T_1 possible. This is often the case in the presence of heavy atoms. From the T_1 state the molecule can relax to S_0 either without radiation or with emission of light (phosphorescence).^[46]

In case of a small energy difference between S_1 and T_1 reverse ISC from T_1 back to S_1 might also occur, if the lifetime of T_1 is long enough. Afterwards the molecule relaxes from S_1 to S_0 by emission of light, leading to delayed fluorescence. Delayed fluorescence can be obtained by triplet-triplet annihilation or by thermal activation (thermally activated delayed fluorescence (TADF)).^[46]

1.3 Organic Light Emitting Diodes (OLEDs)

Organic Light Emitting Diodes (OLEDs) are electroluminescent devices, which are considered as possible replacements for lighting technologies, such as light bulbs, energy-saving lamps and fluorescent tubes.^[47]

One of the main applications for OLEDs are semi-transparent or bendable displays. This is due to several advantages of these materials like high contrast, bright colours, wide viewing angle, thin emissive layers, low energy consumption and fast response speed.^[47-48]

OLEDs are typically set up in a multilayer design, which is placed on a glass substrate. The generation of light is based on the formation of excitons by combination of hole and electron in the emission layer. The “hole” is a positive charge that moves from the anode into the direction of the cathode from molecule to molecule by movement of electrons to the anode. From the anode (usually consisting of a composite of In_2O_3 and SnO_2 “indium tin oxide” (ITO)) the holes move through the hole transport layer (HTL) to the emission layer (EML). On the opposite side electrons are injected from a metal cathode through a thin electron injection and protection layer and the electron transport layer (ETL) into the EML (Figure 2).^[49]

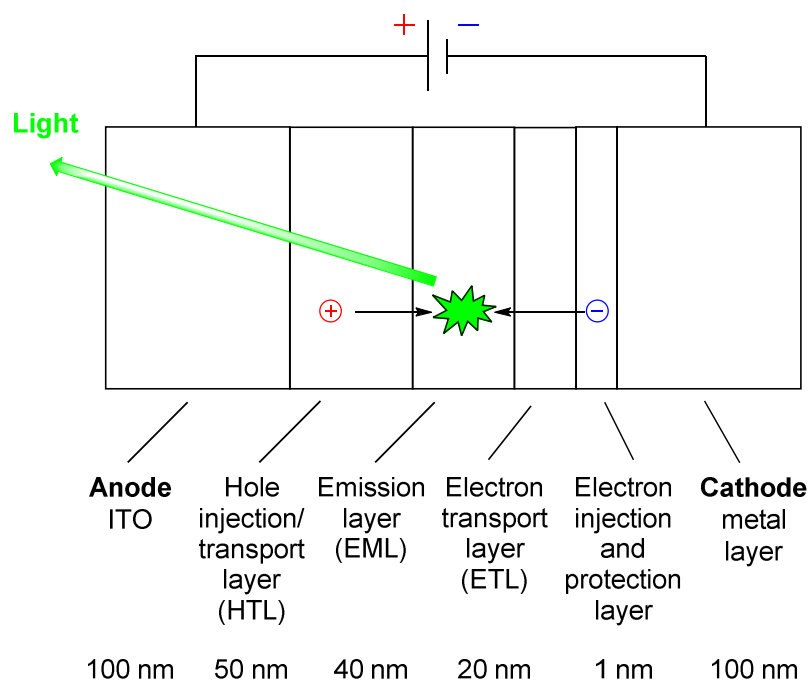


Figure 2: Basic set-up of an OLED. The layers are not drawn to scale.^[49]

Due to spin statistics 25% of the excitons formed are in the singlet state, while the remaining 75% are in the triplet state. This means the relaxation mechanism of the emitter material is of significant importance for the performance of an OLED.^[47]

The first examples of OLEDs used purely fluorescent emitters, of which only the excitons in the singlet state can generate light, while the triplet excitons cannot be harvested. Therefore these devices have only low performance, but in some devices fluorescent materials are still in use, especially to obtain blue emission, because no satisfying alternatives have been found to date.^[47]

In contrast to the fluorescent emitters, it is theoretically possible to reach an internal quantum efficiency of 100% by using phosphorescent emitters. As phosphorescent emitters mostly complexes with heavy metals are under investigation, due to their high SOC, which makes fast ISC possible. Also the spin-forbidden transition from T_1 to S_0 becomes more allowed. In this mechanism all excitons from the singlet and the triplet state are collected *via* the triplet state. Therefore this is called the *triplet harvesting* effect. Currently, although quite expensive, phosphorescent emitters based on platinum and iridium are the most efficient materials.^[47]

The third type of emitters, which is of interest for OLEDs, is TADF emitters. As described above (see 1.2) in the case of delayed fluorescence the emission is caused by the transition from S_1 to S_0 , which is why this process is called *singlet harvesting*. This leads to a possible internal quantum efficiency of 100%, like for phosphorescent emitters. TADF emitters at the moment are mostly based on Cu(I) complexes or on purely organic molecules.^[47]

1.4 Previous work on picolylphosphine based luminescent compounds

First investigations on bis(picolyl)phosphines indicate a versatile and interesting coordination behaviour.^[12a] This is due to the picolyl substituent at phosphorus. Additional nitrogen atoms in the pyridine ring cause a variable coordination capability and the methylene group between phosphorus

and the pyridine ring gives the ligand flexibility and adaptability upon coordination. On the other hand in complexes the ligand is rigid and held by the metal atom. According to first investigations by *C. Hettstedt* this special coordination situation is expressed in special and unexpected properties of the complexes.^[12a] For instance zinc complexes showed blue luminescence under irradiation with UV light in the solid state.^[12a] This finding is especially interesting given the high demand of stable and inexpensive blue emitter materials.

1.5 Aims of the project

The scope of this project was the synthesis of a series of new bis- and tris(picolyl)phosphine based compounds and to investigate their coordination behaviour towards zinc and copper(I).

Structural investigations on the hydrochlorides of some mono(picolyl)phosphine based compounds shall be performed to gain insight into the interactions between the molecules in the solid state.

The materials which are currently in use for the production of OLEDs are based on very expensive elements, such as iridium and platinum. This means that cheaper materials are of interest for the lighting industry. Some of the most promising materials are complexes of zinc and copper(I). Therefore zinc chloride and copper(I) halide complexes of bis- and tris(picolyl)phosphine based ligands shall be synthesised and tested for potential applications as emitter materials.

Further the influence of a fluorescent moiety in one of the organic substituents on the coordination behaviour and the luminescent properties is investigated. Therefore P,N ligands with a substituent containing the Bodipy moiety are synthesised and corresponding complexes with manganese, zinc and copper(I) are prepared and investigated.

1.6 References

- [1] a) S. Liu, C. Ren, N. Zhao, Y. Shen, Z. Li, *Macromol. Rapid Commun.* **2018**, *39*, e1800485; b) M. Cokoja, M. E. Wilhelm, M. H. Anthofer, W. A. Herrmann, F. E. Kuhn, *ChemSusChem* **2015**, *8*, 2436-2454.
- [2] a) P. Sutra, A. Igau, *Coord. Chem. Rev.* **2016**, *308*, 97-116; b) P. W. N. M. van Leeuwen, P. C. J. Kamer, *Catal. Sci. Technol.* **2018**, *8*, 26-113.
- [3] a) S. Demkowicz, J. Rachon, M. Daško, W. Kozak, *RSC Adv.* **2016**, *6*, 7101-7112; b) J. B. Rodriguez, C. Gallo-Rodriguez, *ChemMedChem* **2019**, *14*, 190-216.
- [4] F.-W. Yang, Y.-X. Li, F.-Z. Ren, R. Wang, G.-F. Pang, *Environ. Chem. Lett.* **2019**, *17*, 1769-1785.
- [5] a) S. Wendels, T. Chavez, M. Bonnet, K. A. Salmeia, S. Gaan, *Materials* **2017**, *10*; b) S. D. Jadhav, *Pharma Innovation* **2018**, *7*, 380-386.
- [6] a) D. Joly, P. A. Bouit, M. Hissler, *J. Mater. Chem. C* **2016**, *4*, 3686-3698; b) T. Delouche, A. Mocanu, T. Roisnel, R. Szucs, E. Jacques, Z. Benko, L. Nyulaszi, P. A. Bouit, M. Hissler, *Org. Lett.* **2019**, *21*, 802-806.
- [7] a) H. Klöcker, J. C. Tendyck, L. Keweloh, A. Hepp, W. Uhl, *Chem. Eur. J.* **2019**, *25*, 4793-4807; b) R. H. Laitinen, H. Riihimäki, M. Haukka, S. Jääskeläinen, T. A. Pakkanen, J. Pursiainen, *Eur. J. Inorg. Chem.* **1999**, *1999*, 1253-1258; c) K. V. Rajendran, L. Kennedy, D. G. Gilheany, *Eur. J. Org. Chem.* **2010**, *2010*, 5642-5649; d) R. Popp, R. Gleiter, G. Haberhauer, F. Rominger, *Eur. J. Org. Chem.* **2018**, *2018*, 2795-2805; e) C. Hettstedt, M. Unglert, R. J. Mayer, A. Frank, K. Karaghiosoff, *Eur. J. Inorg. Chem.* **2016**, *2016*, 1405-1414; f) M. L. Clarke, G. L. Holliday, A. M. Z. Slawin, J. D. Woollins, *Dalton Trans.* **2002**, 1093-1103; g) T. Bauer, S. Schulz, M. Nieger, Z. Anorg. Allg. Chem. **2001**, *627*, 266-270; h) Y. V. Svyaschenko, B. B. Barnych, D. M. Volochnyuk, N. V. Shevchuk, A. N. Kostyuk, *J. Org. Chem.* **2011**, *76*, 6125-6133; i) G. Ewart, D. S. Payne, A. L. Porte, A. P. Lane, *J. Chem. Soc.* **1962**, 3984-3990; j) L. Maier, *Helv. Chim. Acta* **1964**, *47*, 2129-2137; k) F. Siméon, P.-A. Jaffrès, D. Villemin, *Tetrahedron* **1998**, *54*, 10111-10118; l) T. A. Van der Knaap, T. C. Klebach, R. Lourens, M. Vos, F. Bickelhaupt, *J. Am. Chem. Soc.* **1983**, *105*, 4026-4032; m) O. Oms, J. L. Bideau, A. Vioux, D. Leclercq, *J. Organomet. Chem.* **2005**, *690*, 363-370; n) D. B. G. Williams, T. E. Netshiozwi, *Tetrahedron* **2009**, *65*, 9973-9982; o) D. Yakhvarov, E. Trofimova, O. Sinyashin, O. Kataeva, Y. Budnikova, P. Lonnecke, E. Hey-Hawkins, A. Petr, Y. Krupskaya, V. Kataev, R. Klingeler, B. Buchner, *Inorg. Chem.* **2011**, *50*, 4553-4558; p) A. Orthaber, J. H. Albering, F. Belaj, R. Pietschnig, *J. Fluorine Chem.* **2010**, *131*, 1025-1031.
- [8] J.-L. Montchamp, *Acc. Chem. Res.* **2014**, *47*, 77-87.
- [9] a) J. E. Borger, A. W. Ehlers, J. C. Slootweg, K. Lammertsma, *Chem. Eur. J.* **2017**, *23*, 11738-11746; b) <https://www.essentialchemicalindustry.org/chemicals/phosphorus.html>, 06.07.2020.
- [10] a) A. N. Tavitkin, S. A. Toloraya, E. E. Nifant'ev, I. E. Nifant'ev, *Tetrahedron Lett.* **2011**, *52*, 824-825; b) N. Weferling, *Z. Anorg. Allg. Chem.* **1987**, *548*, 55-62; c) K. Diemert, B. Kottwitz, W. Kuchen, *Phosphorus Sulfur Relat. Elem.* **1986**, *26*, 307-320; d) S. A. Reiter, S. D. Nogai, H. Schmidbaur, *Dalton Trans.* **2005**, 247-255; e) U. Berens, U. Englert, S. Geyser, J. Runsink, A. Salzer, *Eur. J. Org. Chem.* **2006**, *2006*, 2100-2109; f) A. N. Huryeva, A. P. Marchenko, G. N. Koidan, A. A. Yurchenko, E. V. Zarudnitskii, A. M. Pinchuk, A. N. Kostyuk, *Heteroat. Chem.* **2010**, *21*, 103-118.
- [11] a) K. Toyota, Y. Matsushita, N. Shinohara, M. Yoshifuji, *Heteroat. Chem.* **2001**, *12*, 418-423; b) M. Yoshifuji, T. Niitsu, D. Shiomi, N. Inamoto, *Tetrahedron Lett.* **1989**, *30*, 5433-5436; c) A. Hinke, W. Kuchen, *Phosphorus Sulfur Relat. Elem.* **2006**, *15*, 93-98; d) M. Höhne, N. Peulecke, K. Konieczny, B. H. Müller, U. Rosenthal, *ChemCatChem* **2017**, *9*, 2467-2472; e) M. D. Sorensen, L. K. Blaehr, M. K. Christensen, T. Hoyer, S. Latini, P. J. Hjarnaa, F. Bjorkling, *Bioorg. Med. Chem.* **2003**, *11*, 5461-5484; f) M. Fild, M. Vahldiek, *Phosphorus Sulfur Relat. Elem.*

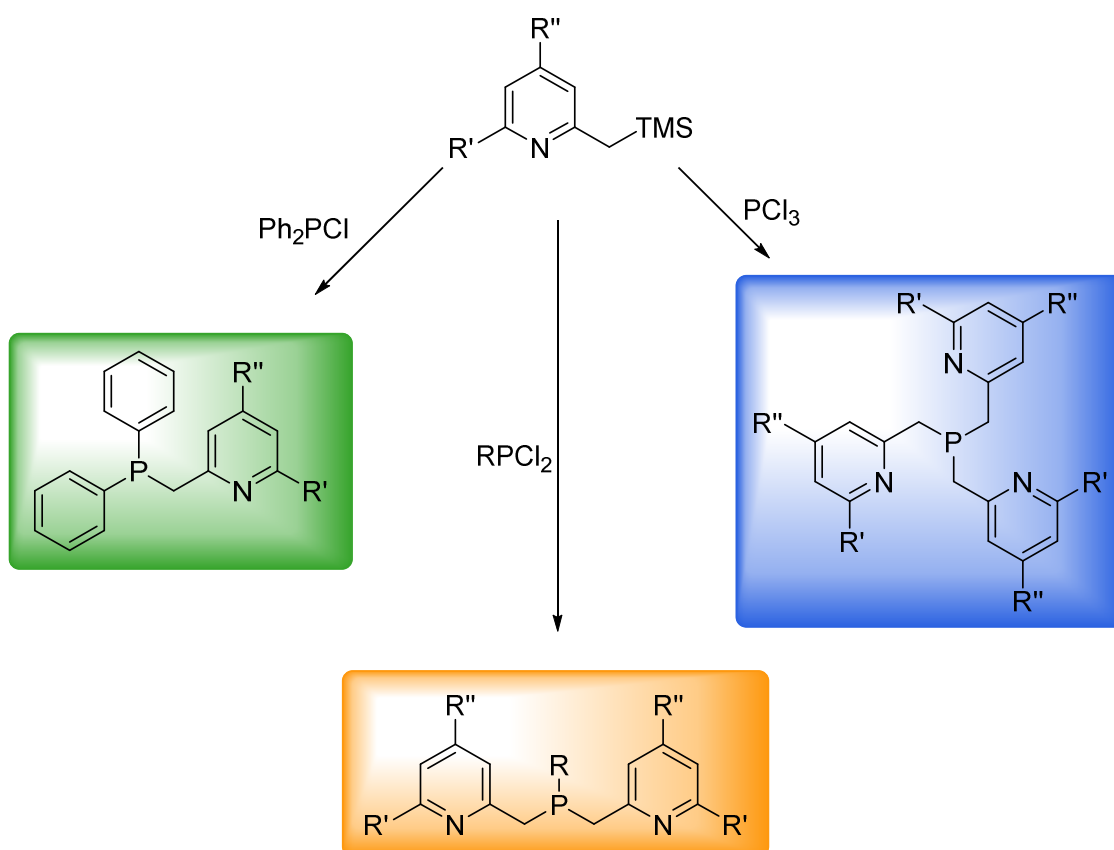
- 1988**, *40*, 207-213; g) R. T. Boéré, J. D. Masuda, P. Tran, *J. Organomet. Chem.* **2006**, *691*, 5585-5591; h) S. Amberg, J. W. Engels, *Helv. Chim. Acta* **2002**, *85*, 2503-2517.
- [12] a) C. Hettstedt, PhD thesis, Ludwig-Maximilians-Universität München **2015**; b) A. Krasovskiy, V. Malakhov, A. Gavryushin, P. Knochel, *Angew. Chem., Int. Ed.* **2006**, *45*, 6040-6044; c) A. Boudier, L. O. Bromm, M. Lotz, P. Knochel, *Angew. Chem., Int. Ed.* **2000**, *39*, 4414-4435; d) P. Knochel, W. Dohle, N. Gommermann, F. F. Kneisel, F. Kopp, T. Korn, I. Sapountzis, V. A. Vu, *Angew. Chem., Int. Ed.* **2003**, *42*, 4302-4320.
- [13] J. Escudie, C. Couret, H. Ranaivonjatovo, M. Lazraq, J. Satge, *Phosphorus Sulfur Relat. Elem.* **1987**, *31*, 27-31.
- [14] K. B. Dillon, M. A. Fox, V. C. Gibson, H. P. Goodwin, L. J. Sequeira, *J. Organomet. Chem.* **2017**, *830*, 113-119.
- [15] M. Scherer, D. Stein, F. Breher, J. Geier, H. Schönberg, H. Grützmacher, *Z. Anorg. Allg. Chem.* **2005**, *631*, 2770-2774.
- [16] a) J. G. Cordaro, D. Stein, H. Grützmacher, *J. Am. Chem. Soc.* **2006**, *128*, 14962-14971; b) R. Appel, A. Westerhaus, *Tetrahedron Lett.* **1981**, *22*, 2159-2160.
- [17] a) d. Koe Pieter, F. Bickelhaupt, *Z. Naturforsch. B* **2003**, *58*, 782; b) M. Carreira, M. Charernsuk, M. Eberhard, N. Fey, R. v. Ginkel, A. Hamilton, W. P. Mul, A. G. Orpen, H. Phetmung, P. G. Pringle, *J. Am. Chem. Soc.* **2009**, *131*, 3078-3092.
- [18] a) F. Allouch, N. V. Vologdin, H. Cattey, N. Pirio, D. Naoufal, A. Kanj, R. V. Smaliy, A. Savateev, A. Marchenko, A. Hurieva, H. Koidan, A. N. Kostyuk, J.-C. Hierso, *J. Organomet. Chem.* **2013**, *735*, 38-46; b) A. Koner, M. Kunz, G. Schnakenburg, R. Streubel, *Eur. J. Inorg. Chem.* **2018**, *2018*, 3778-3784; c) P. K. Majhi, A. Koner, G. Schnakenburg, Z. Kelemen, L. Nyulászi, R. Streubel, *Eur. J. Inorg. Chem.* **2016**, *2016*, 3559-3573; d) A. Koner, S. C. Serin, G. Schnakenburg, B. O. Patrick, D. P. Gates, R. Streubel, *Dalton Trans.* **2017**, *46*, 10504-10514; e) A. Beganskiene, N. Kongprakaiwoot, R. L. Luck, E. Urnezis, *Z. Anorg. Allg. Chem.* **2006**, *632*, 1879-1884; f) A. Tarasevych, I. Shevchenko, A. B. Rozhenko, G.-V. Rösenthaller, *Eur. J. Inorg. Chem.* **2010**, *2010*, 1552-1558.
- [19] a) W. Voskuil, J. F. Arens, *Org. Synth.* **1968**, *48*, 47; b) J. Campos, M. F. Espada, J. Lopez-Serrano, E. Carmona, *Inorg. Chem.* **2013**, *52*, 6694-6704; c) S. Sasaki, F. Murakami, M. Murakami, M. Watanabe, K. Kato, K. Sutoh, M. Yoshifuji, *J. Organomet. Chem.* **2005**, *690*, 2664-2672; d) S. Sasaki, K. Ogawa, M. Watanabe, M. Yoshifuji, *Organometallics* **2010**, *29*, 757-766; e) S. Sasaki, M. Murakami, F. Murakami, M. Yoshifuji, *Heteroat. Chem.* **2011**, *22*, 506-513.
- [20] a) A. Fukazawa, J. Usuba, R. A. Adler, S. Yamaguchi, *Chem. Commun.* **2017**, *53*, 8565-8568; b) S. Torker, A. Müller, R. Sigrist, P. Chen, *Organometallics* **2010**, *29*, 2735-2751; c) Z. M. Xie, P. Wisian-Neilson, R. H. Neilson, *Organometallics* **1985**, *4*, 339-344; d) B. Neuwald, L. Falivene, L. Caporaso, L. Cavallo, S. Mecking, *Chem. Eur. J.* **2013**, *19*, 17773-17788.
- [21] a) F. Eisenträger, A. Göthlich, I. Gruber, H. Heiss, C. A. Kiener, C. Krüger, J. Ulrich Notheis, F. Rominger, G. Scherhag, M. Schultz, B. F. Straub, M. A. O. Volland, P. Hofmann, *New J. Chem.* **2003**, *27*, 540-550; b) R. Zhang, Y. Zhou, *Synthesis* **1987**, *1987*, 938-939; c) M. Xue, J. Li, J. Peng, Y. Bai, G. Zhang, W. Xiao, G. Lai, *Appl. Organometal. Chem.* **2014**, *28*, 120-126; d) M. D. Fryzuk, G. S. Bates, C. Stone, *J. Org. Chem.* **1988**, *53*, 4425-4426; e) I. P. Beletskaya, V. V. Afanasiev, M. A. Kazankova, I. V. Efimova, *Org. Lett.* **2003**, *5*, 4309-4311.
- [22] a) M. K. Rong, K. van Duin, T. van Dijk, J. J. de Pater, B. J. Deelman, M. Nieger, A. W. Ehlers, J. C. Slootweg, K. Lammertsma, *Organometallics* **2017**, *36*, 1079-1090; b) M. Yam, C.-W. Tsang, D. P. Gates, *Inorg. Chem.* **2004**, *43*, 3719-3723.
- [23] a) M. Maumela, K. Blann, H. de Bod, J. Dixon, W. Gabrielli, D. B. Williams, *Synthesis* **2007**, *2007*, 3863-3867; b) A. N. Kornev, N. V. Belina, V. V. Sushev, G. K. Fukin, E. V. Baranov, Y. A. Kurskiy, A. I. Poddelskii, G. A. Abakumov, P. Lonnecke, E. Hey-Hawkins, *Inorg. Chem.* **2009**, *48*, 5574-5583.

- [24] a) W.-W. DuMont, S. Kubiniok, T. Severengiz, *Z. Anorg. Allg. Chem.* **1985**, 531, 21-25; b) I. Kovacs, H. Krautscheid, E. Matern, G. Fritz, *Z. Anorg. Allg. Chem.* **1994**, 620, 1369-1374; c) S. Yogendra, S. S. Chitnis, F. Hennesdorf, M. Bodensteiner, R. Fischer, N. Burford, J. J. Weigand, *Inorg. Chem.* **2016**, 55, 1854-1860.
- [25] a) R. B. Bedford, S. L. Hazelwood, P. N. Horton, M. B. Hursthouse, *Dalton Trans.* **2003**, 4164-4174; b) H. Hacklin, G.-V. Rösenthaller, *Phosphorus Sulfur Relat. Elem.* **1988**, 36, 165-169.
- [26] K. V. Katti, N. Pillarsetty, K. Raghuraman, in *New Aspects in Phosphorus Chemistry III* (Ed.: J.-P. Majoral), Springer Berlin Heidelberg, Berlin, Heidelberg, **2003**, pp. 121-141.
- [27] a) B. Stewart, A. Harriman, L. J. Higham, *Organometallics* **2011**, 30, 5338-5343; b) R. M. Hiney, L. J. Higham, H. Müller-Bunz, D. G. Gilheany, *Angew. Chem., Int. Ed.* **2006**, 45, 7248-7251; c) L. H. Davies, B. Stewart, R. W. Harrington, W. Clegg, L. J. Higham, *Angew. Chem., Int. Ed.* **2012**, 51, 4921-4924; d) A. Ficks, C. Sibbald, S. Ojo, R. W. Harrington, W. Clegg, L. J. Higham, *Synthesis* **2013**, 45, 265-271; e) M. Brynda, *Coord. Chem. Rev.* **2005**, 249, 2013-2034; f) R. Noble-Eddy, S. L. Masters, D. W. Rankin, D. A. Wann, H. E. Robertson, B. Khater, J. C. Guillemin, *Inorg. Chem.* **2009**, 48, 8603-8612.
- [28] J. T. Fleming, L. J. Higham, *Coord. Chem. Rev.* **2015**, 297-298, 127-145.
- [29] K. R. Prabhu, P. N. Kishore, H. Gali, K. V. Katti, *Curr. Sci.* **2000**, 78, 431-439.
- [30] a) M. T. Honaker, J. M. Hovland, R. Nicholas Salvatore, *Curr. Org. Synth.* **2007**, 4, 31-45; b) A. Kermagoret, P. Braunstein, *Organometallics* **2008**, 27, 88-99; c) L. D. Quin, *A Guide to Organophosphorus Chemistry*, John Wiley & Sons, New York, **2000**.
- [31] S. Xu, Z. He, *RSC Adv.* **2013**, 3, 16885.
- [32] a) J. J. Li, E. J. Corey, *Name Reactions for Functional Group Transformations*, pp. 85-158; b) Y. G. Gololobov, L. F. Kasukhin, *Tetrahedron* **1992**, 48, 1353-1406; c) Y. G. Gololobov, I. N. Zhmurova, L. F. Kasukhin, *Tetrahedron* **1981**, 37, 437-472.
- [33] a) Z. Lao, P. H. Toy, *Beilstein J. Org. Chem.* **2016**, 12, 2577-2587; b) L. Longwitz, T. Werner, *Pure Appl. Chem.* **2019**, 91, 95-102.
- [34] a) R. H. Beddoe, H. F. Sneddon, R. M. Denton, *Org. Biomol. Chem.* **2018**, 16, 7774-7781; b) S. Fletcher, *Org. Chem. Front.* **2015**, 2, 739-752; c) T. Y. But, P. H. Toy, *Chem. Asian J.* **2007**, 2, 1340-1355.
- [35] a) A. Jordan, R. M. Denton, H. F. Sneddon, *ACS Sustainable Chem. Eng.* **2020**, 8, 2300-2309; b) H. A. van Kalker, F. L. van Delft, F. P. J. T. Rutjes, *Pure Appl. Chem.* **2012**, 85, 817-828.
- [36] H. Pellissier, *Tetrahedron* **2017**, 73, 2831-2861.
- [37] Z. Wang, X. Xu, O. Kwon, *Chem. Soc. Rev.* **2014**, 43, 2927-2940.
- [38] a) Y. Xiao, Z. Sun, H. Guo, O. Kwon, *Beilstein J. Org. Chem.* **2014**, 10, 2089-2121; b) S. B. Nallapati, S.-C. Chuang, *Asian J. Org. Chem.* **2018**, 7, 1743-1757; c) H. Guo, Y. C. Fan, Z. Sun, Y. Wu, O. Kwon, *Chem. Rev.* **2018**, 118, 10049-10293; d) J. L. Methot, W. R. Roush, *Adv. Synth. Catal.* **2004**, 346, 1035-1050.
- [39] a) Y. Wei, M. Shi, *Chem. Asian J.* **2014**, 9, 2720-2734; b) H. Ni, W. L. Chan, Y. Lu, *Chem. Rev.* **2018**, 118, 9344-9411.
- [40] a) J. P. Genet, *Pure Appl. Chem.* **2002**, 74, 77-83; b) R. Noyori, T. Ohkuma, *Pure Appl. Chem.* **1999**, 71, 1493-1501; c) W. Liu, B. Sahoo, K. Junge, M. Beller, *Acc. Chem. Res.* **2018**, 51, 1858-1869; d) J.-H. Xie, D.-H. Bao, Q.-L. Zhou, *Synthesis* **2014**, 47, 460-471; e) R. H. Morris, *Acc. Chem. Res.* **2015**, 48, 1494-1502.
- [41] a) T. Hayashi, *Catal. Today* **2000**, 62, 3-15; b) T. Hayashi, *Catal. Surv. Jpn.* **1999**, 3, 127-135; c) T. Hayashi, *J. Synth. Org. Chem., Jpn.* **1994**, 52, 900-911; d) L. C. Misal Castro, H. Li, J.-B. Sortais, C. Darcel, *Green Chem.* **2015**, 17, 2283-2303.
- [42] a) G. Cavinato, L. Toniolo, *Molecules* **2014**, 19, 15116-15161; b) C. Godard, B. K. Munoz, A. Ruiz, C. Claver, *Dalton Trans.* **2008**, 853-860; c) A. M. Trzeciak, J. J. Ziolkowski, *Coord. Chem. Rev.* **2005**, 249, 2308-2322.
- [43] a) T. Hayashi, *J. Organomet. Chem.* **2002**, 653, 41-45; b) R. B. Bedford, C. S. J. Cazin, D. Holder, *Coord. Chem. Rev.* **2004**, 248, 2283-2321; c) U. Christmann, R. Vilar, *Angew. Chem.,*

- Int. Ed.* **2005**, *44*, 366-374; d) R. Chinchilla, C. Najera, *Chem. Soc. Rev.* **2011**, *40*, 5084-5121; e) M. Nielsen, *Synthesis* **2016**, *48*, 2732-2738; f) A. S. Guram, *Org. Process Res. Dev.* **2016**, *20*, 1754-1764; g) C. M. Lavoie, M. Stradiotto, *ACS Catal.* **2018**, *8*, 7228-7250; h) B. T. Ingoglia, C. C. Wagen, S. L. Buchwald, *Tetrahedron* **2019**, *75*, 4199-4211; i) W. Fu, W. Tang, *ACS Catal.* **2016**, *6*, 4814-4858; j) K. Tamao, *J. Organomet. Chem.* **2002**, *653*, 23-26.
- [44] a) M. Pujadas, L. Rodríguez, *Coord. Chem. Rev.* **2020**, *408*, 213179; b) I. D. Strel'nik, V. V. Sizov, V. V. Gurzhiy, A. S. Melnikov, I. E. Kolesnikov, E. I. Musina, A. A. Karasik, E. V. Grachova, *Inorg. Chem.* **2020**, *59*, 244-253; c) E. Leoni, J. Mohanraj, M. Holler, M. Mohankumar, I. Nierengarten, F. Monti, A. Sournia-Saquet, B. Delavaux-Nicot, N. Jean-Franco Is, N. Armaroli, *Inorg. Chem.* **2018**, *57*, 15537-15549; d) J. L. Chen, Z. H. Guo, H. G. Yu, L. H. He, S. J. Liu, H. R. Wen, J. Y. Wang, *Dalton Trans.* **2016**, *45*, 696-705; e) B. Hupp, C. Schiller, C. Lenczyk, M. Stanoppi, K. Edkins, A. Lorbach, A. Steffen, *Inorg. Chem.* **2017**, *56*, 8996-9008; f) L. R. V. Favarin, P. P. Rosa, L. Pizzuti, A. Machulek, A. R. L. Caires, L. S. Bezerra, L. M. C. Pinto, G. Maia, C. C. Gatto, D. F. Back, A. dos Anjos, G. A. Casagrande, *Polyhedron* **2017**, *121*, 185-190; g) M. A. Esteruelas, E. Oñate, A. U. Palacios, *Organometallics* **2017**, *36*, 1743-1755; h) S. E. Angell, C. W. Rogers, Y. Zhang, M. O. Wolf, W. E. Jones, *Coord. Chem. Rev.* **2006**, *250*, 1829-1841; i) F. Yu, W.-K. Chu, C. Shen, Y. Luo, J. Xiang, S.-Q. Chen, C.-C. Ko, T.-C. Lau, *Eur. J. Inorg. Chem.* **2016**, *2016*, 3892-3899.
- [45] a) M. Z. Shafikov, A. F. Suleymanova, A. Schinabeck, H. Yersin, *J. Phys. Chem. Lett.* **2018**, *9*, 702-709; b) L. H. He, Y. S. Luo, B. S. Di, J. L. Chen, C. L. Ho, H. R. Wen, S. J. Liu, J. Y. Wang, W. Y. Wong, *Inorg. Chem.* **2017**, *56*, 10311-10324; c) L.-L. Hu, C. Shen, W.-K. Chu, J. Xiang, F. Yu, G. Xiang, Y. Nie, C.-L. Kwok, C.-F. Leung, C.-C. Ko, *Polyhedron* **2017**, *127*, 203-211; d) A. Kobayashi, T. Hasegawa, M. Yoshida, M. Kato, *Inorg. Chem.* **2016**, *55*, 1978-1985; e) X. Hong, B. Wang, L. Liu, X.-X. Zhong, F.-B. Li, L. Wang, W.-Y. Wong, H.-M. Qin, Y. H. Lo, *J. Lumin.* **2016**, *180*, 64-72; f) H. Chen, L.-X. Xu, L.-J. Yan, X.-F. Liu, D.-D. Xu, X.-C. Yu, J.-X. Fan, Q.-A. Wu, S.-P. Luo, *Dyes Pigm.* **2020**, *173*, 108000; g) Q. Wei, R. Zhang, L. Liu, X. X. Zhong, L. Wang, G. H. Li, F. B. Li, K. A. Alamry, Y. Zhao, *Dalton Trans.* **2019**, *48*, 11448-11459; h) A. Neshat, R. B. Aghakhanpour, P. Mastroilli, S. Todisco, F. Molani, A. Wojtczak, *Polyhedron* **2018**, *154*, 217-228; i) S. Keller, A. Prescimone, H. Bolink, M. Sessolo, G. Longo, L. Martinez-Sarti, J. M. Junquera-Hernandez, E. C. Constable, E. Orti, C. E. Housecroft, *Dalton Trans.* **2018**, *47*, 14263-14276; j) C. Bizzarri, A. P. Arndt, S. Kohaut, K. Fink, M. Nieger, *J. Organomet. Chem.* **2018**, *871*, 140-149.
- [46] B. Valeur, *Molecular Fluorescence: Principles and Applications*, Wiley-VCH, Weinheim, **2002**.
- [47] M. J. Leitzl, D. M. Zink, A. Schinabeck, T. Baumann, D. Volz, H. Yersin, *Top. Curr. Chem.* **2016**, *374*, 25.
- [48] L.-P. Liu, R. Zhang, L. Liu, X.-X. Zhong, F.-B. Li, L. Wang, W.-Y. Wong, G.-H. Li, H.-J. Cong, N. S. Alharbi, Y. Zhao, *New J. Chem.* **2019**, *43*, 3390-3399.
- [49] H. Yersin, W. J. Finkenzeller, in *Highly Efficient OLEDs with Phosphorescent Materials* (Ed.: H. Yersin), **2008**, pp. 1-97.

Chapter 2

P,N Ligands



$R = \text{Ph}, i\text{Pr}$

$R', R'' = \text{H,H} / \text{Me,H} / \text{Me,Me}$

2.1 Introduction

Due to the presence of both a soft phosphorus and a hard nitrogen coordination site in P,N ligands, they are multidentate, hemilabile ligands, which have a very versatile coordination behaviour.^[1]

The combination of tertiary phosphines with pyridine moieties has been investigated in numerous studies.^[2] Phosphines with picolyl (Pic), lutidynyl (Lut) and collidynyl (Col) substituents contain a methylene group between the phosphorus atom and the pyridine ring (Figure 1), which gives the molecule greater flexibility and allows coordination of both the phosphorus and the nitrogen to the same metal atom forming a five-membered chelate ring.^[1a, 1b, 2b]

As usual for P,N ligands picolylphosphine based ligands can coordinate to metal atoms either *via* only one of the coordination sites (phosphorus or nitrogen) or with both the phosphorus and the nitrogen atom.^[3] In most cases picolylphosphine related compounds act as multidentate ligands,^[4] but often the coordination of the nitrogen atom to the metal is weaker than the coordination of the phosphorus atom.^[5]

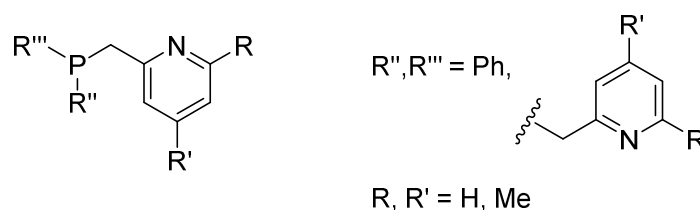


Figure 1: Examples for picolylphosphine based compounds synthesised in this thesis.

In the literature various examples of mono(picolyl)phosphine based compounds and corresponding metal complexes are described.^[2a, 2c, 6]

In contrast only a small number of bis(picolyl)phosphine based compounds and their complexes has been reported to date. The most extensively studied bis(picolyl)phosphine is PhPPic₂, which was first synthesised in 1983 by *E. Lindner et al.*^[3, 7] The only known examples of other bis(picolyl)phosphine related compounds have been reported during the last years by the research group of *K. Karaghiosoff.*^[1c, 8]

In the case of tris(picolyl)phosphine based compounds, PPic₃ and complexes thereof are the only compounds referenced in the literature.^[1c, 9]

Complexes of picolylphosphine based compounds can be used as catalysts for reactions like hydrogenations,^[10] dehydrogenations,^[11] aminations,^[2a] carbonylations,^[12] oligomerisations^[7e, 13] and Atom Transfer Radical Polymerisation.^[14]

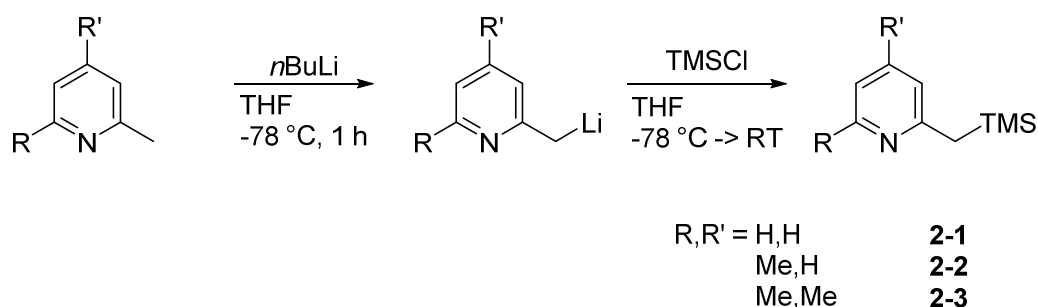
Also first examples of complexes of picolylphosphine related ligands with luminescent properties have been reported.^[8b, 15]

2.2 Results and discussion

2.2.1 Synthesis

2.2.1.1 Silyl compounds

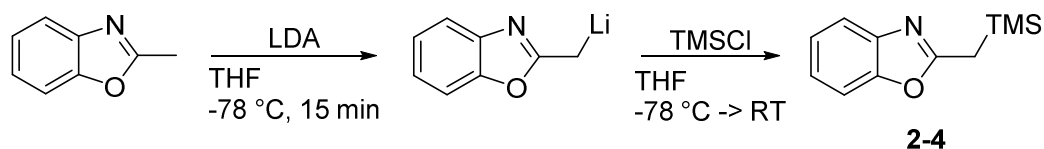
The silyl compounds **2-1–2-3** have been synthesised according to the procedure of C. Hettstedt.^[1c] The corresponding methyl pyridine derivatives were deprotonated at the 2-methyl group with *n*-butyl lithium at -78°C and the lithiated compounds were reacted with an excess of TMSCl to obtain **2-1–2-3** (Scheme 1).



Scheme 1: Synthesis of silyl compounds **2-1–2-3**.

The reaction mixture was then allowed to warm up to RT overnight and the solvent was removed *in vacuo*. After extraction with pentane and removal of the precipitated lithium chloride the solvent was removed *in vacuo*. The desired compounds were obtained as colourless liquids in good yields after vacuum distillation. **2-1–2-3** are soluble in THF, pentane and chloroform and sensitive towards hydrolysis.

2-((Trimethylsilyl)methyl)benzoxazole **2-4** could be synthesised only in very poor yields by using the same synthetic procedure. Therefore it was synthesised according to the synthesis described by S. Pailloux *et al.* to synthesise 2-[(phosphinoyl)methyl]benzoxazole ligands.^[16] 2-Methylbenzoxazole was deprotonated at the methyl group with freshly prepared LDA at -78°C . Afterwards the lithiated compound was allowed to react with an excess of TMSCl instead of a chlorophosphine to obtain **2-4** (Scheme 2).



Scheme 2: Synthesis of 2-((trimethylsilyl)methyl)benzoxazole **2-4**.

The reaction mixture was allowed to warm up to RT overnight and the solvent was removed *in vacuo*. After extraction with pentane and removal of the precipitated lithium chloride the solvent was removed *in vacuo*. The desired compound was obtained as a colourless liquid in 22% yield after vacuum distillation. **2-4** is soluble in THF, pentane and chloroform and sensitive towards hydrolysis.

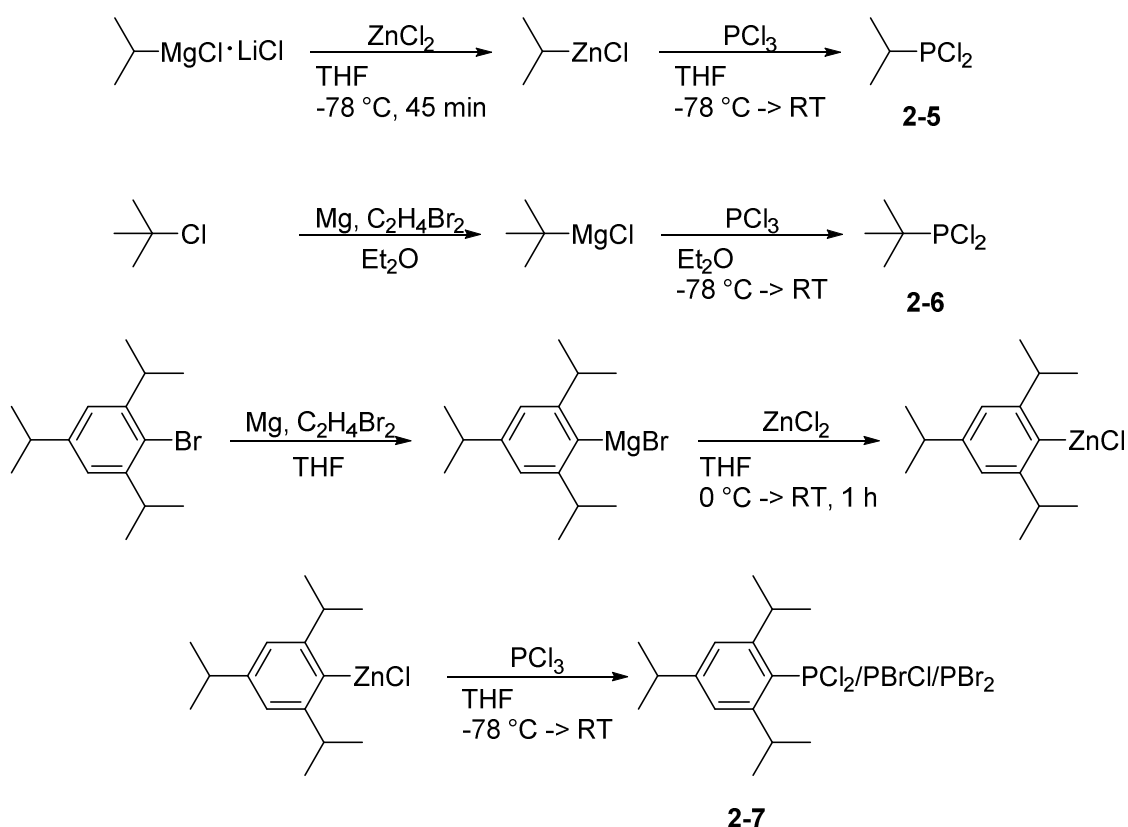
2.2.1.2 Chlorophosphines

The dichlorophosphines **2-5–2-7** have been synthesised according to literature procedures (Scheme 3).

*iso*Propyldichlorophosphine **2-5** was synthesised starting from the *Turbo-Grignard* reagent as described by W. Samstag and J. W. Engels, except that THF was used as solvent instead of Et₂O.^[17] After transmetalation to zinc, the organometallic reagent was allowed to react with trichlorophosphine. This synthetic procedure was chosen, because the zinc reagent is more selective than the *Grignard* reagent and therefore leads to higher yields of the desired dichlorophosphine.

*tert*Butyldichlorophosphine **2-6** was produced according to the synthesis of Y. Liu *et al.*, although the reaction was done in Et₂O instead of THF.^[18] After *Grignard* reaction of *tert*butyl chloride, *tert*butylmagnesium chloride was allowed to react with PCl₃.

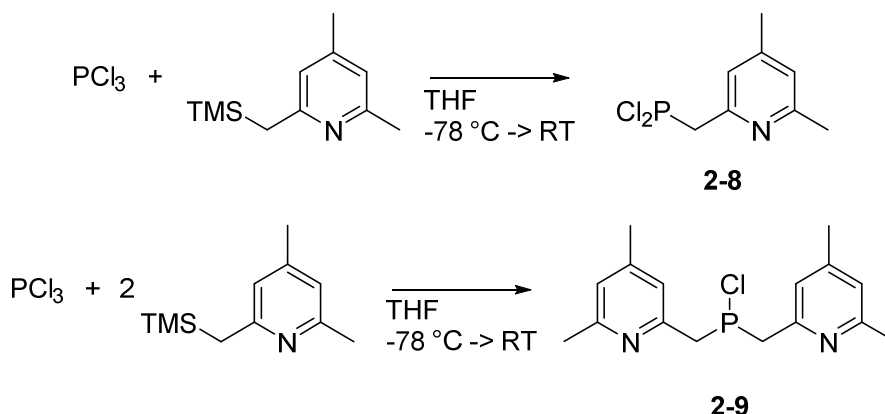
The synthesis of triisopropylphenyldichlorophosphine **2-7** was based on the procedure of M. I. Arz *et al.* starting from triisopropylphenylbromide.^[19] After reaction with magnesium in THF, the *Grignard* reagent was transmetalated to zinc. Then the zinc reagent was allowed to react with PCl₃.



Scheme 3: Synthesis of the dichlorophosphines **2-5–2-7**.

After the reactions were completed the salts, which were formed during the reaction, were removed by filtration. **2-5** and **2-6** were purified by distillation, while **2-7** did not need further purification. **2-6** and **2-7** were dried under vacuum. In the case of **2-7** a mixture of the dichlorophosphine with the corresponding bromochlorophosphine and dibromophosphine was obtained due to the presence of bromine in the reaction mixture.

Reactions of one or two equivalents of **2-3** with PCl_3 were supposed to yield dichlorophosphine **2-8** and chlorophosphine **2-9** respectively (Scheme 4). Therefore the silyl compound was added slowly to a solution of PCl_3 in THF at -78°C and the reaction mixture was allowed to warm up to room temperature overnight.



Scheme 4: Reactions of **2-3** with PCl_3 .

Both reactions resulted in an orange-brown solution with a yellow precipitate. The precipitate was separated by filtration and dissolved in DCM. The reaction solutions and the precipitated solids were analysed by ^{31}P NMR spectroscopy.

The ^{31}P NMR spectra of the reaction mixtures showed various signals between -50 ppm and 220 ppm (Figure 2).

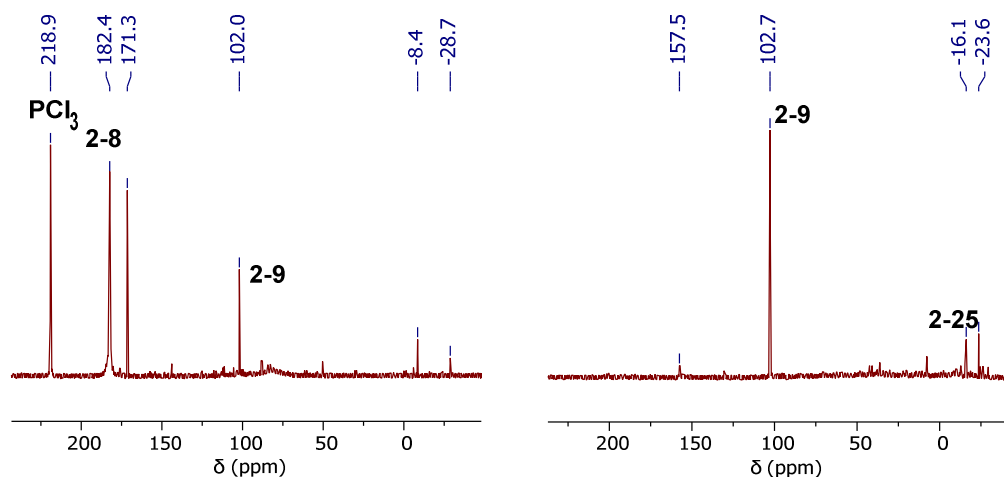


Figure 2: ^{31}P NMR spectra of the reaction mixtures of the reactions of **2-3** with PCl_3 in ratios of 1:1 (left) and 2:1 (right) in THF.

In the ^{31}P NMR spectrum of the reaction mixture of the reaction in a 1:1 ratio a signal at 218.9 ppm can be observed, which can be assigned to unreacted PCl_3 . The signal at 182.4 ppm probably is caused by the desired dichlorophosphine **2-8**. These two signals cannot be seen in the ^{31}P NMR spectrum of the reaction mixture of the reaction in the ratio of 2:1. Due to the larger amount of **2-3** all of the PCl_3 has reacted and also the intermediately formed dichlorophosphine **2-8** was consumed in the reaction to form chlorophosphine **2-9**. The spectra of both reactions show a signal at $102.0/102.7$ ppm, which indicates that **2-9** was formed. In the reaction with 2 equivalents of **2-3** also

a small amount of the corresponding tertiary phosphine **2-25** is formed, which causes a signal at -16.1 ppm in the ^{31}P NMR spectrum.

None of the products from the reaction mixtures could be isolated.

The ^{31}P NMR spectra of the precipitates of both reactions look quite different (Figure 3).

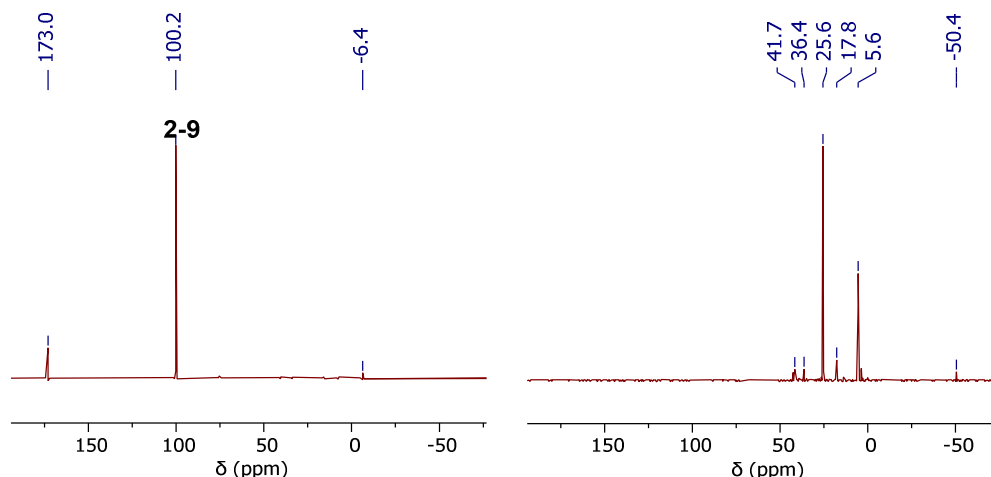


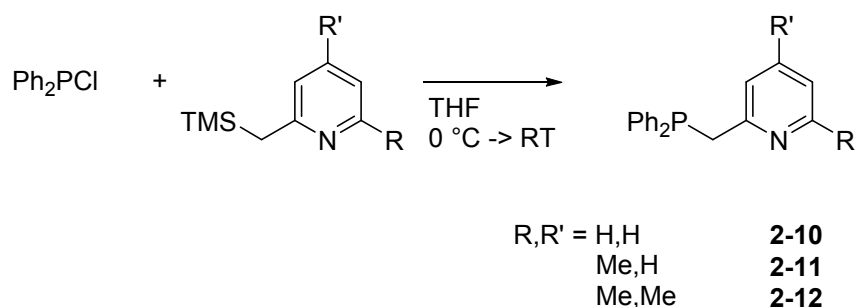
Figure 3: ^{31}P NMR spectra of the precipitates from the reactions of **2-3** with PCl_3 in ratios of 1:1 (left) and 2:1 (right) in DCM.

The ^{31}P NMR spectrum of the precipitate of the reaction in the ratio 1:1 shows a large signal at 100.2 ppm, which can be assigned to chlorophosphine **2-9**. This was confirmed by ^1H and ^{13}C NMR and mass spectroscopy. The other signals represent minor impurities, which could not be identified. The ^{31}P NMR spectrum of the precipitate of the reaction in the ratio 2:1 shows a signal at -50.4 ppm and various other signals between 0 ppm and 50 ppm. None of these signals could be assigned to the desired products of the reaction and therefore the mixture was not further investigated.

Compound **2-8** could not be isolated, instead the reaction in the ratio 1:1 yielded in approx. 35% of **2-9**. From the reaction in the ratio 2:1 no products could be isolated.

2.2.1.3 Picolylphosphine based compounds

To synthesise **2-10–2-12**, the corresponding silyl compounds were reacted with Ph_2PCl in THF in a 1:1 ratio, according to the synthetic route by *C. Hettstedt et al.* (Scheme 5).^[1c]

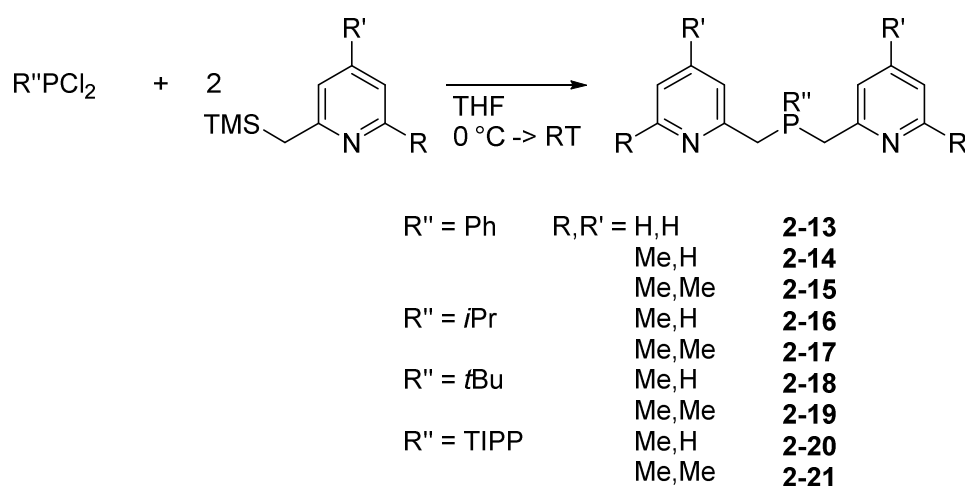


Scheme 5: Synthesis of picolylphosphine based compounds **2-10–2-12**.

After removing the solvent *in vacuo* compounds **2-11** and **2-12** were obtained as viscous colourless oils at room temperature, while compound **2-10** is a colourless solid. The yields were 79–86%. Compounds **2-10–2-12** are soluble in pentane, THF, DCM and chloroform. All three compounds are sensitive towards oxidation and are slowly hydrolysed.

2.2.1.4 Bis(picoly)phosphine based compounds

To synthesise **2-13–2-21**, the corresponding silyl compounds were reacted with PhPCl_2 , $i\text{PrPCl}_2$, $t\text{BuPCl}_2$ or TIPPPCl_2 in THF in a 2:1 ratio, according to the synthetic route by C. Hettstedt *et al.* (Scheme 6).^[1c]



Scheme 6: Synthesis of bis(picoly)phosphine based compounds **2-13–2-21**.

After removing the solvent *in vacuo*, the phosphines **2-13–2-17** were extracted with Et_2O or, in case of **2-15**, pentane. After removal of the solvent *in vacuo* compounds **2-13–2-17** were obtained in good yields of 72–91%. Compound **2-13** was a yellow solid, **2-14** a viscous yellow liquid, **2-15** a viscous amber coloured liquid and **2-16** and **2-17** were amber coloured liquids at room temperature. **2-13–2-17** are soluble in Et_2O , THF, DCM and chloroform. All compounds are sensitive towards oxidation and are slowly hydrolysed.

Compounds **2-20** and **2-21** could not be isolated pure.

The reactions to obtain **2-18** and **2-19** did not yield in the desired products. The ^{31}P NMR spectra of the reaction mixtures after warming up to room temperature showed that most of the dichlorophosphine (201.4/201.1 ppm) did not react (Figure 5). Only little conversion to the corresponding chlorophosphines **2-22** (127.4 ppm) and **2-23** (127.1 ppm) could be observed (Figure 4).

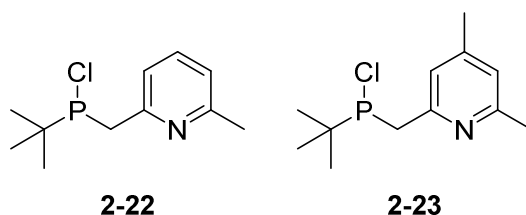


Figure 4: Chlorophosphines **2-22** and **2-23**, formed during the reactions to obtain **2-18** and **2-19**.

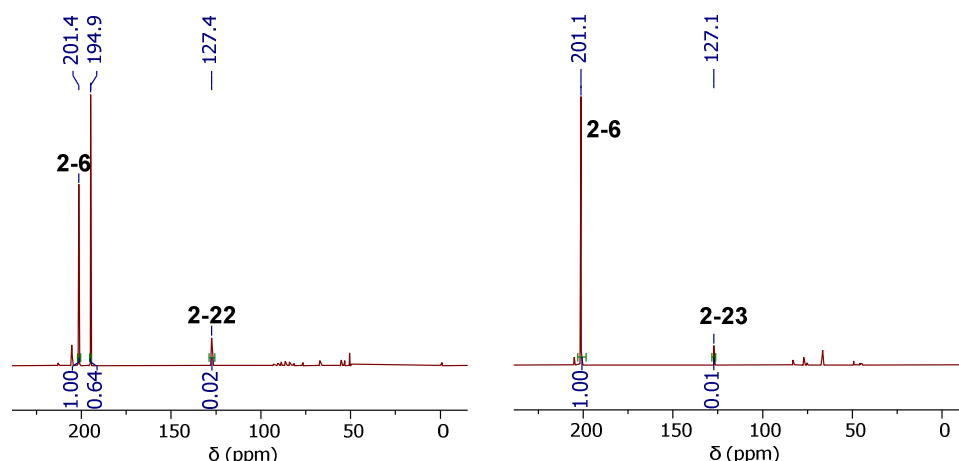


Figure 5: ^{31}P NMR spectra of the reaction mixtures to synthesise **2-18** (left) and **2-19** (right) in THF after warming up to room temperature.

The reaction mixtures were heated to reflux for 22 h to speed up the reaction. The ^{31}P NMR spectra of the reaction mixtures after refluxing showed that the reaction that occurs even at higher temperatures is the substitution of only one of the chlorine atoms bound to the phosphorus with a Lut or Col substituent (Figure 6). In the reaction mixtures there is still starting material present, but the conversion of **2-6** to **2-22** and **2-23** respectively could be increased to 64–74%.

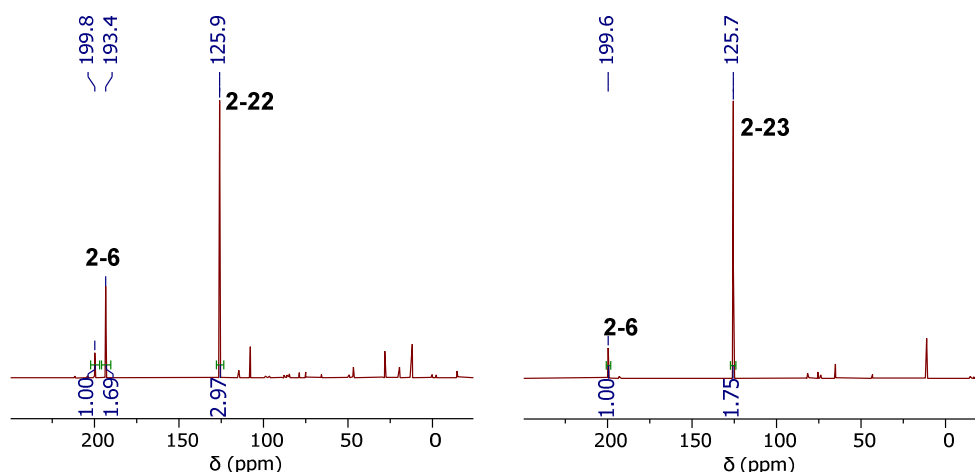
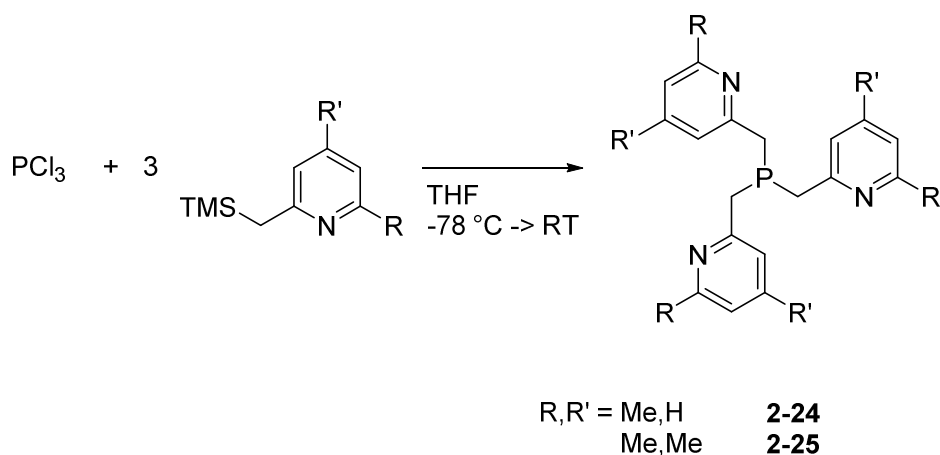


Figure 6: ^{31}P NMR spectra of the reaction mixtures to synthesise **2-18** (left) and **2-19** (right) in THF after refluxing.

Probably due to the steric hindrance of the *tert*butyl group the desired products **2-18** and **2-19** respectively were not formed in these reactions. Possibly the reactivity could be increased by using the lithiated 2-methyl pyridine derivatives in the reaction with **2-6**. This could also lead to the desired compounds **2-18** and **2-19**.

2.2.1.5 Tris(picolyl)phosphine based compounds

To synthesise **2-24** and **2-25**, the corresponding silyl compounds were allowed to react with PCl_3 in THF at -78°C in a 3:1 ratio, according to the synthetic route by C. Hettstedt *et al.* (Scheme 7).^[1c]

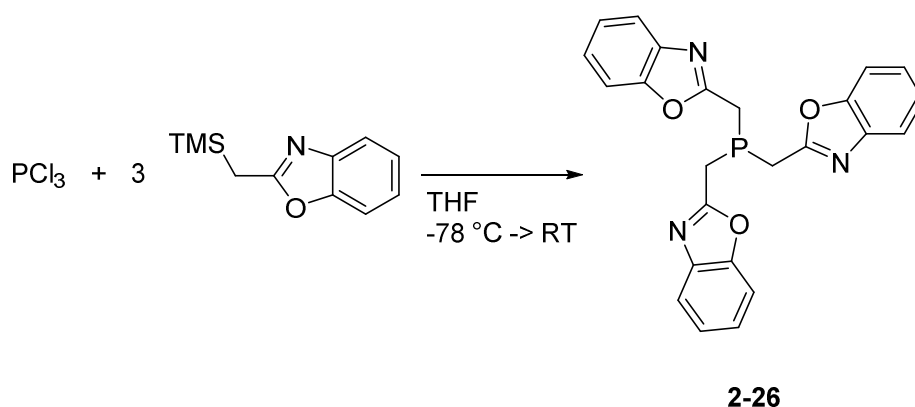


Scheme 7: Synthesis of tris(picolyl)phosphine based compounds **2-24** and **2-25**.

After removal of the solvent *in vacuo* phosphine **2-24** was extracted with pentane and **2-25** was extracted with Et₂O and pentane. The solvent was removed *in vacuo* and the products were obtained as very viscous yellow (**2-24**) or amber coloured (**2-25**) liquids in good yields of 68–84%. **2-24** and **2-25** are soluble in pentane, Et₂O, THF, DCM and chloroform. Both compounds are sensitive towards oxidation and are slowly hydrolysed.

2.2.1.6 Tris(benzoxazol-2-ylmethyl)phosphine

The synthesis of tris(benzoxazol-2-ylmethyl)phosphine **2-26** has been carried out according to the procedure of *C. Hettstedt*.^[1c] PCl₃ was dissolved in THF and reacted with an excess of **2-4** at –78°C (Scheme 8).



Scheme 8: Synthesis of Tris(benzoxazol-2-ylmethyl)phosphine **2-26**.

The reaction mixture was allowed to warm up to RT overnight and the solvent was removed *in vacuo*. The product was isolated in good yield (67%) as yellow solid. Phosphine **2-26** is soluble in THF and chloroform and very sensitive towards oxidation.

2.2.2 NMR data

2.2.2.1 2-((Trimethylsilyl)methyl)benzoxazole

The ^1H , ^{13}C and ^{31}P NMR chemical shifts of 2-((trimethylsilyl)methyl)benzoxazole **2-4** are listed in Table 1.

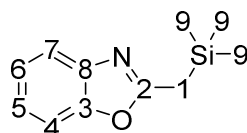


Figure 7: Numbering of carbon atoms in compound **2-4** for ^1H and ^{13}C NMR spectroscopic data assignments.

Table 1: ^1H , ^{13}C and ^{31}P NMR data of phosphines **2-5–2-7** in CDCl_3 .
Chemical shifts δ are in ppm, coupling constants J in Hz.

δ_{Si}	4.0	δ_{C}	
		C1	20.0
δ_{H}		C2	167.2
H1	2.42	C3	151.0
H4	7.60	C4	119.0
H5/6	7.23	C5/6	123.7/123.9
H7	7.42	C7	109.9
H9	0.14	C8	142.2
		C9	-1.3

The assignment of the signals is based on 2D NMR spectra and comparison with literature values of benzofuran, 1*H*-indole and methylbenzoxazole.^[20]

The chemical shift of the ^{29}Si NMR signal of **2-4** is 4.0 ppm, which is in the typical range of aliphatic trimethylsilyl groups (+10 to -20 ppm).^[21]

The ^1H NMR signal at 0.14 ppm is caused by the protons of the trimethylsilyl group (H9) and the signal at 2.42 ppm can be assigned to the methylene group (H1). Both signals appear as singlets, because the 4J coupling is not resolved. Comparisons with the NMR data with benzofuran and 1*H*-indole allow assigning the multiplets at 7.60 ppm (H4) and 7.42 ppm (H7). The chemical shifts of the signals caused by H5 and H6 are almost identical, which leads to an overlap of the signals.

The $^1\text{H}^{13}\text{C}$ HMQC spectrum allows assigning of the ^{13}C NMR signals at 119.0 ppm (C4) and 109.9 ppm (C7). The ^1H NMR signal at 7.23 ppm correlates with the ^{13}C NMR signals at 123.7 ppm and 123.9 ppm, but further assignment is not possible.

The ^{13}C NMR chemical shifts are almost identical to those of methylbenzoxazole, except C1 and C2.^[20b] Both signals are shifted 3.7 ppm and 6.3 ppm, respectively, towards lower field by substitution of one proton by the trimethylsilyl group. Also in the literature the signals of C5 and C6 cannot be differed from each other, because of their very similar chemical shifts.^[20b]

2.2.2.2 Picolylphosphine based compounds

The ^1H , ^{13}C and ^{31}P NMR chemical shifts of the picolylphosphine based compounds **2-10–2-12** are listed in Table 2.

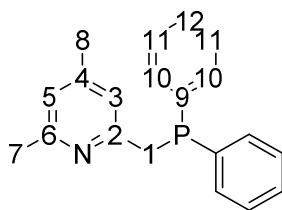


Figure 8: Numbering of carbon atoms in compounds **2-10–2-12** for ^1H and ^{13}C NMR spectroscopic data assignments.

Table 2: ^1H , ^{13}C and ^{31}P NMR data of phosphines **2-10–2-12** in CDCl_3 . Chemical shifts δ are in ppm, coupling constants J in Hz.

	2-10	2-11	2-12		2-10	2-11	2-12
δ_{P}	−9.4	−10.2	−9.7	δ_{C}			
$^3J_{\text{PH10}}$	7.5	7.4	7.4	C1	39.0	38.8	38.7
				C2	158.3	157.3	157.0
δ_{H}				C3	123.8	120.6	121.7
H1	3.64	3.61	3.56	C4	136.2	136.3	147.3
H3	6.98	6.74	6.58	C5	121.1	120.6	121.6
H4	7.45	7.32	–	C6	149.5	158.0	157.7
H5	7.04	6.89	6.73	C7	–	24.6	24.4
H6	8.50	–	–	C8	–	–	20.8
H7	–	2.49	2.45	C9	138.3	138.4	138.5
H8	–	–	2.15	C10	133.0	133.1	133.1
H10	7.45	7.45	7.45	C11	128.5	128.4	128.4
H11	7.32	7.32	7.31	C12	128.8	128.7	128.7
H12	7.32	7.32	7.31	$^1J_{\text{PC1}}$	16.2	16.5	16.2
$^3J_{\text{H3H4}}$	7.8	7.7	–	$^2J_{\text{PC2}}$	8.1	7.8	8.0
$^4J_{\text{H3H5}}$	2.2	–	–	$^3J_{\text{PC3}}$	6.2	4.2	3.0
$^5J_{\text{H3H6}}$	1.0	–	–	$^4J_{\text{PC4}}$	1.1	1.2	–
$^3J_{\text{H4H5}}$	7.5	7.6	–	$^5J_{\text{PC5}}$	2.3	–	1.6
$^4J_{\text{H4H6}}$	1.9	–	–	$^4J_{\text{PC6}}$	1.1	1.2	1.1
$^3J_{\text{H5H6}}$	4.9	–	–	$^1J_{\text{PC9}}$	15.0	15.0	14.8
$^6J_{\text{PH5}}$	1.1	–	–	$^2J_{\text{PC10}}$	18.9	18.8	18.8
				$^3J_{\text{PC11}}$	6.5	6.6	6.7

In the ^{31}P NMR spectra the chemical shifts of the signals of compounds **2-10–2-12** are in the range of −9.4 ppm to −10.2 ppm, which is typical for tertiary phosphines.^[22] In the ^1H coupled ^{31}P NMR spectra the coupling of the *ortho* phenyl protons with the phosphorus causes quintets with coupling constants of 7.4 Hz to 7.5 Hz. The coupling with the methylene protons H1 is very small and cannot be resolved.

In the ^1H NMR spectra of compounds **2-10–2-12** the signals of the phenyl protons H10–H12 appear as two multiplets with chemical shifts of 7.31–7.32 ppm and 7.45 ppm. The signals of the pyridine protons are shifted towards higher field by the introduction of additional methyl groups at the pyridine ring.

The ^1H NMR signal of H5 of compound **2-10** resolves a long range coupling with the phosphorus atom over six bonds.

In the ^{13}C NMR spectra the chemical shifts of the signals of the phenyl carbon atoms C9–C12 are almost identical for compounds **2-10–2-12**. The signals of C1 and C2 are slightly shifted towards higher field from **2-10** to **2-12**. Introduction of the methyl groups at C4 and C6 respectively leads to a

shift of approx. 10 ppm of the corresponding signals towards lower field. The signals of the other carbon atoms vary by a maximum of 3.2 ppm from **2-10** to **2-12**.

Remarkably the $^2J_{PC}$ coupling constants to C10 (18.8–18.9 Hz) are slightly larger than the $^1J_{PC}$ coupling constants (14.8–16.5 Hz) with C9.

2.2.2.3 Bis(picolyl)phosphine based compounds

The 1H , ^{13}C and ^{31}P NMR chemical shifts of the bis(picolyl)phosphine based compounds **2-13–2-17** are listed in Table 3.

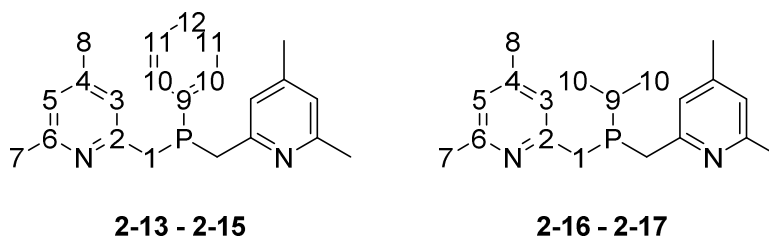


Figure 9: Numbering of carbon atoms in compounds **2-13–2-17** for 1H and ^{13}C NMR spectroscopic data assignments.

Table 3: 1H , ^{13}C and ^{31}P NMR data of phosphines **2-13–2-17** in $CDCl_3$. Chemical shifts δ are in ppm, coupling constants J in Hz.

	2-13	2-14	2-15	2-16	2-17		2-13	2-14	2-15	2-16	2-17
δ_P	-13.1	-13.1	-13.1	0.7	1.4	δ_C					
$^3J_{PH10}$	7.4	7.3	7.5	13.3	13.3	C1	37.8	37.6	37.5	34.4	34.4
						C2	158.2	157.4	157.1	158.6	158.3
δ_H						C3	123.8	120.6	121.6	120.6	121.6
H1a	3.40	3.34	3.28	3.03	2.97	C4	136.2	136.2	147.2	136.3	147.3
H1b	3.32	3.24	3.21	2.99	2.97	C5	121.0	120.3	121.4	120.1	121.3
H3	7.00	6.79	6.58	7.00	6.79	C6	149.2	157.7	157.3	157.7	157.3
H4	7.44	7.29	–	7.37	–	C7	–	24.5	24.2	24.6	24.3
H5	7.00	6.83	6.66	6.86	6.68	C8	–	–	20.7	–	20.9
H6	8.44	–	–	–	–	C9	136.8	137.1	137.4	25.0	25.3
H7	–	2.43	2.38	2.45	2.41	C10	132.8	132.8	132.8	19.2	19.2
H8	–	–	2.10	–	2.17	C11	128.4	128.1	128.0	–	–
H9	–	–	–	1.67	1.68	C12	129.2	129.0	128.9	–	–
H10	7.44	7.42	7.43	1.05	1.06	$^1J_{PC1}$	18.8	18.7	18.3	21.1	20.6
H11	7.28	7.29	7.25	–	–	$^2J_{PC2}$	5.8	5.8	5.9	5.7	6.2
H12	7.28	7.26	7.25	–	–	$^3J_{PC3}$	5.4	5.7	6.0	6.0	6.4
$^2J_{H1aH1b}$	13.4	13.3	13.3	13.6	–	$^4J_{PC4}$	–	1.0	–	–	0.8
$^3J_{H3H4}$	–	7.7	–	7.7	–	$^5J_{PC5}$	2.1	2.1	2.1	1.8	1.7
$^4J_{H3H5}$	–	0.5	–	–	–	$^4J_{PC6}$	–	1.0	0.8	–	0.6
$^5J_{H3H6}$	1.0	–	–	–	–	$^1J_{PC9}$	18.2	18.4	18.2	13.8	13.6
$^3J_{H4H5}$	–	7.6	–	7.6	–	$^2J_{PC10}$	20.0	19.8	19.7	13.5	13.1
$^4J_{H4H6}$	1.9	–	–	–	–	$^3J_{PC11}$	7.0	7.0	6.9	–	–
$^3J_{H5H6}$	4.9	–	–	–	–	$^4J_{PC12}$	–	0.7	–	–	–
$^3J_{H9H10}$	–	–	–	7.1	7.0						
$^2J_{PH9}$	–	–	–	2.0	1.7						
$^2J_{PH1a}$	1.7	1.7	1.2	–	–						

In the ^{31}P NMR spectra the chemical shifts of the signals of compounds **2-13–2-15** are -13.1 ppm, while the ^{31}P NMR signals of **2-16** and **2-17** appear at chemical shifts of 0.7 ppm and 1.4 ppm respectively. In the ^1H coupled ^{31}P NMR spectra the coupling of the *ortho* phenyl protons of **2-13–2-15** with the phosphorus causes triplets with coupling constants of 7.3 Hz to 7.5 Hz. The $^3J_{\text{PH10}}$ coupling constants of compounds **2-16** and **2-17** are 13.3 Hz. The coupling with the methylene protons H1 in compounds **2-13–2-17** cannot be resolved.

In the ^1H NMR spectra of compounds **2-13–2-15** the signals of the phenyl protons H10–H12 appear as two multiplets with chemical shifts of 7.25 – 7.29 ppm and 7.42 – 7.44 ppm.

The signals of the protons of the *isopropyl* groups of **2-16** and **2-17** appear at 1.05 – 1.06 ppm (H10) and 1.67 – 1.68 ppm (H9) respectively.

As for the picolylphosphine based compounds **2-10–2-12** for the bis(picolyl)phosphine based compounds **2-13–2-15** and **2-16–2-17** respectively, the signals of the protons of the organic moieties are shifted towards higher field by the introduction of additional methyl groups at the pyridine ring.

In the case of phosphines **2-13–2-15** the protons at the methylene group H1 are diastereotopic and therefore cause two signals with $^2J_{\text{HH}}$ of 13.3 – 13.4 Hz. The signals of H1a resolve a small $^2J_{\text{PH}}$ coupling constant of 1.2 – 1.7 Hz, while no $^2J_{\text{PH}}$ coupling can be observed for H1b. In the ^1H NMR spectra of **2-16** and **2-17** the signals of H1a and H1b move closer towards each other. The signals of H1a and H1b of **2-16** resolve a $^2J_{\text{HH}}$ coupling constant of 13.6 Hz, but no $^2J_{\text{PH}}$ coupling. In the ^1H NMR spectrum of **2-17** the signal of H1 is a singlet (Figure 10).

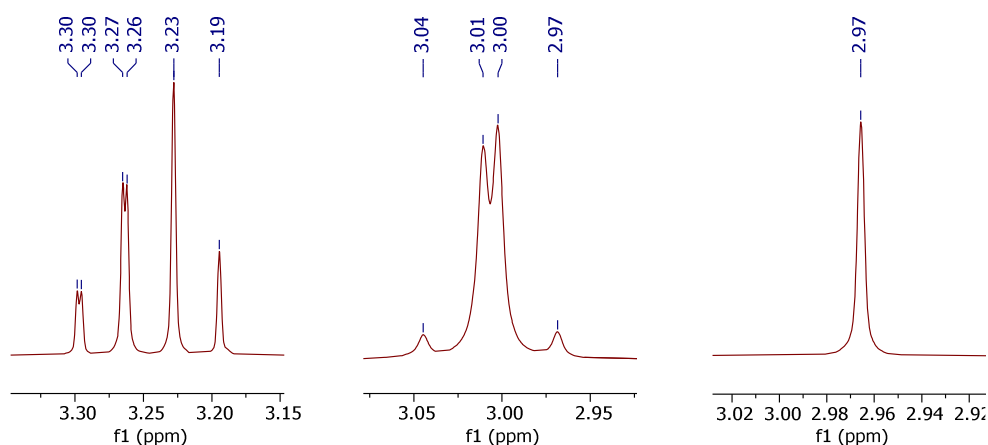


Figure 10: ^1H NMR signals of H1 of **2-15** (left), **2-16** (middle) and **2-17** (right).

In the ^{13}C NMR spectra the chemical shifts of the signals of the phenyl carbon atoms C9–C12 are almost identical for compounds **2-13–2-15** and similar to those of **2-10–2-12**. Upon introduction of additional methyl groups at the pyridine rings the same trends as in the NMR data of the **2-10–2-12** can be observed for the **2-13–2-15** and **2-16–2-17** respectively. Especially the chemical shifts of the ^{13}C NMR signals of C3–C8 are almost identical for **2-14** and **2-16** and **2-15** and **2-17** respectively. Replacement of the phenyl group with an *isopropyl* group leads to a slight low field shift of the signals of C1 and a slight high field shift of the signals of C2. The chemical shifts of the other ^{13}C NMR signals are not affected.

As for **2-10–2-12** the $^2J_{\text{PC}}$ coupling constants with C10 are larger than the $^1J_{\text{PC}}$ coupling constants with C9 for compounds **2-13–2-15**. These coupling constants of **2-13–2-15** are slightly larger than of **2-10–2-12**. The $^1J_{\text{PC1}}$ coupling constants are also increased, whilst the $^2J_{\text{PC2}}$ coupling constants are slightly decreased from **2-10–2-12** to **2-13–2-15**. The $^1J_{\text{PC1}}$ coupling constants are increased by 2.3 – 2.4 Hz upon replacement of the phenyl group with an *isopropyl* group.

2.2.2.4 Tris(picolyl)phosphine based compounds

The ^1H , ^{13}C and ^{31}P NMR chemical shifts of the tris(picolyl)phosphine based compounds **2-24–2-25** are listed in Table 4.

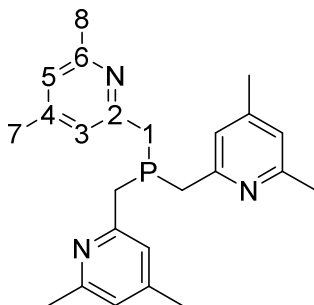


Figure 11: Numbering of carbon atoms in compounds **2-24** and **2-25** for ^1H and ^{13}C NMR spectroscopic data assignments.

Table 4: ^1H , ^{13}C and ^{31}P NMR data of phosphines **2-24** and **2-25** in CDCl_3 .
Chemical shifts δ are in ppm, coupling constants J in Hz.

	2-24	2-25		2-24	2-25
δ_{P}	-12.2	-12.2	δ_{C}		
			C1	35.8	36.3
δ_{H}			C2	157.8	157.8
H1	3.00	3.00	C3	120.7	121.8
H3	6.83	6.71	C4	136.2	147.3
H4	7.35	–	C5	120.2	121.4
H5	7.01	6.84	C6	157.6	157.5
H7	2.43	2.43	C7	24.5	24.4
H8	–	2.19	C8	–	20.9
$^3J_{\text{H3H4}}$	7.7	–	$^1J_{\text{PC1}}$	21.2	20.5
$^3J_{\text{H4H5}}$	7.7	–	$^2J_{\text{PC2}}$	4.9	5.2
$^2J_{\text{PH1}}$	1.6	0.8	$^3J_{\text{PC3}}$	5.0	5.5
			$^4J_{\text{PC4}}$	0.7	–
			$^5J_{\text{PC5}}$	1.9	1.8
			$^4J_{\text{PC6}}$	0.8	0.7

In the ^{31}P NMR spectra the signals of compounds **2-24** and **2-25** are at a chemical shift of –12.2 ppm. The coupling with the methylene protons H1 cannot be resolved in the ^1H coupled ^{31}P NMR spectra. In the ^1H and ^{13}C NMR spectra of compounds **2-24** and **2-25** the same trends as for the pairs **2-11/12** and **2-14/15** can be observed.

In the rows **2-11/14/24** and **2-12/15/25** the ^1H NMR signals of H1 are shifted towards higher field, while the signals of H3 and H5 are shifted towards lower field.

The ^{13}C NMR signals of C5 are shifted towards higher field in the same rows.

Upon introduction of more Lut/Col substituents at the phosphorus $^1J_{\text{PC1}}$ is increased, while $^2J_{\text{PC2}}$ decreases.

2.2.2.5 Tris(benzoxazol-2-ylmethyl)phosphine

The ^1H , ^{13}C and ^{31}P NMR chemical shifts of **2-26** are listed in Table 5.

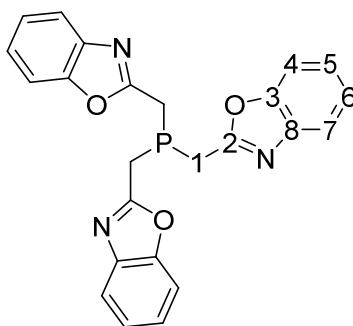


Figure 12: Numbering of carbon atoms in compound **2-26** for ^1H and ^{13}C NMR spectroscopic data assignments.

Table 5: ^1H , ^{13}C and ^{31}P NMR data of phosphine **2-26** in CDCl_3 .
Chemical shifts δ are in ppm, coupling constants J in Hz.

δ_{P}	-24.9	δ_{C}	
$^2J_{\text{PH1}}$	3.9	C1	25.7
		C2	162.7
δ_{H}		C3	150.9
H1	3.50	C4	119.7
H4	7.60	C5/6	124.3/124.8
H5/6	7.29	C7	110.4
H7	7.40	C8	141.4
		$^1J_{\text{PC1}}$	22.2
		$^2J_{\text{PC2}}$	5.5
		$^4J_{\text{PC3}}$	0.8

The ^{31}P NMR signal of **2-26** appears at -24.9 ppm, which is in the typical range of tertiary phosphines.^[22] In the ^1H coupled ^{31}P NMR spectrum a splitting of the signal into a septet with a coupling constant of 3.9 Hz due to coupling with the methylene protons can be observed.

Correspondingly the signal of H1 in the ^1H NMR spectrum appears at a chemical shift of 3.50 ppm as a doublet with a coupling constant of 3.9 Hz. Compared to the corresponding ^1H NMR signal of **2-4** the signal of H1 is shifted approx. 1 ppm towards lower field, due to the higher electronegativity of the phosphorus compared to silicon.

As for **2-4** the ^1H and ^{13}C NMR signals have been assigned according to the 2D NMR spectra and comparisons with literature values of similar compounds.

The ^1H and ^{13}C NMR chemical shifts of the aromatic atoms 3–8 are almost identical to those of **2-4**.

The ^{13}C NMR signal of C1 is shifted towards lower field, while the signal of C2 is shifted towards higher field compared to **2-4**.

2.2.3 Photophysical data of 2-26

Compound **2-26** shows blue emission in the solid state (Figure 13). In Figure 14 the fluorescence emission spectrum of **2-26** is shown. The emission maximum is at 496 nm.

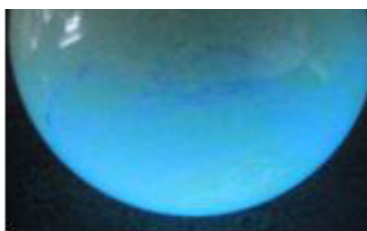


Figure 13: Luminescence of **2-26** under UV light.

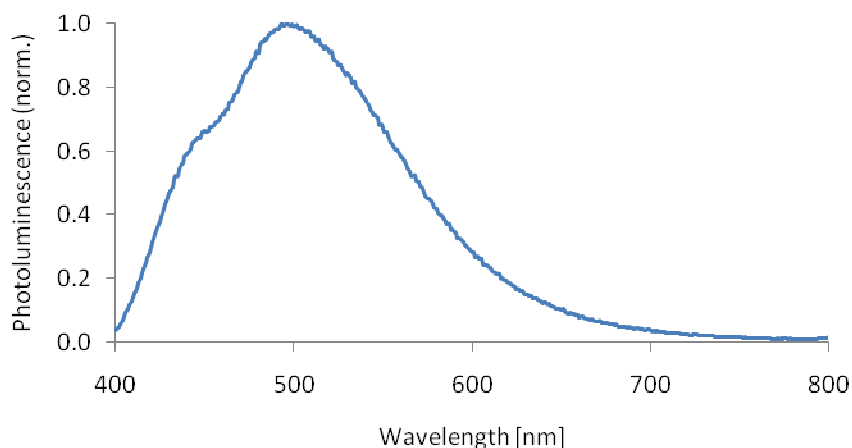


Figure 14: Fluorescence emission spectrum of phosphine **2-26** in the solid state.

Time-correlated Single Photon Counting (TCSPC) is a method which is used to determine the relaxation times of luminescent compounds. From the relaxation times it is possible to draw conclusions on the processes involved in the relaxation of a compound.

In the TCSPC measurement the time until a single photon is emitted after excitation of a sample is determined. After fitting the data from a multitude of measuring points with an exponential function the relaxation times are obtained from the fit parameters.

In the solid state interactions between the molecules, such as diffusion effects or radiationless deactivation *via* vibrations, occur in competition to the luminescence. Therefore it is necessary to use a biexponential function to fit the data, which leads to two relaxation times τ_1 and τ_2 . The observed relaxation mechanism is described by τ_1 , while τ_2 describes the competing processes.

From TCSPC measurements the relaxation times of **2-26** of $\tau_1 = 1.115 \pm 0.015$ ns and $\tau_2 = 3.54 \pm 0.04$ ns in the solid state could be determined (Figure 15). These relaxation times are in the time range, which is typical for fluorescence (0.01–10 ns)^[23] and indicate that **2-26** probably is a singlet emitter, which is typical for purely organic emitters.

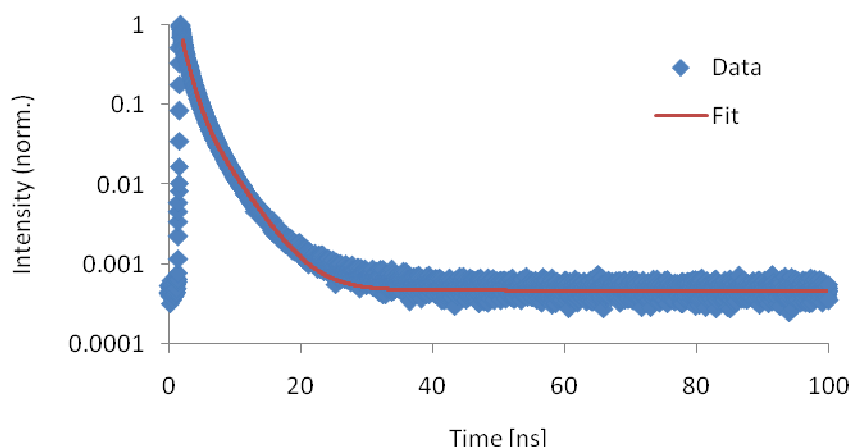


Figure 15: Results of the TCSPC measurements of **2-26**.

2.2.4 Crystal structure of tris(benzoxazol-2-ylmethyl)phosphine oxide **2-27**

By slow diffusion of MeCN in a solution of **2-26** in THF colourless crystals suitable for X-ray diffraction analysis were obtained.

The structure showed, that the phosphine had been oxidised during the crystallization, probably because of oxygen, that entered the flask during crystallization. The phosphine oxide **2-27** is soluble in THF and chloroform.

2-27 crystallises in the triclinic space group *P*-1 with two formula units in the unit cell. The asymmetric unit comprises one molecule of the phosphine oxide and one molecule of MeCN. The asymmetric unit of **2-27** is shown in Figure 16.

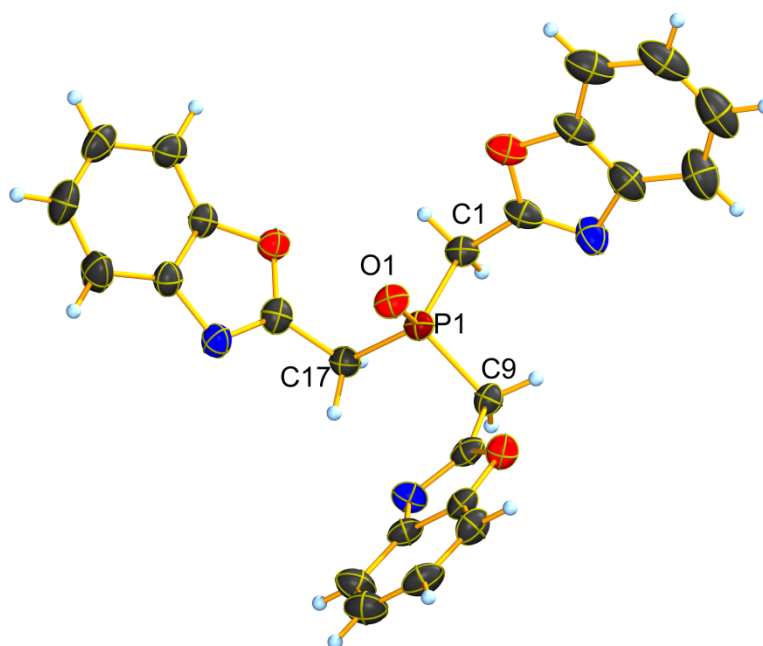


Figure 16: Molecular structure of **2-27**. Thermal ellipsoids are drawn at 50% probability level. The solvent molecule has been omitted for clarity. Selected bond lengths [Å] and angles [°]: P1–C1: 1.806(2), P1–C9: 1.810(3), P1–C17: 1.815(2), P1–O1: 1.480(2), C1–P1–C9: 106.1(1), C1–P1–C17: 105.2(1), C1–P1–O1: 113.6(1), C9–P1–C17: 106.2(1), C9–P1–O1: 112.4(1), C17–P1–O1: 112.8(1).

The P–O bond length of 1.480(2) Å is comparable to the P–O bond length of 1.488(4) Å in tribenzylphosphine oxide described in the literature.^[24] The P–C bond lengths are between 1.806(2) Å and 1.815(2) Å, which is slightly shorter than the literature value of the P–C bonds of tribenzylphosphine oxide (1.823(3) Å).^[24]

The C–P–O angles of compound **2-27** are between 112.4(1) ° and 113.6(1) °, which is slightly larger than the ideal tetrahedral angle of 109.5 °. The C–P–C angles are between 105.2(1) ° and 106.2(1) ° and slightly smaller than the tetrahedral angle.

The phosphine oxide molecules are parallel stacked along the *a* axis (Figure 17). The distance between the molecules is 4.890(1) Å, meaning that there are probably no attractive π - π interactions, despite the parallel arrangement.

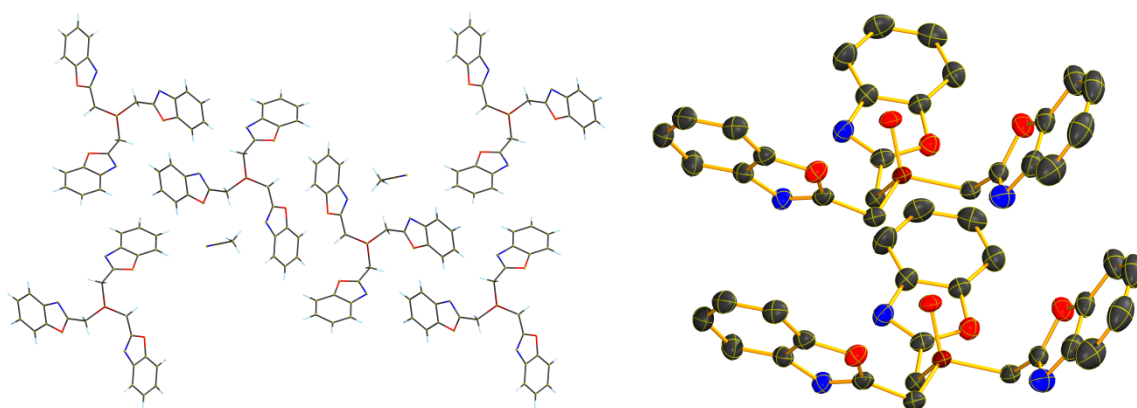


Figure 17: Crystal structure of **2-27**. View along the *a* axis (left) and stacking of the molecules along the *a* axis (right, thermal ellipsoids are drawn at 50% probability level, H atoms and solvent molecules have been omitted for clarity).

2.3 Summary

The phosphines **2-8–2-26** have been synthesised by reaction of one of the silyl compounds **2-1–2-4** with a P–Cl compound according to the procedure of *C. Hettstedt*.^[1c] **2-10–2-17** and **2-24–2-26** could be completely characterised by NMR spectroscopy. The eleven new phosphines can be used as multidentate P,N ligands and **2-26** contains even seven atoms which are able to coordinate to metals: one phosphorus atom, three nitrogen atoms and three oxygen atoms.

Remarkably **2-26** shows blue fluorescence under UV light. The fact that the compound does not contain any metals indicates that it is most likely a pure singlet emitter, which is confirmed by the short relaxation times measured in the TCSPC.

The phosphines could not be crystallised and therefore no crystal structures could be obtained. But during the experiments to crystallise **2-26**, crystals of the corresponding phosphine oxide **2-27** were isolated and the structure could be determined (Figure 18).

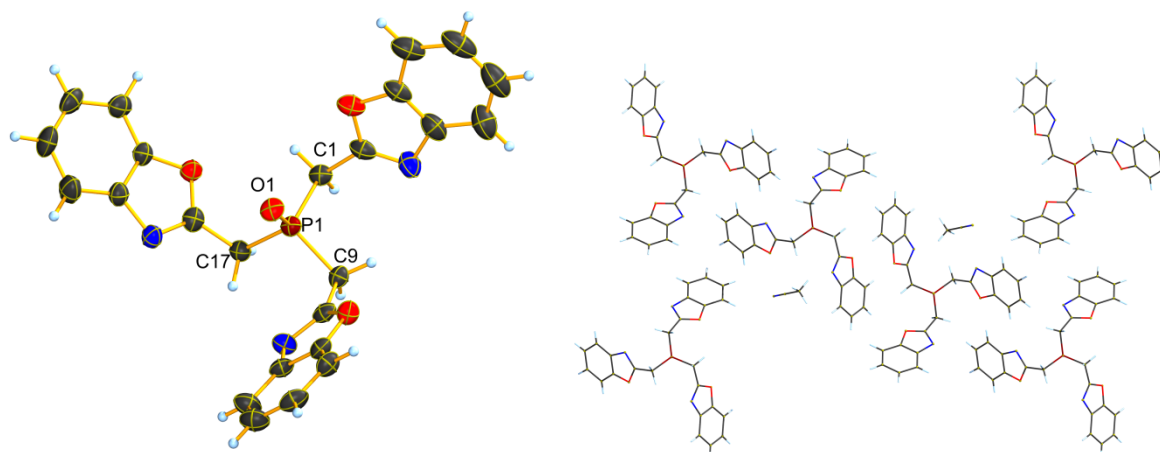


Figure 18: Molecular structure (left) and crystal structure (right) of **2-27**.

Reaction of PCl_3 with one equivalent of **2-3** yielded approx. 35% of **2-9** instead of **2-8** as expected. The reaction of PCl_3 with two equivalents of **2-3** was expected to yield **2-9**, but no product could be isolated from this reaction. It was not possible to isolate **2-8** from one of these reactions.

The reactions to obtain the bis(picolyl)phosphine related compounds **2-20** and **2-21** led to the desired products, but the compounds could not be obtained pure.

In contrast to the reactions to synthesise the bis(picolyl)phosphine based compounds **2-13–2-17**, **2-20** and **2-21** the reactions towards **2-18** and **2-19** did not yield the expected products. These reactions stopped after substitution of one of the chlorine atoms bound to the phosphorus with a Lut/Col group at the chlorophosphines **2-22** and **2-23** respectively. Also these two reactions were much slower than the other reactions and needed heating to reflux to get significant amounts of product. This is probably due to the steric demand of the *tert*butyl group at the phosphorus. Likely the reaction could be sped up by using the more reactive lithiated methyl pyridine derivatives instead of the silyl compounds. It might also be possible to get to the tertiary phosphines with this reaction.

2.4 Experimental

2.4.1 General

2.4.1.1 Schlenk technique

All reactions, unless mentioned otherwise, were performed under inert gas using Schlenk line techniques. As inert gas argon from Messer Griesheim with a purity of 5.0 in 50 L steel bottles was used. Glass equipment was stored in an oven with a temperature of 110°C before use. The glass equipment was greased with high vacuum quality grease (Glisseal®) from Borer or Korasilon-Paste (medium) from Kurt Obermeier GmbH & Co. KG. Before starting a reaction the setup was heated under vacuum (10^{-3} mbar) and purged with argon three times.

2.4.1.2 Preparation of NMR samples under Schlenk conditions

For preparation of NMR samples of air or moisture sensitive substances a special sample holder was used. This consists of an approx. 7 cm long glass tube with a Schlenk tap in the upper third. The upper end can be sealed with a stopper and the lower end can be sealed with a QuickFit®, in which a perforated silicone septum is inserted. A NMR tube can be pushed through the hole in the septum from above until the setup can be sealed and through the tap the apparatus can be evacuated, heated and purged with inert gas. The sample is filled in under inert gas counter flow with a 1 mL syringe. Afterwards the NMR tube is pushed up until the lid can be put on under inert gas counter flow.

2.4.1.3 Solvents

THF, pentane, Et₂O and toluene were dried over sodium/benzophenone and sodium respectively. DCM was dried over calcium hydride and MeCN was dried over phosphorus pentoxide. All solvents were distilled prior to use.

2.4.1.4 Chemicals

All starting materials were purchased from Merk, Fluka/Aldrich/Riedl-De-Hähn, Acros Organics, ABCR and TCI and used as received or were present in the research group *Klapötke/Karaghiosoff*. *n*BuLi and the “Turbo-Grignard” reagent were donated by Albemarle (Rockwood Lithium GmbH).

2.4.1.5 NMR spectroscopy

NMR spectra were recorded with a JEOL 400 Eclipse instrument, a Bruker AV400 instrument or a Bruker AV400TR instrument. Chemical shifts were referenced to Me₄Si (¹H, ¹³C, ²⁹Si) and 85 % H₃PO₄ (³¹P) as external standards. All spectra were measured at 25°C, if not mentioned otherwise. The assignment of the signals in the ¹H and ¹³C NMR spectra is based on 2D (¹H, ¹H COSY45, ¹H, ¹³C HMQC and ¹H, ¹³C HMBC) experiments. For the 2D NMR spectra sinebell window function and zero filling in both directions was applied resulting in a 4k × 4k matrix.

2.4.1.6 Mass spectrometry

Mass spectrometric data were obtained with a JEOL MStation JMS 700 spectrometer using the FAB mode or a MAT 95 or a MAT 90 spectrometer using the direct ESI mode.

2.4.1.7 Elemental analysis

Elemental analysis was performed either on an Elementar Vario El analyser or an Elementar Vario micro cube for C, H and N.

2.4.1.8 Single crystal X-ray diffraction

For data collection an Xcalibur3 diffractometer equipped with a Spellman generator (voltage 50 kV, current 40 mA) and a Kappa CCD detector with an X-ray radiation wavelength of 0.71073 Å was used or a D8 Venture system equipped with a Bruker D8 Venture TXS rotating-anode X-ray tube (Mo K α , λ = 0.71073 Å) and a multilayer mirror optics monochromator. Air sensitive crystals were taken out of the vessel under inert gas and immediately put in a drop of perfluorinated oil (KEL-F®) on an object holder.

2.4.1.9 Data collection from the diffractometer and solving of the crystal structures

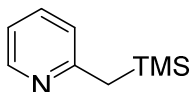
Data collection from the Xcalibur3 diffractometer was performed with the CrysAlis CCD software^[25] and the data reduction with the CrysAlis RED software.^[26] For the Bruker D8 software provided by Bruker was used for data collection,^[27] data reduction^[28] and cell refinement.^[29] The structures were solved with SHELXS-97,^[30] refined with SHELXL-2014^[31] and finally checked using PLATON.^[32] The absorptions were corrected using the SCALE3 ABSPACK multiscan method.^[33] Finally cif-files were checked with the online available checkCIF service of the International Union of Crystallography.^[34] Representations of molecular and crystal structures were generated with DIAMOND.

2.4.1.10 PL spectroscopy and TCSPC measurements

PL spectra and TCSPC measurements were recorded by *Dr. Andreas Jakowetz* from the research group of *Prof. Bein* on a FluoTime 300 spectrometer of PicoQuant. The sample was excited with a 378 nm laser (LDH-P-C-375, PicoQuant). The light was p-polarised, pulse length was approx. 100 ps and the pulse intensity was 2 μJcm^{-2} . The emitted light was collected with a 2'' lens and scattered light was filtered with a 400 nm interference filter (FELH0400, Thorlabs) and polarised under the magic angle (54.7 °). Subsequently the light was spectrally separated with a monochromator (Omni- λ 300, Zolix) and detected with a sensitive photomultiplier (PMA 192, PicoQuant). TCSPC histograms were recorded with a TimeHarp 260 P (PicoQuant). Data were fitted with the PicoQuant FluoFit 4.6.6.0 software using the biexponential function $I(t) = \sum_{i=1}^n A_i e^{-\frac{t-t_f}{\tau_i}}$.

2.4.2 Syntheses

2.4.2.1 2-((Trimethylsilyl)methyl)pyridine 2-1



2-Methylpyridine (10.0 mL, 100 mmol, 1 eq) was dissolved in 100 mL dry THF and cooled to -78°C. *n*BuLi (78.2 mL, 1.45 M in hexane, 100 mmol, 1 eq) was added dropwise and the deep red solution was stirred for 1 h at -78°C. TMSCl (15 mL, 118 mmol, 1.2 eq) was added dropwise and the solution returned to colourless, while it was allowed to warm up to RT overnight. The solvent was removed *in vacuo* and the crude product was extracted with 100 mL of pentane. The white precipitate was filtered off and the solvent was removed *in vacuo*.

After vacuum distillation (10^{-3} mbar, 31°C, oil bath 43°C) the product was obtained as colourless liquid (12.3 g, 74.4 mmol, 74%).

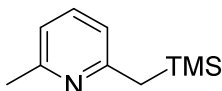
^1H NMR (400 MHz, CDCl_3) δ = 8.39 (ddd, J = 4.9, 1.9, 1.0 Hz, 1H), 7.44 (td, J = 7.6, 1.9 Hz, 1H), 6.91 (m, 2H), 2.31 (s, 2H), -0.02 (s, 9H).

^{13}C NMR (101 MHz, CDCl_3) δ = 161.4, 149.1, 135.8, 122.2, 119.2, 30.4, -1.6.

^{29}Si NMR (79 MHz, CDCl_3) δ = 2.3.

The NMR chemical shifts correspond with the literature values.^[1c, 35]

2.4.2.2 2-Methyl-6-((trimethylsilyl)methyl)pyridine 2-2



2,6-Dimethylpyridine (11.7 mL, 100 mmol, 1 eq) was dissolved in 100 mL dry THF and cooled to -78°C. *n*BuLi (78.1 mL, 1.28 M in hexane, 100 mmol, 1 eq) was added dropwise and the deep red solution was stirred for 1 h at -78°C. TMSCl (15 mL, 118 mmol, 1.2 eq) was added dropwise and the solution returned to colourless, while it was allowed to warm up to RT overnight. The solvent was removed *in vacuo* and the crude product was extracted with 100 mL of pentane. The white precipitate was filtered off and the solvent was removed *in vacuo*.

After vacuum distillation (10^{-3} mbar, 27°C, oil bath 41°C) the product was obtained as colourless liquid (17.3 g, 96.5 mmol, 97%).

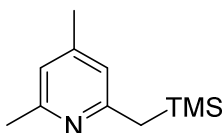
^1H NMR (400 MHz, CDCl_3) δ = 7.34 (t, $^3J_{\text{HH}}$ = 7.7 Hz, 1H), 6.79 (dd, $^3J_{\text{HH}}$ = 7.6 Hz, $^4J_{\text{HH}}$ = 0.5 Hz, 1H), 6.72 (d, $^3J_{\text{HH}}$ = 7.8 Hz, 1H), 2.45 (s, 3H), 2.29 (s, 2H), -0.02 (s, 9H).

^{13}C NMR (101 MHz, CDCl_3) δ = 160.6, 157.5, 136.1, 119.0, 118.6, 30.3, 24.7, -1.6.

^{29}Si NMR (80 MHz, CDCl_3) δ = 2.1.

The ^1H and ^{13}C NMR chemical shifts correspond with the literature values.^[35a]

2.4.2.3 2,4-Dimethyl-6-((trimethylsilyl)methyl)pyridine 2-3



2,4,6-Trimethylpyridine (13.2 mL, 100 mmol, 1 eq) was dissolved in 120 mL dry THF and cooled to -78°C. *n*BuLi (1.6 M in hexane, 62.6 mL, 100 mmol, 1 eq) was added dropwise and the orange solution was stirred for 1 h at -78°C. TMSCl (14.8 mL, 116 mmol, 1.2 eq) was added dropwise and the solution changed back to colourless while it was allowed to warm up to RT overnight. The solvent was removed *in vacuo* and the crude product was extracted with 120 mL of dry pentane. The white precipitate was removed by filtration and the solvent was removed *in vacuo*.

After vacuum distillation (10^{-3} mbar, 37°C, oil bath 45–50°C) the product was obtained as colourless liquid (13.6 g, 71 mmol, 71%).

^1H NMR (400 MHz, CDCl_3) δ = 6.65 (s, 1H), 6.56 (s, 1H), 2.42 (s, 3H), 2.25 (s, 2H), 2.21 (s, 3H), -0.01 (s, 9H).

^{13}C NMR (101 MHz, CDCl_3) δ = 160.4, 157.2, 147.0, 120.0, 119.8, 29.9, 24.4, 20.9, -1.6.

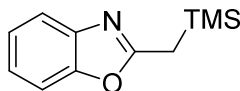
^{29}Si NMR (79 MHz, CDCl_3) δ = 1.9.

EA: Found: C, 68.5; H, 9.9; N, 7.9%. Calc. for $\text{C}_{11}\text{H}_{19}\text{NSi}$: C, 68.3; H, 9.9; N, 7.2.

m/z (FAB⁺) [%]: 194.1348 (100).

The ¹H and ¹³C NMR chemical shifts correspond with the literature values.^[35a]

2.4.2.4 2-((Trimethylsilyl)methyl)benzoxazole 2-4



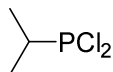
Diisopropyl amine (0.70 mL, 5.0 mmol, 1 eq) was dissolved in 10 mL dry THF and cooled to -78°C . *n*BuLi (1.4 M in hexane, 3.45 mL, 5.0 mmol, 1 eq) was added dropwise and the yellow solution was stirred for 10 min at -78°C . 2-Methylbenzoxazole (0.59 mL, 5.0 mmol, 1 eq) was dissolved in 10 mL dry THF and cooled to -78°C . The LDA solution was added dropwise and the yellow-orange solution was stirred for 15 min. TMSCl (0.75 mL, 5.9 mmol, 1.2 eq) was added dropwise and the pale yellow solution was allowed to warm up to RT overnight. The solvent was removed *in vacuo* and the crude product was extracted with 5 mL of dry pentane. The white precipitate was filtered off and the solvent was removed *in vacuo*.

After vacuum distillation ($2 \cdot 10^{-3}$ mbar, 40°C , 95°C oil bath) the product was obtained as colourless liquid (0.21 g, 1.0 mmol, 20%).

¹H NMR (400 MHz), ¹³C NMR (101 MHz) and ²⁹Si NMR (80 MHz) see Table 1.

EA: Found: C, 62.2; H, 7.3; N, 6.55. Calc. for C₁₁H₁₅NOSi: C, 64.3; H, 7.4; N, 6.8%.

2.4.2.5 *iso*Propyldichlorophosphine 2-5



Zinc chloride (1 M in THF, 60 mL, 60 mmol, 1.2 eq) was added dropwise to *i*-PrMgCl·LiCl (1.1 M in THF, 46 mL, 50 mmol, 1 eq) at -78°C and stirred for 45 min at -78°C . Afterwards the grey suspension was added dropwise to a solution of PCl₃ (5.3 mL, 60 mmol, 1.2 eq) in 60 mL of dry THF at -78°C and the reaction mixture was allowed to warm up to RT overnight. The white precipitate was filtered off and the solvent was removed by distillation. The crude product was extracted with 60 mL of dry pentane and the white precipitate was removed by filtration. After distillation the product was obtained as a colourless liquid (2.65 g, 18.3 mmol, 37% in THF/pentane).

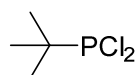
¹H NMR (400 MHz, CDCl₃) δ = 2.24 (dhept, ²J_{PH} = 16.8 Hz, ³J_{HH} = 7.0 Hz, 1H), 1.27 (dd, ³J_{PH} = 15.7 Hz, ³J_{HH} = 7.0 Hz, 6H).

¹³C NMR (101 MHz, CDCl₃) δ = 38.7 (d, ¹J_{PC} = 43.1 Hz), 15.9 (d, ²J_{PC} = 16.9 Hz).

³¹P NMR (162 MHz, CDCl₃) δ = 199.9 (dhept, ²J_{PH} = 30.4 Hz, ³J_{PH} = 16.1 Hz).

The ³¹P NMR chemical shift corresponds with the literature value.^[17]

2.4.2.6 *tert*Butyldichlorophosphine 2-6



Magnesium (3.1 g 127 mmol, 1.3 eq) was suspended in 100 mL of dry diethyl ether. Five drops of 1,2-Dibromo ethane were added and the mixture was refluxed using a hot air gun for approx. 10 min. *tert*Butyl chloride (11 mL, 100 mmol, 1 eq) was added slowly during the next 2 h and the reaction mixture was heated to reflux with a hot air gun for 30 min. After another 30 min the grey suspension of *tert*butylmagnesium chloride was added dropwise to a solution of PCl_3 (8.8 mL, 100 mmol, 1 eq) in 100 mL of dry diethyl ether at -78°C . The grey suspension turned colourless, while it was allowed to warm up to RT overnight. The white precipitate was filtered off and the solvent was removed by distillation. The crude product was extracted with 40 mL of dry diethyl ether and after distillation (160°C) the product was dried *in vacuo*. The product was obtained as colourless solid (3.7 g, 23.5 mmol, 24%).

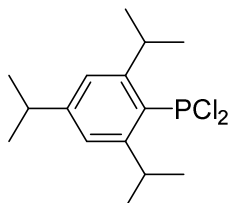
^1H NMR (400 MHz, CDCl_3) δ = 1.23 (d, $^3J_{\text{PH}}$ = 15.0 Hz, 9H).

^{13}C NMR (101 MHz, CDCl_3) δ = 38.9 (d, $^1J_{\text{PC}}$ = 45.1 Hz), 23.8 (d, $^2J_{\text{PC}}$ = 21.1 Hz).

^{31}P NMR (162 MHz, CDCl_3) δ = 200.3.

The NMR chemical shifts correspond with the literature values.^[18, 36]

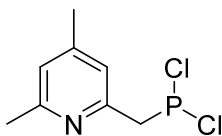
2.4.2.7 Triisopropylphenyldichlorophosphine 2-7



Magnesium (3.3 g, 135 mmol, 2.3 eq) was suspended in 100 mL of dry THF. Five drops of 1,2-dibromo ethane were added and the mixture was stirred for 1 h. 2-Bromo-1,3,5-triisopropylbenzene (15 mL, 59 mmol, 1 eq) was added dropwise, while the solution was kept refluxing with a hot air gun. After complete addition of the 2-bromo-1,3,5-triisopropylbenzene the dark grey solution was refluxed for five more minutes. Zinc chloride (101 mL, 1 M in THF, 101 mmol, 1.7 eq) was added dropwise at 0°C . After warming up to RT the mixture was stirred for 1 h. The grey suspension was added dropwise to a solution of PCl_3 (8.8 mL, 100 mmol, 1 eq) in 100 mL of dry THF. After the reaction mixture was allowed to warm up to RT overnight the white precipitate was filtered off. The solvent was removed *in vacuo* and the product was obtained as pale yellow solid (13.8 g, 41.9 mmol, 71%). The product was obtained as a mixture of TIPPPCl_2 (78%), TIPPPClBr (11%) and TIPPPBr_2 (11%).

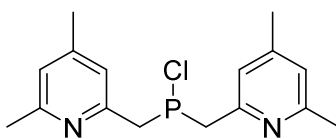
^{31}P NMR (162 MHz, CDCl_3) δ = 166.17 (TIPPPCl_2), 166.14 (TIPPPClBr), 166.12 (TIPPPBr_2).

2.4.2.8 Attempted synthesis of dichloro(4,6-dimethylpyridin-2-ylmethyl)phosphine 2-8



PCl_3 (0.44 mL, 5.0 mmol, 1 eq) was dissolved in 10 mL dry THF and cooled down to -78°C . **2-3** (0.97 g, 5.0 mmol, 1 eq) was added dropwise and the solution was allowed to warm up to room temperature overnight. The reaction mixture turned orange and a yellow precipitate was formed. The precipitate was filtered off and dried under vacuum.

The main compound of the precipitate was identified as bis(4,6-dimethylpyridin-2-ylmethyl)chlorophosphine **2-9**.



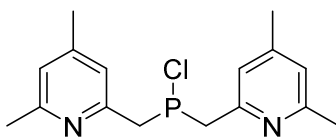
$^1\text{H NMR}$ (400 MHz, CDCl_3) δ = 7.37 (s, 2H), 7.21 (s, 2H), 4.14 (d, $^2J_{\text{PH}} = 8.8$ Hz, 4H), 2.71 (s, 6H), 2.45 (s, 6H).

$^{13}\text{C NMR}$ (101 MHz, CDCl_3) δ = 158.6, 152.9, 149.8 (d, $^2J_{\text{PC}} = 8.8$ Hz), 126.1 (d, $^5J_{\text{PC}} = 1.3$ Hz), 125.6 (d, $^3J_{\text{PC}} = 5.2$ Hz), 37.2 (d, $^1J_{\text{PC}} = 41.7$ Hz), 22.1, 19.2.

$^{31}\text{P NMR}$ (162 MHz, CDCl_3) δ = 98.8.

m/z (FAB $^+$) [%]: 271.1342 (43).

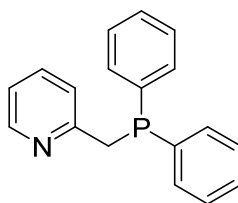
2.4.2.9 Attempted synthesis of bis(4,6-dimethylpyridin-2-ylmethyl)chlorophosphine 2-9



PCl_3 (0.44 mL, 5.0 mmol, 1 eq) was dissolved in 10 mL dry THF and cooled down to -78°C . **2-3** (1.93 g, 10.0 mmol, 2 eq) was added dropwise and the solution was allowed to warm up to room temperature overnight. The reaction mixture turned orange-brown and a yellow precipitate was formed. The precipitate was filtered off and dried under vacuum.

$^{31}\text{P NMR}$ spectra of the solution and the precipitate showed several signals. The $^{31}\text{P NMR}$ spectrum of the solution showed a signal at 102.7 ppm, which is probably caused by **2-9**, but the product could not be isolated (see 2.2.1.2). The signals in the $^{31}\text{P NMR}$ spectrum of the precipitate could not be assigned (see 2.2.1.2).

2.4.2.10 Diphenyl(pyridin-2-ylmethyl)phosphine 2-10



Diphenylchlorophosphine (1.79 mL, 10.0 mmol, 1 eq) was dissolved in anhydrous THF (10 mL) and cooled to 0°C. **2-1** (1.65 g, 10.0 mmol, 1 eq) was added dropwise and the reaction mixture was left to warm to room temperature overnight. The solvent was removed *in vacuo* and the product was obtained as colourless solid (2.39 g, 8.62 mmol, 86%).

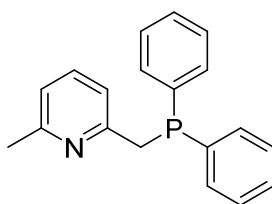
$^1\text{H NMR}$ (400 MHz), $^{13}\text{C NMR}$ (101 MHz) and $^{31}\text{P NMR}$ (162 MHz) see Table 2.

EA: Found: C, 76.5; H, 5.8; N, 4.9. Calc. for $\text{C}_{18}\text{H}_{16}\text{NP}$: C, 78.0; H, 5.8; N, 5.05%.

m/z (ESI) [%]: 278.10962 (17), 200.06264 (3), 98.03546 (1).

The NMR chemical shifts correspond with the literature values.^[37]

2.4.2.11 Diphenyl(6-methylpyridin-2-ylmethyl)phosphine 2-11



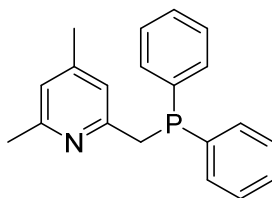
Diphenylchlorophosphine (1.79 mL, 10.0 mmol, 1 eq) was dissolved in anhydrous THF (10 mL) and cooled to 0°C. **2-2** (1.79 g, 10.0 mmol, 1 eq) was added dropwise and the reaction mixture was left to warm to room temperature overnight. The solvent was removed *in vacuo* and the product was obtained as colourless liquid (2.29 g, 7.86 mmol, 79%).

$^1\text{H NMR}$ (400 MHz), $^{13}\text{C NMR}$ (101 MHz) and $^{31}\text{P NMR}$ (162 MHz) see Table 2.

EA: Found: C, 77.3; H, 6.4; N, 5.1. Calc. for $\text{C}_{19}\text{H}_{18}\text{NP}$: C, 78.3; H, 6.2; N, 4.8%.

m/z (ESI) [%]: 292.12490 (23), 214.07808 (3).

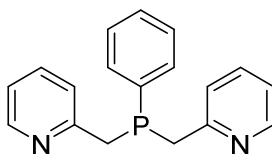
2.4.2.12 Diphenyl(4,6-dimethylpyridin-2-ylmethyl)phosphine 2-12



Diphenylchlorophosphine (1.79 mL, 10.0 mmol, 1 eq) was dissolved in anhydrous THF (10 mL) and cooled to 0°C. **2-3** (1.93 g, 10.0 mmol, 1 eq) was added dropwise and the reaction mixture was left to warm to room temperature overnight. The solvent was removed *in vacuo* and the product was obtained as colourless liquid (2.59 g, 8.49 mmol, 85%).

^1H NMR (400 MHz), ^{13}C NMR (101 MHz) and ^{31}P NMR (162 MHz) see Table 2.
EA: Found: C, 78.6; H, 6.5; N, 4.4. Calc. for $\text{C}_{20}\text{H}_{20}\text{NP}$: C, 78.7; H, 6.6; N, 4.6%.
 m/z (ESI) [%]: 306.14091 (27), 228.09399 (3).

2.4.2.13 Phenyl-bis(pyridin-2-ylmethyl)phosphine 2-13



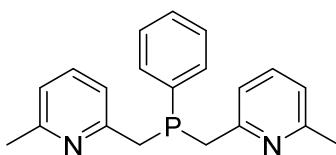
Phenyldichlorophosphine (2.30 mL, 16.9 mmol, 1 eq) was dissolved in 40 mL dry THF and cooled to 0°C. **2-1** (5.59 g, 33.8 mmol, 2 eq) was added dropwise and the solution turned yellow-orange, while it was allowed to warm up to RT overnight. The solvent was removed *in vacuo* and the crude product was extracted with 20 mL of dry Et_2O . The precipitate was filtered off and the solvent was removed *in vacuo*.

The product was obtained as yellow solid (4.37 g, 15.0 mmol, 89%).

^1H NMR (400 MHz), ^{13}C NMR (101 MHz) and ^{31}P NMR (162 MHz) see Table 3.

The ^1H and ^{13}C NMR chemical shifts correspond with the literature values.^[7e, 7g]

2.4.2.14 Phenyl-bis(6-methylpyridin-2-ylmethyl)phosphine 2-14



Phenyldichlorophosphine (0.68 mL, 5 mmol, 1 eq) was dissolved in 10 mL dry THF and cooled to 0°C. **2-2** (1.8 g, 10 mmol, 2 eq) was added dropwise and the solution turned yellow-orange, while it was allowed to warm up to RT overnight. The solvent was removed *in vacuo* and the crude product was extracted with 10 mL dry Et_2O . The precipitate was filtered off and the solvent was removed *in vacuo*.

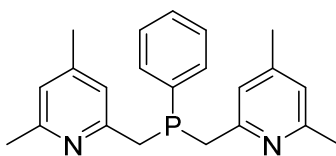
The product was obtained as very viscous yellow liquid (1.29 g, 4.0 mmol, 80%).

^1H NMR (400 MHz), ^{13}C NMR (101 MHz) and ^{31}P NMR (162 MHz) see Table 3.

EA: Found: C, 74.5; H, 6.7; N, 8.2. Calc. for $\text{C}_{20}\text{H}_{21}\text{N}_2\text{P}$: C, 75.0; H, 6.6; N, 8.7%.

m/z (FAB⁺) [%]: 321.1505 (100).

2.4.2.15 Phenyl-bis(4,6-dimethylpyridin-2-ylmethyl)phosphine 2-15



Phenyldichlorophosphine (0.68 mL, 5 mmol, 1 eq) was dissolved in 10 mL dry THF and cooled to 0°C. **2-3** (2.0 g, 10.3 mmol, 2.1 eq) was added dropwise and the solution turned yellow-orange, while it was allowed to warm up to RT overnight. The solvent was removed *in vacuo* and the crude product was extracted with 10 mL of dry Et₂O.

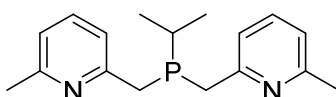
The precipitate was filtered off and the solvent was removed *in vacuo*. The crude product was extracted with 10 mL of dry pentane. The precipitate was filtered off and the solvent was removed *in vacuo*. The product was obtained as very viscous amber coloured liquid (1.27 g, 3.64 mmol, 72%).

¹H NMR (400 MHz), ¹³C NMR (101 MHz) and ³¹P NMR (162 MHz) see Table 3.

EA: Found: C, 74.7; H, 7.3; N, 8.4. Calc. for C₂₂H₂₅N₂P: C, 75.8; H, 7.2; N, 8.0%.

m/z (ESI) [%]: 349.18359 (51), 228.09406 (19).

2.4.2.16 isoPropyl-bis(6-methylpyridin-2-ylmethyl)phosphine 2-16



2-5 (4.1 g, 28.2 mmol, 1 eq) was dissolved in 60 mL dry THF and cooled to 0°C. **2-2** (10.0 g, 55.8 mmol, 2 eq) was added dropwise and the solution turned yellow, while it was allowed to warm up to RT overnight. The solvent was removed *in vacuo* and the crude product was extracted with 40 mL Et₂O. The precipitate was filtered off and the solvent was removed *in vacuo*. The crude product was extracted with 60 mL Et₂O. The precipitate was filtered off and the solvent was removed *in vacuo*.

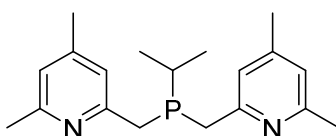
The product was obtained as amber coloured liquid (6.7 g, 23.2 mmol, 83%).

¹H NMR (400 MHz), ¹³C NMR (101 MHz) and ³¹P NMR (162 MHz) see Table 3.

EA: Found: C, 68.4; H, 8.0; N, 10.05. Calc. for C₁₇H₂₃N₂P: C, 71.3; H, 8.1; N, 9.8%.

m/z (FAB⁺) [%]: 287.1637 (100).

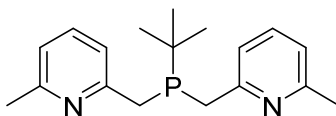
2.4.2.17 isoPropyl-bis(4,6-dimethylpyridin-2-ylmethyl)phosphine 2-17



2-5 (2.65 g, 18.3 mmol, 1 eq) was dissolved in 20 mL dry THF and cooled to 0°C. **2-3** (7.1 g, 36.6 mmol, 2 eq) was added dropwise and the solution turned yellow-orange, while it was allowed to warm up to RT overnight. The solvent was removed *in vacuo* and the crude product was extracted with 20 mL dry Et₂O. The precipitate was filtered off and the solvent was removed *in vacuo*. The product was obtained as amber coloured liquid (5.22 g, 16.6 mmol, 91%).

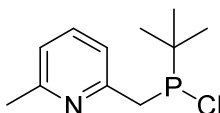
^1H NMR (400 MHz), ^{13}C NMR (101 MHz) and ^{31}P NMR (162 MHz) see Table 3.
EA: Found: C, 71.3; H, 8.6; N, 8.65. Calc. for $\text{C}_{19}\text{H}_{27}\text{N}_2\text{P}$: C, 72.6; H, 8.7; N, 8.9%.
 m/z (FAB $^+$) [%]: 315.1967 (100).

2.4.2.18 Attempted synthesis of *tert*butyl-bis(6-methylpyridin-2-ylmethyl)phosphine 2-18



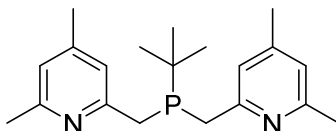
A solution of **2-6** (1 M in THF, 12.0 mL, 12.0 mmol, 1 eq) was cooled down to 0°C and **2-2** (4.22 g, 24.0 mmol, 2 eq) was added dropwise. The reaction mixture was allowed to warm up to room temperature overnight in which the solution turned yellow. The reaction mixture was heated to reflux for 22 h, in which the solution turned orange.

From the ^{31}P NMR spectrum of the reaction mixture the main product was identified as *tert*butyl-(6-methylpyridin-2-ylmethyl)-chlorophosphine.



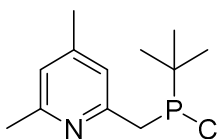
^{31}P NMR (162 MHz, THF) δ = 126.5.

2.4.2.19 Attempted synthesis of *tert*butyl-bis(4,6-dimethylpyridin-2-ylmethyl)phosphine 2-19



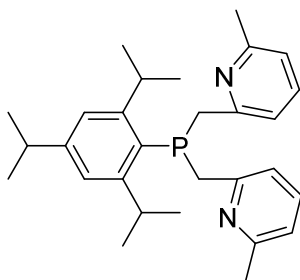
A solution of **2-6** (1 M in THF, 12.0 mL, 12.0 mmol, 1 eq) was cooled down to 0°C and **2-3** (4.54 g, 23.5 mmol, 2 eq) was added dropwise. The reaction mixture was allowed to warm up to room temperature overnight in which the solution turned reddish. The reaction mixture was heated to reflux for 22 h, in which the solution turned red-brown.

From the ^{31}P NMR spectrum of the reaction mixture the main product was identified as *tert*butyl-(4,6-dimethylpyridin-2-ylmethyl)-chlorophosphine.



^{31}P NMR (162 MHz, THF) δ = 126.2.

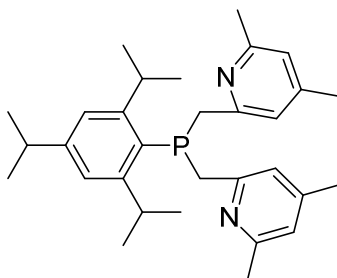
2.4.2.20 Triisopropylphenyl-bis(6-methylpyridin-2-ylmethyl)phosphine 2-20



A solution of **2-7** (0.5 M in THF, 10.0 mL, 5.0 mmol, 1 eq) was cooled down to 0°C and **2-2** (1.8 g, 10.0 mmol, 2 eq) was added dropwise. The reaction mixture was allowed to warm up to room temperature overnight in which the solution turned yellow. The solvent was removed *in vacuo*. A very viscous yellow liquid was obtained. The product could not be isolated pure.

^{31}P NMR (162 MHz, CDCl_3) $\delta = -21.8$.

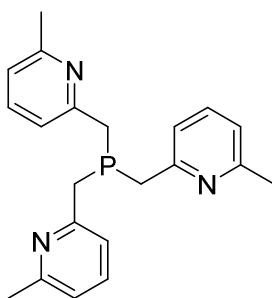
2.4.2.21 Triisopropylphenyl-bis(4,6-dimethylpyridin-2-ylmethyl)phosphine 2-21



A solution of **2-7** (0.5 M in THF, 10.0 mL, 5.0 mmol, 1 eq) was cooled down to 0°C and **2-3** (1.94 g, 10.0 mmol, 2 eq) was added dropwise. The reaction mixture was allowed to warm up to room temperature overnight in which the solution turned yellow. The solvent was removed *in vacuo* and the crude product was extracted with 10 mL of pentane. The precipitate was filtered off and the product was extracted with MeCN (3x5 mL). The solvent was removed *in vacuo*. A very viscous yellow liquid was obtained. The product could not be isolated pure.

^{31}P NMR (162 MHz, CDCl_3) $\delta = -22.7$.

2.4.2.22 Tris(6-methylpyridin-2-ylmethyl)phosphine 2-24

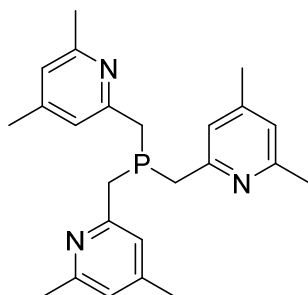


PCl_3 (0.87 mL, 10 mmol, 1 eq) was dissolved in 10 mL dry THF and cooled to -78°C . **2-2** (5.4 g, 30 mmol, 3 eq) was added dropwise and the solution turned amber coloured, while it was allowed to warm up to RT overnight. The solvent was removed *in vacuo* and the crude product was extracted with 10 mL dry pentane. The precipitate was filtered off and the solvent was removed *in vacuo*. The product was obtained as very viscous yellow liquid (1.46 g, 4.2 mmol, 84%).

^1H NMR (400 MHz), ^{13}C NMR (101 MHz) and ^{31}P NMR (162 MHz) see Table 4.

m/z (FAB $^+$) [%]: 350.1768 (100).

2.4.2.23 Tris(4,6-dimethylpyridin-2-ylmethyl)phosphine 2-25



PCl_3 (0.44 mL, 5.0 mmol, 1 eq) was dissolved in 15 mL dry THF and cooled to -78°C . **2-3** (2.9 g, 15 mmol, 3 eq) was added dropwise and the solution turned yellow-orange, while it was allowed to warm up to RT overnight. The solvent was removed *in vacuo* and the crude product was extracted with 10 mL dry Et_2O . The precipitate was filtered off and the solvent was removed *in vacuo*. The crude product was extracted with 10 mL of dry pentane. The precipitate was filtered off and the solvent was removed *in vacuo*.

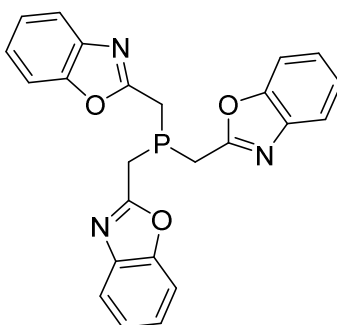
The product was obtained as very viscous amber coloured liquid (1.34 g, 3.4 mmol, 68%).

^1H NMR (400 MHz), ^{13}C NMR (101 MHz) and ^{31}P NMR (162 MHz) see Table 4.

EA: Found: C, 72.1; H, 7.7; N, 10.3. Calc. for $\text{C}_{24}\text{H}_{30}\text{N}_3\text{P}$: C, 73.6; H, 7.7; N, 10.7%.

m/z (ESI) [%]: 392.22525 (7), 271.13598 (5).

2.4.2.24 Tris(benzoxazol-2-ylmethyl)phosphine 2-26



PCl_3 (0.18 mL, 2.0 mmol, 1 eq) was dissolved in 5 mL dry THF and cooled down to -78°C . **2-4** (1.33 g, 6.5 mmol, 3.3 eq) was added dropwise and the solution was allowed to warm up to room temperature overnight. The solvent was removed *in vacuo* and the product was obtained as yellow solid (0.48 g, 1.35 mmol, 67%).

^1H NMR (400 MHz), ^{13}C NMR (101 MHz) and ^{31}P NMR (162 MHz) see Table 5.

2.4.3 Crystallographic data

Table 6: Crystallographic data of **2-27**.

Identification code	mx398
Empirical formula	C ₂₆ H ₂₁ N ₄ O ₄ P
Formula weight [g·mol ⁻¹]	484.44
Temperature [K]	143(2)
Crystal size [mm ³]	0.08 × 0.14 × 0.38
Colour, shape	Colourless rod
Crystal system	Triclinic
Space group	<i>P</i> -1
<i>a</i> [Å]	4.8902(3)
<i>b</i> [Å]	13.5057(8)
<i>c</i> [Å]	19.4914(9)
α [°]	109.652(5)
β [°]	90.931(5)
γ [°]	100.161(5)
<i>V</i> [Å ³]	1189.35(12)
<i>Z</i>	2
ρ_{calc} [g·cm ⁻³]	1.353
Radiation [Å]	MoK α = 0.71073
μ [cm ⁻¹]	0.156
<i>F</i> (000)	504
Index ranges	-6 ≤ <i>h</i> ≤ 6 -15 ≤ <i>k</i> ≤ 16 -24 ≤ <i>l</i> ≤ 23
θ range [°]	4.195 ≤ θ ≤ 26.371
Reflections collected	8884
Independent reflections	4801
Observed reflections	3483
Data/restraints/parameters	4801/0/334
<i>R</i> _{int}	0.0375
<i>R</i> ₁ , <i>wR</i> ₂ [<i>I</i> > 2σ(<i>I</i>)]	0.0467, 0.0947
<i>R</i> ₁ , <i>wR</i> ₂ [all data]	0.0689, 0.1093
Goof	1.021
$\delta\rho_{\text{max}}$, $\delta\rho_{\text{min}}$ [e·nm ⁻³]	0.361, -0.303

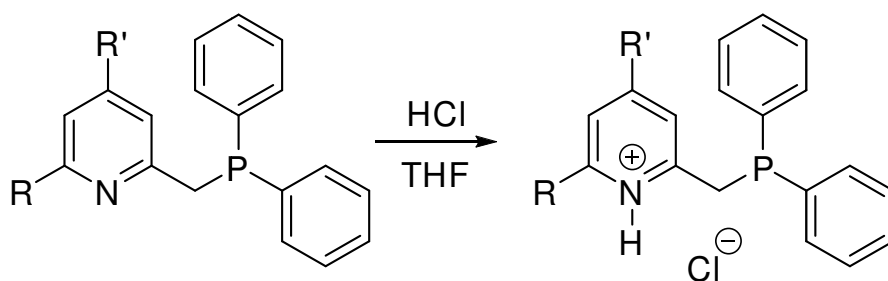
2.5 References

- [1] a) C. Hettstedt, P. Koestler, E. Ceylan, K. Karaghiosoff, *Tetrahedron* **2016**, 72, 3162-3170; b) A. Murso, D. Stalke, *Dalton Trans.* **2004**, 2563-2569; c) C. Hettstedt, M. Unglert, R. J. Mayer, A. Frank, K. Karaghiosoff, *Eur. J. Inorg. Chem.* **2016**, 2016, 1405-1414.
- [2] a) H. Jaafar, H. Li, L. C. Misal Castro, J. Zheng, T. Roisnel, V. Dorcet, J.-B. Sortais, C. Darcel, *Eur. J. Inorg. Chem.* **2012**, 2012, 3546-3550; b) F. Hung-Low, K. K. Klausmeyer, *Inorg. Chim. Acta* **2008**, 361, 1298-1310; c) A. Jansen, S. Pitter, *Monatsh. Chem.* **1999**, 130, 783-794.
- [3] S. Liu, R. Peloso, P. Braunstein, *Dalton Trans.* **2010**, 39, 2563-2572.
- [4] M. Devillard, C. Alvarez Lamsfus, V. Vreeken, L. Maron, J. I. van der Vlugt, *Dalton Trans.* **2016**, 45, 10989-10998.
- [5] J. T. Mague, S. W. Hawbaker, *J. Chem. Crystallogr.* **1997**, 27, 603-608.
- [6] a) W. V. Dahlhoff, T. R. Dick, S. M. Nelson, *J. Chem. Soc. A* **1969**, 2919-2923; b) E. De la Encarnacion, J. Pons, R. Yanez, J. Ros, *Inorg. Chim. Acta* **2006**, 359, 745-752; c) H. Yang, N. Lugan, R. Mathieu, *Organometallics* **1997**, 16, 2089-2095.
- [7] a) E. Lindner, H. Rauleder, W. Hiller, *Z. Naturforsch., B: Anorg. Chem., Org. Chem.* **1983**, 38B, 417-425; b) E. Lindner, H. Rauleder, P. Wegner, *Z. Naturforsch., B: Anorg. Chem., Org. Chem.* **1984**, 39B, 1224-1229; c) S. Liu, R. Peloso, R. Pattacini, P. Braunstein, *Dalton Trans.* **2010**, 39, 7881-7883; d) I. Objartel, D. Leusser, F. Engelhardt, R. Herbst-Irmer, D. Stalke, *Z. Anorg. Allg. Chem.* **2013**, 639, 2005-2012; e) A. Kermagoret, F. Tomicki, P. Braunstein, *Dalton Trans.* **2008**, 2945-2955; f) K. K. Klausmeyer, F. Hung, *Acta Crystallogr., Sect. E: Struct. Rep. Online* **2006**, 62, m2415-m2416; g) F. Hung-Low, A. Renz, K. K. Klausmeyer, *Eur. J. Inorg. Chem.* **2009**, 2009, 2994-3002; h) G. Jin, L. Vendier, Y. Coppel, S. Sabo-Etienne, S. Bontemps, *Dalton Trans.* **2015**, 44, 7500-7505.
- [8] a) C. Hettstedt, R. J. Mayer, J. F. Martens, S. Linert, K. Karaghiosoff, *Eur. J. Inorg. Chem.* **2016**, 2016, 726-735; b) C. Hettstedt, PhD thesis, Ludwig-Maximilians-Universität München **2015**; c) S. Linert, S. Wagner, P. Schmidt, L. Higham, C. Hepples, P. Waddell, K. Karaghiosoff, *Phosphorus Sulfur Relat. Elem.* **2019**, 194, 565-568.
- [9] a) C. J. Whiteoak, J. D. Nobbs, E. Kiryushchenkov, S. Pagano, A. J. P. White, G. J. P. Britovsek, *Inorg. Chem.* **2013**, 52, 7000-7009; b) B. Chiswell, *Aust. J. Chem.* **1967**, 20, 2533-2534.
- [10] a) D. Wei, A. Bruneau-Voisine, T. Chauvin, V. Dorcet, T. Roisnel, D. A. Valyaev, N. Lugan, J.-B. Sortais, *Adv. Synth. Catal.* **2018**, 360, 676-681; b) C. Perez-Zuniga, C. Negrete-Vergara, V. Guerschais, H. Le Bozec, S. A. Moya, P. Aguirre, *Mol. Catal.* **2019**, 462, 126-131; c) T. Miura, I. E. Held, S. Oishi, M. Naruto, S. Saito, *Tetrahedron Lett.* **2013**, 54, 2674-2678.
- [11] a) P. J. Lauridsen, Z. Lu, J. J. A. Celaje, E. A. Kedzie, T. J. Williams, *Dalton Trans.* **2018**, 47, 13559-13564; b) R. Langer, A. Gese, D. Gesevicius, M. Jost, B. R. Langer, F. Schneck, A. Venker, W. Xu, *Eur. J. Inorg. Chem.* **2015**, 2015, 696-705.
- [12] P. A. Aguirre, C. A. Lagos, S. A. Moya, C. Zuniga, C. Vera-Oyarce, E. Sola, G. Peris, J. C. Bayon, *Dalton Trans.* **2007**, 5419-5426.
- [13] a) G. Mueller, M. Klinga, P. Osswald, M. Leskelae, B. Rieger, *Z. Naturforsch., B: Chem. Sci.* **2002**, 57, 803-809; b) G. Si, Y. Na, C. Chen, *ChemCatChem* **2018**, 10, 5135-5140.
- [14] a) Z. Xue, T. B. L. Nguyen, S. K. Noh, W. S. Lyoo, *Angew. Chem., Int. Ed.* **2008**, 47, 6426-6429; b) Z. Xue, S. K. Noh, W. S. Lyoo, *J. Polym. Sci., Part A: Polym. Chem.* **2008**, 46, 2922-2935.
- [15] a) A.-F. Ma, H.-H. Seo, S.-H. Jin, U. C. Yoon, M. H. Hyun, S. K. Kang, Y.-I. Kim, *Bull. Korean Chem. Soc.* **2009**, 30, 2754-2758; b) N. S. Pennington, M. M. Richter, B. Carlson, *Dalton Trans.* **2010**, 39, 1586-1590.
- [16] S. Pailloux, C. E. Shirima, E. N. Duesler, K. A. Smith, R. T. Paine, *Polyhedron* **2011**, 30, 2746-2757.
- [17] W. Samstag, J. W. Engels, *Angew. Chem.* **1992**, 104, 1367-1369.
- [18] Y. Liu, B. Ding, D. Liu, Z. Zhang, Y. Liu, W. Zhang, *Res. Chem. Intermed.* **2017**, 43, 4959-4966.

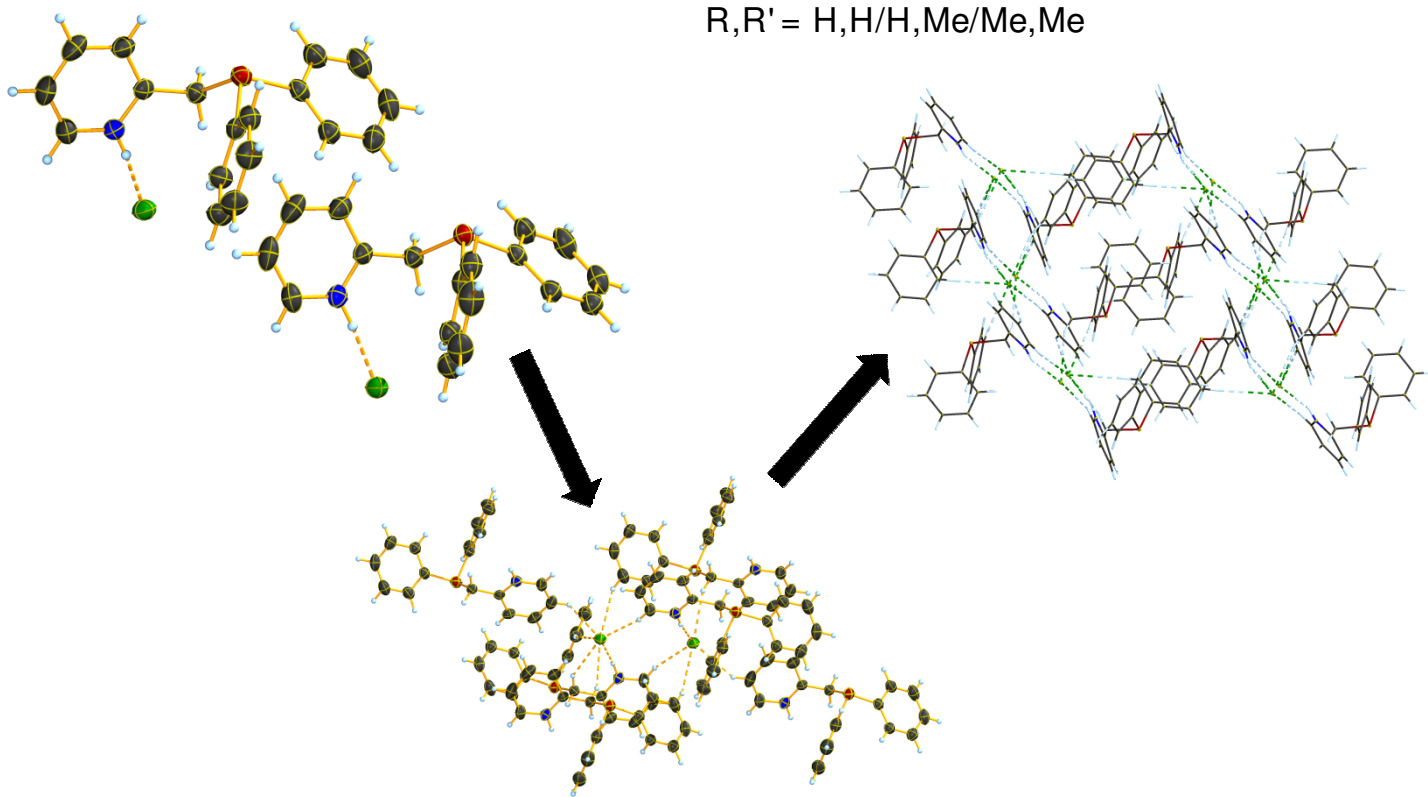
- [19] M. I. Arz, V. T. Annibale, N. L. Kelly, J. V. Hanna, I. Manners, *J. Am. Chem. Soc.* **2019**, *141*, 2894-2899.
- [20] a) R. J. Abraham, M. Reid, *J. Chem. Soc., Perkin Trans. 2* **2002**, 1081-1091; b) J. Llinares, J. P. Galy, R. Faure, E. J. Vincent, J. Elguero, *Can. J. Chem.* **1979**, *57*, 937-945.
- [21] <https://www.pascal-man.com/periodic-table/29Si.pdf>, 01.07.2020.
- [22] S. Braun, S. Berger, H.-O. Kalinowski, *NMR-Spektroskopie von Nichtmetallen*, Georg Thieme Verlag, New York, **1993**.
- [23] B. Valeur, *Molecular Fluorescence: Principles and Applications*, Wiley-VCH, Weinheim, **2002**.
- [24] D. A. H. Novoa, H. Perez, O. M. Peeters, N. M. Blaton, R. C. J. De, J. M. Lopez, *Acta Crystallogr. C* **2000**, *56*, E98-99.
- [25] M. S. Hain, Y. Fukuda, C. Rojas Ramírez, B. Y. Winer, S. E. Winslow, R. D. Pike, D. C. Bebout, *Cryst. Growth Des.* **2014**, *14*, 6497-6507.
- [26] S. Foxon, J.-Y. Xu, S. Turba, M. Leibold, F. Hampel, F. W. Heinemann, O. Walter, C. Würtele, M. Holthausen, S. Schindler, *Eur. J. Inorg. Chem.* **2007**, *2007*, 429-443.
- [27] S. Soudani, V. Ferretti, C. Jelsch, F. Lefebvre, C. Ben Nasr, *Inorg. Chem. Commun.* **2015**, *61*, 187-192.
- [28] L. V. De Freitas, A. L. d. S. F. Dos Santos, F. C. Da Costa, J. B. Calixto, P. V. P. Miranda, T. J. J. Silva, E. S. Pereira, W. R. Rocha, W. B. De Almeida, L. A. De Souza, M. C. R. Freitas, *J. Mol. Stru.* **2018**, *1169*, 119-129.
- [29] S. Badoğlu, Ş. Yurdakul, *J. Struct. Chem.* **2018**, *59*, 1010-1021.
- [30] G. M. Sheldrick, SHELXS-97, Program for Crystal Structure Solution, **1997**, University of Göttingen, Germany.
- [31] G. M. Sheldrick, *Acta Crystallogr., Sect. C: Struct. Chem.* **2015**, *71*, 3-8.
- [32] A. L. Spek, PLATON, A Multipurpose Crystallographic Tool, **1999**, Utrecht University, The Netherlands.
- [33] SCALE3 ABSPACK - An Oxford Diffraction program (v. 1.0.4, gui:1.0.3); **2005**, Oxford Diffraction Ltd., Oxfordshire, UK.
- [34] <https://checkcif.iucr.org/>.
- [35] a) C.-K. Kim, E. Park, B.-Y. Son, *J. Korean Chem. Soc.* **1994**, *38*, 570-575; b) A. Kermagoret, P. Braunstein, *Organometallics* **2008**, *27*, 88-99; c) S. Schwieger, R. Herzog, C. Wagner, D. Steinborn, *J. Organomet. Chem.* **2009**, *694*, 3548-3558.
- [36] D. Dakternieks, R. D. Giacomo, *Phosphorus Sulfur Relat. Elem.* **2006**, *24*, 217-224.
- [37] J. Flapper, H. Kooijman, M. Lutz, A. L. Spek, P. W. N. M. van Leeuwen, C. J. Elsevier, P. C. J. Kamer, *Organometallics* **2009**, *28*, 1180-1192.

Chapter 3

Synthesis, molecular and crystal structures of picolyl, lutidinyl and collidinyl phosphine hydrochlorides



$R, R' = H, H / H, Me / Me, Me$



S. Linert, D. Shiels, M. P. Dean, T. Colgan, L. J. Higham, K. Karaghiosoff
To be submitted to European Journal of Inorganic Chemistry

3.1 Introduction

Hemilabile P,N ligands, which include both a soft phosphorus and a hard nitrogen centre, exhibit very interesting complexing attributes, as the properties of both atoms can be individually fine-tuned.^[1] A lot of research has been done on these ligands and complexes with various transition metals, such as Fe, Pt, Rh, Pd, Ni, Cu and many others are known for bifunctional ligands of this type.^[2] Complexes of P,N ligands are commonly used as catalysts for a series of different reactions like e.g. hydrogenations, alkylations, aminations, hydrogen isotope exchange reactions, polycondensations and oligomerisations.^[1a, 1d, 3] Due to their fluorescent properties some of these complexes also are of interest for the lighting industry, in areas such as OLEDs and sensors.^[4]

The bifunctionality of such ligands means that there are both hard and soft centres within the molecule, ultimately meaning that in theory, it is possible to be selective about which atom will coordinate, depending on the hard/soft properties of the metal which is binding.^[5]

In many complexes though P,N ligands act as chelating ligands and coordinate via both the phosphorus and the nitrogen atom.^[5b]

The steric effects of the phenyl rings, which regularly feature in such ligands on the phosphorus atom, can strongly influence the coordination geometry in metal complexes.^[5a] Furthermore, due to the free rotation which is present around the P–C bond which leads to the pyridine ring, the N can take up a favourable position allowing coordination with a metal.^[6]

Diphenyl(pyridin-2-ylmethyl)phosphine (Ph₂PPic) **2-10** (Figure 1) is a well-known example for such P,N ligands. It was first synthesised in 1968 and structures of complexes with Fe, Ir, Ni and multiple other transition metals are known.^[7] By contrast, the extremely similar phosphine ligand, Diphenyl(6-methylpyridin-2-ylmethyl)phosphine (Ph₂PLut) **2-11** (Figure 1), has not been extensively researched. Although the ligand was synthesised for the first time in 1969, only a limited number of publications mention it.^[8] Moreover, Diphenyl(4,6-dimethylpyridin-2-ylmethyl)phosphine (Ph₂PCol) **2-12** (Figure 1) has not been referenced to date.

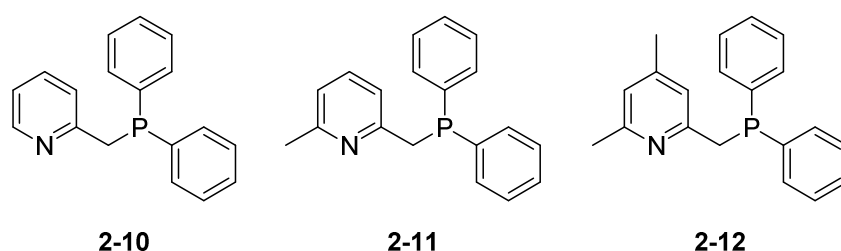


Figure 1: P,N ligands Diphenyl(pyridin-2-ylmethyl)phosphine (Ph₂PPic) **2-10**, Diphenyl(6-methylpyridin-2-ylmethyl)phosphine (Ph₂PLut) **2-11** and Diphenyl(4,6-dimethylpyridin-2-ylmethyl)phosphine (Ph₂PCol) **2-12**.

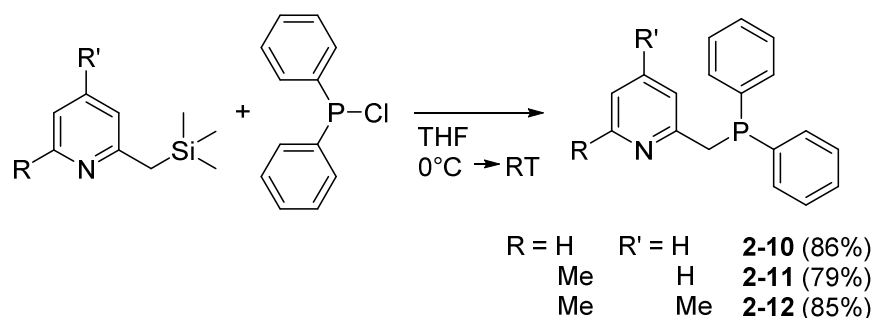
Since all 3 molecules only differ slightly by one or two methyl groups, it could be argued that the properties of these compounds are very similar to each other, and the phosphines could possibly be applied in fluorescence research or in homogenous catalysis.

Phosphine **2-10** is described as a viscous oil at room temperature.^[9] Ionic compounds often are much easier to crystallise than neutral compounds. As it proved to be difficult to crystallise the free ligands, it might be much easier to crystallise the hydrochloride salts than the pure phosphines. Since the crystal structures of the hydrochlorides can be determined, this might help to understand some key aspects of the molecules, such as geometry and orientation of the aryl rings.

3.2 Results and discussion

3.2.1 Synthesis

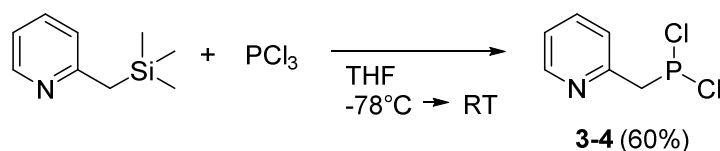
To synthesise **2-10–2-12**, the corresponding silyl compounds were allowed to react with $\text{Ph}_2\text{P-Cl}$ in a 1:1 ratio, according to the synthetic routes adopted by *Braunstein et al.*^[10] and *Hettstedt et al.*^[1b] The reaction was performed in THF allowing the solution to warm up from 0°C to RT (Scheme 1).



Scheme 1: Synthetic route towards phosphines **2-10–2-12**.

Compounds **2-10–2-12** are soluble in pentane, THF, DCM and chloroform. All three compounds are sensitive towards oxidation and are slowly hydrolysed. Compounds **2-11** and **2-12** are viscous colourless oils at room temperature, while compound **2-10** in contrast to the findings in the literature is a colourless solid.

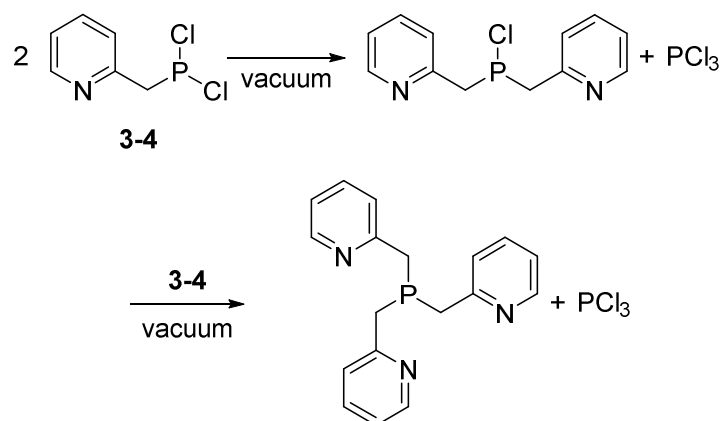
Instead of using diphenylchlorophosphine, as with preceding experiments, PCl_3 was used to synthesise (pyridin-2-ylmethyl)dichlorophosphine (PicP-Cl_2) **3-4** (Scheme 2).



Scheme 2: Synthetic route towards dichlorophosphine **3-4**.

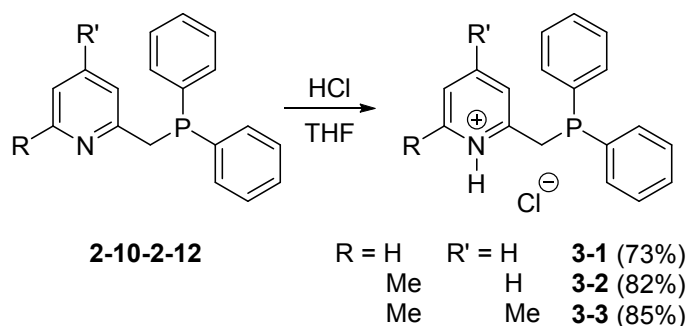
The reaction was performed by adding 2-((trimethylsilyl)methyl)pyridine to PCl_3 in a 1:1 ratio, in THF allowing the solution to warm up from -78°C to RT. From the ^{31}P NMR spectrum of the reaction solution can be determined that 60% of the phosphorus in solution has formed the desired product ($\delta = 183.6$ ppm (t, $^2J_{\text{PH}} = 13.1$ Hz)). 20% of the phosphorus was unreacted PCl_3 and small amounts of $\text{Pic}_2\text{P-Cl}$ (6%, $\delta = 87.9$ ppm) and Pic_3P (1%, $\delta = -7.3$ ppm) have been formed. Also some unidentified phosphorus containing impurities were present in the mixture.

The formation of dichlorophosphine **3-4** has been observed before, but it could not be isolated due to a dismutation reaction that occurs when the compound is dried under vacuum (Scheme 3).^[1b, 11]



Scheme 3: Dismutation reaction of **3-4** under vacuum.

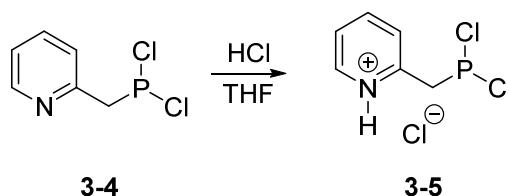
The hydrochlorides **3-1–3-3** were synthesised by addition of a solution of HCl in Et₂O to a solution of the corresponding phosphines (Scheme 4).



Scheme 4: Synthesis of hydrochlorides **3-1–3-3**.

Compounds **3-1–3-3** are insoluble in pentane and moderately soluble in THF. Compounds **3-2** and **3-3** show high solubility in DCM and chloroform, but compound **3-1** is only moderately soluble in these two solvents. All three compounds are colourless solids at room temperature and sensitive towards oxidation in air and are slowly hydrolysed. Upon hydrolysis after a few days the P–C_{Alk} bond is cleaved and in contact with oxygen the corresponding 2-pyridyl carboxylic acid is formed. Compounds **3-1–3-3** can easily be deprotonated to regenerate the corresponding phosphines with triethylamine. Therefore it is possible to purify compounds **2-10-2-12** *via* the corresponding hydrochlorides.

By addition of HCl to compound **7** the corresponding hydrochloride **3-5** (Scheme 5) was formed.



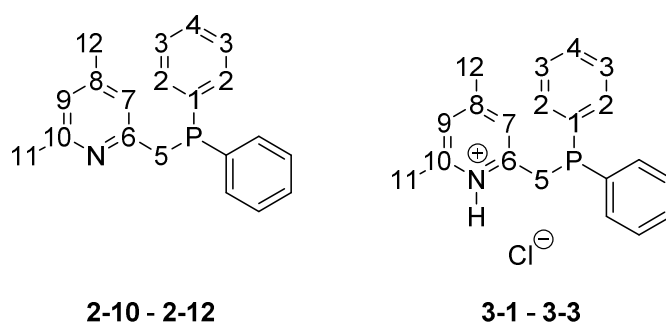
Scheme 5: Synthesis of hydrochloride compound **3-5**.

This compound is a pale yellow solid, which is stable under vacuum. The hydrochloride is not soluble in pentane and has a low solubility in THF, acetonitrile, DCM and chloroform. Due to the low solubility it was not possible to purify the substance. From the ³¹P NMR spectrum can be determined that 73% of the phosphorus in the mixture has formed the desired product ($\delta = 169.5$ ppm). The mixture probably also contains the hydrochloride of Pic₂PCl (18%, $\delta = 98.6$ ppm) and 9% of another

unidentified impurity. In the ^1H NMR spectrum a broad signal at 17.85 ppm is probably caused by the proton at the pyridine nitrogen and a signal at 4.45 ppm by the methylene group. The pyridine protons cause four signals at 8.75, 8.62, 8.40 and 7.84 ppm, which cannot further be assigned. The solubility of compound **3-5** was too low to obtain ^{13}C NMR data.

3.2.2 NMR data

The ^1H , ^{13}C and ^{31}P NMR chemical shifts of compounds **2-10–2-12** and **3-1–3-3** are listed in Tables 1 and 2.



N-H = 13 for ^1H NMR

Figure 2: Numbering of carbon atoms in compounds **2-10–2-12** and **3-1–3-3** for ^1H and ^{13}C NMR spectroscopic data assignments.

Table 1: ^1H NMR data of phosphines **2-10–2-12** and **3-1–3-3** in CDCl_3 . Chemical shifts δ are in ppm, coupling constants J in Hz.

δ_{H}	2-10	2-11	2-12	3-1	3-2	3-3
H2	7.45	7.45	7.45	7.54	7.56	7.55
H3	7.32	7.32	7.31	7.37	7.36	7.35
H4	7.32	7.32	7.31	7.37	7.36	7.35
H5	3.64	3.61	3.56	4.16	4.23	4.14
H7	6.98	6.74	6.58	7.46	7.13	6.88
H8	7.45	7.32	—	8.09	7.89	—
H9	7.04	6.89	6.73	7.59	7.30	7.07
H10	8.50	—	—	8.49	—	—
H11	—	2.49	2.45	—	2.86	2.79
H12	—	—	2.15	—	—	2.35
H13	—	—	—	18.25	17.65	17.22
$^3J_{\text{H7H8}}$	7.8	7.7	—	8.0	8.0	—
$^4J_{\text{H7H9}}$	2.2	—	—	—	—	—
$^5J_{\text{H7H10}}$	1.0	—	—	—	—	—
$^3J_{\text{H8H9}}$	7.5	7.6	—	6.6	7.8	—
$^4J_{\text{H8H10}}$	1.9	—	—	—	—	—
$^3J_{\text{H9H10}}$	4.9	—	—	5.2	—	—
$^6J_{\text{PH9}}$	1.1	—	—	—	—	—

In the ^1H NMR spectra of compounds **2-10–2-12** and **3-1–3-3** the signals of the phenyl protons (H2–H4) appear as two multiplets with chemical shifts between 7.31–7.37 ppm and 7.45–7.56 ppm.

Protonation of the pyridine nitrogen leads to a shift of almost all signals towards lower field. For the signals of the phenyl protons H2–H4 only a minor shift of 0.04–0.11 ppm is observed. The ^1H NMR signals of the protons at the picolyl based substituent are shifted much more, except the signal of H10 of compound **2-10** and **3-1** respectively, which is not shifted. For the signals of H7, H8, H9 and H11 the low field shift of the signals is smaller, the more methyl substituents are attached to the pyridine ring. The ^1H NMR signal of H9 of compound **2-10** resolves a long range coupling with the phosphorus atom over six bonds.

Table 2: ^{13}C and ^{31}P NMR data of phosphines **2-10–2-12** and **3-1–3-3** in CDCl_3 . Chemical shifts δ are in ppm, coupling constants J in Hz.

	2-10	2-11	2-12	3-1	3-2	3-3
δ_{P}	−9.4	−10.2	−9.7	−3.1	−3.0	−3.8
$^3J_{\text{PH2}}$	7.5	7.4	7.4	–	–	–
δ_{C}						
C1	138.3	138.4	138.5	135.0	135.3	135.5
C2	133.0	133.1	133.1	133.2	133.3	133.3
C3	128.5	128.4	128.4	129.1	129.0	128.9
C4	128.8	128.7	128.7	129.9	129.8	129.7
C5	39.0	38.8	38.7	33.6	33.2	32.8
C6	158.3	157.3	157.0	155.1	155.0	153.8
C7	123.8	120.6	121.7	127.2	124.2	124.8
C8	136.2	136.3	147.3	144.5	143.8	157.1
C9	121.1	120.6	121.6	123.9	124.4	125.0
C10	149.5	158.0	157.7	140.6	154.1	153.0
C11	–	24.6	24.4	–	19.6	19.3
C12	–	–	20.8	–	–	22.1
$^1J_{\text{PC1}}$	15.0	15.0	14.8	14.6	14.9	14.3
$^2J_{\text{PC2}}$	18.9	18.8	18.8	19.9	19.8	19.5
$^3J_{\text{PC3}}$	6.5	6.6	6.7	6.5	6.8	6.2
$^1J_{\text{PC5}}$	16.2	16.5	16.2	22.7	22.4	21.5
$^2J_{\text{PC6}}$	8.1	7.8	8.0	9.7	9.3	9.2
$^3J_{\text{PC7}}$	6.2	4.2	3.0	7.4	7.5	7.4
$^4J_{\text{PC8}}$	1.1	1.2	–	–	–	–
$^5J_{\text{PC9}}$	2.3	–	1.6	–	–	–
$^4J_{\text{PC10}}$	1.1	1.2	1.1	–	–	–

In the ^{31}P NMR spectra the chemical shifts of the signals of compounds **2-10–2-12** and **3-1–3-3** are in the range of −3.0 to −10.2 ppm, which is typical for tertiary phosphines. Protonation at the pyridine nitrogen leads to a minor shift towards lower field of 6.5–7.2 ppm. In the ^1H coupled ^{31}P NMR spectra of the non-protonated compounds **2-10–2-12** the coupling of the *ortho* phenyl protons with the phosphorus causes quintets with coupling constants of 7.4 to 7.5 Hz. The coupling with the methylene protons H5 is very small and cannot be resolved. Because of slight broadening of the signals due to the protonation no coupling can be observed in the ^1H coupled ^{31}P NMR spectra of compounds **3-1–3-3**.

In the ^{13}C NMR spectra the chemical shifts of the signals of C2–C4 are almost identical for compounds **1–3** and the corresponding protonated compounds **3-1–3-3** and are shifted towards lower field for at most 1.1 ppm. The signals of C1 are shifted towards higher field for 3.0–3.3 ppm.

The coupling constants of the signals of C1 are slightly decreased and those of the signals of C2 are increased by 0.7 to 1.0 Hz.

As observed for the signals of the ^1H NMR spectra the impact of the protonation on the chemical shifts of the NMR signals is larger for the atoms of the picolyl based moiety than of the phenyl groups. The signals of the carbon atoms in *ortho* position to the nitrogen C5, C6, C10 and C11 are shifted towards higher field, while the signals of C7, C8, C9 and C12 are shifted towards lower field. The coupling constant observed for C5 is increased by 5.9 to 6.5 Hz.

3.2.3 Crystal structures

Single crystals of **3-1**, **3-3** and **3-5** suitable for single crystal X-ray analysis were obtained by slow solvent evaporation from solutions in THF. Single crystals of **3-2** were obtained by slow diffusion of diethyl ether into a solution in dichloromethane.

Compound **3-1** crystallises in the triclinic space group *P*-1 and contains two crystallographically independent units of the hydrochloride (Figure 3).

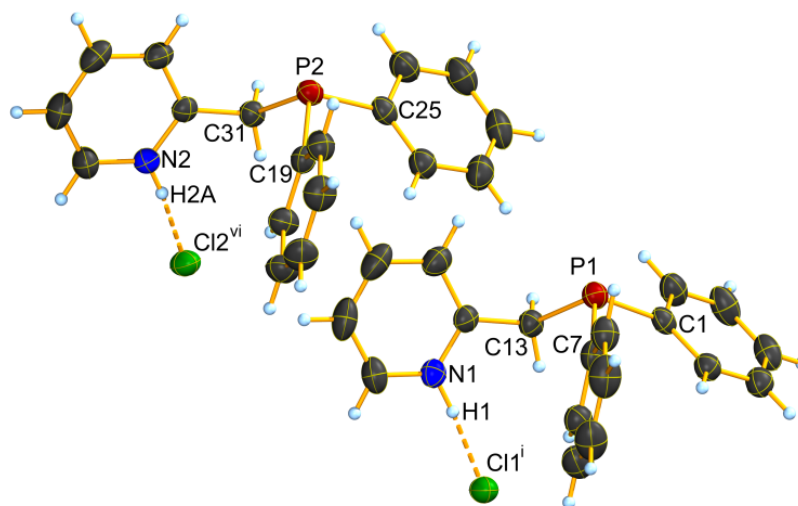


Figure 3: Molecular structure of hydrochloride **3-1**. Thermal ellipsoids are drawn at 50% probability level. Selected bond lengths [Å] and angles [°]: P1–C1: 1.835(2), P1–C7: 1.828(2), P1–C13: 1.870(2), P2–C19: 1.826(2), P2–C25: 1.835(2), P2–C31: 1.865(2), N1–H1: 0.92(2), N2–H2A: 0.83(2), H1...Cl1ⁱ: 2.12(2), H2A...Cl2^{vi}: 2.20(1), N1...Cl1ⁱ: 3.002(2), N2...Cl2^{vi}: 2.994(2), C1–P1–C7: 103.5(1), C1–P1–C13: 97.0(1), C7–P1–C13: 102.7(1), C19–P2–C25: 103.0(1), C19–P2–C31: 103.6 (1), C25–P2–C31: 98.4(1), sum of angles around P1: 303.2, sum of angles around P2: 305.0, N1–H1–Cl1ⁱ: 159.7(7), N2–H2A–Cl2^{vi}: 160.2(7). i: -x, 1-y, 1-z, vi: x, -1+y, 1+z.

Compound **3-2** crystallises in the orthorhombic space group *Pbca*. The molecular structure is shown in Figure 4.

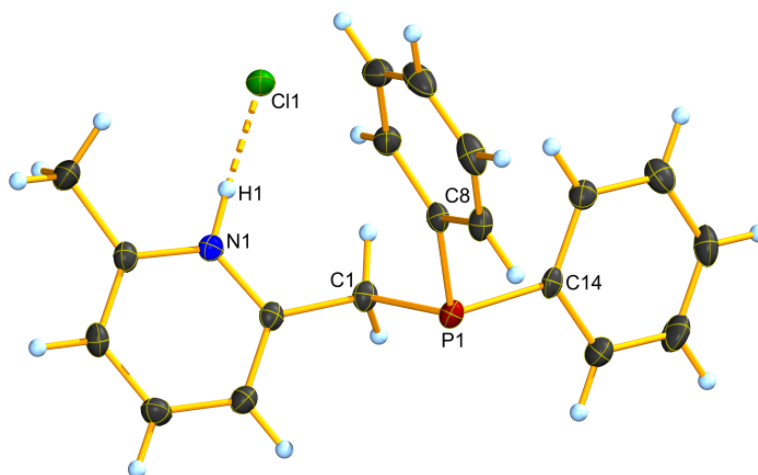


Figure 4: Molecular structure of hydrochloride **3-2**. Thermal ellipsoids are drawn at 50% probability level. Selected bond lengths [Å] and angles [°]: C1–P1: 1.868(2), P1–C8: 1.826(2), P1–C14: 1.841(2), N1–H1: 0.96(3), H1···Cl1: 2.02(2), N1···Cl1: 2.975(2), C1–P1–C8: 104.0(1), C1–P1–C14: 98.7(1), C8–P1–C14: 102.2(1), sum of angles around P1: 304.9, N1–H1–Cl1: 167(2).

Compound **3-3** crystallises in the triclinic space group *P*–1. The molecular structure is shown in Figure 5.

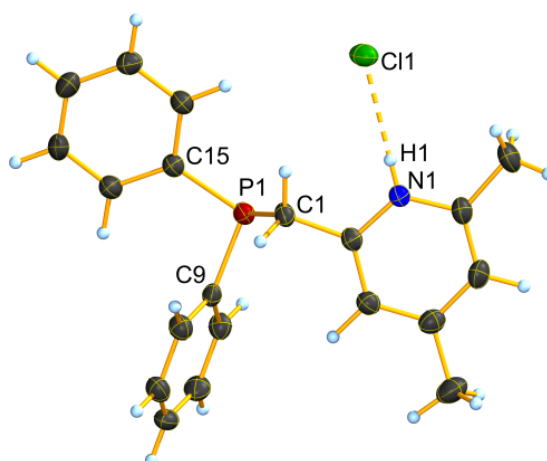


Figure 5: Molecular structure of hydrochloride **3-3**. Thermal ellipsoids are drawn at 50% probability level. Selected bond lengths [Å] and angles [°]: P1–C1: 1.864(2), P1–C9: 1.831(2), P1–C15: 1.835(2), N1–H1: 0.78(2), H1···Cl1: 2.25(2), N1···Cl1: 3.023(2), C1–P1–C9: 102.2(1), C1–P1–C15: 98.7(1), C9–P1–C15: 103.4(1), sum of angles around P1: 304.3, N1–H1–Cl1: 171(1).

The P–C_{Alk} bonds (1.870(2)–1.864(2) Å) are notably longer than the P–C_{Ar} (1.826(2)–1.841(2) Å) bonds for compounds **3-1–3-3**. The distances between the phosphorus and the aromatic carbon atoms are quite similar to the bond lengths found in triphenylphosphine, whereby the P–C distances are 1.822(5) to 1.831(5) Å.^[12] Comparing the P–C_{Alk} distances to those found in tribenzylphosphine 1.855(2) Å to 1.858(2) Å the P–C_{Alk} distances found in the structures of **3-1–3-3** are slightly longer.^[13] For compounds **3-1–3-3** the C–P–C angles are between 97.0(1) ° and 104.0(1) ° and are in a similar range as the angles of literature known phosphines.^[12–13] The corresponding angles in the structure of tribenzylphosphine are 97.7(1)–99.5(1) ° and 102.1(2)–103.6(2) ° for triphenylphosphine.^[12–13] The sums of the angles around the phosphorus atoms in compounds **3-1–3-3** are 303.2–305.0 °, which means that the molecules deviate significantly from planarity and lean more towards a pyramidal shape.

An area where the bond lengths differ quite much in the molecular structures are the N–H (0.78(2)–0.96(3) Å) and H···Cl distances (2.02(2)–2.25(2) Å). In general, the shorter the N–H distances, the longer are the H···Cl distances.

Therefore, although the N–H and H···Cl distances of **3-1**–**3-3** vary over 0.18 Å (N–H) and 0.23 Å (H···Cl), the N···Cl distances are similar for all three compounds (2.975(2)–3.023(2) Å).

For pyridine based hydrochlorides N–H distances of 0.85–0.93 Å and H···Cl distances of 2.08–2.24 Å are usual.^[14] An exception is pyridinium hydrochloride, which has a very long N–H distance of 1.14 Å and a short H···Cl distance of 1.92 Å.^[15] The N–H and H···Cl distances of compounds **3-1** and **3-2** are comparable to those found in the literature, whilst the N–H distance (0.78(2) Å) in compound **3-3** is very short with a long H···Cl distance (2.25(2) Å) respectively.

An area where compound **3-1** differs to compounds **3-2** and **3-3** is the N–H···Cl angle. The N–H···Cl angles of **3-1** (159.7(7)° and 160.2(7)°) are slightly more bent than those of compounds **3-2** and **3-3** (**3-2**: 167(2)°; **3-3**: 171(1)°).

From the crystal structure of **3-1** (Figure 6) can be seen, that the chloride ion forms a hydrogen bond with the hydrogen atom in *ortho* position to the nitrogen atom. In compounds **3-2** and **3-3** this hydrogen atom is replaced by a methyl group, which influences the hydrogen bonding of the chloride and thus the N–H···Cl angle.

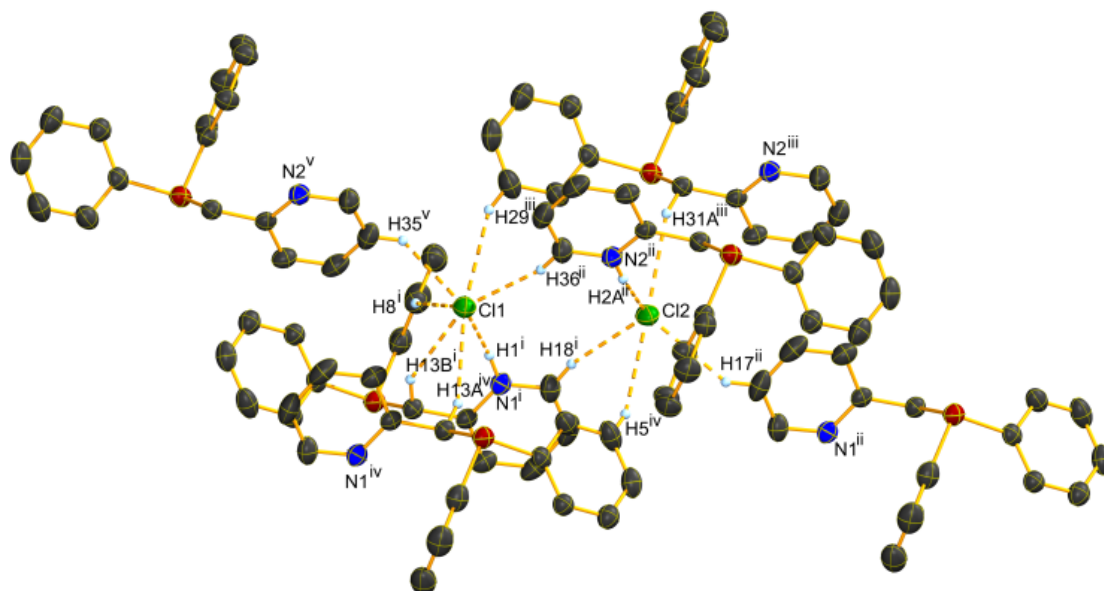


Figure 6: Hydrogen bonding in the crystal structure of **3-1**. Thermal ellipsoids are drawn at 50% probability level. H atoms not interacting with the shown Cl atoms have been omitted for clarity. Selected bond lengths [Å]: H1ⁱ···Cl1: 2.12(2), H8ⁱ···Cl1: 2.91(1), H13Bⁱ···Cl1: 2.85(1), H13A^{iv}···Cl1: 2.72(1), H29ⁱⁱⁱ···Cl1: 2.85(1), H35^v···Cl1: 2.71(2), H36ⁱⁱ···Cl1: 2.54(2), H2Aⁱⁱ···Cl2: 2.20(1), H5^{iv}···Cl2: 2.85(2), H17ⁱⁱ···Cl2: 2.75(2), H18ⁱ···Cl2: 2.64(2), H31Aⁱⁱⁱ···Cl2: 2.75(1). i: -x, 1-y, 1-z, ii: x, 1+y, -1+z, iii: 1-x, 1-y, 1-z, iv: x, y, -1+z, v: 1-x, -y, 1-z.

The crystal structures of all three hydrochlorides are strongly determined by hydrogen bonding of different H atoms to the chloride ions. The strongest hydrogen bond is the N–H···Cl interaction, but in all crystal structures several C–H···Cl hydrogen bonds can be observed. According to Aakeröy *et al.* for the discussion of the crystal structures presented in this work C–H···Cl hydrogen bonds are considered present, if the H···Cl distance is shorter than 3.0 Å and the C–H···Cl angle is larger than 90°.^[16]

In the crystal structure of **3-1** Cl1 forms hydrogen bonds with seven hydrogen atoms, while Cl2 interacts with only five H atoms. The strongest C–H···Cl interactions are between the Cl atoms and the H atoms in *ortho* position to the N atoms with H···Cl distances of 2.54(2) Å and 2.64(2) Å. The C–

H...Cl angles are 165(1)° and 163.3(9)° respectively. Through these hydrogen bonds the two molecules form dimers.

The dimers form hydrogen-bonded chains in the crystal along the *b* axis through weak interactions of the Cl atoms with H atoms of the methylene groups, the H atoms in *meta* position at the phenyl rings and the H atoms in *meta* position to the N atoms of the pyridine rings (Figure 7). The H...Cl distances are between 2.71(2) Å and 2.91(1) Å and the C–H...Cl angles are 135.8(5)–157(1)°.

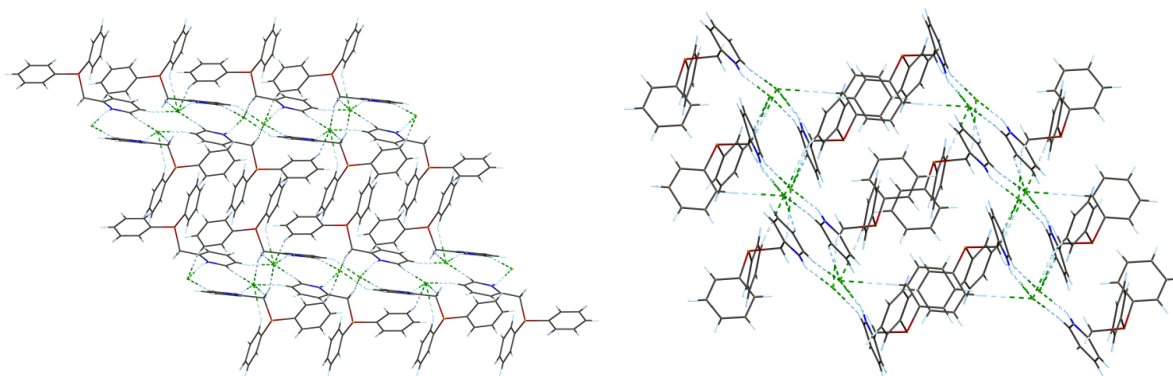


Figure 7: Crystal structure of **3-1**. View along the *a* axis (left) and *b* axis (right).

The chloride ion of compound **3-2** forms one strong hydrogen bond with the H atom at the pyridine nitrogen and six weak hydrogen bonds to carbon bonded H atoms (Figure 8).

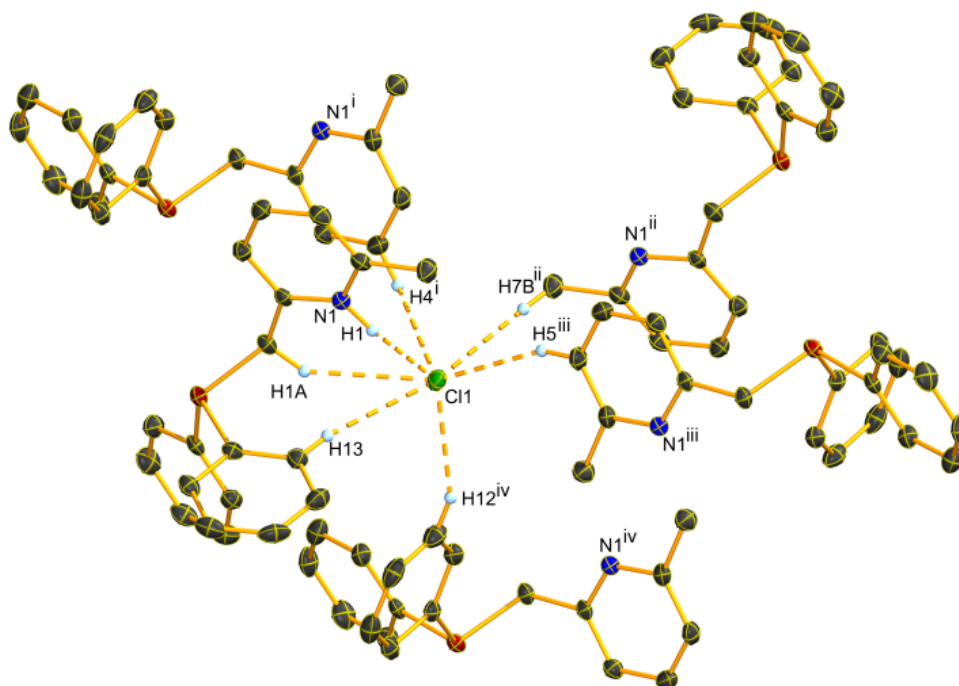


Figure 8: Hydrogen bonding in the crystal structure of **3-2**. Thermal ellipsoids are drawn at 50% probability level. H atoms not interacting with the shown Cl atom have been omitted for clarity. Selected bond lengths [Å]: H1...Cl1: 2.02(2), H1A...Cl1: 2.83(1), H4ⁱ...Cl1: 2.85(1), H5ⁱⁱⁱ...Cl1: 2.69(1), H7Bⁱⁱ...Cl1: 2.76(1), H12^{iv}...Cl1: 2.70(1), H13...Cl1: 2.85(1). i: 0.5–*x*, 0.5+*y*, *z*, ii: 1–*x*, 1–*y*, 1–*z*, iii: 0.5+*x*, 0.5–*y*, 1–*z*, iv: 1.5–*x*, 0.5+*y*, *z*.

The H...Cl distances of the C–H...Cl hydrogen bonds are between 2.69(1) Å and 2.85(1) Å and the C–H...Cl angles are 137.5(1)–174.8(1)°.

Through these weak hydrogen bonding interactions a three-dimensional network is formed in the crystal structure (Figure 9).

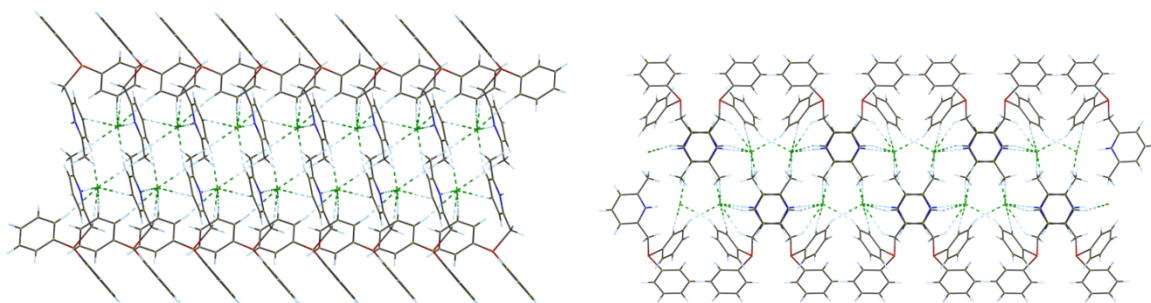


Figure 9: Crystal structure of **3-2**. View along the *a* axis (left) and *b* axis (right).

The chloride ion of compound **3-3** forms hydrogen bonds with the H atom at the pyridine nitrogen and five carbon bonded H atoms (Figure 10).

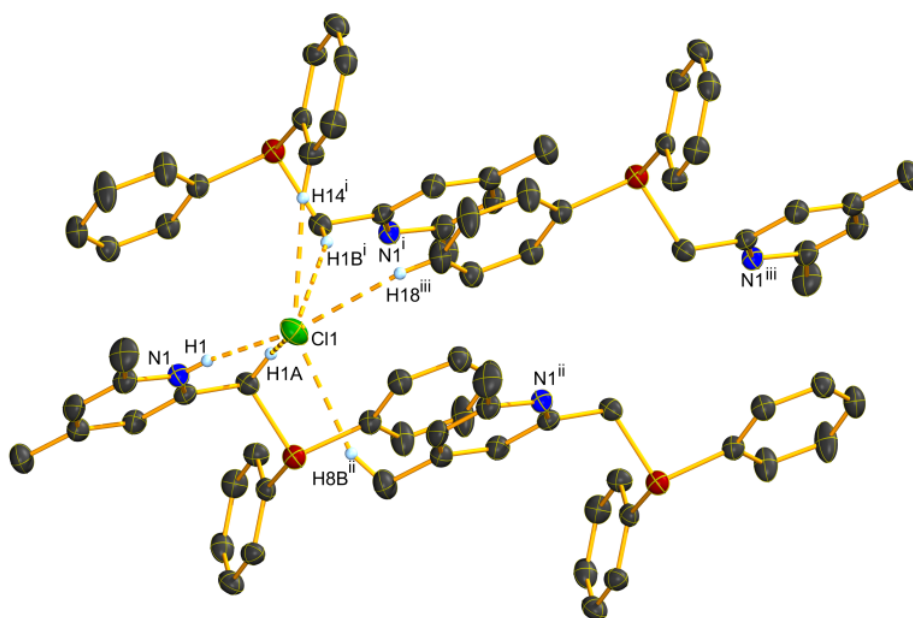


Figure 10: Hydrogen bonding in the crystal structure of **3-3**. Thermal ellipsoids are drawn at 50% probability level. H atoms not interacting with the shown Cl atom have been omitted for clarity. Selected bond lengths [Å]: H1 \cdots Cl1: 2.25(2), H1A \cdots Cl1: 2.96(1), H1B \cdots Cl1: 2.88(1), H8B \cdots Cl1: 2.89(2), H14 \cdots Cl1: 2.86(2), H18 \cdots Cl1: 2.93(1). i: 1-*x*, 1-*y*, 1-*z*, ii: -1+*x*, *y*, *z*, iii: -*x*, 1-*y*, 1-*z*.

The H \cdots Cl distances of the C-H \cdots Cl hydrogen bonds are between 2.86(1) Å and 2.96(1) Å and the C-H \cdots Cl angles are 135.9(6)–173(1) °.

Through these weak hydrogen bonding interactions a three-dimensional network is formed in the crystal structure (Figure 11).

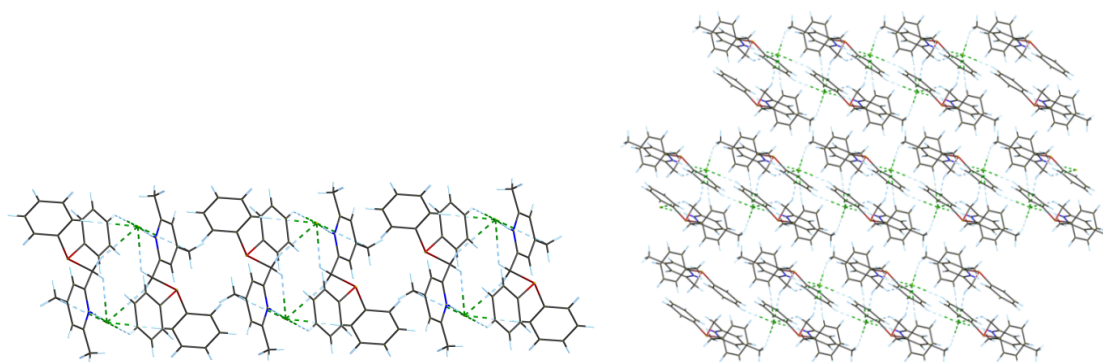


Figure 11: Crystal structure of **3-3**. View along the *a* axis (left) and *c* axis (right).

Compound **3-5** crystallises in the triclinic space group *P*-1. The molecular structure is shown in Figure 12.

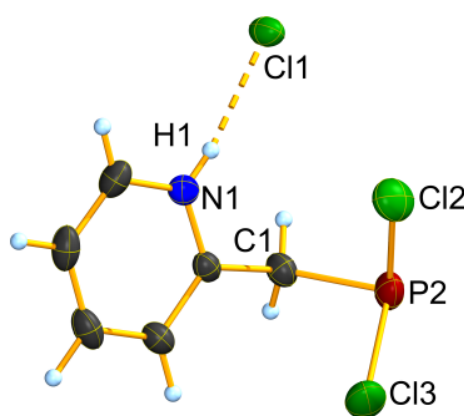


Figure 12: Molecular structure of **3-5**. Thermal ellipsoids are drawn at 50 % probability level. Selected bond lengths [Å] and angles [°]: P1–C1: 1.837(2), P1–Cl2: 2.043(1), P1–Cl3: 2.055(1), N1–H1: 0.78(2), H1···Cl1: 2.26(2), N1···Cl1: 3.015(2), C1–P1–Cl2: 100.3(1), C1–P1–Cl3: 100.6(1), Cl2–P1–Cl3: 100.9(1), sum of angles around P1: 301.8, N1–H1–Cl1: 166(1).

The lengths of the P–Cl bonds differ slightly (2.043(1) Å and 2.055(1) Å and fit well to P–Cl distances found in the structures of other dichlorophosphines (2.053(1)–2.087(1) Å).^[17]

The N–H, H···Cl and N···Cl distances in the structure of **3-5** are very similar to those found for compound **3-3**.

The geometry at the phosphorus atom features a quite pyramidal shape, with the angles summing up to 301.8°. The three angles are all in the same range between 100.3(1)° and 100.9(1)°. The N–H···Cl angle (166(1)°) deviates slightly from 180°.

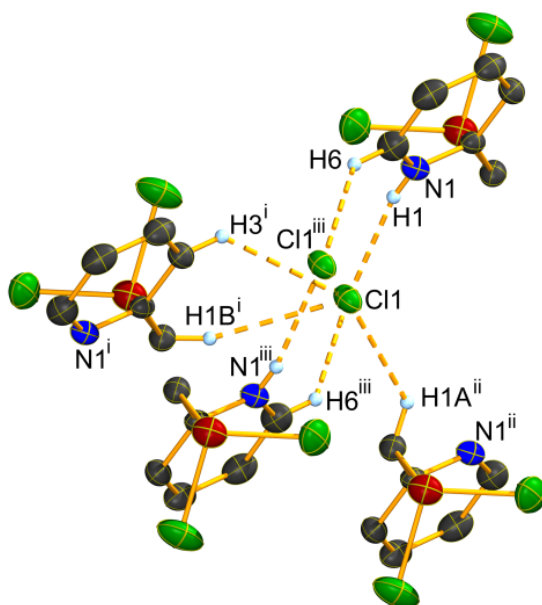


Figure 13: Hydrogen bonding in the crystal structure of **3-5**. Thermal ellipsoids are drawn at 50% probability level. H atoms not interacting with the shown Cl1 atom have been omitted for clarity. Selected bond lengths [Å]: H1 \cdots Cl1: 2.26(2), H1A $^{ii}\cdots$ Cl1: 2.88(1), H1B $^i\cdots$ Cl1: 2.75(1), H3 $^i\cdots$ Cl1: 2.94(1), H6 $^{iii}\cdots$ Cl1: 2.76(2). i: $-1+x, y, z$, ii: $1-x, -y, 2-z$, iii: $-x, 1-y, 2-z$.

As observed in the crystal structure of compound **3-1** the molecules form hydrogen bonded dimers with each chloride anion interacting with the *ortho* pyridine hydrogen atom of the opposite molecule (Figure 13). Through another three C–H \cdots Cl hydrogen bonds these dimers form layers in the crystal along the *ab* plane. In these layers two of the pyridine rings are stacked above each other, with the attached CH₂PCl₂ moieties pointing away to opposite directions (Figure 14).

This arrangement is favoured probably because of π – π stacking interactions between the pyridine rings in a slipped conformation. The distance between the centres of the rings is 3.638(1) Å with an angle of 0.0(1) ° of the planes through the rings to each other. The distance is within the range in which non-covalent interactions between π -systems in a face-to-face conformation can be found (3.3–3.8 Å).^[18]

In the π – π stacking the pyridine rings are arranged antiparallel. This conformation is favoured probably due to the dipole moment of the pyridine rings.

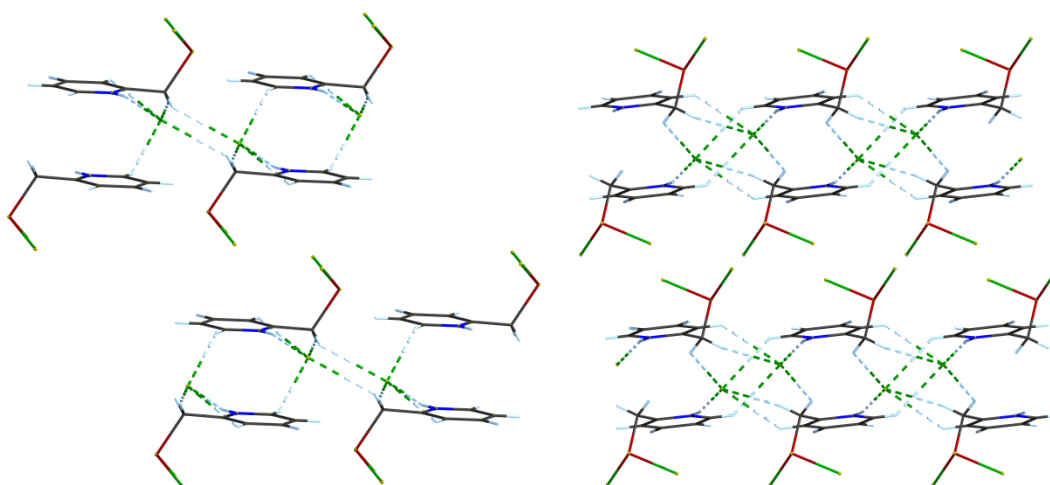


Figure 14: Crystal structure of **3-5**. View along the *a* axis (left) and *b* axis (right).

3.2.4 DFT calculations

Both chemical properties and reactivity are known to depend on the nature and energy of the frontier orbitals present in a molecule.^[19] Specifically, for compounds **2-10–2-12**, examination of these orbitals can give insight into the chemical differences between the phosphorus and nitrogen present in the ligands (both of which have potential to act as nucleophiles and bases). It will also allow investigation of the influence the methyl groups, present in **2-11** and **2-12** have on the electronic properties of the ligands.

Geometry optimisation of compounds **2-10–2-12** and the all carbon analogue benzyldiphenylphosphine (BnPPh₂, Figure 16) was carried out using density functional calculations, with the B3LYP functional and 6-31G* basis set.^[20] Optimisation was considered complete when there was an absence of negative frequencies in the vibrational spectra. From this, the nature and energy of the HOMO, LUMO, and several other molecular orbitals for compounds **2-10–2-12** and BnPPh₂ were identified. The percentage contributions of atoms or groups to molecular orbitals were calculated using the approach outlined by *La Porta et. al.* and were confirmed using the Chemissian package.^[21]

The first thing that is clear from these calculations is that there is very little variation in both the composition and energy of the frontier orbitals present in compounds **2-10–2-12** (Figure 15). They are also very close in energy to BnPPh₂ (HOMO and LUMO energies of -5.85 eV and -0.47 eV respectively) suggesting that the presence of nitrogen has little to no effect on the HOMO/LUMO energy.

The HOMO is localised on the PPh₂ unit present in **2-10–2-12** (88–90% of the orbital localised on PPh₂), with very little incorporation of the pyridine ring. This is comparable to that observed in BnPPh₂ (Figure 16) but differs from the distribution of, previously reported, PPh₃ in which the HOMO is spread across all three rings.^[22] This may suggest that the presence of the saturated methylene spacer prevents delocalisation of the phosphorus lone pair into the pyridine ring.

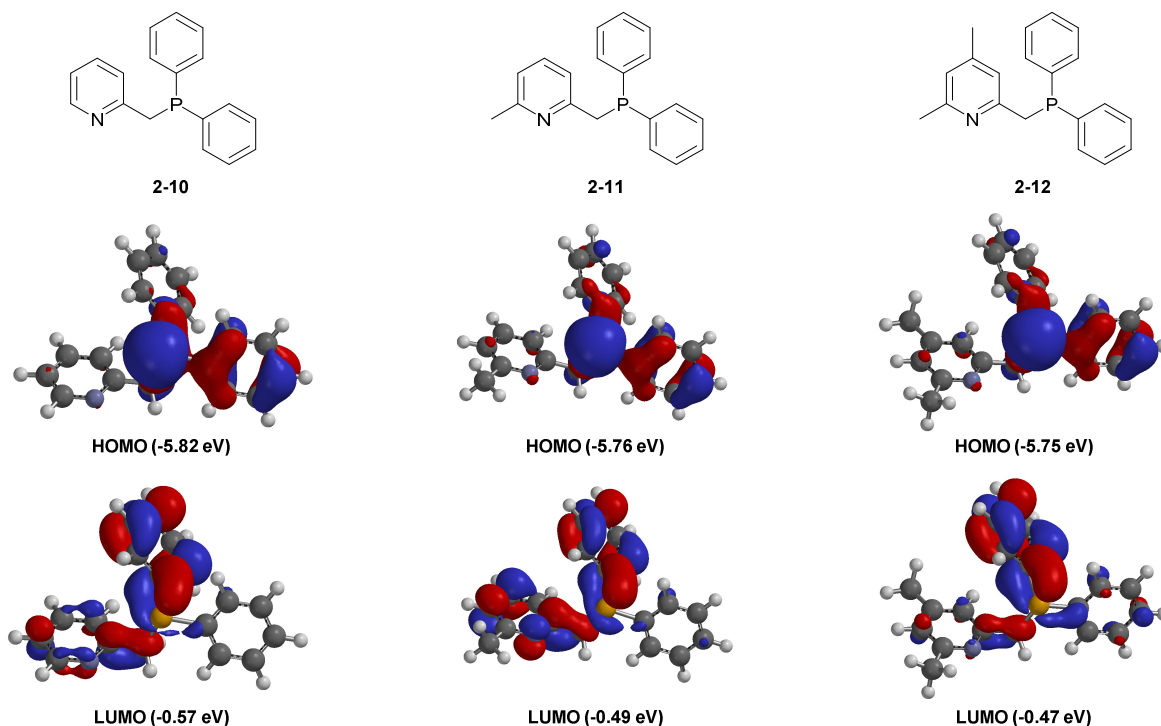


Figure 15: Frontier orbitals and their respective energies for compounds **2-10–2-12**. The orbitals and energies were generated using the Spartan 14 software package using Density Functional Theory, B3LYP functional, and 6-31G* basis set.

The presence of the methyl groups in **2-11** and **2-12** has very little effect on the distribution or energy of the HOMO. This is likely because the N-heterocycle, on which the methyl groups are added, is not incorporated into the HOMO.

There is more variation in the nature of the LUMO across the series (Figure 15). The LUMOs all contain significant contribution from one phenyl ring and the phosphorus atom (50–72% localised on PPh). However, they vary in the level of incorporation of the pyridine ring, with 33% of the LUMO localised on the N-heterocycle for **2-11**, compared to 13% for **2-10** and 6% for **2-12**. The LUMOs of compounds **2-10–2-12** also differ significantly from the LUMO of BnPPH₂ (Figure 16), in which the LUMO spreads across the PPh₂ unit.

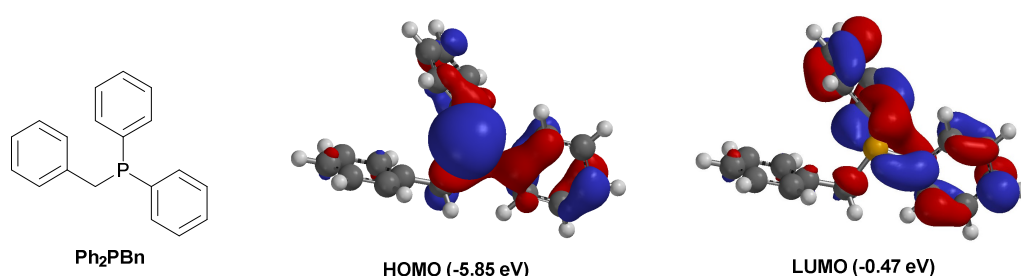


Figure 16: Molecular orbital diagrams for the HOMO and LUMO of Ph₂PBn and their respective energies.

It is apparent that the HOMOs of compounds **2-10–2-12** do not contain significant contribution from the nitrogen lone pair. This means that information about the reactivity of this lone pair, which is important when considering protonation or metal coordination, cannot be obtained by examining the HOMO. Therefore, it follows that there is another molecular orbital responsible for reaction at nitrogen.

The idea of expanding the set of frontier orbitals beyond simply the HOMO and LUMO is not uncommon for compounds containing more than one reactive site. In these systems additional molecular orbitals can be used to gain insight into the reactivity present at additional reactive sites. Previously these orbitals have been referred to as frontier effective-for-reaction molecular orbitals (FERMOs),^[23] but in this work the term HOMO_N will be used for the highest occupied molecular orbital that can be used to describe the reactivity of the nitrogen lone pair.

The molecular orbital that controls reaction at nitrogen should be localised on nitrogen, at least to some degree, and have the appropriate shape for reaction. Analysis of the next highest occupied molecular orbitals in **2-10–2-12** (i.e. HOMO–1 to HOMO–5) reveals that the HOMO–3 for **2-10** and HOMO–2 for **2-11** and **2-12** contain nitrogen character of 43, 56, and 58% for compounds **2-10**, **2-11**, and **2-12** respectively. Furthermore, they contain significant nitrogen p-character which is typical of the nitrogen lone pair (Figure 17). This suggests that these molecular orbitals are much more suitable for describing reactions at nitrogen in these systems (HOMO_N).

Analysis of the energies of these orbitals shows a small rise in the energy of the HOMO_N as the methyl groups are added, which is expected as these groups are electron-donating. Furthermore, this rise in energy may be the reason the HOMO_N moves from HOMO–3 in **2-10** to HOMO–2 in **2-11** and **2-12**.

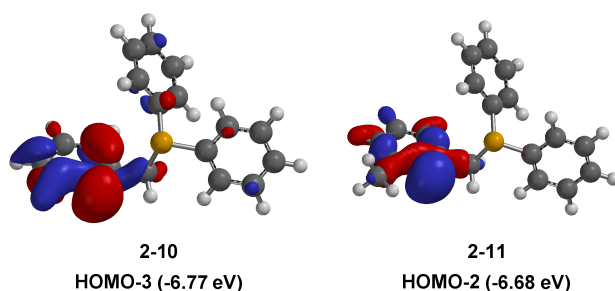


Figure 17: Molecular orbital diagrams showing HOMO-3 for compound **2-10** and HOMO-2 for compound **2-11**. These orbitals contain significant contribution from nitrogen.

By expanding the range of frontier orbitals to include the HOMO, LUMO and HOMO_N (either HOMO-2 or HOMO-3) we have a better picture of the electronics of our systems and the influence of incorporation of methyl groups. The HOMO is 0.85–0.95 eV higher in energy than the HOMO_N for compounds **2-10–2-12**. This is consistent with the lower electronegativity of phosphorus compared to nitrogen, which results in a higher energy lone pair. Additionally, this energy difference can also be used to describe the difference in hardness between the sites.^[23] The absolute hardness (η) of a compound/site is given by:

$$\eta = \frac{E_{LUMO} - E_{HOMO}}{2}$$

Harder compounds have larger HOMO–LUMO gaps and, therefore, higher values of η .^[23a] For compounds **2-10–2-12**, the average values are $\eta_P = 2.63(\pm 0.01)$ eV and $\eta_N = 3.09(\pm 0.02)$ eV, where η_P and η_N represent the absolute hardness of P and N respectively. This is consistent with nitrogen being the harder site and may explain why, for example, it is the N-heterocycle that is protonated in the reactions with HCl (H^+ is a hard cation) rather than the phosphorus.

A full computational study in the protonation of **2-10–2-12** would be required to determine whether protonation occurs directly at the nitrogen atom, and therefore implying the use of the HOMO_N, or if compounds **3-1–3-3** are a result of initial protonation at the phosphorus atom followed by rearrangement. However, given that the molecular orbital analysis supports the formation of a *N*-protonated species, which is what was observed experimentally, a full mechanistic study is beyond the scope of this work.

3.3 Summary

Through synthesis of the corresponding hydrochlorides of four picolylphosphine derivatives it has been possible to learn and understand about the unknown structures and geometries of the phosphines.

Compounds **2-10–2-12** and **3-1–3-3** have been fully characterised by 1H , ^{13}C and ^{31}P NMR spectroscopy.

The higher conformational stability given by the hydrochloride enhances the ability of the molecule to crystallise, allowing the structure to be measured and ultimately providing interesting information as to the details of the molecular make-up. The crystal structures of the hydrochlorides **3-1–3-3** and **3-5** are strongly determined by the hydrogen bonds formed by the chloride anions.

Theoretical investigations of phosphines **2-10–2-12** have shown that the HOMO strongly influences the reactivity at the phosphorus atom, while the reactivity of the nitrogen atom is determined by molecular orbitals of lower energy (HOMO-3 and HOMO-2 respectively).

3.4 Experimental

For general information about methods and analytical instruments used see 2.4.1

3.4.1 DFT calculations

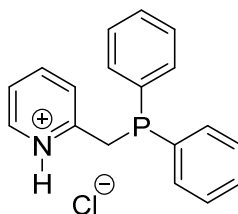
Optimised geometries of the compounds were calculated at the DFT level of theory, with the B3LYP functional and 6-31G* basis set, using the Spartan 14 program.^[24] Optimisation was considered complete when there was an absence of negativity frequencies in the vibrational spectrum. All molecular orbitals were visualised using the Spartan 14 program.^[24] Orbital compositions were calculated using the formula given below, where $\sum \phi_X^2$ is the sum of the squares of the eigenvalues associated with the atomic orbitals of X and $\sum \phi_{all}^2$ is the sum of the squares of the eigenvalues of all atomic orbitals contributing to that molecular orbital, and were confirmed using the Chemissian software package.^[21a, 25]

$$\% \text{ Character of } X = \frac{\sum \phi_X^2}{\sum \phi_{all}^2} \times 100$$

3.4.2 Syntheses

For syntheses and analytical data of **2-10-2-12** see 2.4.2.

3.4.2.1 2-((Diphenylphosphino)methyl)pyridine-1-ium chloride **3-1**.



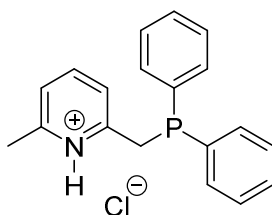
Compound **2-10** (2.8 g, 10 mmol, 1 eq) was dissolved in THF (10 mL) and HCl (37% in H₂O, 0.83 mL, 10 mmol, 1 eq) was added. The reaction mixture was stirred for 1 h at room temperature. The product formed a precipitate, which was separated by filtration and dried under vacuum. The product was obtained as colourless solid (2.3 g, 7.3 mmol, 73%).

¹H NMR data are listed in Table 1, ¹³C and ³¹P NMR data in Table 2.

EA: Found: C, 66.9; H, 5.7; N, 4.1. Calc. for C₁₈H₁₇ClNP: C, 68.9; H, 5.5%; N, 4.5%.

m/z (ESI) [%]: 278.10944 (23), 200.06254 (2), 150.12783 (13), 98.03541 (1).

3.4.2.2 2-((Diphenylphosphino)methyl)-6-methylpyridine-1-ium chloride **3-2**.



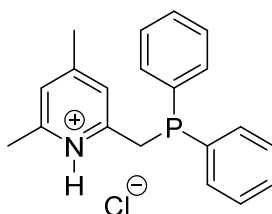
Compound **3-2** was synthesised in the same manner as **3-1** using **2-11** (1.1 g, 3.6 mmol, 1 eq) and HCl (37% in H₂O, 0.30 mL, 3.6 mmol, 1 eq). The product was obtained as colourless solid (2.7 g, 8.2 mmol, 82%).

¹H NMR data are listed in Table 1, ¹³C and ³¹P NMR data in Table 2.

EA: Found: C, 68.15; H, 5.8; N, 4.1. Calc. for C₁₉H₁₉NPCL: C, 69.6; H, 5.8; N, 4.3%.

m/z (ESI) [%]: 292.12484 (100), 214.07804 (9), 130.15908 (1).

3.4.2.3 2-((Diphenylphosphino)methyl)-4,6-dimethylpyridine-1-ium chloride **3-3**.



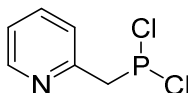
Compound **3-3** was synthesised in the same manner as **3-1** using **2-12** (3.1 g, 10 mmol, 1 eq) and HCl (37% in H₂O, 0.83 mL, 10 mmol, 1 eq). The product was obtained as colourless solid (2.9 g, 8.5 mmol, 85%).

¹H NMR data are listed in Table 1, ¹³C and ³¹P NMR data in Table 2.

EA: Found: C, 70.2; H, 6.3; N, 4.1. Calc. for C₂₀H₂₁NPCL: C, 70.3; H, 6.2; N, 4.1%.

m/z (ESI) [%]: 306.14078 (11), 152.07071 (1).

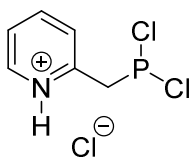
3.4.2.4 (Pyridin-2-ylmethyl)dichlorophosphine **3-4**.



PCl₃ (0.87 mL, 10 mmol, 1 eq) was dissolved in anhydrous THF (10 mL) and cooled to -78°C. 2-((Trimethylsilyl)methyl)pyridine (1.7 g, 10 mmol, 1 eq) was added dropwise and the reaction mixture was left to warm to room temperature overnight.

³¹P NMR (109 MHz, THF): δ = 183.6 (²J_{PH} = 13.1 Hz).

3.4.2.5 2-((Dichloro-phosphino)methyl)-pyridin-1-ium chloride 3-5.



To the solution of compound **3-4** HCl (2.0 M in Et₂O, 5.0 mL, 10 mmol, 1 eq) was added and stirred for 1 h at room temperature. The product formed a precipitate, which was separated by filtration and dried under vacuum. The resulting pale yellow solid (0.84 g) contained the product **3-5** in a purity of 73%.

³¹P NMR (162 MHz, CDCl₃): δ = 169.5.

3.4.3 Molecular Orbital Contributions

Table 3: Percentage contributions of both phosphorus and nitrogen to the 6 highest occupied molecular orbitals of compounds **2-10–2-12** and Ph₂PBn. The percentage contributions were calculated using the approaches outlined by La Porta *et al.* and were confirmed using the Chemissian software package.^[21a, 25] The numbers highlighted show the respective orbitals P/N contribute most to in each compound.

	Ph ₂ PPic		Ph ₂ PLut		Ph ₂ PCol		Ph ₂ PBn	
	%P	%N	%P	%N	%P	%N	%P	%N
HOMO	49%	0%	49%	1%	49%	1%	49%	N/A
HOMO-1	8%	6%	7%	0%	7%	0%	10%	N/A
HOMO-2	2%	19%	1%	56%	1%	58%	1%	N/A
HOMO-3	1%	43%	2%	0%	2%	0%	2%	N/A
HOMO-4	4%	0%	1%	2%	2%	6%	1%	N/A
HOMO-5	2%	7%	4%	2%	3%	2%	4%	N/A

3.4.4 Crystallographic data

Table 4: Crystallographic data of **3-1–3-3** and **3-5**.

	3-1	3-2	3-3	3-5
Identification code	mx006	wv538	lx573	mx049
Empirical formula	C ₁₈ H ₁₇ ClNP	C ₁₉ H ₁₉ ClNP	C ₂₀ H ₂₁ ClNP	C ₆ H ₇ Cl ₃ NP
Formula weight [g·mol ⁻¹]	313.74	327.77	341.80	230.45
Temperature [K]	173(2)	143(2)	173(2)	173(2)
Crystal size [mm ³]	0.20× 0.25× 0.35	0.02× 0.02× 0.08	0.10× 0.15× 0.20	0.10× 0.15× 0.20
Colour, shape	Colourless block	Colourless rod	Colourless block	Colourless block
Crystal system	Triclinic	Orthorhombic	Triclinic	Triclinic
Space group	<i>P</i> –1	<i>Pbca</i>	<i>P</i> –1	<i>P</i> –1
<i>a</i> [Å]	11.3434(5)	11.2194(3)	8.3366(7)	7.0252(4)
<i>b</i> [Å]	12.8823(5)	8.0120(2)	10.4295(8)	8.2249(6)
<i>c</i> [Å]	12.9619(5)	38.1816(10)	11.1284(10)	9.5689(6)
α [°]	62.779(4)	90	102.643(7)	72.668(6)
β [°]	81.518(3)	90	105.496(8)	77.134(5)
γ [°]	85.686(3)	90	96.248(7)	65.783(6)
<i>V</i> [Å ³]	1665.85(13)	3432.14(15)	895.28(14)	478.14(6)
<i>Z</i>	4	8	2	2
ρ_{calc} [g·cm ⁻³]	1.251	1.269	1.268	1.601
Radiation [Å]	MoK α = 0.71073	MoK α = 0.71073	MoK α = 0.71073	MoK α = 0.71073
μ [cm ⁻¹]	0.318	0.312	0.302	1.061
<i>F</i> (000)	656	1376	360	232
Index ranges	–16 ≤ <i>h</i> ≤ 16 –18 ≤ <i>k</i> ≤ 18 –18 ≤ <i>l</i> ≤ 18	–13 ≤ <i>h</i> ≤ 13 –9 ≤ <i>k</i> ≤ 9 –47 ≤ <i>l</i> ≤ 47	–11 ≤ <i>h</i> ≤ 11 –14 ≤ <i>k</i> ≤ 14 –14 ≤ <i>l</i> ≤ 15	–10 ≤ <i>h</i> ≤ 10 –11 ≤ <i>k</i> ≤ 11 –13 ≤ <i>l</i> ≤ 13
θ range [°]	4.203 ≤ θ ≤ 30.508	3.170 ≤ θ ≤ 26.018	4.414 ≤ θ ≤ 30.505	4.118 ≤ θ ≤ 30.507
Reflections collected	33930	30280	9372	9371
Independent reflections	10123	3327	5419	2890
Observed reflections	7178	2750	3680	2264
Data/restraints/parameters	10123/0/411	3327/0/204	5419/0/226	2890/0/105
<i>R</i> _{int}	0.0360	0.0536	0.0363	0.0297
<i>R</i> ₁ , <i>wR</i> ₂ [<i>I</i> > 2 σ (<i>I</i>)]	0.0446, 0.1032	0.0389, 0.0864	0.0518, 0.1103	0.0377, 0.0892
<i>R</i> ₁ , <i>wR</i> ₂ [all data]	0.0710, 0.1204	0.0506, 0.0920	0.0880, 0.1320	0.0535, 0.0987
GooF	1.029	1.055	1.031	1.024
$\delta\rho_{\text{max}}$, $\delta\rho_{\text{min}}$ [e·nm ⁻³]	0.623, –0.230	0.892, –0.216	0.640, –0.292	0.462, –0.319

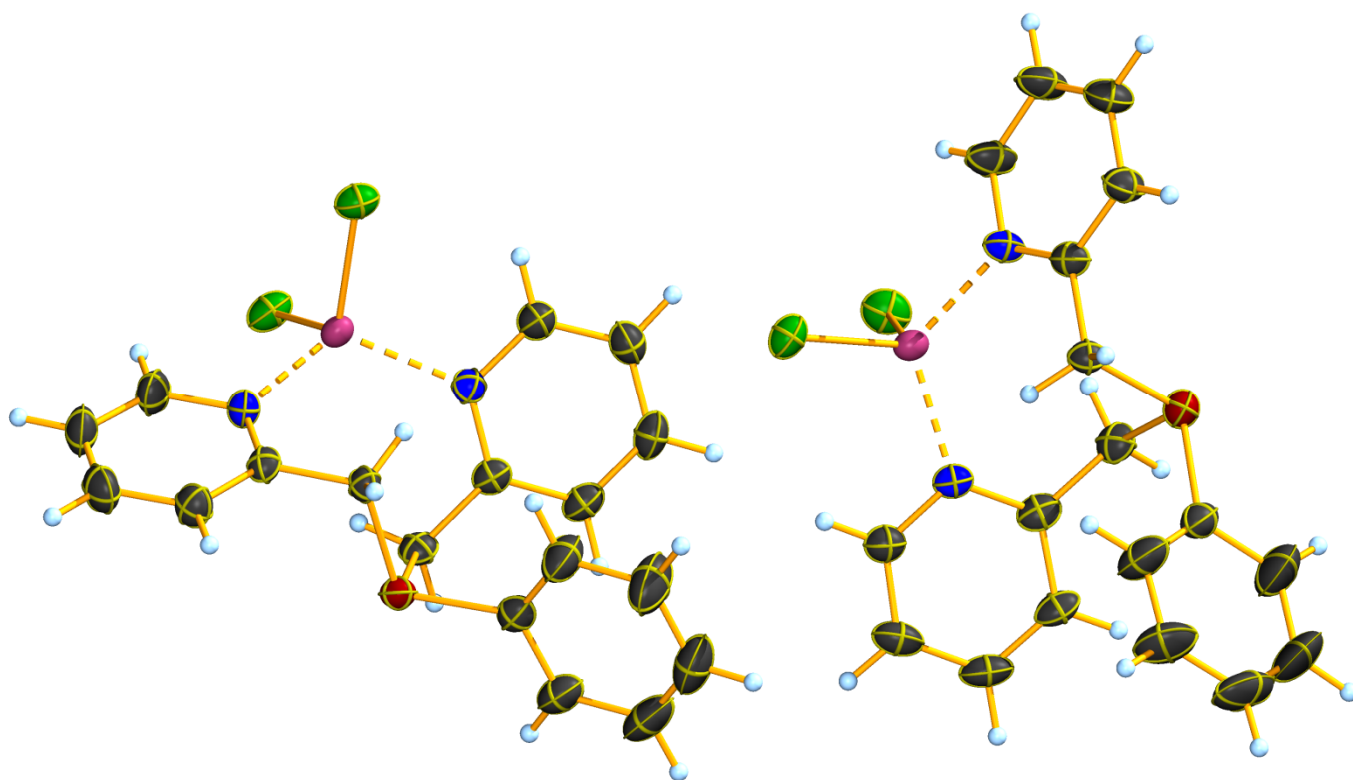
3.5 References

- [1] a) M. P. Carroll, P. J. Guiry, *Chem. Soc. Rev.* **2014**, 43, 819-833; b) C. Hettstedt, M. Unglert, R. J. Mayer, A. Frank, K. Karaghiosoff, *Eur. J. Inorg. Chem.* **2016**, 2016, 1405-1414; c) V. Vasilenko, T. Roth, C. K. Blasius, S. N. Intorp, H. Wadepohl, L. H. Gade, *Beilstein J. Org. Chem.* **2016**, 12, 846-853; d) B. V. Rokade, P. J. Guiry, *ACS Catal.* **2017**, 8, 624-643.
- [2] a) D. Benito-Garagorri, W. Lackner-Warton, C. M. Standfest-Hauser, K. Mereiter, K. Kirchner, *Inorg. Chim. Acta* **2010**, 363, 3674-3679; b) M. Melník, P. Mikuš, *J. Organomet. Chem.* **2017**, 828, 30-37; c) K. Wajda-Hermanowicz, A. Kochel, R. Wróbel, *J. Organomet. Chem.* **2018**, 860, 30-48; d) C. Braun, M. Nieger, S. Bräse, *Chem. Eur. J.* **2017**, 23, 16452-16455; e) B. Choubey, P. S. Prasad, J. T. Mague, M. S. Balakrishna, *Eur. J. Inorg. Chem.* **2018**, 2018, 1707-1714; f) M. K. Rong, F. Holtrop, J. C. Slootweg, K. Lammertsma, *Coord. Chem. Rev.* **2019**, 382, 57-68.
- [3] a) S. F. Zhu, Q. L. Zhou, *Acc. Chem. Res.* **2017**, 50, 988-1001; b) F. Speiser, P. Braunstein, L. Saussine, *Acc. Chem. Res.* **2005**, 38, 784-793; c) S.-Y. Liu, L.-Y. Xu, C.-Y. Liu, Z.-G. Ren, D. J. Young, J.-P. Lang, *Tetrahedron* **2017**, 73, 2374-2381; d) S. Hameury, C. Gourlaouen, M. Sommer, *Polym. Chem.* **2018**, 9, 3398-3405; e) M. Valero, D. Becker, K. Jess, R. Weck, J. Atzrodt, T. Bannenberg, V. Derdau, M. Tamm, *Chem. Eur. J.* **2019**, 25, 6517-6522; f) W. I. Lai, M. P. Leung, P. Y. Choy, F. Y. Kwong, *Synthesis* **2019**, 51, 2678-2686.
- [4] a) D. M. Zink, T. Baumann, J. Friedrichs, M. Nieger, S. Bräse, *Inorg. Chem.* **2013**, 52, 13509-13520; b) B. Carlson, B. E. Eichinger, W. Kaminsky, G. D. Phelan, *J. Phys. Chem. C* **2008**, 112, 7858-7865; c) Q. M. Zhu, L. Song, W. X. Chai, H. Y. Shen, Q. H. Wei, L. S. Qin, *Acta Crystallogr. C Struct. Chem.* **2018**, 74, 62-68.
- [5] a) E. Essoun, R. Wang, M. A. S. Aquino, *Inorg. Chim. Acta* **2017**, 454, 97-106; b) I. Angurell, E. Puig, O. Rossell, M. Seco, P. Gómez-Sal, A. Martín, *J. Organomet. Chem.* **2012**, 716, 120-128.
- [6] F. Hung-Low, K. K. Klausmeyer, *Inorg. Chim. Acta* **2008**, 361, 1298-1310.
- [7] a) E. Uhlig, M. Schaefer, *Z. Anorg. Allg. Chem.* **1968**, 359, 67-77; b) A. Murso, D. Stalke, *Dalton Trans.* **2004**, 2563-2569; c) C. Dubs, T. Yamamoto, A. Inagaki, M. Akita, *Chem. Commun.* **2006**, 1962-1964; d) J. T. Mague, S. W. Hawbaker, *J. Chem. Crystallogr.* **1997**, 27, 603-608.
- [8] a) W. V. Dahlhoff, T. R. Dick, S. M. Nelson, *J. Chem. Soc. A* **1969**, 2919-2923; b) C.-H. Lin, V. N. Nesterov, M. G. Richmond, *J. Organomet. Chem.* **2013**, 744, 24-34.
- [9] W. J. Knebel, R. J. Angelici, *Inorg. Chim. Acta* **1973**, 7, 713-716.
- [10] A. Kermagoret, P. Braunstein, *Organometallics* **2008**, 27, 88-99.
- [11] C. Hettstedt, PhD thesis, Ludwig-Maximilians-Universität München, **2015**.
- [12] J. J. Daly, *J. Chem. Soc.* **1964**, 3799-3810.
- [13] W. Levason, D. Pugh, G. Reid, *Acta Crystallogr. C* **2013**, 69, 560-564.
- [14] a) S. Ma, M. Chen, F.-F. Fan, A.-Q. Jia, Q.-F. Zhang, *J. Chem. Crystallogr.* **2018**, 48, 64-71; b) N. Lu, R. J. Wei, K. Y. Lin, M. Alagesan, Y. S. Wen, L. K. Liu, *Acta Crystallogr. C Struct. Chem.* **2017**, 73, 343-349; c) S. M. Fellows, T. J. Prior, *Acta Crystallogr. E Crystallogr. Commun.* **2016**, 72, 436-439; d) Effendy, P. C. Junk, C. J. Kepert, L. M. Louis, T. C. Morien, B. W. Skelton, A. H. White, *Z. anorg. allg. Chem.* **2006**, 632, 1312-1325; e) M. Mastalir, M. Schroffenegger, B. Stoger, M. Weil, K. Kirchner, *Acta Crystallogr. E Crystallogr. Commun.* **2016**, 72, 331-333; f) G. M. de Lima, J. L. Wardell, R. A. Howie, S. M. S. V. Wardell, *J. Chem. Crystallogr.* **2012**, 43, 36-43.
- [15] D. Mootz, J. Hocken, *Z. Naturforsch., B: Chem. Sci.* **1989**, 44, 1239-1246.
- [16] C. B. Aakeröy, T. A. Evans, K. R. Seddon, I. Palinko, *New J. Chem.* **1999**, 23, 145-152.
- [17] a) H. Klöcker, M. Layh, A. Hepp, W. Uhl, *Dalton Trans.* **2016**, 45, 2031-2043; b) A. Orthaber, F. Belaj, J. H. Albering, R. Pietschnig, *Eur. J. Inorg. Chem.* **2010**, 2010, 34-37; c) S. Greenberg, D. W. Stephan, *Inorg. Chem.* **2009**, 48, 8623-8631; d) D. Vidovic, Z. Lu, G. Reeske, J. A. Moore, A. H. Cowley, *Chem. Commun.* **2006**, 3501-3503; e) V. Plack, J. R. Goerlich, A. Fischer, H. Thoennessen, P. G. Jones, R. Schmutzler, *Z. Anorg. Allg. Chem.* **1995**, 621, 1080-1092.

- [18] C. Janiak, *Dalton Trans.* **2000**, 3885-3896.
- [19] K. Fukui, *Angew. Chem. Int. Ed.* **1982**, 21, 801-809.
- [20] Y. Zhang, L. Y. Chen, W. X. Yin, J. Yin, S. B. Zhang, C. L. Liu, *Dalton Trans.* **2011**, 40, 4830-4833.
- [21] a) F. A. La Porta, R. T. Santiago, T. C. Ramalho, M. P. Freitas, E. F. F. Da Cunha, *Int. J. Quantum Chem.* **2010**, 110, 2015-2023; b) S. Lindsay, S. K. Lo, O. R. Maguire, E. Bill, M. R. Probert, S. Sproules, C. R. Hess, *Inorg. Chem.* **2013**, 52, 898-909.
- [22] B. Stewart, A. Harriman, L. J. Higham, *Organometallics* **2011**, 30, 5338-5343.
- [23] a) R. R. Da Silva, T. C. Ramalho, J. M. Santos, J. D. Figueroa-Villar, *J. Phys. Chem. A* **2006**, 110, 1031-1040; b) R. R. da Silva, J. M. Santos, T. C. Ramalho, J. D. Figueroa-Villar, *J. Braz. Chem. Soc.* **2006**, 17, 223-226.
- [24] Spartan 14v112, **2013**, Wavefunction Inc., Irvine, <https://www.wavefun.com/spartan>.
- [25] <https://www.chemissian.com/>.

Chapter 4

Zinc complexes



4.1 Introduction

4.1.1 Coordination chemistry of zinc

The normal oxidation state of the zinc ion is +2.^[1] Due to the d^{10} configuration of Zn(II) it has no ligand field stabilisation energy, which means that the geometry and coordination number can be adapted to best fulfil the requirements of the coordinating ligands.^[2]

For example in zinc dialkyls the zinc atom is often coordinated only by two carbon atoms.^[1a, 3] With other ligands containing e.g. nitrogen, oxygen or halide atoms the coordination number usually varies between four and six (Figure 1).^[1a, 2a, 3-4] The corresponding polyhedrons can easily be distorted from the ideal geometry.^[4b]

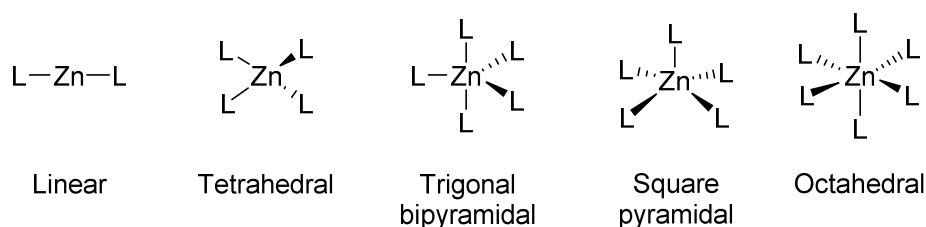


Figure 1: Typical coordination geometries found in zinc complexes.

There are not many examples of zinc complexes with phosphine ligands and in the literature known complexes often additional *O*- or *N*-donors are present.^[5]

4.1.2 Luminescent properties of Zn complexes

Luminescent zinc complexes are of special interest for the development of blue or white emitting OLEDs.

Usually the emission of zinc complexes is based on fluorescence and only a small number of compounds, which exhibit phosphorescence or TADF, are known.^[6]

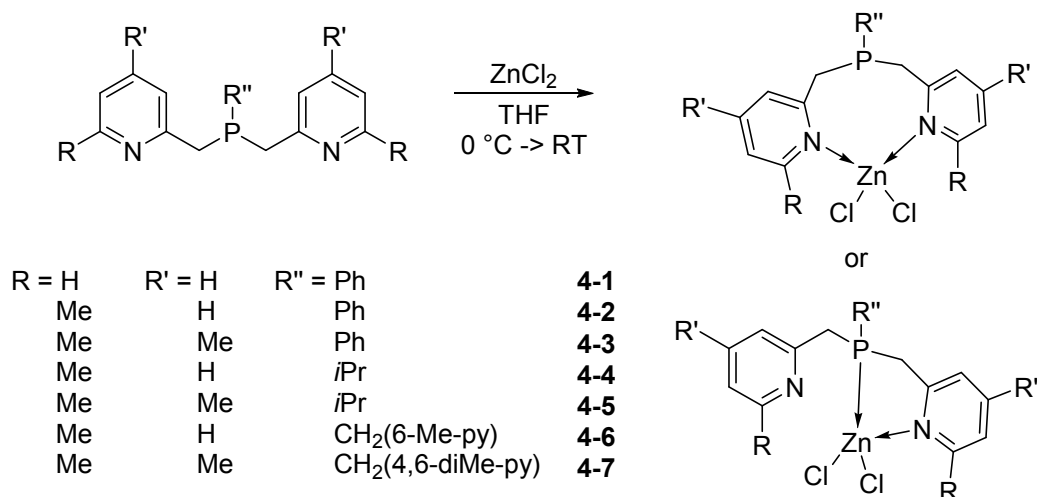
In d^{10} metal complexes there are no $d-d$ transitions possible. Therefore the fluorescence is usually caused by ligand centred excited states or LLCT.^[6b]

The main function of the metal atom often is to stabilise the ligand and its geometry. This means that the wavelength and intensity of the emission and the stability of the complex can strongly be influenced by modification of the ligand.^[6b]

4.2 Results and discussion

4.2.1 Synthesis

The zinc complexes have been synthesised by adding solutions of the corresponding phosphines to a solution of zinc chloride in THF (Scheme 1).



Scheme 1: Synthesis of the zinc chloride complexes.

The reaction to prepare **4-1** formed a colourless precipitate, which was isolated by filtration and dried under vacuum. The complex is soluble in DCM and chloroform, but insoluble in MeCN, Et₂O and pentane.

Compounds **4-2–4-7** were obtained as pale yellow solids after removal of the solvent *in vacuo* in moderate to good yields of 47–71%. All complexes are soluble in polar solvents like MeCN, THF, DCM and chloroform, but insoluble in non-polar solvents like Et₂O and pentane. All compounds are sensitive towards air and moisture.

4.2.2 NMR data

The ¹H, ¹³C and ³¹P NMR chemical shifts of complexes **4-1–4-7** are listed in Tables 1 and 2.

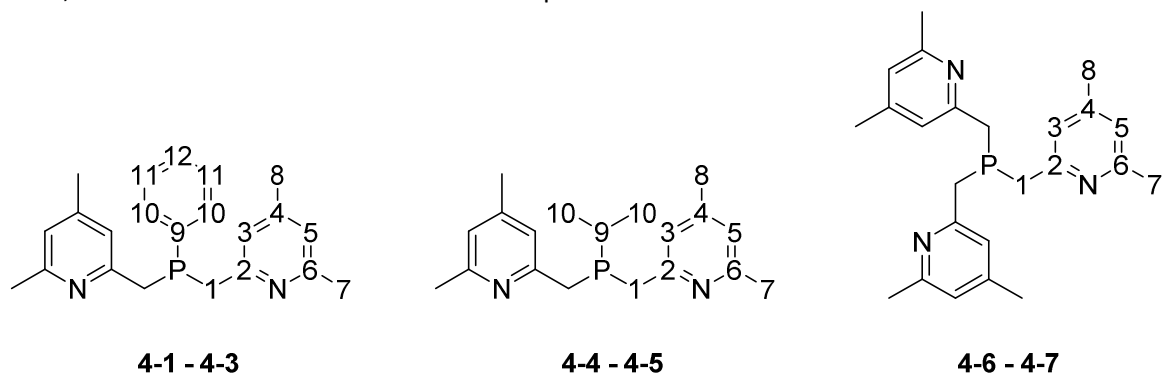


Figure 2: Numbering of carbon atoms of the ligands in compounds **4-1** and **4-7** for ¹H and ¹³C NMR spectroscopic data assignments.

Table 1: ^1H , ^{13}C and ^{31}P NMR data of the ligands in complexes **4-1–4-5** in CDCl_3 . Chemical shifts δ in ppm, coupling constants J in Hz.

	4-1	4-2	4-3	4-4	4-5		4-1	4-2	4-3	4-4	4-5
δ_{P}	−9.1	−24.1	−23.3	−11.8	−10.9	δ_{C}					
$^3J_{\text{PH10}}$	5.8	–	–	17.7	17.4	C1	32.3	33.1	33.0	29.0	28.8
						C2	156.8	153.3	152.9	153.8	153.4
δ_{H}						C3	126.4	122.5	123.8	122.7	123.2
H1a	3.42	3.81	3.78	3.56	3.35	C4	140.2	138.8	150.9	139.2	150.3
H1b	3.30	3.62	3.60	3.42	3.25	C5	122.9	123.1	124.0	123.2	123.6
H3	6.88	7.07	6.96	7.20	6.90	C6	149.5	159.0	158.3	159.0	158.3
H4	7.71	7.51	–	7.56	–	C7	–	24.6	24.3	24.5	24.2
H5	7.42	7.02	6.83	7.04	6.78	C8	–	–	21.0	–	20.8
H6	9.08	–	–	–	–	C9	132.7	125.6	125.8	23.1	23.0
H7	–	2.64	2.62	2.67	2.55	C10	132.0	133.6	133.7	18.3	18.2
H8	–	–	2.24	–	2.20	C11	128.9	129.3	131.1	–	–
H9	–	–	–	2.37	2.27	C12	130.3	132.1	132.1	–	–
H10	6.98	7.75	7.84	1.26	1.23	$^1J_{\text{PC1}}$	27.3	16.2	15.4	14.2	13.7
H11	7.27	7.39	7.44	–	–	$^2J_{\text{PC2}}$	–	1.5	–	2.0	2.0
H12	7.36	7.45	7.48	–	–	$^3J_{\text{PC3}}$	2.7	4.6	4.6	4.3	4.3
$^2J_{\text{H1aH1b}}$	13.7	15.3	15.0	15.5	15.3	$^5J_{\text{PC5}}$	0.7	2.8	2.9	2.5	2.5
$^3J_{\text{H3H4}}$	9.1	7.8	–	7.7	–	$^1J_{\text{PC9}}$	18.1	33.0	31.9	16.8	16.3
$^3J_{\text{H4H5}}$	6.6	7.7	–	7.7	–	$^2J_{\text{PC10}}$	20.5	13.9	14.0	3.9	3.9
$^3J_{\text{H5H6}}$	5.6	–	–	–	–	$^3J_{\text{PC11}}$	7.0	10.5	10.4	–	–
$^4J_{\text{H4H6}}$	1.8	–	–	–	–	$^4J_{\text{PC12}}$	–	2.4	2.3	–	–
$^5J_{\text{H3H6}}$	0.8	–	–	–	–						
$^3J_{\text{H9H10}}$	–	–	–	7.1	7.1						
$^2J_{\text{PH9}}$	–	–	–	1.8	1.1						
$^2J_{\text{PH1a}}$	3.6	9.0	10.0	9.5	9.7						
$^2J_{\text{PH1b}}$	4.5	6.6	6.0	6.5	6.0						

Table 2: ^1H , ^{13}C and ^{31}P NMR data of the ligands in complexes **4-6–4-7** in CDCl_3 . Chemical shifts δ in ppm, coupling constants J in Hz.

	4-6	4-7		4-6	4-7
δ_{P}	−23.8	−20.9	δ_{C}		
			C1	30.7	30.7
δ_{H}			C2	153.6	153.2
H1	3.48	3.42	C3	122.1	123.3
H3	7.13	6.98	C4	138.3	150.2
H4	7.53	–	C5	122.6	123.5
H5	7.01	6.83	C6	158.8	158.0
H7	2.57	2.53	C7	24.5	24.2
H8	–	2.25	C8	–	21.0
$^3J_{\text{H3H4}}$	7.7	–	$^1J_{\text{PC1}}$	14.7	12.6
$^3J_{\text{H4H5}}$	7.7	–	$^2J_{\text{PC2}}$	2.4	2.2
$^2J_{\text{PH1}}$	7.7	7.5	$^3J_{\text{PC3}}$	4.7	3.6
			$^5J_{\text{PC5}}$	2.4	2.6

The ^{31}P NMR signals of **4-2-4-7** are shifted 8.7–12.5 ppm towards higher field compared to the signals of the free ligands. This coordination induced shift (CIS) $\Delta\delta$ is slightly larger for the signals of the complexes with the ligands without the 4-methyl group at the pyridine rings than the corresponding complexes with these methyl groups. In contrast the ^{31}P NMR signal of **4-1** is shifted only 3.4 ppm towards lower field compared to the signal of the free ligand **2-13**. This indicates that the coordination of the ligand to zinc in complex **4-1** might be different from the coordination in the other complexes. The crystal structure of **4-1** (see 4.2.4) shows that in this complex the zinc is coordinated by only the nitrogen atoms of the ligands. It is likely that the additional 6-methyl groups to the ligands makes *N,N* coordination sterically much more difficult and therefore in the other complexes *P,N* coordination might be found.

The $^3J_{\text{PH}10}$ coupling constants resolved in the proton coupled ^{31}P NMR spectra of **4-4** and **4-5** are increased by 4.4 Hz and 4.1 Hz respectively compared to those of the free ligands. In contrast the $^3J_{\text{PH}10}$ coupling constant of **4-1** is decreased by 1.6 Hz compared to that of **2-13**. In the proton coupled ^{31}P NMR spectra of **4-2** and **4-3** no $^3J_{\text{PH}10}$ coupling is resolved.

Low temperature ^{31}P NMR measurements of **4-5** at -80°C showed four signals instead of only one signal as the ^{31}P NMR spectrum taken at room temperature (Figure 3). After return to room temperature the same spectrum as before cooling is obtained. This indicates that at room temperature there are four different species in the solution, which are in a rapid equilibrium and therefore cause only one signal in the NMR spectrum.

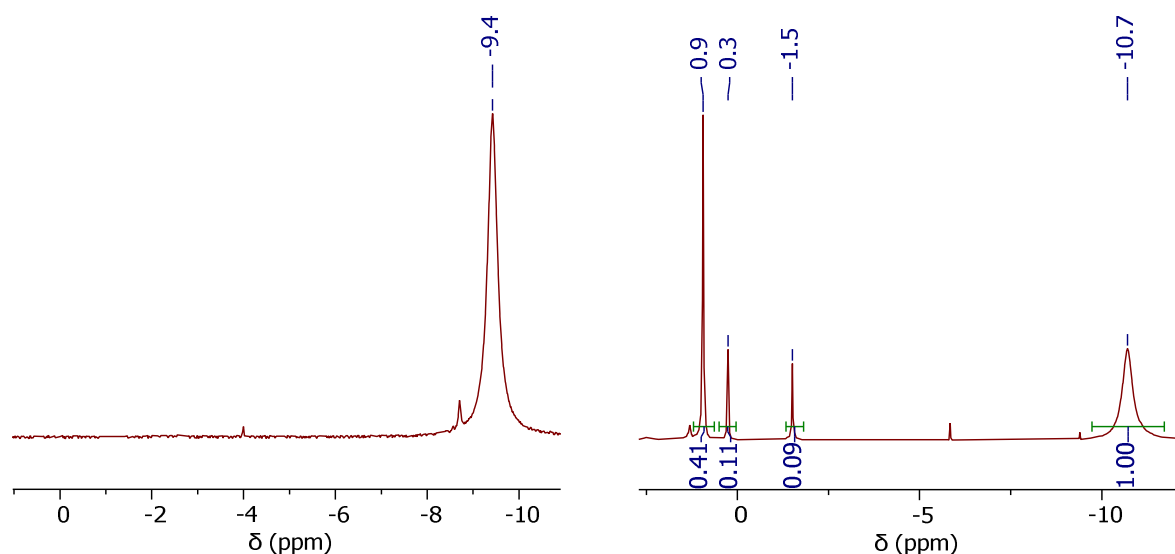


Figure 3: ^{31}P NMR spectra of **4-5** in CD_2Cl_2 at room temperature (left) and -80°C (right).

The chemical shift of the signal of the free ligand at -80°C is 1.1 ppm. The signal at 0.9 ppm in the NMR spectrum of the complex at -80°C might be caused by free ligand, which is present in the solution in an amount of approx. 25%. The signal at a chemical shift of -10.7 ppm (62%) is probably caused by the complex. Also two more species containing the ligand are present in the solution in minor amounts of 6–7% causing signals at -1.5 ppm and 0.3 ppm. One of these species might be a complex with *N,N* coordination or only one of the nitrogen atoms coordinating to the zinc (Figure 4). Also the formation of dimers as shown in Figure 4 might be possible.

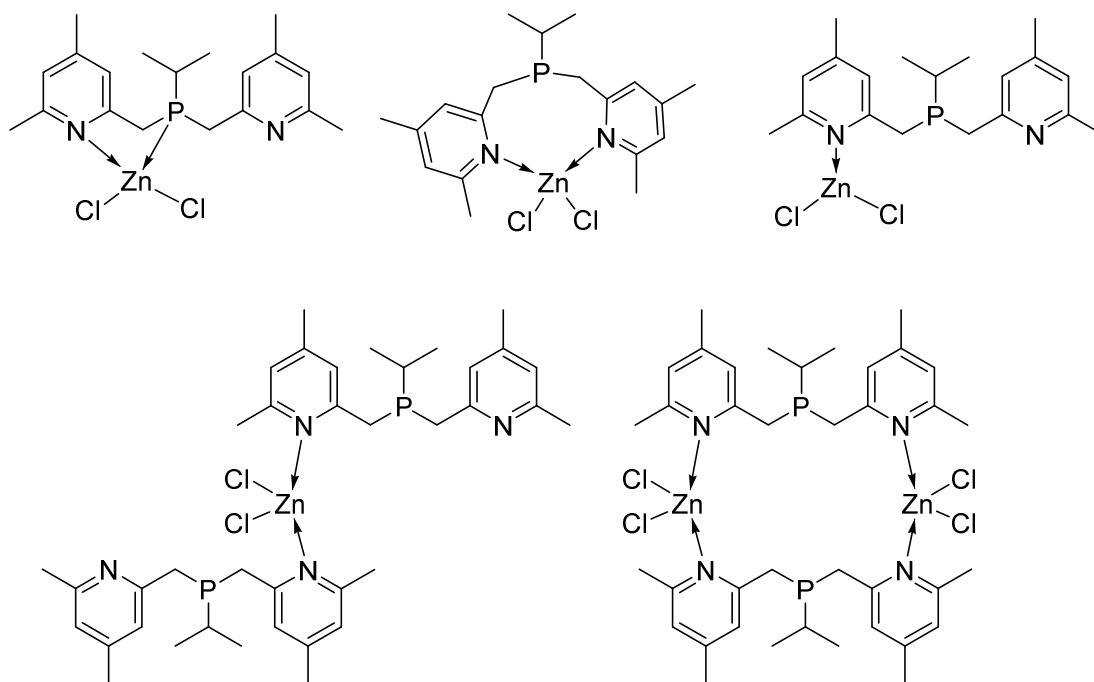


Figure 4: Possible structures of species, which might be present in the solution of **4-5**.

On the contrary in the ^{31}P NMR spectrum of **4-1** at -80°C only one signal can be observed (Figure 5). This means that there is no equilibrium in solutions of **4-1**, but only one species is present.

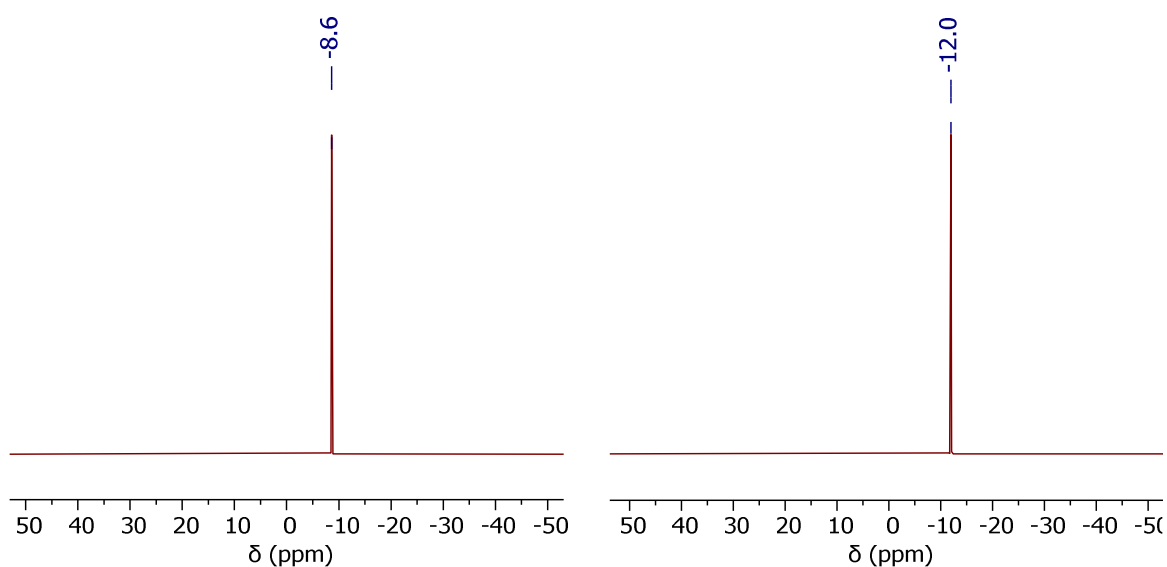


Figure 5: ^{31}P NMR spectra of **4-1** in CD_2Cl_2 at room temperature (left) and -80°C (right).

Probably due to the equilibrium in solution it is much more difficult to crystallise the Zn complexes of the ligands with the lutidynyl or collidynyl substituents.

For the following discussion of the ^1H and ^{13}C NMR it should be considered, that the chemical shifts and coupling constants of **4-5** and probably **4-2-4-4** as well as **4-6** and **4-7** are only average values due to the equilibrium in the solution.

All signals in the ^1H NMR spectra of **4-2-4-7** are shifted 0.10–0.70 ppm towards lower field in comparison to the signals found for the free ligands, except the signals for H5 of **4-6** and **4-7**, which

show no CIS. The ^1H NMR signals for H3, H10 and H11 of compound **4-1** are shifted towards higher field (H3: 0.12 ppm, H10: 0.46 ppm, H11: 0.01 ppm) with respect to the corresponding signals of **2-13**, while the signals of H4, H5, H6 and H12 are shifted towards lower field (H4: 0.27 ppm, H5: 0.42 ppm, H6: 0.64 ppm, H12: 0.08 ppm). The signals for H1 of **4-6** and **4-7** are also shifted 0.42–0.48 ppm towards lower field.

The signals for the diastereotopic protons H1a and H1b of **4-1–4-5** are moved further apart from each other compared to the signals of the free ligands. While in the spectra of **2-16** and **2-17** the signals of H1a and H1b showed significant overlap, the corresponding signals in the spectra of **4-4** and **4-5** are clearly separated. The signals of H1 of compounds **4-2–4-5** are shifted 0.28–0.53 ppm towards lower field compared to those of the free ligands. On the contrary the signal of H1a of **4-1** is shifted only 0.02 ppm towards lower field, while the signal of H1b is shifted 0.02 ppm towards higher field.

In comparison to the free ligand **2-13** the $^2J_{\text{H1aH1b}}$ coupling constant of **4-1** is slightly increased by 0.3 Hz. Also the $^2J_{\text{PH1}}$ coupling constants of **4-1** are increased by 1.9 Hz and 4.5 Hz compared to **2-13**. In the case of **4-2–4-4** the $^2J_{\text{H1aH1b}}$ coupling constants are increased 1.7–2.0 Hz and the $^2J_{\text{PH1}}$ coupling constants are increased 6.0–9.7 Hz compared to those of the corresponding ligands.

Comparison of the ^{13}C NMR spectra of **4-1–4-7** with the spectra of the free ligands shows the largest effect of the complexation on the signals of C1, C2 and C9 ($\Delta\delta$: C1: 4.5–5.6 ppm, C2: 1.4–4.9 ppm, C9: 1.9–11.6 ppm). The other signals have CIS of a maximum of 4.0 ppm compared to the signals of the ligands. The signals of C1, C2, C8 and C9 are shifted towards higher field, while the signals of C3–6, C11 and C12 are shifted towards lower field compared to the signals of the ligand. The signals of C7 are shifted 0.1 ppm towards lower field for **4-2** and **4-3** and 0.1–0.2 ppm towards higher field for **4-4**, **4-5** and **4-7** and the signals of C10 are shifted 0.8–0.9 ppm towards lower field for **4-2** and **4-3**, while they are shifted 0.8–1.0 ppm towards higher field for **4-1**, **4-4** and **4-5**. For the signal of C2 of compound **4-1** the shift is only 1.6 ppm, but for **4-2–4-7** the shift is between 4.1 ppm and 5.0 ppm. Also the signal of C9 for compound **4-1** is shifted only 4.1 ppm towards higher field, while the corresponding signals of **4-2** and **4-3** are shifted 11.5 ppm. These differences also indicate that the coordination in **4-1** might be different from the coordination found in **4-2** and **4-3**.

The coupling constants J_{PC} of the signals of C1–C4, C6 and C10 are decreased by 0.6–9.6 Hz for compounds **4-2–4-7**, while the coupling constants of the signals of C5, C9, C11 and C12 are increased by 0.7–14.6 Hz compared to the coupling constants found for the signals of the free ligands. Especially the coupling constants of the signals of C9 of **4-2** and **4-3** are significantly increased by 14.6 Hz and 13.7 Hz respectively. This strong influence on the signal of C9 might result from coordination of the neighbouring phosphorus atom to the zinc. On the contrary the coupling constant of the signal of C1 for compound **4-1** is increased 8.5 Hz compared to $^1J_{\text{PC1}}$ of **2-13**. The coupling constants of the signals of the phenyl carbon atoms of **4-1** are comparable to those found for the signals of **2-13**.

The ^1H and ^{13}C NMR spectra of **4-1** at $-80\text{ }^\circ\text{C}$ are very similar to those at room temperature. In the ^1H and ^{13}C NMR spectra of **4-5** at $-80\text{ }^\circ\text{C}$ the signals of the species present in the solution can be seen, but assignment of the signals is not possible.

4.2.3 Photophysical data

None of the complexes shows luminescence in solution, but in the solid state the complexes show blue luminescence under UV light (Figure 6).

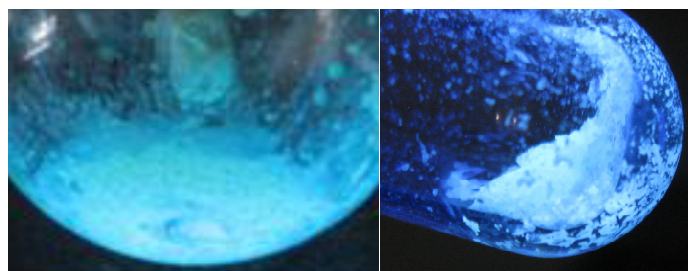


Figure 6: Luminescence of **4-1** (left) and **4-5** (right) under UV light.

The emission maximum of **4-1** in the solid state is at 486 nm (Figure 7).

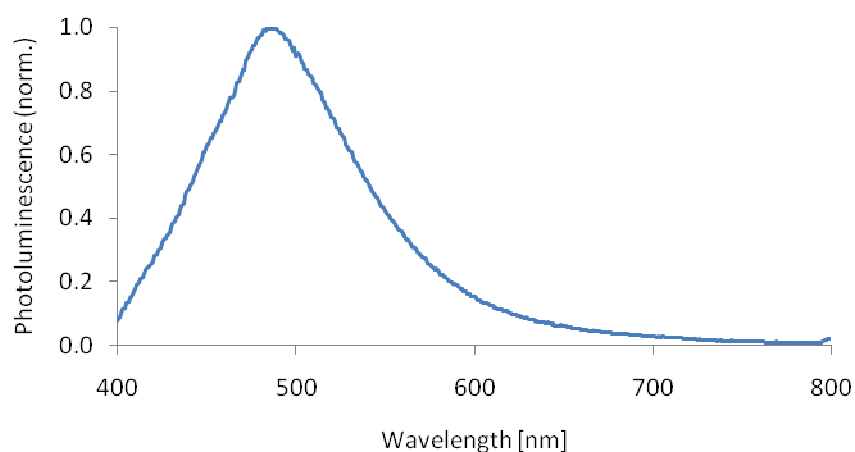


Figure 7: Fluorescence emission spectrum of **4-1** in the solid state.

From TCSPC measurements the relaxations times of **4-1** in the solid state could be determined (Figure 8). From a biexponential fit of the results the relaxation times of $\tau_1 = 2.23 \pm 0.04$ ns and $\tau_2 = 8.93 \pm 0.12$ ns were determined. These relaxation times are in the time range, which is typical for fluorescence (0.01–10 ns).^[7] This indicates that **4-1** probably is a singlet emitter, like most luminescent zinc complexes.

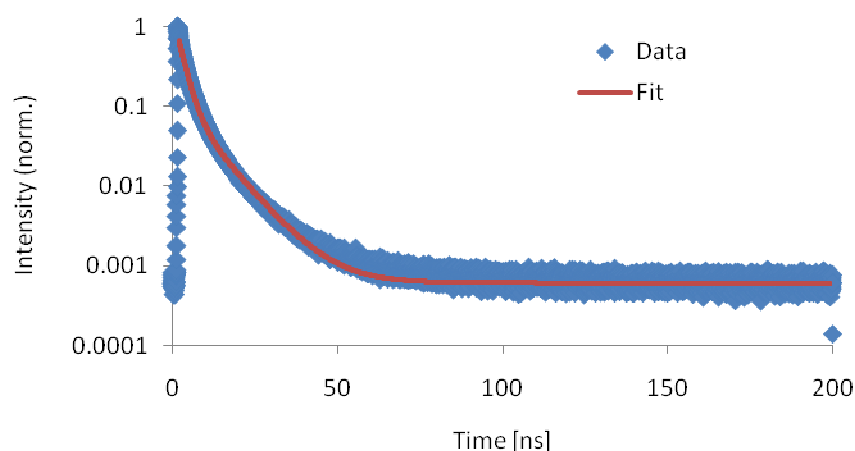


Figure 8: Results of the TCSPC measurements of **4-1**.

4.2.4 Crystal structure of 4-1

Crystals of **4-1** suitable for single crystal X-ray diffraction have been obtained from a solution in chloroform. The complex crystallises in the triclinic space group $P\bar{1}$ with two formula units in the unit cell. The asymmetric unit comprises two molecules of the complex. The asymmetric unit is depicted in Figure 9.

The zinc atoms are coordinated distorted tetrahedrally by two nitrogen atoms of one ligand and two chloride anions.

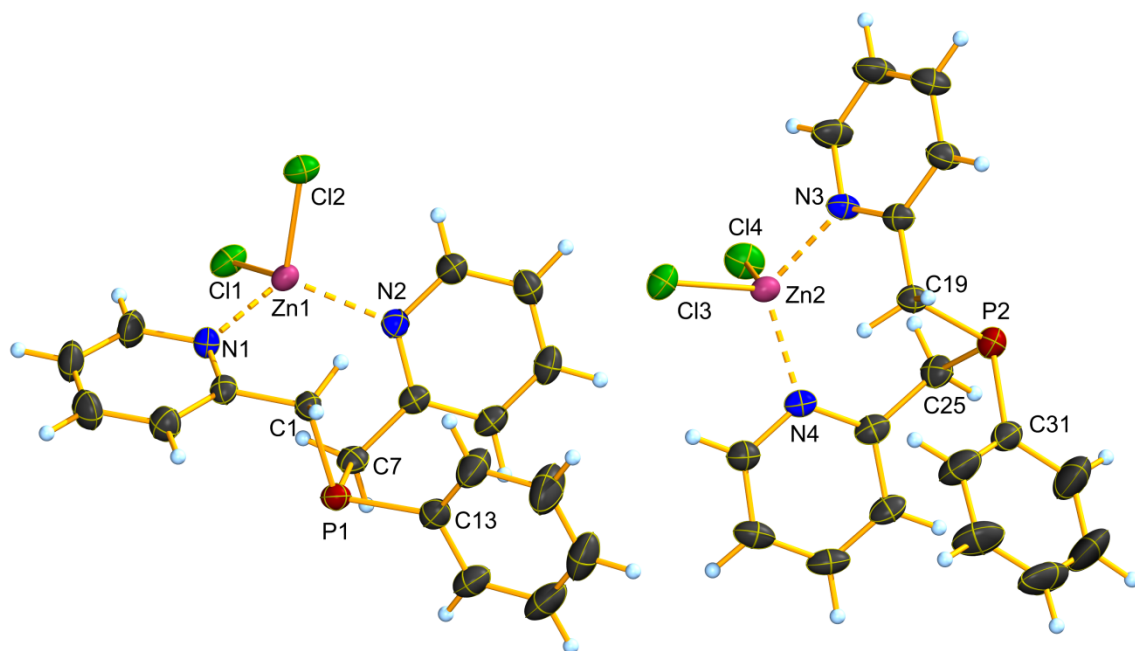


Figure 9: Asymmetric unit of **4-1**. Thermal ellipsoids are drawn at 50% probability level. Selected bond lengths [Å] and angles [°]: Zn1–Cl1: 2.230(1), Zn1–Cl2: 2.235(1), Zn1–N1: 2.057(2), Zn1–N2: 2.046(2), Zn2–Cl3: 2.229(1), Zn2–Cl4: 2.243(1), Zn2–N3: 2.057(3), Zn2–N4: 2.060(2), P1–C1: 1.852(3), P1–C7: 1.873(2), P1–C13: 1.823(4), P2–C19: 1.847(2), P2–C25: 1.871(3), P2–C31: 1.825(3), Cl1–Zn1–Cl2: 116.8(1), Cl1–Zn1–N1: 105.6(1), Cl1–Zn1–N2: 106.9(1), Cl2–Zn1–N1: 105.9(1), Cl2–Zn1–N2: 105.3(1), N1–Zn1–N2: 116.9(1), Cl3–Zn2–Cl4: 115.8(1), Cl3–Zn2–N3: 104.8(1), Cl3–Zn2–N4: 110.1(1), Cl4–Zn2–N3: 104.1(1), Cl4–Zn2–N4: 105.4(1), N3–Zn2–N4: 117.0(1), C1–P1–C7: 100.8(1), C1–P1–C13: 102.1(1), C7–P1–C13: 102.5(1), C19–P2–C25: 101.5(1), C19–P2–C31: 102.7(1), C25–P2–C31: 102.4(1).

The only examples of zinc chloride complexes of bis(picolyl)phosphines in the literature are the complexes synthesised by *C. Hettstedt*.^[8] In these complexes the zinc atom is coordinated in the same way by the nitrogen atoms of the picolyl substituents.

This coordination type can also be found in zinc chloride complexes of bis(picolyl)amines,^[9] bis(picolyl)silane^[10] and a bis(picolyl)-pyridinyl-butyne ligand (Figure 10).^[11]

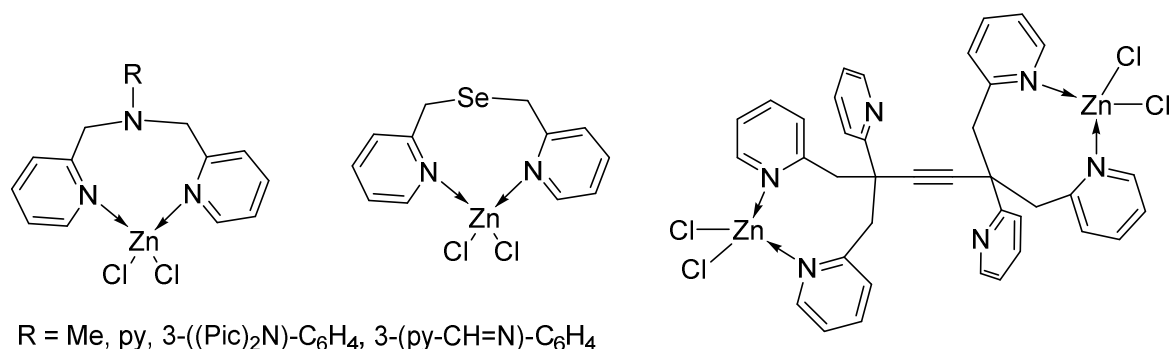


Figure 10: Literature known zinc chloride complexes of bis(picoly)amines, bis(picoly)selane and a bis(picoly)-pyridinyl-butyne ligand.

The Zn–N distances are between 2.046(2) and 2.060(2) Å, which is only slightly shorter than the mean Zn–N distance of four-coordinate zinc atoms with pyridine ligands (2.064 Å)^[12] and corresponds with the Zn–N distances of the zinc chloride complexes of bis(picoly)phosphines and tris(picoly)phosphine (2.041(2)–2.084(5) Å).^[8]

The Zn–Cl distances are in the range from 2.229(1) to 2.243(1) Å. This is slightly shorter than the mean Zn–Cl distance of four-coordinate zinc atoms (2.253 Å),^[12] but concurs with the literature values of the complexes of *C. Hettstedt* (2.204(2)–2.254(1) Å).^[8]

The P–C_{Alk} bond lengths of **4-1** are between 1.847(2) Å and 1.873(2) Å. This is slightly longer than the mean P–C_{Alk} bonds in complexes of triethylphosphine, tri-*n*-propylphosphine, methyldiphenylphosphine and dimethyl(phenyl)phosphine (1.825–1.832 Å),^[12] but the P–C_{Alk} bond lengths found in the complexes of *C. Hettstedt* (1.850(6)–1.893(1) Å) are in the same range as those of **4-1**.^[8]

The P–C_{Ar} bond lengths of **4-1** are 1.823(4) Å and 1.824(3) Å, which is comparable to the mean P–C_{Ar} bond lengths in complexes of triphenylphosphine, methyldiphenylphosphine and dimethyl(phenyl)phosphine (1.823–1.828 Å)^[12] and the P–C_{Ar} bond length of the *o*-methoxyphenylbis(picoly)phosphine zinc chloride complex (1.830(2) Å) and the *p*-methoxyphenylbis(picoly)phosphine zinc chloride complex (1.820(1) Å).^[8]

The angles around the Zn atoms vary from 104.8(1) ° to 117.0(1) °. The N–Zn–N angles (116.9(1) ° and 117.0(1) °) and Cl–Zn–Cl angles (115.8(1) ° and 116.8(1) °) are larger than the N–Zn–Cl angles (104.8(1)–110.1(1) °). The N–Zn–N and Cl–Zn–Cl angles are all larger than the ideal tetrahedral angle of 109.5 °, while the N–Zn–Cl angles are, with one exception of 110.1(1) °, slightly smaller than the ideal tetrahedral angle. Comparison of the angles with the literature values of ZnCl₂ complexes of tris(picoly)phosphine, *o*-methoxyphenylbis(picoly)phosphine and *p*-methoxyphenylbis(picoly)phosphine shows similarity of the angles.^[8]

The C–P–C angles of **4-1** range from 100.8(1) ° to 102.7(1) °, which is comparable to the literature values found in zinc chloride complexes of bis(picoly)phosphines and tris(picoly)phosphine (95.8(7)–104.0(4) °).^[8] The sums of the angles around the phosphorus atoms are 305.4 ° and 306.5 ° respectively, meaning that the conformation around the phosphorus atoms is pyramidal.

Figure 11 shows the crystal structure of **4-1** along the *c* axis. The pyridine rings containing N2 and N4 are arranged parallel to each other. The distance between the centres of the rings is 3.784(1) Å and the angle of the rings to each other is 2.2(1) °. This suggests, that the crystal structure is stabilised by weak attractive π - π interactions.

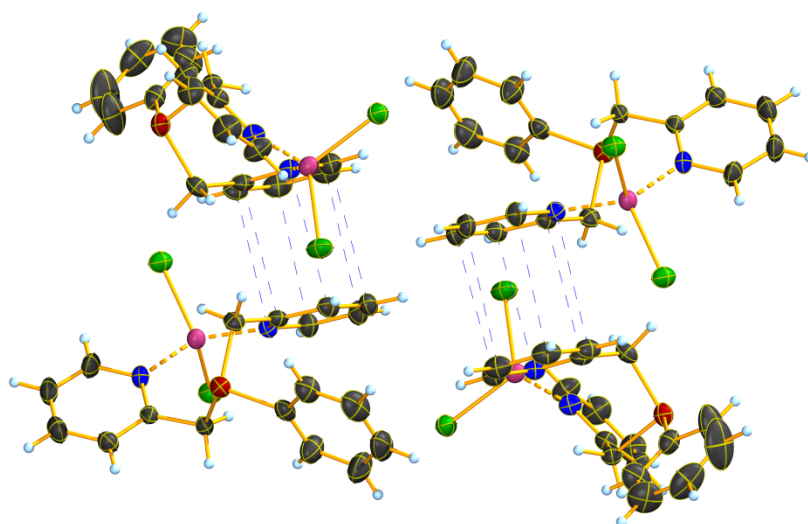


Figure 11: Crystal structure of **4-1**. View along the *c* axis. Thermal ellipsoids are drawn at 50% probability level.

4.2.5 DFT calculations

From the frontier orbitals of a molecule a lot of information about the chemical properties and the reactivity of a molecule can be obtained.^[13] The energy gap between the HOMO and the LUMO gives information about the chemical stability of a molecule.^[13b]

Geometry optimisation has been performed with the Gaussian 16 package with the B3LYP functional and 6-31G+(d,p) basis set.^[14] For the optimum geometry of complex **4-1** the distribution and energies of the highest occupied and the lowest unoccupied molecular orbitals were determined. The HOMO–1, HOMO, LUMO and LUMO+1 are depicted in Figure 12.

The HOMO is centred at the chlorine atoms, while the contributions of the metal atom and the phosphine ligand are rather small. The main part of the HOMO–1 is localised at the phosphine ligand, but also contributions of the chlorine atoms are present.

The LUMO is centred at one of the pyridine rings of the ligand, while the LUMO+1 is centred at the other pyridine ring. Both orbitals also have small contributions of the phosphorus atom, but the phenyl ring is only weakly involved in the composition of these orbitals.

The energy gap between HOMO and LUMO of 4.92 eV (252.0 nm) is rather large.

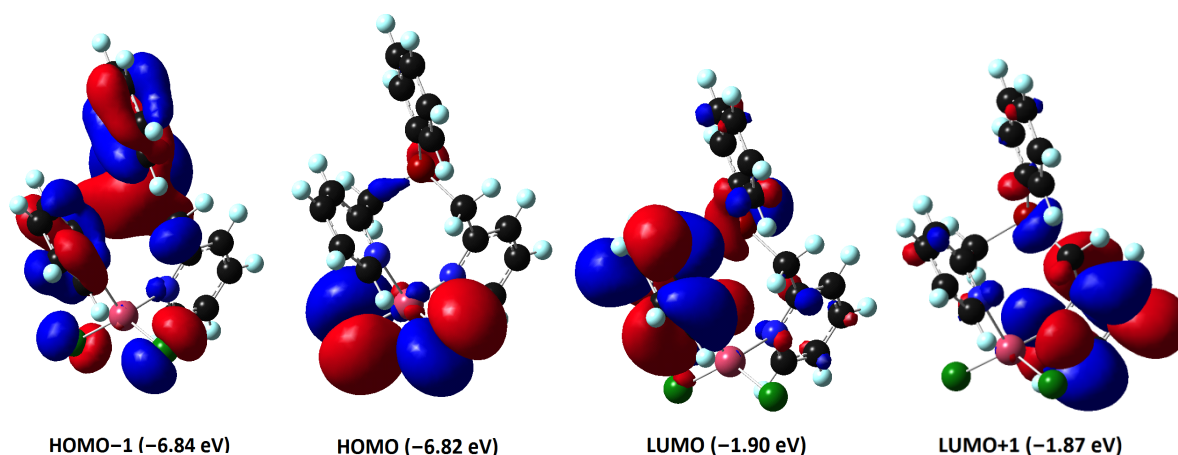


Figure 12: HOMO–1, HOMO, LUMO and LUMO+1 of **4-1**.

The UV/Vis spectrum of **4-1** was calculated with the TD-DFT method at the B3LYP/6-31G+(d,p) level of theory.^[14] The calculated absorption spectrum shows a maximum at 291 nm (Figure 13). The most prominent contribution to the absorption comes from a singlet transition at 291.4 nm from HOMO-1 and HOMO to the LUMO. With respect to the distribution of the orbitals involved in this transition it is obvious that the luminescence of complex **4-1** is based on LC and LLCT states.

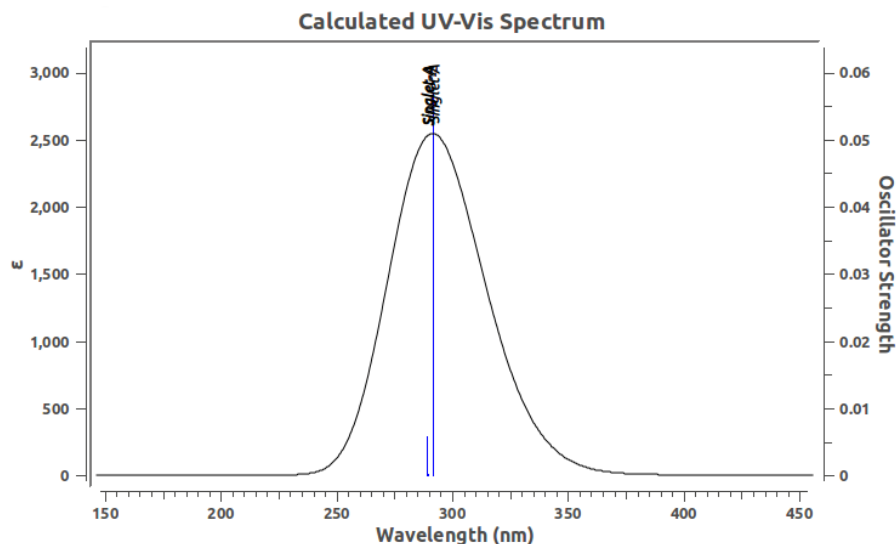


Figure 13: Calculated absorption spectrum of **4-1**.

4.3 Summary

Seven new zinc chloride complexes of bis- and tris(picoly)phosphine based ligands have been synthesised and characterised.

The ³¹P NMR chemical shifts of solutions of the complexes indicated that in complex **4-1** the ligand possibly might coordinate to the metal in a different way than in complexes **4-2–4-5**. This needs to be confirmed by X-ray crystallography.

Low temperature ³¹P NMR measurements at –80°C revealed that in the case of **4-1** only one species is present in the solution, while in the case of **4-5** a rapid equilibrium of four species in the solution causes one averaged signal at room temperature. Probably due to the presence of this equilibrium the zinc complexes of lutidinyl or collidinyl substituted phosphines are more difficult to crystallise and no crystal structures of these compounds could be determined.

All seven complexes emit blue luminescence under UV-light. The short relaxation times determined in TSCPC measurements of **4-1** indicate that the observed emission is caused by singlet state transitions.

The crystal structure of complex **4-1** could be determined by X-ray crystallography. From the molecular structure it is obvious that the zinc is coordinated only by the nitrogen atoms of the ligand and does not interact with the phosphorus. In the molecular structure π - π -stacking interactions between the pyridine rings can be observed.

DFT calculations revealed that the HOMO is centred mostly at the chlorine atoms, while the LUMO is centred at the pyridine moiety of the phosphine ligand. Excitation leads to a charge transfer from the chloride ions to the ligand.

4.4 Experimental

For general information about methods and analytical instruments used see 2.4.1.

Compounds **4-2–4-7** were obtained from the reaction mixtures after removal of the solvent without further purification. NMR data indicated that a mixture of several species might have been obtained. Therefore no yields and data from elemental analysis are listed for these compounds.

4.4.1 DFT calculations

Geometry optimisation, vibrational calculations and calculations of molecular orbitals have been performed with the Gaussian 16 package with the B3LYP functional and the 6-31G+(d,p) basis set starting from the molecular geometries determined from the crystal structures.^[14] Optimisations have been considered complete when no negative frequencies were present in the vibrational spectrum. UV/Vis spectra of the optimised structures were calculated with the TD-DFT method at the B3LYP/6-31G+(d,p) level of theory.^[14]

4.4.2 Syntheses

4.4.2.1 Phenyl-bis(pyridin-2-ylmethyl)phosphine zinc chloride complex 4-1

A solution of **2-13** (2.0 mL, 0.5 M in MeCN, 1.0 mmol, 1 eq) was added dropwise to a solution of ZnCl₂ (1.0 mL, 1 M in Et₂O, 1.0 mmol, 1 eq), which led to a colourless precipitate. The suspension was stirred overnight. The solid was filtered off and dried *in vacuo*. The product was obtained as colourless solid (90 mg, 0.21 mmol, 21%).

¹H NMR (400 MHz), ¹³C NMR (101 MHz) and ³¹P NMR (162 MHz) see Table 1.

m/z (ESI) [%]: 293.12027 (74), 200.06235 (51).

4.4.2.2 Phenyl-bis(6-methylpyridin-2-ylmethyl)phosphine zinc chloride complex 4-2

A solution of **2-14** (2.0 mL, 0.5 M in MeCN, 1.0 mmol, 1 eq) was added dropwise to a solution of ZnCl₂ (1.0 mL, 1 M in THF, 1.0 mmol, 1 eq), which led to a clouding of the solution. The reaction solution was stirred overnight before the solvent was removed *in vacuo*. The product was obtained as colourless solid (265 mg).

¹H NMR (400 MHz), ¹³C NMR (101 MHz) and ³¹P NMR (162 MHz) see Table 1.

m/z (FAB⁺) [%]: 419.0430 (100).

m/z (FAB⁻) [%]: 35.0 (1).

4.4.2.3 Phenyl-bis(4,6-dimethylpyridin-2-ylmethyl)phosphine zinc chloride complex 4-3

A solution of **2-15** (2.0 mL, 0.5 M in MeCN, 1.0 mmol, 1 eq) was added dropwise to a solution of ZnCl₂ (1.0 mL, 1 M in THF, 1.0 mmol, 1 eq), which led to a clouding of the solution. The reaction

solution was stirred overnight and the product precipitated after addition of dry Et₂O. The colourless solid was filtered off and dried *in vacuo*. The product was obtained as colourless solid (226 mg).

¹H NMR (400 MHz), ¹³C NMR (101 MHz) and ³¹P NMR (162 MHz) see Table 1.

m/z (FAB⁺) [%]: 447.0719 (100).

m/z (FAB⁻) [%]: 35.0 (1).

4.4.2.4 *iso*Propyl-bis(6-methylpyridin-2-ylmethyl)phosphine zinc chloride complex 4-4

A solution of **2-16** (2.0 mL, 0.5 M in MeCN, 1.0 mmol, 1 eq) was added dropwise to a solution of ZnCl₂ (1.0 mL, 1 M in THF, 1.0 mmol, 1 eq). The reaction solution was stirred overnight and the solvent was removed *in vacuo*. The product was obtained as pale yellow solid (302 mg).

¹H NMR (400 MHz), ¹³C NMR (101 MHz) and ³¹P NMR (162 MHz) see Table 1.

4.4.2.5 *iso*Propyl-bis(4,6-dimethylpyridin-2-ylmethyl)phosphine zinc chloride complex 4-5

A solution of **2-17** (2.2 mL, 0.5 M in MeCN, 1.1 mmol, 1 eq) was added dropwise to a solution of ZnCl₂ (1.1 mL, 1 M in THF, 1.0 mmol, 1 eq), which led to a clouding of the solution. The reaction solution was stirred overnight and the solvent was removed *in vacuo*. The product was obtained as colourless solid (237 mg).

¹H NMR (400 MHz), ¹³C NMR (101 MHz) and ³¹P NMR (162 MHz) see Table 1.

m/z (FAB⁺) [%]: 413.0910 (100).

m/z (FAB⁻) [%]: 35 (1).

4.4.2.6 Tris(6-methylpyridin-2-ylmethyl)phosphine zinc chloride complex 4-6

A solution of **2-24** (1.5 mL, 0.5 M in MeCN, 0.75 mmol, 1 eq) was added dropwise to a solution of ZnCl₂ (0.5 mL, 1.5 M in THF, 0.75 mmol, 1 eq). The reaction solution was stirred overnight and the solvent was removed *in vacuo*. The product was obtained as colourless solid (289 mg).

¹H NMR (400 MHz), ¹³C NMR (101 MHz) and ³¹P NMR (162 MHz) see Table 2.

4.4.2.7 Tris(4,6-dimethylpyridin-2-ylmethyl)phosphine zinc chloride complex 4-7

A solution of **2-25** (2.0 mL, 0.5 M in MeCN, 1.0 mmol, 1 eq) was added dropwise to a solution of ZnCl₂ (1.0 mL, 1 M in THF, 1.0 mmol, 1 eq), which led to a clouding of the solution. The reaction solution was stirred overnight and the solvent was removed *in vacuo*. The product was obtained as colourless solid (277 mg).

¹H NMR (400 MHz), ¹³C NMR (101 MHz) and ³¹P NMR (162 MHz) see Table 2.

m/z (FAB⁺) [%]: 490.1134 (12).

m/z (FAB⁻) [%]: 35 (1).

4.4.3 Crystallographic data

Table 3: Crystallographic data of compound **4-1**.

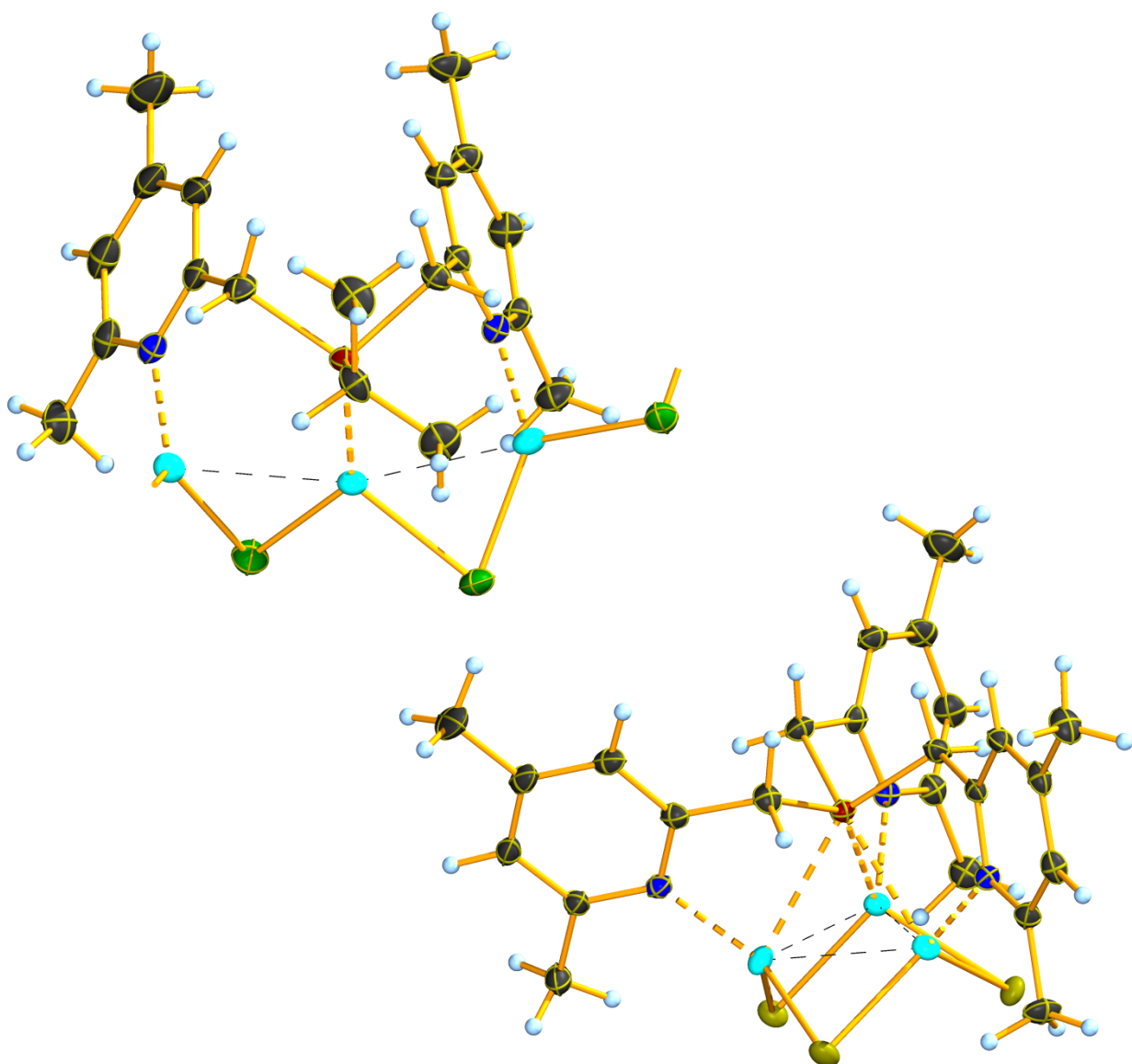
Identification code	mx399
Empirical formula	C ₁₈ H ₁₇ Cl ₂ N ₂ PZn
Formula weight [g·mol ⁻¹]	428.57
Temperature [K]	143(2)
Crystal size [mm ³]	0.20× 0.33× 0.39
Colour, shape	Colourless block
Crystal system	Triclinic
Space group	<i>P</i> -1
<i>a</i> [Å]	11.9745(4)
<i>b</i> [Å]	14.0085(6)
<i>c</i> [Å]	15.0123(6)
α [°]	62.197(4)
β [°]	89.218(3)
γ [°]	73.498(4)
<i>V</i> [Å ³]	2114.71(16)
<i>Z</i>	4
ρ_{calc} [g·cm ⁻³]	1.346
Radiation [Å]	MoK α = 0.71073
μ [cm ⁻¹]	1.491
<i>F</i> (000)	872
Index ranges	-15≤ <i>h</i> ≤15 -18≤ <i>k</i> ≤18 -11≤ <i>l</i> ≤19
θ range [°]	4.372≤ θ ≤ 27.481
Reflections collected	18629
Independent reflections	9647
Observed reflections	7521
Data/restraints/parameters	9647/0/433
<i>R</i> _{int}	0.0277
<i>R</i> ₁ , <i>wR</i> ₂ [<i>I</i> >2σ(<i>I</i>)]	0.0429, 0.1108
<i>R</i> ₁ , <i>wR</i> ₂ [all data]	0.0610, 0.1221
GooF	1.050
$\delta\rho_{\text{max}}$, $\delta\rho_{\text{min}}$ [e·nm ⁻³]	0.750, -0.433

4.5 References

- [1] a) H. Vahrenkamp, *Chem. Unserer Zeit* **1988**, 22, 73-84; b) G.-J. Chen, S.-X. Zeng, C.-H. Lee, Y.-L. Chang, C.-J. Chang, S. Ding, H.-Y. Chen, K.-H. Wu, I. J. Chang, *Polymer* **2020**, 194.
- [2] a) S. Di Bella, A. Colombo, C. Dragonetti, S. Righetto, D. Roberto, *Inorganics* **2018**, 6; b) F. Mancin, P. Tecilla, *New J. Chem.* **2007**, 31.
- [3] H. Vahrenkamp, *Dalton Trans.* **2007**, 4751-4759.
- [4] a) A. Terenzi, A. Lauria, A. M. Almerico, G. Barone, *Dalton Trans.* **2015**, 44, 3527-3535; b) A. Erxleben, *Coord. Chem. Rev.* **2003**, 246, 203-228.
- [5] I. D'Auria, M. Lamberti, M. Mazzeo, S. Milione, G. Roviello, C. Pellicchia, *Chem. Eur. J.* **2012**, 18, 2349-2360.
- [6] a) Y. Sakai, Y. Sagara, H. Nomura, N. Nakamura, Y. Suzuki, H. Miyazaki, C. Adachi, *Chem. Commun.* **2015**, 51, 3181-3184; b) A. Barbieri, G. Accorsi, N. Armaroli, *Chem. Commun.* **2008**, 2185-2193; c) F. Dumur, *Synth. Met.* **2014**, 195, 241-251.
- [7] B. Valeur, *Molecular Fluorescence: Principles and Applications*, Wiley-VCH, Weinheim, **2002**.
- [8] C. Hettstedt, PhD thesis, Ludwig-Maximilians-Universität München **2015**.
- [9] a) A. Beitat, S. P. Foxon, C. C. Brombach, H. Hausmann, F. W. Heinemann, F. Hampel, U. Monkowius, C. Hirtenlehner, G. Knor, S. Schindler, *Dalton Trans.* **2011**, 40, 5090-5101; b) S. Lindsay, S. K. Lo, O. R. Maguire, E. Bill, M. R. Probert, S. Sproules, C. R. Hess, *Inorg. Chem.* **2013**, 52, 898-909; c) S. Foxon, J.-Y. Xu, S. Turba, M. Leibold, F. Hampel, F. W. Heinemann, O. Walter, C. Würtele, M. Holthausen, S. Schindler, *Eur. J. Inorg. Chem.* **2007**, 2007, 429-443; d) F. Pop, J. Ding, L. M. L. Daku, A. Hauser, N. Avarvari, *RSC Adv.* **2013**, 3, 3218; e) Y. Zhang, L. Y. Chen, W. X. Yin, J. Yin, S. B. Zhang, C. L. Liu, *Dalton Trans.* **2011**, 40, 4830-4833.
- [10] M. S. Hain, Y. Fukuda, C. Rojas Ramírez, B. Y. Winer, S. E. Winslow, R. D. Pike, D. C. Bebout, *Cryst. Growth Des.* **2014**, 14, 6497-6507.
- [11] S. Kumar, D. Mandon, *Inorg. Chem.* **2015**, 54, 7481-7491.
- [12] A. J. C. Wilson, E. Prince, *International Tables for Crystallography, Vol. C Mathematical, physical and chemical tables*, 2nd ed., Kluwer Academic Publishers, Dordrecht/Boston/London, **1999**.
- [13] a) K. Fukui, *Science* **1982**, 218, 747-754; b) S. Badoğlu, Ş. Yurdakul, *J. Struct. Chem.* **2018**, 59, 1010-1021.
- [14] M. J. Frisch, G. W. Trucks, H. B. Schlegel, G. E. Scuseria, M. A. Robb, J. R. Cheeseman, G. Scalmani, V. Barone, G. A. Petersson, H. Nakatsuji, X. Li, M. Caricato, A. V. Marenich, J. Bloino, B. G. Janesko, R. Gomperts, B. Mennucci, H. P. Hratchian, J. V. Ortiz, A. F. Izmaylov, J. L. Sonnenberg, D. Williams-Young, F. Ding, F. Lipparini, F. Egidi, J. Goings, B. Peng, A. Petrone, T. Henderson, D. Ranasinghe, V. G. Zakrzewski, J. Gao, N. Rega, G. Zheng, W. Liang, M. Hada, M. Ehara, K. Toyota, R. Fukuda, J. Hasegawa, M. Ishida, T. Nakajima, Y. Honda, O. Kitao, H. Nakai, T. Vreven, K. Throssell, J. Montgomery, J. A., J. E. Peralta, F. Ogliaro, M. J. Bearpark, J. J. Heyd, E. N. Brothers, K. N. Kudin, V. N. Staroverov, T. A. Keith, R. Kobayashi, J. Normand, K. Raghavachari, A. P. Rendell, J. C. Burant, S. S. Iyengar, J. Tomasi, M. Cossi, J. M. Millam, M. Klene, C. Adamo, R. Cammi, J. W. Ochterski, R. L. Martin, K. Morokuma, O. Farkas, J. B. Foresman, D. J. Fox, Gaussian 16, Revision A.03 ed., Gaussian, Inc., Wallingford CT, **2016**.

Chapter 5

Copper(I) complexes



Parts of this chapter have been published in
S. Linert, S. Wagner, P. Schmidt, L. Higham, C. Hepples, P. Waddell, K. Karaghiosoff
Phosphorus Sulfur, **2019**, 194, 565–568.

5.1 Introduction

5.1.1 Copper(I) complexes

Copper(I) has a very manifold and interesting coordination behaviour. The usual coordination modes of copper(I) are tetrahedral, trigonal planar and linear.^[1] In the literature many copper halide complexes with various structural motifs are described. Numerous examples exist of monomeric, square/rhomboid dimeric, cubane tetrameric, “stair step” oligomeric and zigzag polymeric complexes (Figure 1).^[1-2]

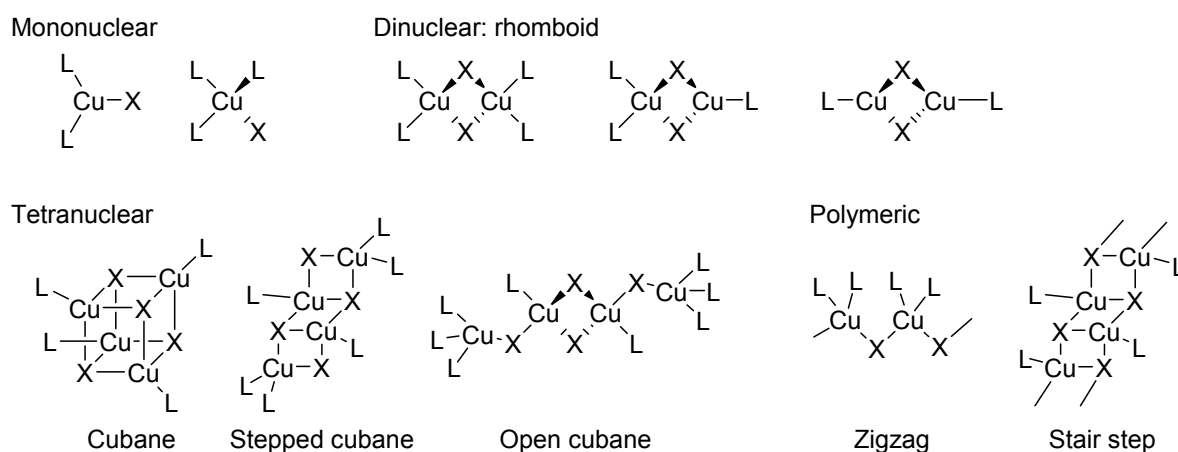


Figure 1: Typical coordination modes and structures of copper(I) complexes.

The most common ligand to metal stoichiometries are 1:1, 1:2 and 1:4. Fewer examples are known of complexes with other ligand to metal ratios.^[2a]

In many copper(I) clusters Cu...Cu distances that are shorter than the sum of the *van der Waals* radii (2.8 Å) can be found.^[3] In 2012 S. Dinda and A. G. Samuelson published a study about Cu...Cu interactions, which concluded in the statement, that Cu...Cu interactions are comparable to weak hydrogen bonds.^[4]

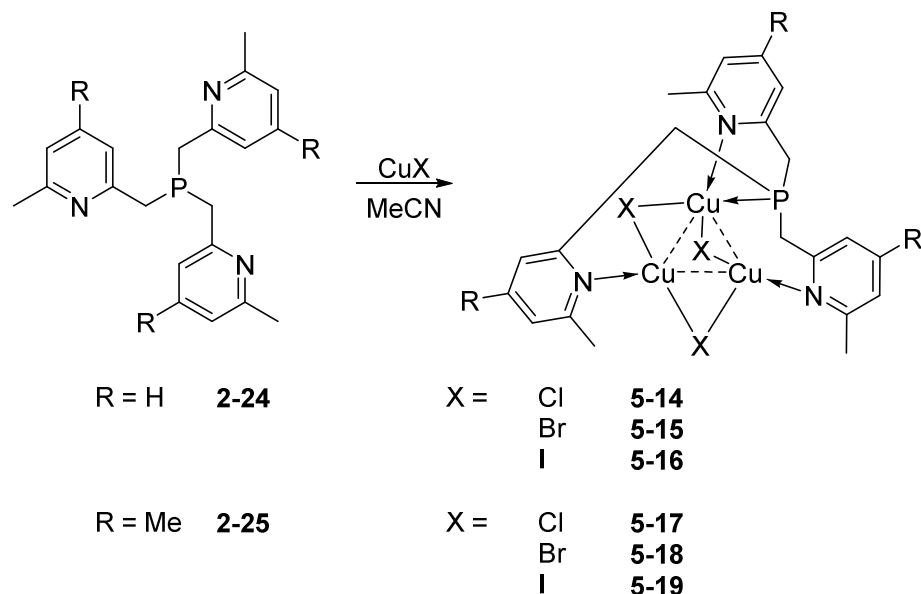
5.1.2 Luminescent properties of Cu(I) complexes

In the literature a large number of copper(I) complexes is described, which exhibit luminescent properties.^[5] The colours of the luminescence cover the entire spectrum of visible light from red to blue.^[6]

A lot of the investigations that can be found in the literature have been made on copper(I) halide complexes. Although the research is mostly focused on di- and tetranuclear complexes of the types Cu₂X₂L₄ and Cu₄X₄L₄,^[5e, 6] also mononuclear complexes and coordination polymers with luminescent properties have been referenced.^[5b, 7]

The emission of copper(I) complexes is often caused by metal-to-ligand charge transfer processes (MLCT) or ligand centred (LC) π - π^* transitions.^[8] Additionally in clusters a d-p transition from the halides to the copper atoms (XMCT) is possible, which is called the cluster-centred (CC) state.^[8] Some complexes also exhibit TADF.^[8]

The wavelength of the emission maximum can be fine-tuned by the choice of the halide and by the reduction potential of the ligand.^[6]



Scheme 3: Synthesis of copper(I) complexes **5-14** to **5-19** of **2-24** and **2-25**.

In the beginning reactions were performed with a ligand/metal ratio of 1:1. After the first crystal structures (**5-4** and **5-14**, see 5.2.3.1 and 5.2.3.5) had been obtained it was obvious that the bis- and tris(picolyl)phosphine based ligands react in a ligand/metal ratio of 1:2 or 1:3 with the copper(I) salts. Therefore the ratio was adjusted correspondingly for further reactions.

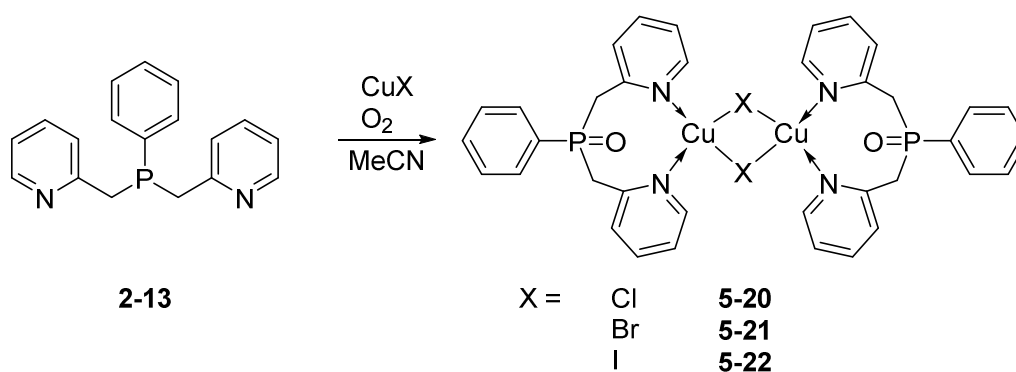
The complexes formed colourless precipitates, which were separated from the solution by filtration and dried *in vacuo*.

The complexes are insoluble in unpolar solvents like Et₂O, pentane and toluene and also almost insoluble in DCM and chloroform. The solubility in acetonitrile is very poor, but can be increased upon heating to obtain solutions for crystallisation.

Due to the low solubility it was not possible to obtain NMR spectra of the complexes. The ³¹P NMR spectra of the reaction mixtures of the reactions in a 1:1 ratio showed broad signals shifted slightly towards higher field compared to the signals in the spectra of the pure ligands. These signals are probably caused by free ligand remaining unreacted in the solution.

High resolution mass spectra of the copper halide complexes all show peaks with masses that correspond to LH⁺, LCu⁺ and LCu₂X⁺. Also for all complexes a peak for was found, which corresponds to a ligand fragment in which a P–C bond was cleaved and one of the picolyl based substituents was eliminated. In case of **5-7**, **5-11**, **5-12**, **5-16**, **5-17** and **5-19** small peaks were observed with masses of LCu₃X₂⁺.

To obtain the copper(I) halide complexes of phosphine **2-13** a solution of **2-13** in MeCN was added to suspensions of the copper salts in MeCN (Scheme 4).



Scheme 4: Synthesis of copper(I) complexes **5-20** to **5-22** of the phosphine oxide of **2-13**.

In the ^{31}P NMR spectra of the resulting solutions signals in the range of phosphine oxides were observed. This indicates that probably oxygen was present during the reaction and the phosphine oxide complexes **5-20** to **5-22** were obtained. In case of **5-20** and **5-21** this was confirmed by X-ray crystallography (see 2.3.6).

5.2.2 Photophysical data

Some of the synthesised complexes show green or green-blue luminescence in the solid state. The most intense luminescence was observed for complexes **5-1** and **5-2** (Figure 2). Complexes **5-8**, **5-14**, **5-18** and **5-19** also showed weak luminescence under UV light.

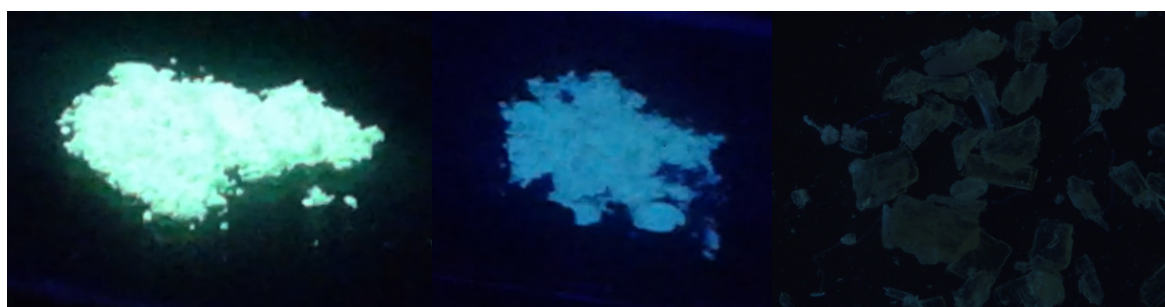


Figure 2: Luminescence of **5-1** (left), **5-2** (middle) and **5-14** (right) under UV light.

In solution no luminescence for any of the complexes could be observed, either because the luminescence is quenched or the solubility of the complexes is too low.

The emission spectrum of **5-14** shows a maximum at a wavelength of 481 nm (Figure 3).

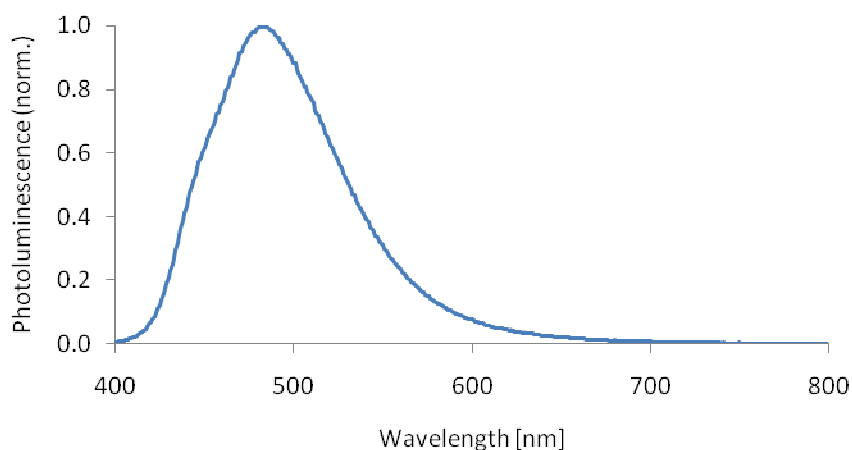


Figure 3: Fluorescence emission spectrum of **5-14** in the solid state.

From TCSPC measurements the relaxations times of **5-14** in the solid state could be determined (Figure 4). From a biexponential fit of the results the relaxation times of $\tau_1 = 0.057 \pm 0.003 \mu\text{s}$ and $\tau_2 = 0.184 \pm 0.002 \mu\text{s}$ were determined. The lifetime of S_1 , which leads to fluorescence is between 0.1 ns and 100 ns, while the lifetime of T_1 (phosphorescence) ranges from 1 μs to 1 s.^[10] The relaxation times of **5-14** indicate that probably triplet states are involved in the relaxation mechanism of the complex. To differ between phosphorescence and TADF temperature dependent TCSPC measurements would be necessary.

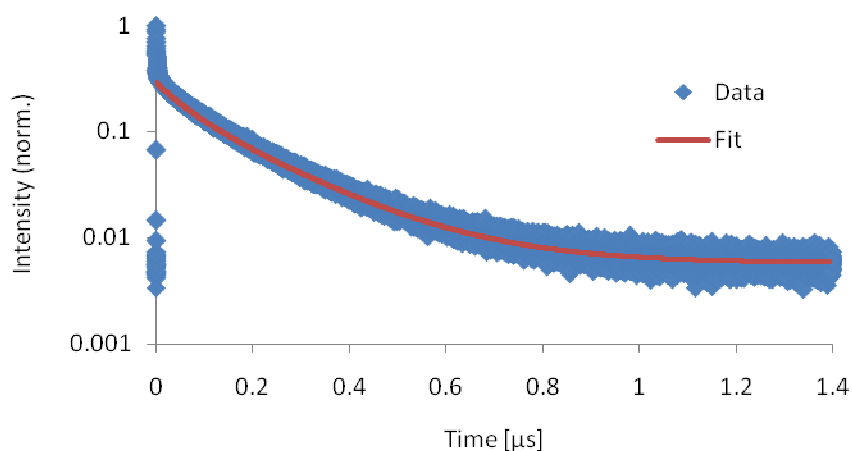


Figure 4: Results of the TCSPC measurements of **5-14**.

The phosphine oxide complexes **5-20–5-22** also show luminescence under UV light in the solid state (Figure 5).

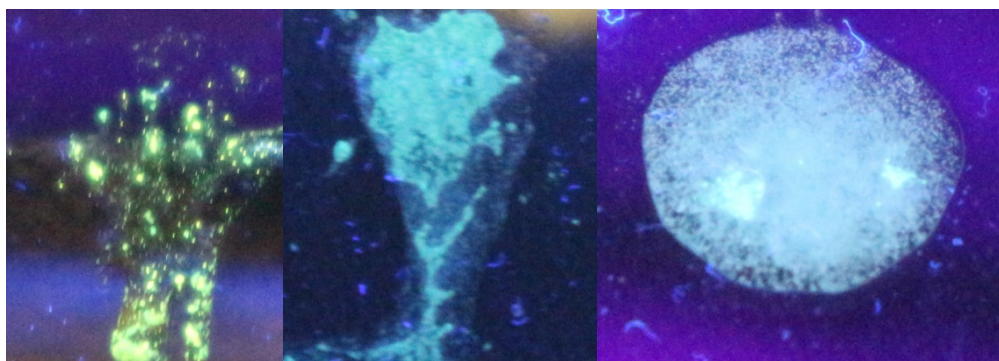


Figure 5: Luminescence of **5-20** (left), **5-21** (middle) and **5-22** (right) under UV light.

From the emission spectra it is evident that the colour of the emission is influenced by the choice of the halide. The emission maximum is blue-shifted upon changing from chloride (**5-20**, 536 nm) to bromide (**5-21**, 512 nm) and iodide (**5-22**, 487 nm) (Figure 6).

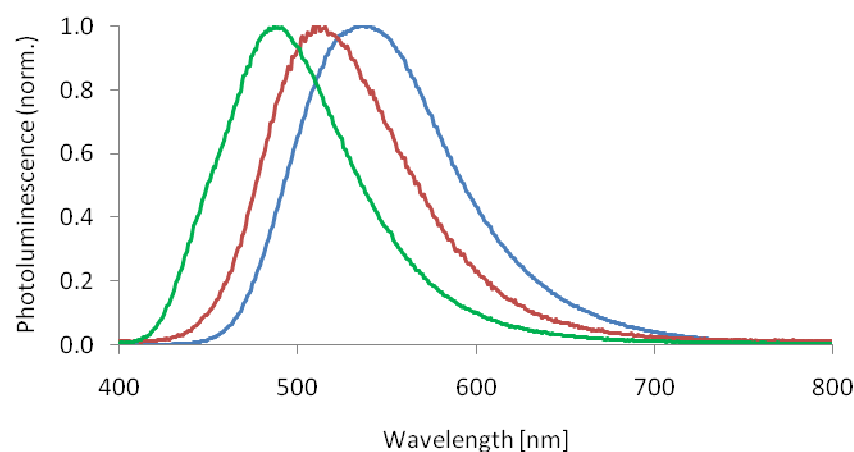


Figure 6: Fluorescence emission spectra of **5-20** (blue), **5-21** (red) and **5-22** (green) in the solid state.

TCSPC measurements of **5-20** ($\tau_1 = 2.06 \pm 0.06 \mu\text{s}$, $\tau_2 = 8.04 \pm 0.04 \mu\text{s}$), **5-21** ($\tau_1 = 1.56 \pm 0.04 \mu\text{s}$, $\tau_2 = 6.45 \pm 0.06 \mu\text{s}$) and **5-22** ($\tau_1 = 2.05 \pm 0.18 \mu\text{s}$, $\tau_2 = 7.71 \pm 0.06 \mu\text{s}$) suggest a relaxation mechanism, in which triplet states are involved.

5.2.3 Crystal structures

5.2.3.1 Crystal structure of 5-4

Single crystals of **5-4** suitable for X-ray crystallography could be obtained by slow diffusion of Et_2O in a solution in MeCN.

The complex crystallises in the monoclinic space group $P2_1/c$ with four formula units in the unit cell. The asymmetric unit comprises one half of the dimeric structure (Figure 7). Although a stoichiometry of 1:1 was used for the reaction in the complex a ligand to metal ratio of 1:2 was observed.

The dimeric molecular structure of **5-4** consists of two ligand molecules and four CuCl units (Figure 7). In the structure Cu1 is coordinated in a distorted tetrahedral conformation by P1, N1, Cl1 and the symmetry generated Cl1ⁱ. The Cu1 and Cl1 atoms form the typical four-membered Cu_2Cl_2 rhomboid. The Cu2 atom is coordinated trigonal planar by N2, Cl1 and Cl2.

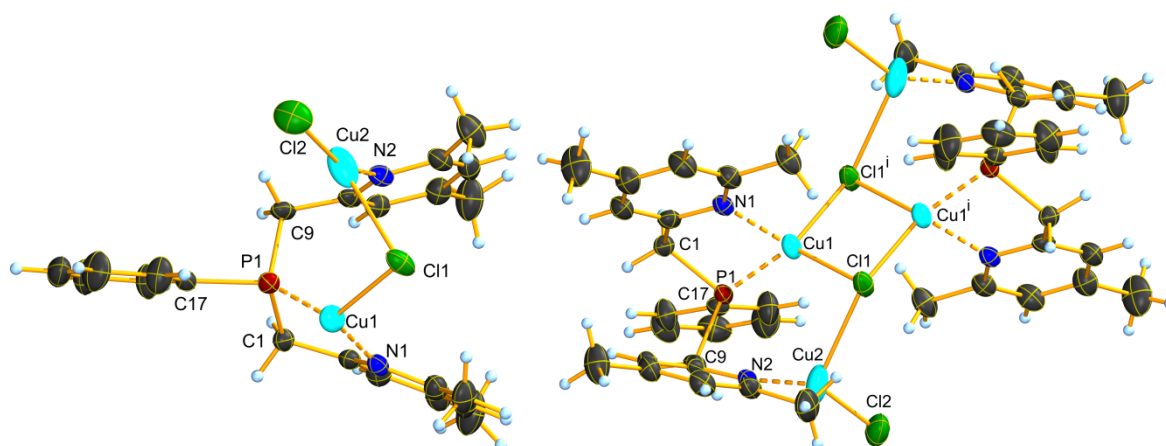


Figure 7: Asymmetric unit (left) and dimeric molecular structure (right) of complex **5-4**. Thermal ellipsoids are drawn at 50% probability level. Selected bond lengths [Å] and angles [°]: Cu1–P1: 2.202(1), Cu1–N1: 2.174(3), Cu1–Cl1: 2.351(1), Cu1–Cl1ⁱ: 2.382(1), Cu2–N2: 1.938(3), Cu2–Cl1: 2.705(1), Cu2–Cl2: 2.116(1), P1–C1: 1.832(3), P1–C9: 1.847(3), P1–C17: 1.816(3), Cu1···Cu1ⁱ: 3.127(1), P1–Cu1–N1: 86.1(1), P1–Cu1–Cl1: 127.4(1), P1–Cu1–Cl1ⁱ: 121.8(1), N1–Cu1–Cl1: 112.6(1), N1–Cu1–Cl1ⁱ: 111.4(1), Cl1–Cu1–Cl1ⁱ: 97.3(1), N2–Cu2–Cl1: 96.7(1), N2–Cu2–Cl2: 152.6(1), Cl1–Cu2–Cl2: 109.4(1), C1–P1–C9: 101.1(2), C1–P1–C17: 103.9(2), C9–P1–C17: 100.3(2). i: 2–x, 1–y, 1–z.

The Cu1–P1 distance of 2.202(1) Å is comparable to the Cu–P distances of literature known bis(picoly)phosphine copper(I) complexes with PN₂X (2.199(6) Å and 2.202(2) Å) or PNX₂ coordination (2.227(10) Å).^[11] Similar Cu–P distances have been found for various copper chloride complexes with Cu₂Cl₂ rings in which the copper atoms are additionally coordinated by PPh₃ and the nitrogen atom of a pyridine derivative (2.189(2)–2.2038(14) Å).^[5c]

The Cu1–N1 distance of 2.174(3) Å is significantly longer than the Cu–N distances found in the (PPh₃)₂(py)₂Cu₂Cl₂ complexes mentioned above (2.0473(14)–2.082(6) Å).^[5c] In contrast to these (PPh₃)₂(py)₂Cu₂Cl₂ complexes in **5-4** the phosphorus is connected to the pyridine ring *via* the methylene bridge. Due to this structure of the ligand a shorter Cu–N distance is probably not possible in **5-4**. The Cu–N distances of the picoly) nitrogen atoms of the bis(picoly)phosphine copper(I) complexes of *C. Hettstedt* (2.236(2) Å and 2.230(1) Å) are even longer than the Cu1–N1 distance of **5-4**.^[11]

The Cu1–Cl1 distance (2.351(1) Å) and the Cu1–Cl1ⁱ distance (2.382(1) Å) are slightly different, which is typical for the structural motif of the Cu₂X₂ ring.^[5c] The Cu1–Cl distances found in the structure of **5-4** are in the same range as the literature values for comparable complexes (2.3604(9)–2.4400(6) Å).^[5c]

The distance between the copper atoms in the four-membered ring Cu1 and Cu1ⁱ of 3.127(1) Å is in the same range as the literature values of complexes with Cu₂Cl₂ rhomboids, in which the other ligands at the copper are PPh₃ and a *N*-heteroaromatic compound (2.8329(4)–3.2299(3) Å).^[5c] This distance is significantly longer than the sum of the *van der Waals* radii, which means that there are no interactions between the copper atoms.

The Cu2–N2 distance of 1.938(3) Å is much shorter than the distance between Cu1 and N1. In other complexes with three coordinate copper(I) atoms coordinated by two halide atoms and a nitrogen atom of a pyridine derivative the Cu–N distances are between 1.9553(16) Å and 1.993(5) Å,^[12] which is only slightly longer than the Cu2–N2 distance of **5-4**.

The Cu2–Cl distances are very different. The Cu2–Cl2 distance of 2.116(1) Å is quite short, while the Cu2–Cl1 distance is very long (2.705(1) Å). The Cu2–Cl2 distance is comparable to the mean Cu–Cl distance of three-coordinate copper(I) atoms with terminal chlorine atoms (2.179 Å).^[13]

The P–C_{alk} bond lengths are 1.832(3) Å and 1.847(3) Å, which is shorter than the mean bond length of P–C_{sp3} bonds (1.855 Å).^[13] The length of the P1–C1 bond (1.832(3) Å) is comparable to the mean

P–C_{Alk} bonds in complexes of triethylphosphine, tri-*n*-propylphosphine, methyldiphenylphosphine and dimethyl(phenyl)phosphine (1.825–1.832 Å).^[13] The P–C_{Ar} bond of **5-4** (1.816(3) Å) is much shorter than the mean P–C_{Ar} bond length (1.836 Å).^[13] In complexes of triphenylphosphine, methyldiphenylphosphine and dimethyl(phenyl)phosphine the mean P–C_{Ar} bond lengths are 1.823–1.828 Å,^[13] which is slightly longer than the P–C_{Ar} bond of **5-4**.

The angles around Cu1 vary in the range from 86.1(1)° to 127.4(1)° around the ideal tetrahedral angle of 109.5°. The Cl1–Cu1–Cl1ⁱ angle is 97.3(1)°, which is slightly smaller than the literature values of 97.74(2)° and 100.98(5)° found in other complexes with Cu₂Cl₂ rhomboids.^[14] The P1–Cu1–N1 angle of 86.1(1)° is approx. 2° larger than the same angle observed in the bis(picolyl)phosphine complexes (84.1(5)° and 84.2(2)°).^[11]

The angles around Cu2 vary over a wide range from 96.7(1)° to 152.6(1)°, but they sum up to 358.7°, which means that the conformation around Cu2 is almost perfectly planar.

The C–P–C angles around P1 vary in a small range from 100.3(1)° to 103.9(1)°, which is slightly smaller than the tetrahedral angle. This implies that the conformation around the phosphorus is distorted tetrahedral.

In the crystal the dimers are arranged in layers in an AB pattern along the *b* and *c* axis (Figure 8).

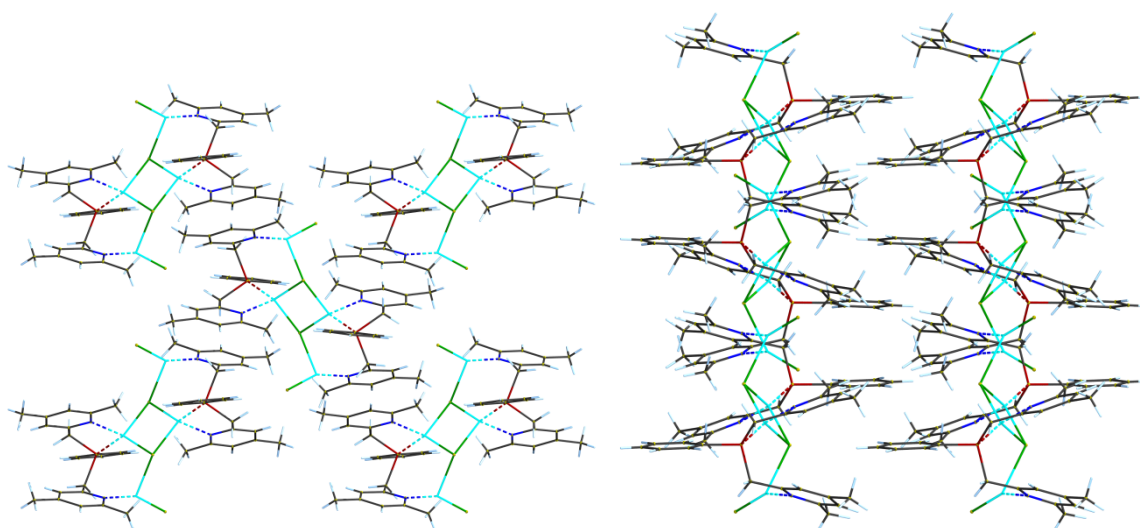


Figure 8: Crystal structure of **5-4**. View along the *a* axis (left) and *c* axis (right).

5.2.3.2 Crystal structures of **5-7** and **5-11**

Single crystals of **5-7** suitable for X-ray crystallography could be obtained by slow diffusion of Et₂O in a solution in MeCN (**5-7a**). From a later reaction to resynthesise complex **5-7** single crystals suitable for X-ray crystallography were obtained from a solution in MeCN. These crystals turned out to be of a structural isomer of **5-7** (**5-7b**).

The complex **5-7a** crystallises in the monoclinic space group *P*2₁/*c* with four formula units in the unit cell.

The molecular structure of **5-7a** consists of one ligand molecule and three CuCl units (Figure 9). In the structure Cu1 is coordinated trigonal planar by N1, Cl1 and Cl2. Cu2 is coordinated in a distorted tetrahedral conformation by P1, N2, Cl1 and Cl3, while Cu3 is coordinated linear by Cl2 and Cl3. The

copper and chlorine atoms form a six-membered ring (Figure 9). A search in the database of the CCDC on July 1st 2020 gave no other results for copper(I) halide complexes with six-membered Cu₃X₃ rings, in which the copper atoms were coordinated tetrahedrally, trigonal planar and linear.

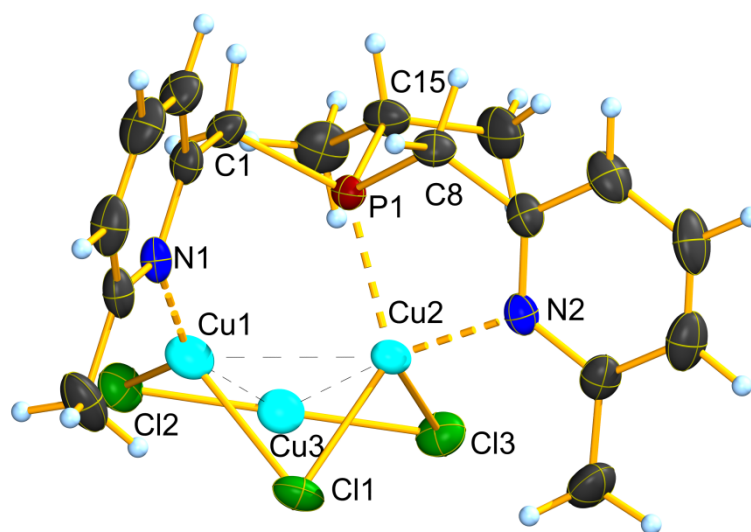


Figure 9: Asymmetric unit of **5-7a**. Thermal ellipsoids are drawn at 50% probability level. Selected bond lengths [Å] and angles [°]: Cu1–N1: 1.979(4), Cu1–Cl1: 2.342(1), Cu1–Cl2: 2.305(1), Cu2–P1: 2.220(1), Cu2–N2: 2.062(3), Cu2–Cl1: 2.321(1), Cu2–Cl3: 2.577(1), Cu3–Cl2: 2.134(1), Cu3–Cl3: 2.126(1), P1–C1: 1.853(4), P1–C8: 1.834(4), P1–C15: 1.843(4), Cu1...Cu2: 2.652(1), Cu1...Cu3: 2.727(1), Cu2...Cu3: 2.590(1), P1...Cu1: 3.023(1), P1...Cu3: 3.543(1), N1–Cu1–Cl1: 116.8(1), N1–Cu1–Cl2: 133.5(1), Cl1–Cu1–Cl2: 108.5(1), P1–Cu2–N2: 88.5(1), P1–Cu2–Cl1: 129.3(1), P1–Cu2–Cl3: 112.9(1), N2–Cu2–Cl1: 117.2(1), N2–Cu2–Cl3: 109.5(1), Cl1–Cu2–Cl3: 99.2(1), Cl2–Cu3–Cl3: 179.5(1), C1–P1–C8: 102.4(2), C1–P1–C15: 100.9(2), C8–P1–C15: 104.6(2).

The tetrahedral coordination situation around Cu2 is often found in copper(I) complexes and the Cu–P (2.220(1) Å), Cu–N (2.062(3) Å) and Cu–Cl1 (2.321(1) Å) distances are in the typical ranges for these types of distances (mean atom distances: Cu–P: 2.252 Å (triphenylphosphine), Cu–N: 2.024 Å (pyridine), Cu–Cl: 2.364 Å (μ_2 -Cl)).^[13] The Cu2–Cl3 distance of 2.577(1) Å is much longer than the mean Cu–Cl distance of four-coordinate Cu(I) atoms to μ_2 -Cl atoms.^[13]

The Cu1–N1 distance (1.979(4) Å) is shorter than the Cu2–N2 distance, but within the range found in the literature for this type of coordination (1.9553(16) Å–1.993(5) Å).^[12] The Cu1–Cl distances (2.342(1) Å and 2.305(1) Å) are longer than the mean Cu–Cl distance for three-coordinate copper(I) atoms (2.275 Å),^[13] but in the same range as the Cu–Cl distances of the N-(2-pyridylmethyl)acetamide CuCl complex (2.2246(4) Å and 2.3997(4) Å).^[12a]

The Cu–Cl distances at Cu3 (2.134(2) Å and 2.126(2) Å) are comparable to those found for the CuCl₂[–] ion (2.036(5)–2.171(5) Å).^[15]

The distances between P1 and Cu1 (3.023(1) Å) or Cu3 (3.543(1) Å) are much longer than the P1–Cu2 distance and too long for any bonding interactions.

The Cu–Cu distances are in the range of 2.590(1)–2.727(1) Å, which is shorter than the sum of the *van der Waals* radii. This means that weak Cu...Cu interactions can be found in the Cu₃Cl₃ cluster of **5-7a**.

The P–C bond lengths are between 1.835(4) Å and 1.853(5) Å, which is in the typical range of P–C_{Alk} bond lengths in complexes of tertiary phosphines (mean bond lengths: 1.825–1.863 Å).^[13]

The angles around Cu2 vary in the range of –21 ° to +20 ° around the ideal tetrahedral angle of 109.5 °. The P1–Cu2–N2 (88.5(1) °) and the Cl1–Cu2–Cl3 (99.2(1) °) angle are smaller than the ideal

tetrahedral angle, while the P1–Cu2–Cl (112.9(1) ° and 129.3(1) °) and the N2–Cu2–Cl (109.5(1) ° and 117.2(1) °) angles are larger than 109.5 °.

The angles around Cu1 vary over a range from 108.5(1) ° to 133.5(1) ° and sum up to 358.8 °, which indicates that the conformation around Cu1 is almost perfectly planar.

The Cl2–Cu3–Cl3 angle of 179.5(1) ° implies an almost perfect linear conformation of Cu3, which resembles the conformation of the copper in the CuCl_2^- ion.

The C–P–C angles around P1 vary in a small range from 100.9(2) ° to 104.6(2) ° and are all smaller than the tetrahedral angle, which indicates a distorted tetrahedral conformation around the phosphorus atom.

In the crystal the molecules are arranged in layers in an AB pattern along the *b* and *c* axis (Figure 10).

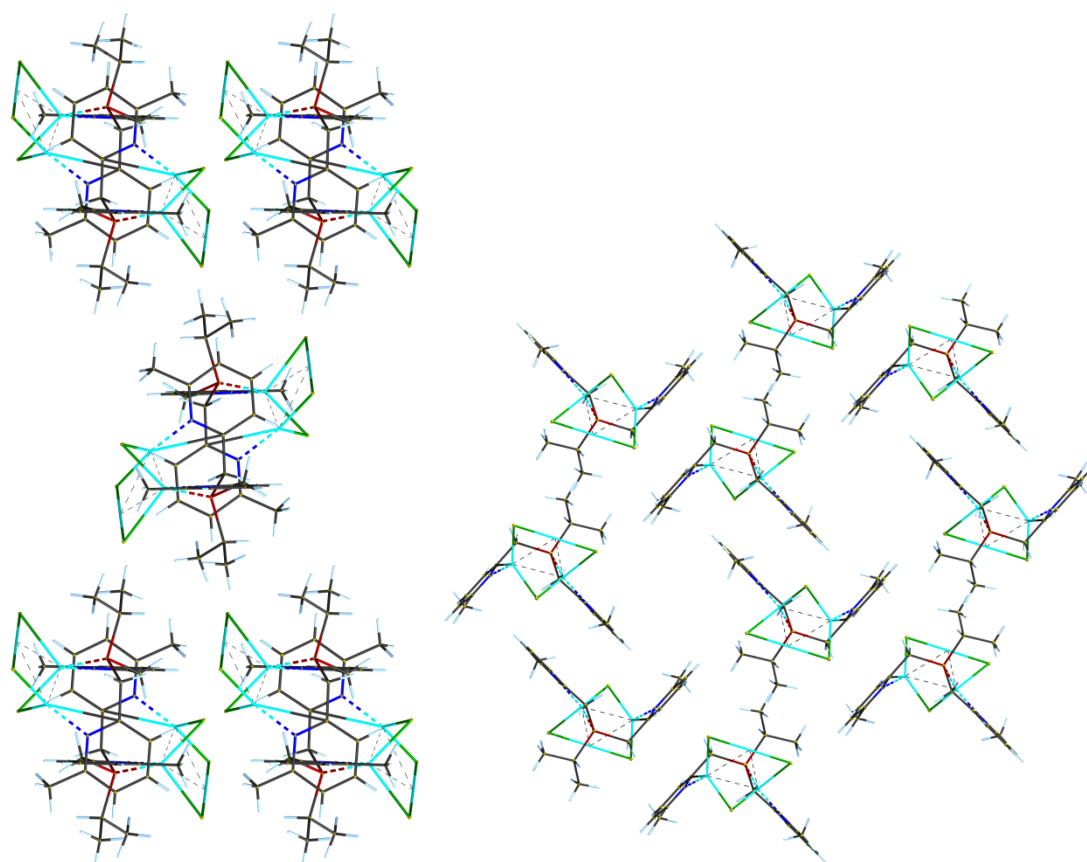


Figure 10: Crystal structure of **5-7a**. View along the *a* axis (left) and *b* axis (right).

The view along the *b* axis shows, that two of the molecules at a time are arranged with the pyridine rings containing N2 side by side. The distance between the centres of the pyridine rings is 3.638(1) Å, which is within the range of attractive π - π interactions of 3.3–3.8 Å (Figure 11).^[16] The pyridine rings are arranged antiparallel to each other.

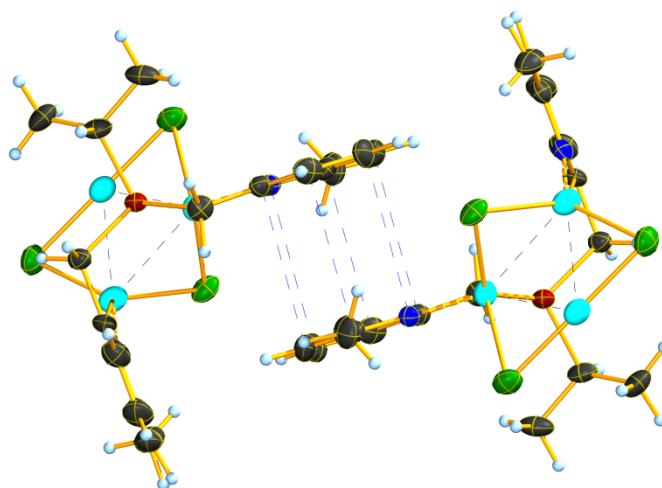


Figure 11: π - π interactions in the crystal of **5-7a**.

Crystals of **5-7b** and **5-11** suitable for single crystal X-ray analysis were obtained from solutions in MeCN. Compound **5-7b** crystallises in the orthorhombic space group *Pba*2 with two ligand molecules and six CuCl units in the asymmetric unit, while **5-11** crystallises in the orthorhombic space group *Pna*2₁ and the asymmetric unit comprises only one molecule of the ligand and three units of CuCl. The structures of **5-7b** and **5-11** are isostructural. All copper atoms are coordinated trigonal planar by each two chlorine atoms and one nitrogen or phosphorus atom of the ligand (Figure 12).

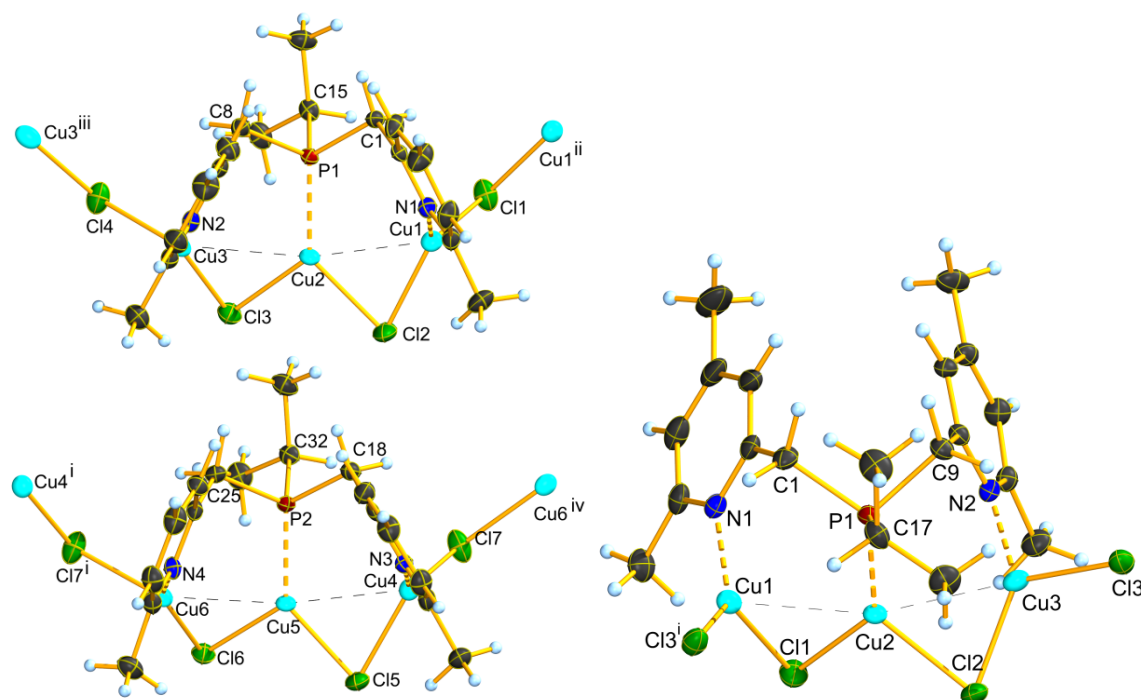


Figure 12: Asymmetric unit of **5-7b** (left) and **5-11** (right). Thermal ellipsoids are drawn at 50% probability level. Selected bond lengths [Å] and angles [°] of **5-7b**: Cu1–N1: 1.990(5), Cu1–Cl1: 2.265(2), Cu1–Cl2: 2.256(2), Cu2–P1: 2.205(2), Cu2–Cl2: 2.288(2), Cu2–Cl3: 2.309(2), Cu3–N2: 1.969(5), Cu3–Cl3: 2.236(2), Cu3–Cl4: 2.286(1), Cu4–N3: 1.978(5), Cu4–Cl5: 2.323(2), Cu4–Cl7: 2.223(2), Cu5–P2: 2.202(2), Cu5–Cl5: 2.269(2), Cu5–Cl6: 2.336(2), Cu6–N4: 1.960(5), Cu6–Cl6: 2.201(2), Cu6–Cl7ⁱ: 2.362(2), Cu1...Cu2: 2.694(1), Cu2...Cu3: 2.850(1), Cu4...Cu5: 2.710(1), Cu5...Cu6: 2.721(1), P1–C1: 1.847(6), P1–C8: 1.847(6), P1–C15: 1.850(6), P2–C18: 1.852(6), P2–C25: 1.850(6), P2–C32: 1.846(6), N1–Cu1–Cl1: 123.6(2), N1–Cu1–Cl2: 119.7(2), Cl1–Cu1–Cl2: 116.6(1), P1–Cu2–Cl2: 133.9(1), P1–Cu2–Cl3: 126.8(1), Cl2–Cu2–Cl3: 98.9(1), N2–Cu3–Cl3: 130.5(2), N2–Cu3–Cl4: 117.0(2), Cl3–Cu3–Cl4: 112.5(1), N3–Cu4–Cl5: 114.7(2), N3–Cu4–Cl7: 130.4(2), Cl5–Cu4–Cl7: 114.9(1), P2–Cu5–Cl5: 136.0(1), P2–Cu5–Cl6: 124.0(1), Cl5–Cu5–Cl6: 99.3(1), N4–Cu6–Cl6: 143.8(2), N4–Cu6–Cl7ⁱ: 109.9(2), Cl6–Cu6–Cl7ⁱ: 106.2(1), Cu1–Cl1–Cu1ⁱⁱ: 103.0(1), Cu1–Cl2–Cu2: 72.7(1), Cu2–Cl3–Cu3: 77.7(1), Cu3–Cl4–Cu3ⁱⁱⁱ: 120.9(1), Cu4–Cl5–Cu5: 72.3(1), Cu5–Cl6–Cu6: 73.6(1), Cu4–Cl7–Cu6^{iv*}: 113.7(1), C1–P1–C8: 103.3(3), C1–P1–C15: 99.9(3), C8–P1–C15:

103.7(3), C18–P2–C25: 103.3(3), C18–P2–C32: 101.4(3), C25–P2–C32: 102.3(3). i: $-0.5+x, 0.5-y, z$, ii: $1-x, 1-y, z$, iii: $-x, 1-y, z$, iv: $0.5+x, 0.5-y, z$. Selected bond lengths [Å] and angles [°] of **5-11**: Cu1–N1: 1.990(3), Cu1–Cl1: 2.341(1), Cu1–Cl3ⁱ: 2.219(1), Cu2–P1: 2.197(1), Cu2–Cl1: 2.257(1), Cu2–Cl2: 2.343(1), Cu3–N2: 1.965(3), Cu3–Cl2: 2.215(1), Cu3–Cl3: 2.345(1), Cu1...Cu2: 2.706(1), Cu2...Cu3: 2.682(1), P1–C1: 1.854(4), P1–C9: 1.850(4), P1–C17: 1.852(4), N1–Cu1–Cl1: 105.7(1), N1–Cu1–Cl3ⁱ: 131.3(1), Cl1–Cu1–Cl3ⁱ: 123.0(1), P1–Cu2–Cl1: 133.1(1), P1–Cu2–Cl2: 125.6(1), Cl1–Cu2–Cl2: 101.0(1), N2–Cu3–Cl2: 138.1(1), N2–Cu3–Cl3: 109.6(1), Cl2–Cu3–Cl3: 112.2(1), Cu1–Cl1–Cu2: 72.1(1), Cu2–Cl2–Cu3: 72.1(1), Cu3–Cl3–Cu1ⁱⁱ: 113.0(1), C1–P1–C9: 103.0(2), C1–P1–C17: 101.1(2), C9–P1–C17: 102.7(2). i: $0.5+x, 1.5-y, z$, ii: $-0.5+x, 1.5-y, z$.

In the structures the Cu–P distances range from 2.197(1) Å to 2.205(2) Å, which is slightly shorter than the Cu–P distance of **5-7a**. A comparison of these distances with literature known structures, in which copper atoms are coordinated trigonal planar by the phosphorus atom of a tertiary phosphine and two chlorine atoms shows that the Cu–P distances of **5-7b** and **5-11** are within the range found in such complexes (2.149(3)–2.211(2) Å).^[17]

The Cu–N distances of complexes **5-7b** and **5-11** (1.960(5)–1.990(5) Å) are comparable to the Cu1–N1 distance (1.979(4) Å) found in the structure of **5-7a**, meaning that the distances are in the typical range of Cu–N distances of complexes with NCuX₂ coordination (1.9553(16) Å–1.993(5) Å).^[12]

The Cu–Cl distances cover a wide range from 2.201(2) Å to 2.362(2) Å around the mean Cu–Cl distance of three-coordinate copper atoms to μ_2 -chlorine atoms (2.275 Å).^[13]

The short Cu...Cu distances of 2.682(1)–2.850(1) Å indicate the presence of weak Cu...Cu interactions, although the distance between Cu2 and Cu3 (2.850(1) Å) in the structure of **5-7b** is slightly longer than the sum of the *van der Waals* radii (2.8 Å).

The P–C bond lengths (1.846(6)–1.854(4) Å) found for **5-7b** and **5-11** are in the same range as those of **5-7a**, which is typical for P–C_{Alk} bonds of tertiary phosphine complexes (mean bond lengths: 1.825–1.863 Å).^[13]

The sums of the angles around the copper atoms of **5-7b** and **5-11** are between 359.3 ° and 360.0 °, meaning that all copper atoms are coordinated almost perfectly trigonal planar. The N–Cu–Cl angles vary strongly from 105.7(1) ° to 143.8(2) °, while the P–Cu–Cl angles cover a smaller range between 124.0(1) ° and 136.0(1) °. The Cl–Cu–Cl angles at the copper atoms coordinated by phosphorus (Cu2 and Cu5; 98.9(1)–101.0(1) °) are smaller than those at the other copper atoms (106.2(1)–123.0(1) °). The Cu–Cl–Cu angles at the chlorine atoms between the ligand units (Cl1, Cl4 and Cl7 in the structure of **5-7b** and Cl3 in the structure of **5-11**; 103.0(1)–120.9(1) °) are significantly larger than the Cu–Cl–Cu angles at the other chlorine atoms (72.1(1)–77.7(1) °). The small Cu–Cl–Cu angles of 72.1(1) ° to 77.7(1) ° correspond to the short Cu...Cu distances.

The C–P–C angles of 99.9(3) ° to 103.7(3) ° are smaller than the ideal tetrahedral angle. This implies that the conformation around the phosphorus atoms is distorted tetrahedral, as usual for tertiary phosphine complexes.

The structures of **5-7b** and **5-11** are polymeric. In the crystal structure the copper and chlorine atoms form (CuCl)_n chains, which are coordinated by the ligand molecules alternating on both sides of the chain (Figure 13).

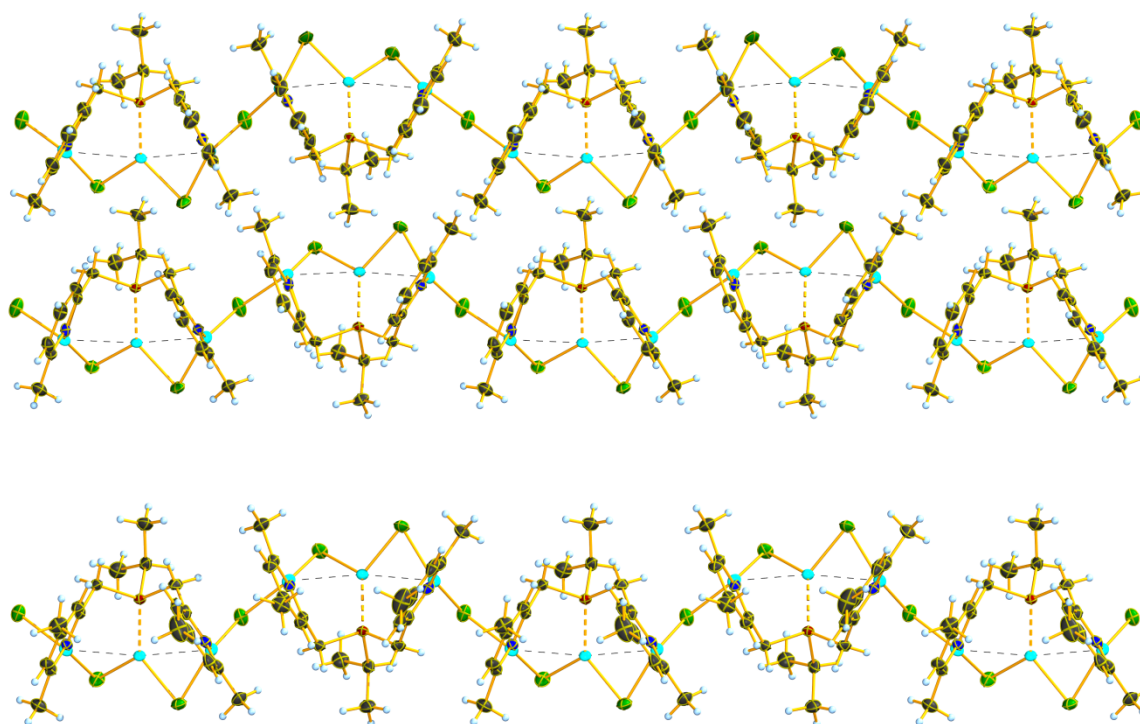


Figure 13: CuCl-chains in the crystal structures of **5-7b** (top) and **5-11** (bottom).

These chains are aligned along the a axis; along the b axis the chains are stacked above each other (Figure 14).

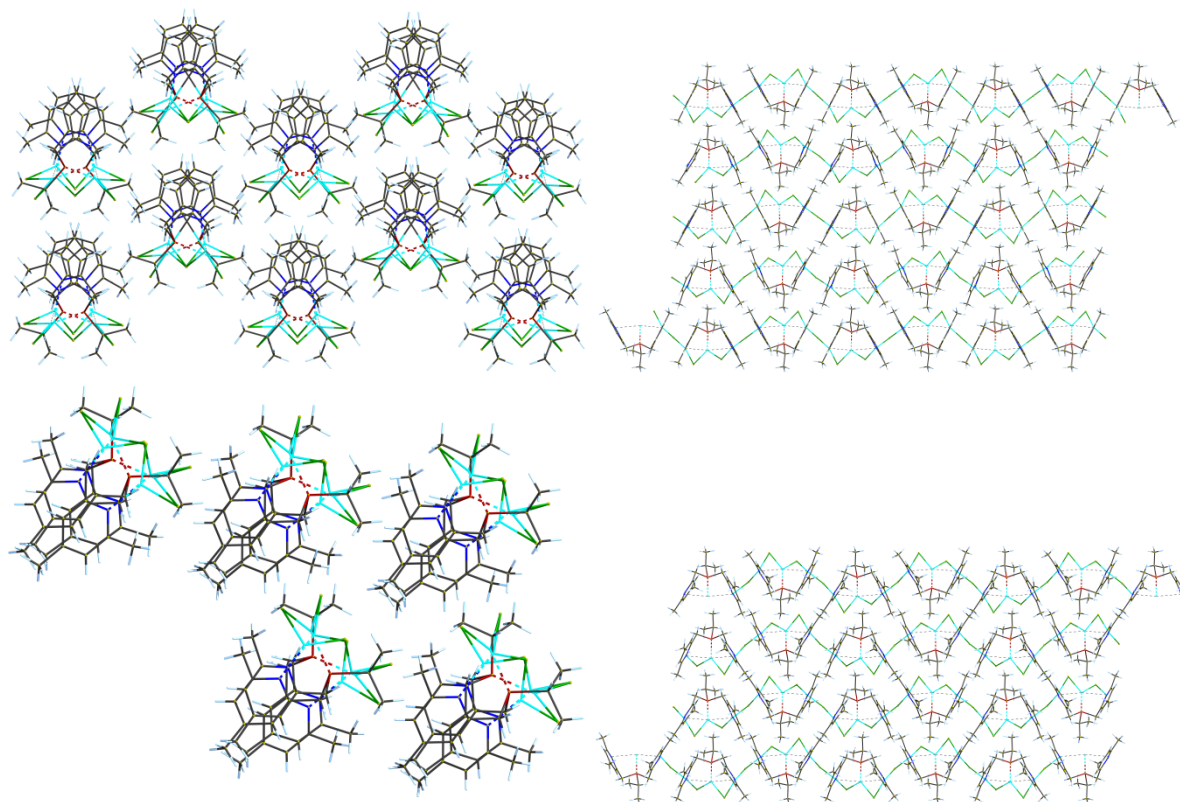


Figure 14: Crystal structures of **5-7b** (top) and **5-11** (bottom). View along the a axis (left) and the c axis (right).

Figure 15 shows the asymmetric units of **5-7a** and **5-7b**. In the direct comparison of the structural isomers of **5-7** several differences can be seen. In the case of **5-7a** a monomeric structure is observed, which is stabilised by π - π interactions. In contrast the structure of **5-7b** is polymeric. Also the coordination of the ligand to the copper atoms is different in these two isomers. While all copper atoms in **5-7b** are coordinated trigonal planar by two chlorine atoms and either phosphorus or a nitrogen atom of the ligand, the three copper atoms in **5-7a** are coordinated in three different structural motifs (distorted tetrahedral, trigonal planar and linear).

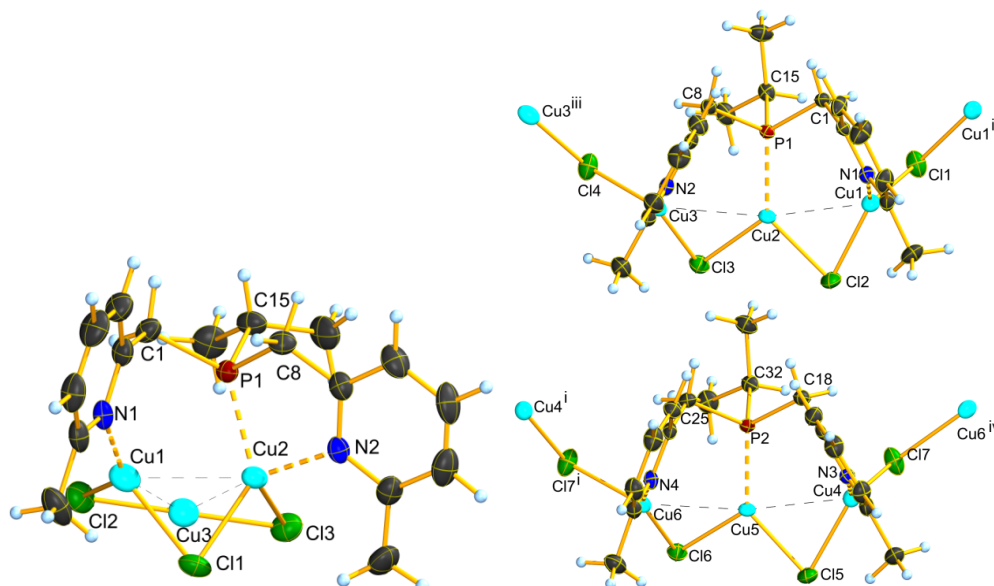


Figure 15: Asymmetric unit of **5-7a** (left) and **5-7b** (right). Thermal ellipsoids are drawn at 50% probability level.

5.2.3.3 Crystal structures of **5-9** and **5-13**

Single crystals of **5-9** suitable for X-ray crystallography could be obtained after leaving a solution in MeCN for three days. Crystals of **5-13** suitable for X-ray crystallography were obtained by slow diffusion of Et₂O into a solution in MeCN.

Complex **5-9** crystallises in the monoclinic space group *Cc* with four formula units in the unit cell, while complex **5-13** crystallises in the orthorhombic space group *Pbca* with eight formula units in the unit cell. As found for the CuCl complexes **5-7b** and **5-11** the structures of the CuI complexes **5-9** and **5-13** with the same ligands are isostructural.

The asymmetric unit of **5-9** comprises two ligand molecules and six CuI units, while the asymmetric unit of **5-13** comprises only one ligand molecule and three units of CuI (Figure 16). These findings also are analogous to those of the CuCl complexes. In each of the structures of **5-9** and **5-13** three copper atoms and three iodine atoms form six-membered rings. Two of the copper atoms in each ring (Cu1, Cu2 and Cu4, Cu5) are coordinated distorted tetrahedrally by each one nitrogen atom of the ligands, two iodine atoms and a bridging phosphorus atom. The other copper atoms (Cu3 and Cu6) are coordinated trigonal planar by three iodine atoms. One of these copper–iodine interactions connects the copper atoms with an iodine atom of the neighbouring six-membered ring (I1 and I4).

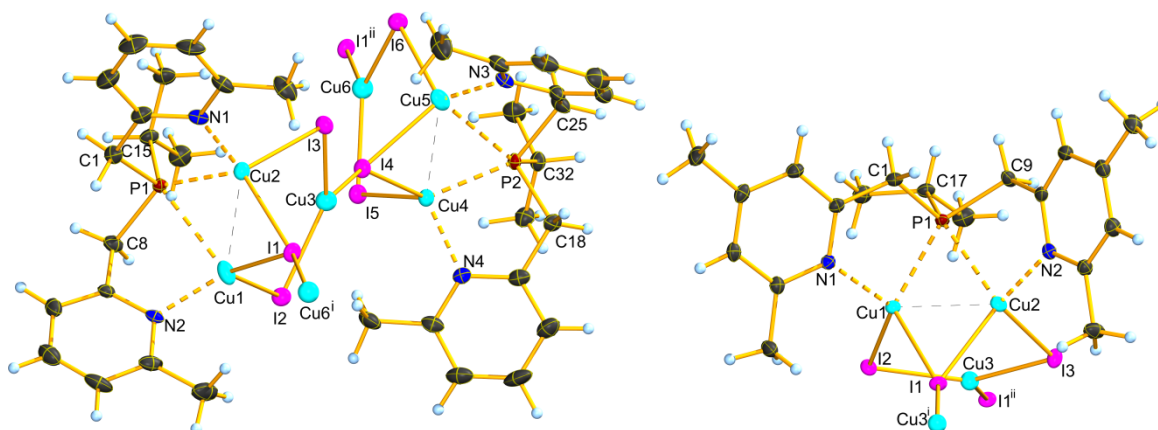


Figure 16: Asymmetric unit of **5-9** (left) and **5-13** (right). Thermal ellipsoids are drawn at 50% probability level. Selected bond lengths [Å] and angles [°] of **5-9**: Cu1–P1: 2.630(2), Cu1–N2: 2.026(5), Cu1–I1: 2.668(1), Cu1–I2: 2.576(1), Cu2–P1: 2.290(2), Cu2–N1: 2.057(5), Cu2–I1: 2.649(1), Cu2–I3: 2.634(1), Cu3–I2: 2.523(1), Cu3–I3: 2.521(1), Cu3–I4: 2.589(1), Cu4–P2: 2.285(2), Cu4–N4: 2.057(5), Cu4–I4: 2.647(1), Cu4–I5: 2.642(1), Cu5–P2: 2.641(2), Cu5–N3: 2.033(5), Cu5–I4: 2.684(1), Cu5–I6: 2.569(1), Cu6–I1: 2.586(1), Cu6–I5: 2.518(1), Cu6–I6: 2.526(1), Cu1...Cu2: 2.545(1), Cu1...Cu3: 3.782(1), Cu2...Cu3: 3.802(1), Cu4...Cu5: 2.539(1), Cu4...Cu6: 3.782(1), Cu5...Cu6: 3.766(1) P1...Cu3: 4.427(2), P2...Cu6: 4.448(2), P1–C1: 1.840(6), P1–C8: 1.859(6), P1–C15: 1.849(6), P2–C18: 1.844(6), P2–C25: 1.860(6), P2–C32: 1.844(6), P1–Cu1–N2: 86.0(2), P1–Cu1–I1: 109.7(1), P1–Cu1–I2: 110.0(1), N2–Cu1–I1: 115.5(1), N2–Cu1–I2: 118.0(1), I1–Cu1–I2: 113.9(1), P1–Cu2–N1: 88.9(2), P1–Cu2–I1: 122.4(1), P1–Cu2–I3: 115.1(1), N1–Cu2–I1: 111.2(1), N1–Cu2–I3: 115.6(1), I1–Cu2–I3: 103.8(1), I2–Cu3–I3: 124.1(1), I2–Cu3–I4: 120.0(1), I3–Cu3–I4: 115.1(1), P2–Cu4–N4: 89.1(2), P2–Cu4–I4: 122.7(1), P2–Cu4–I5: 115.4(1), N4–Cu4–I4: 110.4(1), N4–Cu4–I5: 114.1(1), I4–Cu4–I5: 104.8(1), P2–Cu5–N3: 86.1(2), P2–Cu5–I4: 108.9(1), P2–Cu5–I6: 111.6(1), N3–Cu5–I4: 114.1(1), N3–Cu5–I6: 119.0(1), I4–Cu5–I6: 113.6(1), I1ⁱⁱ–Cu6–I5: 115.7(1), I1ⁱⁱ–Cu6–I6: 118.5(1), I5–Cu6–I6: 124.9(1), Cu1–P1–Cu2: 61.9(1), Cu4–P2–Cu5: 61.6(1), C1–P1–C8: 98.9(3), C1–P1–C15: 102.2(3), C8–P1–C15: 98.4(3), C18–P2–C25: 98.9(3), C18–P2–C32: 102.3(3), C25–P2–C32: 98.6(3). i: x,y,1+z, ii: x,y,-1+z. Selected bond lengths [Å] and angles [°] of **5-13**: Cu1–P1: 2.347(1), Cu1–N1: 2.030(2), Cu1–I1: 2.680(1), Cu1–I2: 2.622(1), Cu2–P1: 2.442(1), Cu2–N2: 2.035(2), Cu2–I1: 2.705(1), Cu2–I3: 2.589(1), Cu3–I1: 2.569(1), Cu3–I2: 2.525(1), Cu3–I3: 2.521(1), Cu1...Cu2: 2.481(1), Cu1...Cu3: 3.888(1), Cu2...Cu3: 3.829(1), P1...Cu3: 4.621(1), P1–C1: 1.836(2), P1–C9: 1.855(2), P1–C17: 1.850(2), P1–Cu1–N1: 89.0(1), P1–Cu1–I1: 118.3(1), P1–Cu1–I2: 116.4(1), N1–Cu1–I1: 111.3(1), N1–Cu1–I2: 117.6(1), I1–Cu1–I2: 104.5(1), P1–Cu2–N2: 88.9(1), P1–Cu2–I1: 114.0(1), P1–Cu2–I3: 117.6(1), N2–Cu2–I1: 115.8(1), N2–Cu2–I3: 113.0(1), I1–Cu2–I3: 107.2(1), I1ⁱⁱ–Cu3–I2: 119.9(1), I1ⁱⁱ–Cu3–I3: 118.6(1), I2–Cu3–I3: 120.5(1), Cu1–P1–Cu2: 62.4(1), C1–P1–C9: 97.5(1), C1–P1–C17: 102.9(1), C9–P1–C17: 97.6(1). i: 1-x,-0.5+y,1.5-z, ii: 1-x,0.5+y,1.5-z.

There is only a small number of copper(I) complexes with bridging phosphine ligands described in the literature.^[18] *F. Leca et al.* reported the first examples in 2005 with a ligand based on 2,5-bis(2-pyridyl)phosphole (Figure 17).^[19]

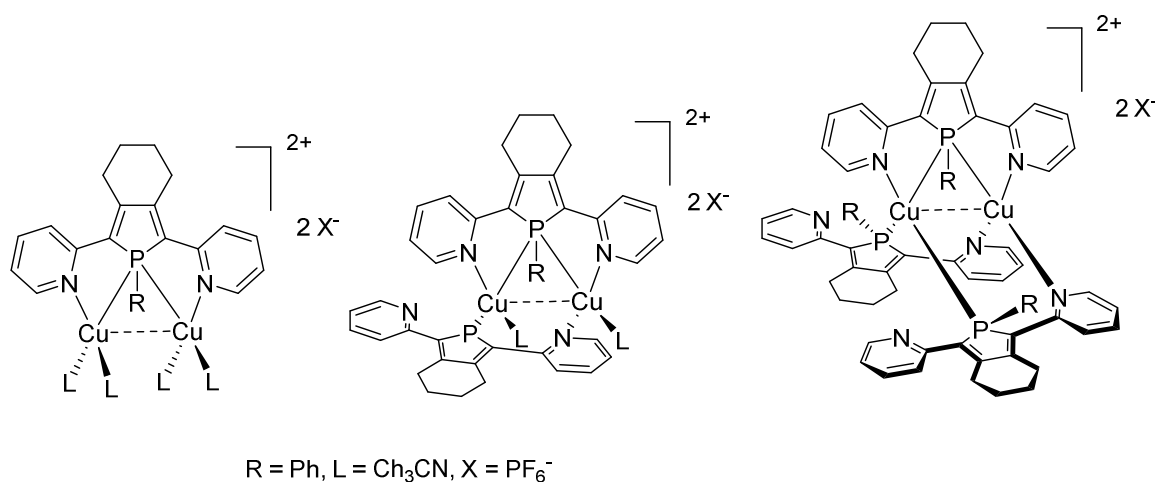


Figure 17: First examples of Cu(I) complexes with bridging phosphine ligands.^[19]

As found for the complexes described in the literature^[18] the coordination of the phosphorus to the copper atoms is asymmetric in complexes **5-9** and **5-13**. The Cu–P distances in complex **5-9** cover a quite wide range from 2.285(2) Å to 2.641(2) Å, while the Cu–P distances of **5-13** are much closer to each other (2.347(1) Å and 2.442(1) Å). All Cu–P distances are in the same range as the Cu–P distances of copper(I) complexes of bridging phosphines discussed in the literature (2.230(3)–2.728(3) Å).^[18]

The Cu–N distances of complexes **5-9** and **5-13** (2.026(5)–2.057(5) Å) are slightly longer than the mean atom distance found in complexes with pyridine nitrogen atoms coordinating to four-coordinate copper atoms (2.024 Å).^[13]

The Cu–I distances range from 2.518(1) Å to 2.705(1) Å. This corresponds with the mean Cu–I distance in complexes with μ_2 -iodine atoms (2.647 Å).^[13] The Cu–I distances at the four-coordinate copper atoms (2.569(1)–2.705(1) Å) are longer than those at the three-coordinate copper atoms (2.518(1)–2.589(1) Å). This is also found in the literature, although the mean atom distances (four-coordinate: 2.830 Å, three-coordinate: 2.661 Å) are longer than the distances found in complexes **5-9** and **5-13**.^[13] The Cu–I distances of the μ_3 -iodine atoms (2.589(1)–2.705(1) Å) are always longer than those of the μ_2 -iodine atoms (2.518(1)–2.642(1) Å) coordinating to the same copper atom. This corresponds to the literature, which reports a mean Cu– μ_2 -I distance of 2.647 Å and a mean Cu– μ_3 -I distance of 2.690 Å.^[13]

The Cu...Cu distances between the pairs Cu1/Cu2 and Cu4/Cu5 (2.481(1)–2.545(1) Å) are quite short, but still in the same range as those reported for other copper complexes of bridging phosphines (2.4882(12)–2.9501(6) Å).^[18] The short Cu...Cu distances of **5-9** and **5-13** are much shorter than the sum of the *van der Waals* radii, which indicates that there are weak Cu...Cu interactions between these copper atoms. The other Cu...Cu distances are much longer (3.766(1)–3.888(1) Å) and clearly no interactions can be found between the copper atoms.

The bond lengths of the P–C bonds (1.836(2)–1.860(6) Å) concur with the mean P–C_{Alk} bonds of tertiary phosphine complexes (1.825–1.863 Å).^[13]

The angles around the tetrahedrally coordinated copper atoms range from 86.0(2) ° to 122.7(1) °. The P–Cu–N angles (86.0(2)–89.1(2) °) are significantly smaller than the ideal tetrahedral angle (109.5 °), but comparable to those of complexes **5-4** and **5-7a**. All N–Cu–I angles (110.4(1)–119.0(1) °) and the P–Cu–I angles (108.9(1)–122.7(1) °) with one exception of 108.9(1) ° are larger than the tetrahedral angle. The I–Cu–I angles (103.8(1)–113.9(1) °) vary around the tetrahedral angle.

The I–Cu–I angles around the trigonal coordinated copper atoms vary in a small range (115.1(1)–124.9(1) °) around 120 °. The sums of the angles around the copper atoms are 359.0–359.2 °, which means that the copper atoms are coordinated almost perfectly planar.

Corresponding to the short Cu...Cu distances the Cu–P–Cu angles (61.6(1)–62.4(1) °) are slightly smaller than those found in the literature (63.2(1)–71.83(3) °).^[18]

Through the Cu6–I1 and Cu3–I4 interactions the six-membered rings form chains in the crystal. The ligands are coordinating to the chains alternating on both sides (Figure 18).

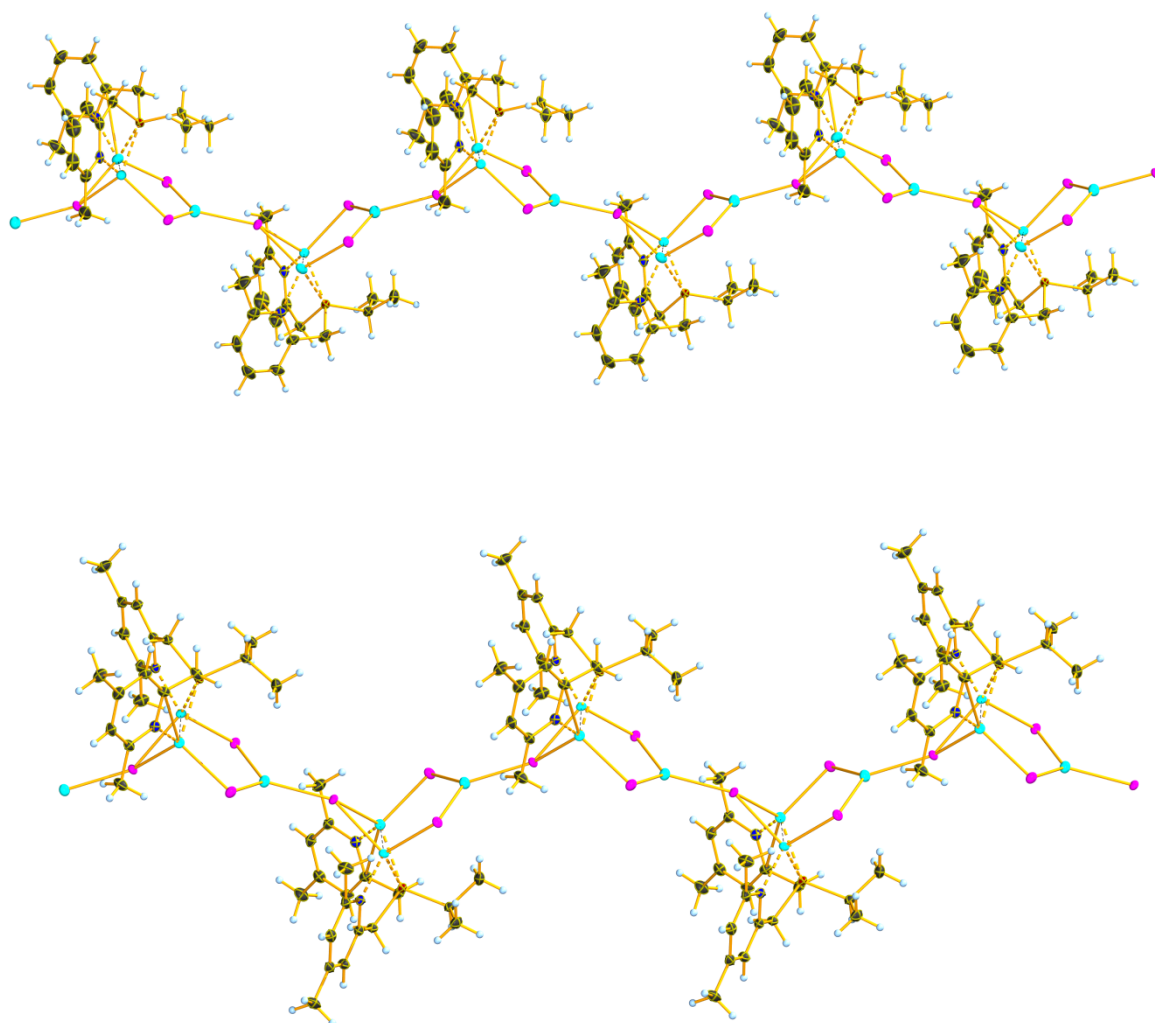


Figure 18: Chain of Cu_3I_3 rings in the crystal structure of **5-9** (top) and **5-13** (bottom).

In the crystal structure the chains are arranged in layers along the a axis (**5-9**) and the c axis (**5-13**) respectively (Figure 19).

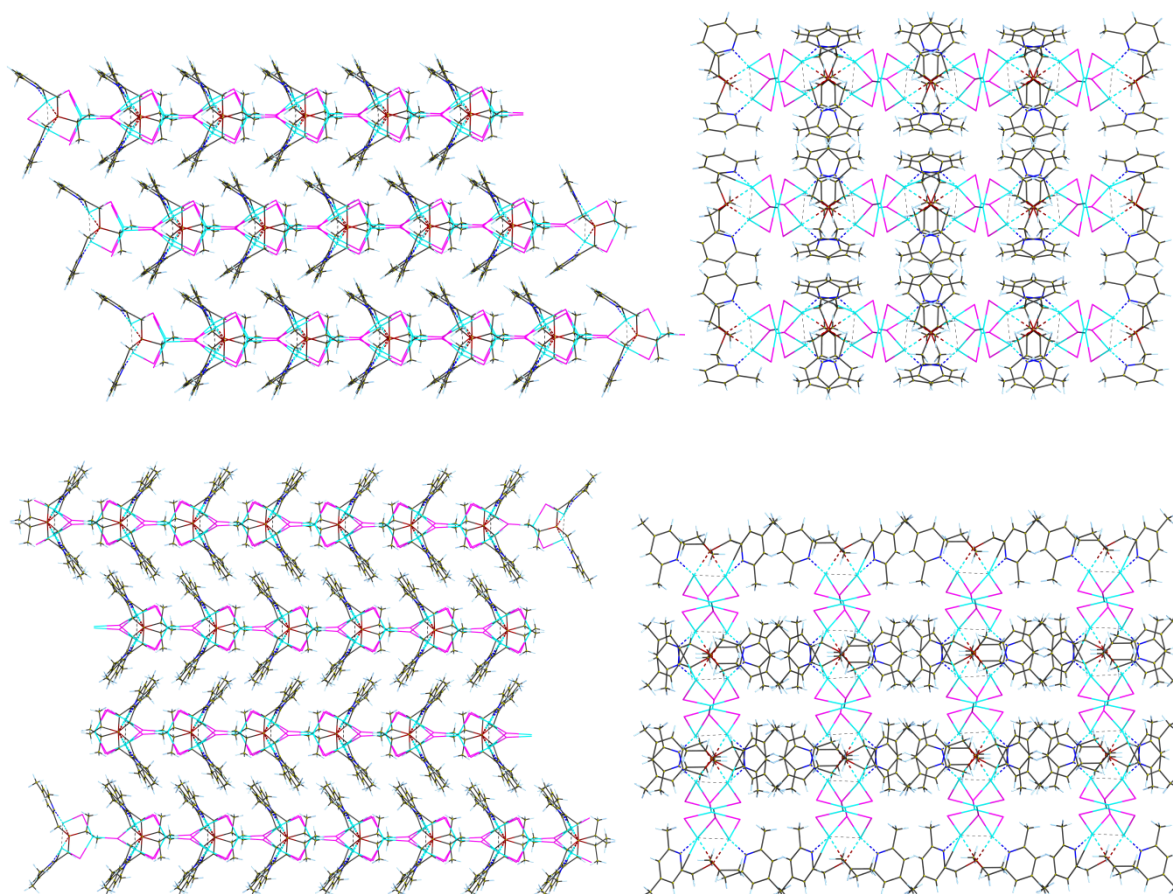


Figure 19: View along the *b* axis (left) and *c* axis (right) of the crystal structure of **5-9** (top) and view along the *a* axis (left) and *b* axis (right) of the crystal structure of **5-13** (bottom)

5.2.3.4 Crystal structure of **5-10**

Single crystals of **5-10** suitable for X-ray crystallography could be obtained by slow diffusion of MeCN in a solution in 4-picoline.

The complex crystallises in the orthorhombic space group *Pbca* with eight formula units in the unit cell. Remarkably in the structure of **5-10** no 4-picoline can be found, although it is a good ligand for Cu(I).

The asymmetric unit of **5-10** comprises one ligand molecule and three units of CuSCN (Figure 20). In the structure two of the copper atoms are coordinated distorted tetrahedrally by each one nitrogen atom of the ligand, two SCN[−] anions – one SCN[−] anion, which coordinates to Cu1 *via* N5 and to Cu2 *via* S1 respectively and to another copper atom *via* the other coordination site and one bridging SCN[−] anion, which coordinates to Cu1 and Cu2 atoms *via* S3 and another copper atom *via* N5 – and the bridging phosphorus atom of the ligand. The third copper atom (Cu3) is coordinated trigonal planar by three SCN[−] anions.

A search in the database of the CCDC on July 1st 2020 gave no other results for CuSCN complexes with the same structural motif.

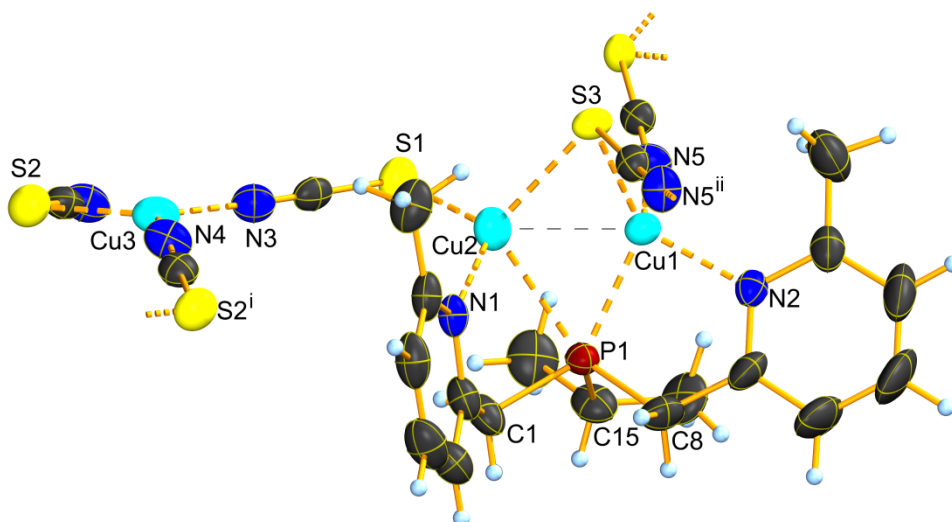


Figure 20: Asymmetric unit of **5-10**. Thermal ellipsoids are drawn at 50% probability level. Selected bond lengths [Å] and angles [°]: Cu1–P1: 2.262(1), Cu1–N2: 2.057(3), Cu1–N5: 1.957(3), Cu1–S3: 2.361(1), Cu2–P1: 2.679(1), Cu2–N1: 2.022(3), Cu2–S1: 2.280(1), Cu2–S3: 2.364(1), Cu3–N3: 1.929(4), Cu3–N4: 1.903(3), Cu3–S2: 2.260(1), Cu1...Cu2: 2.523(1), P1–C1: 1.846(4), P1–C8: 1.826(4), P1–C15: 1.848(4), P1–Cu1–N2: 87.4(1), P1–Cu1–N5: 117.6(1), P1–Cu1–S3: 121.7(1), N2–Cu1–N5: 117.7(1), N2–Cu1–S3: 113.9(1), S3–Cu1–N5: 99.9(1), P1–Cu2–N1: 83.5(1), P1–Cu2–S1: 111.1(1), P1–Cu2–S3: 106.2(1), N1–Cu2–S1: 118.9(1), N1–Cu2–S3: 120.2(1), S1–Cu2–S3: 112.0(1), Cu1–P1–Cu2: 60.7(1), Cu1–S3–Cu2: 64.6(1), N3–Cu3–N4: 121.1(1), N3–Cu3–S2: 115.0(1), N4–Cu3–S2: 123.8(1), sum of angles around Cu3: 359.9, C1–P1–C8: 99.8(2), C1–P1–C15: 100.7(2), C8–P1–C15: 105.2(2). i: $-0.5+x, 0.5-y, 1-z$, ii: $-0.5+x, y, 0.5-z$.

The Cu1–P1 distance (2.262(1) Å) in the structure of **5-10** is much shorter than the Cu2–P1 distance (2.679(1) Å). These distances are similar to the Cu–P distances found for **5-9** and thus within the range of Cu–P distances found in other copper(I) complexes of bridging phosphines discussed in the literature (2.230(3)–2.728(3) Å).^[18]

The Cu–N_{py} distances (2.022(3) Å and 2.057(3) Å) are comparable to the mean atom distance found in complexes with four-coordinate copper atoms coordinated by pyridine nitrogen atoms (2.024 Å).^[13]

The Cu1–N5 distance of 1.957(3) Å is slightly shorter than the Cu–N distances of other CuSCN complexes described in the literature (1.992(1)–2.0132(9) Å).^[20]

The distance between Cu2 and S1 (2.280(1) Å) is significantly shorter than the Cu–S distances of known copper thiocyanate complexes (2.3494(4)–2.4488(8) Å).^[20]

The Cu–S3 distances of 2.361(1) Å and 2.364(1) Å are very close to each other and within the range found for copper complexes with bridging thiocyanate sulphur atoms (2.307(2)–2.868(3) Å).^[21]

The Cu–N distances at Cu3 (1.903(3) Å and 1.929(4) Å) are comparable to the Cu–N distances found for other complexes with N₂CuS coordination (1.868(2)–2.156(1) Å).^[22] The Cu3–S2 distance of 2.260(1) Å concurs with the Cu–S distances of known complexes (2.1581(8)–2.3949(7) Å).^[22]

The short Cu1...Cu2 distance (2.523(1) Å) clearly indicates the presence of weak Cu...Cu interactions between these copper atoms.

The P–C bond lengths are 1.826(4)–1.848(4) Å, which is within the range of the mean P–C_{Alk} bond lengths found in tertiary phosphine complexes (1.825–1.863 Å).^[13]

The angles around Cu1 and Cu2 range from 83.5(1) ° to 121.7(1) °. The P–Cu–N_{py} angles (83.5(1) ° and 87.4(1) °) are significantly smaller than the ideal tetrahedral angle as found in the structures of the copper halide complexes of **2-16** and **2-17** discussed above (see 2.3.2 and 2.3.3). All other angles except from P1–Cu2–S3 (106.2(1) °) and S3–Cu1–N5 (99.9(1) °) are larger than the tetrahedral angle. The angles around Cu3 are all very close to 120 ° (115.0(1)–123.8(1) °) and sum up to 359.9 °. This means that the coordination around Cu3 is almost perfectly planar.

The Cu–P–Cu angle is 60.7(1)° and the Cu–S3–Cu angle 64.6(1)°. Both angles are quite small corresponding to the short distance between Cu1 and Cu2.

In the crystal the complex forms a polymeric network (Figure 21). The Cu3 atoms and the SCN[−] anions containing S2 and N4 form chains, which are connected to Cu2 through the third anion coordinating to Cu3.

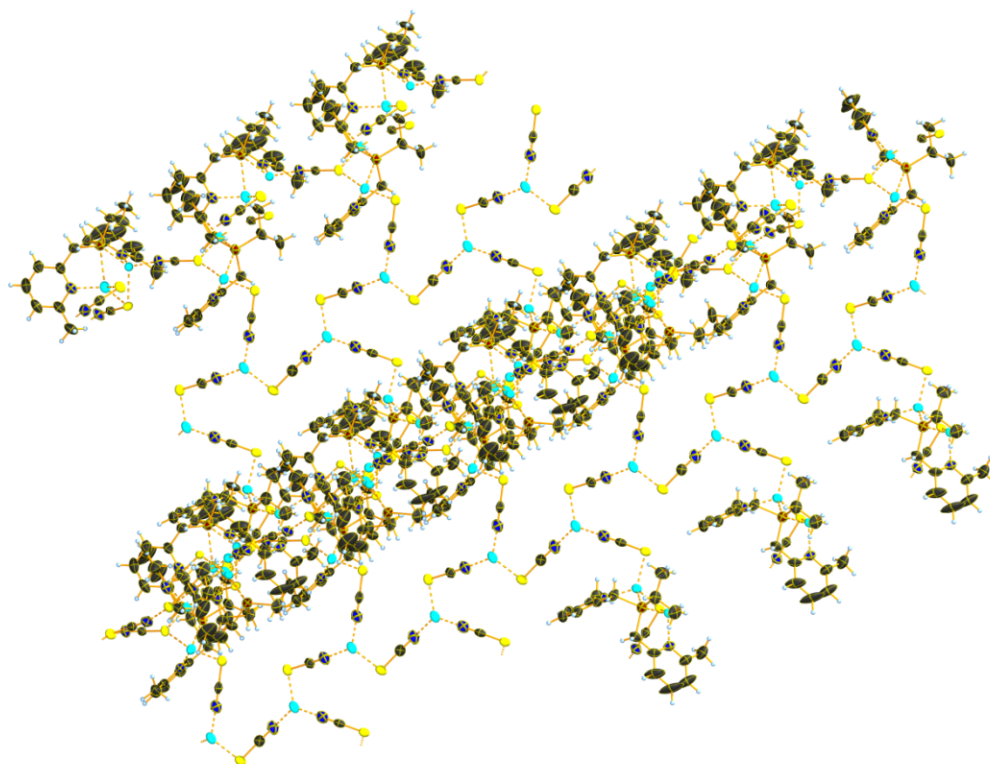


Figure 21: Crystal structure of **5-10**. Thermal ellipsoids are drawn at 50% probability level.

While the copper atoms are coordinated tetrahedrally in the crystal structure of CuSCN,^[23] the copper atoms are coordinated trigonal planar in the CuSCN chains of **5-10**. This means that the coordination situation in the part of the complex differs from the structure of pure CuSCN, although no interaction with the ligands can be observed.

5.2.3.5 Crystal structures of **5-14**, **5-17** and **5-18**

Single crystals of **5-14** and **5-18** suitable for X-ray crystallography could be obtained from solutions in MeCN. Single crystals of **5-17** were obtained by slow diffusion of Et₂O in a solution in MeCN.

Complex **5-14** crystallises in the monoclinic space group *C2/c* with eight formula units in the unit cell, complex **5-17** in the monoclinic space group *P2₁/n* with four formula units in the unit cell and complex **5-18** in the triclinic space group *P-1* with two formula units in the unit cell.

The asymmetric units of **5-14**, **5-17** and **5-18** comprise one ligand molecule and three units of CuCl or CuBr respectively (Figures 22 and 23). In the asymmetric unit of **5-17** an additional solvent molecule is included (Figure 22). In the structures of **5-14** and **5-18** each copper atom is coordinated distorted tetrahedrally by each one nitrogen atom of the ligand, two halide atoms and the phosphorus atom of the ligand. In these two structures the phosphorus atom is centred above the triangle formed by the three copper atoms. In contrast the phosphorus atom in the structure of complex **5-17** is much

closer to Cu1 than to the other copper atoms. This means that in this structure Cu1 is coordinated distorted tetrahedrally by the phosphorus atom, one of the nitrogen atoms of the ligand and two chlorine atoms, while the other two copper atoms are coordinated trigonal by each one of the remaining nitrogen atoms of the ligand and two chlorine atoms.

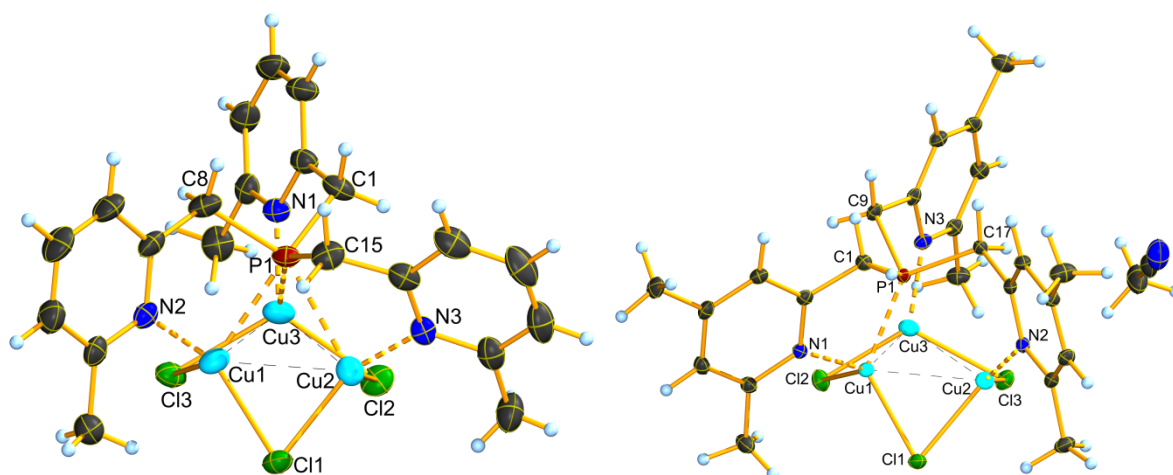


Figure 22: Asymmetric units of **5-14** (left) and **5-17** (right). Thermal ellipsoids are drawn at 50% probability level. Selected bond lengths [Å] and angles [°] of **5-14**: Cu1–P1: 2.418(1), Cu1–N2: 2.031(2), Cu1–Cl1: 2.357(1), Cu1–Cl3: 2.323(1), Cu2–P1: 2.511(1), Cu2–N3: 2.018(2), Cu2–Cl1: 2.344(1), Cu2–Cl2: 2.334(1), Cu3–P1: 2.593(1), Cu3–N1: 2.015(2), Cu3–Cl2: 2.286(1), Cu3–Cl3: 2.356(1), Cu1...Cu2: 2.573(1), Cu1...Cu3: 2.572(1), Cu2...Cu3: 2.613(1), P1–C1: 1.844(3), P1–C8: 1.845(3), P1–C15: 1.841(3), P1–Cu1–N2: 86.0(1), P1–Cu1–Cl1: 109.8(1), P1–Cu1–Cl3: 113.7(1), N2–Cu1–Cl1: 118.5(1), N2–Cu1–Cl3: 114.8(1), Cl1–Cu1–Cl3: 111.5(1), P1–Cu2–N3: 84.2(1), P1–Cu2–Cl1: 107.1(1), P1–Cu2–Cl2: 109.5(1), N3–Cu2–Cl1: 117.2(1), N3–Cu2–Cl2: 118.9(1), Cl1–Cu2–Cl2: 114.5(1), P1–Cu3–N1: 83.0(1), P1–Cu3–Cl2: 108.3(1), P1–Cu3–Cl3: 106.7(1), N1–Cu3–Cl2: 121.0(1), N1–Cu3–Cl3: 116.8(1), Cl2–Cu3–Cl3: 114.6(1), Cu1–Cu2–Cu3: 59.5(1), Cu1–Cu3–Cu2: 59.5(1), Cu2–Cu1–Cu3: 61.0(1), P1–Cu1–Cu2: 60.3(1), P1–Cu1–Cu3: 62.5(1), P1–Cu2–Cu1: 56.8(1), P1–Cu2–Cu3: 60.8(1), P1–Cu3–Cu1: 55.8(1), P1–Cu3–Cu2: 57.7(1), Cu1–P1–Cu2: 62.9(1), Cu1–P1–Cu3: 61.7(1), Cu2–P1–Cu3: 61.6(1), C1–P1–C8: 99.6(1), C1–P1–C15: 100.6(1), C8–P1–C15: 100.4(1). Selected bond lengths [Å] and angles [°] of **5-17**: Cu1–P1: 2.245(1), Cu1–N1: 2.067(2), Cu1–Cl1: 2.337(1), Cu1–Cl2: 2.416(1), Cu2–N2: 1.989(2), Cu2–Cl1: 2.372(1), Cu2–Cl3: 2.239(1), Cu3–N3: 1.995(2), Cu3–Cl2: 2.246(1), Cu3–Cl3: 2.397(1), Cu1...Cu2: 2.616(1), Cu1...Cu3: 2.593(1), Cu2...Cu3: 2.918(1), P1...Cu2: 2.947(1), P1...Cu3: 2.819(1), P1–C1: 1.848(2), P1–C9: 1.844(2), P1–C17: 1.843(2), P1–Cu1–N1: 88.3(1), P1–Cu1–Cl1: 126.0(1), P1–Cu1–Cl2: 111.9(1), N1–Cu1–Cl1: 112.9(1), N1–Cu1–Cl2: 110.4(1), Cl1–Cu1–Cl2: 106.0(1), N2–Cu2–Cl1: 111.5(1), N2–Cu2–Cl3: 135.8(1), Cl1–Cu2–Cl3: 110.8(1), N3–Cu3–Cl2: 128.8(1), N3–Cu3–Cl3: 107.6(1), Cl2–Cu3–Cl3: 120.9(1), sum of angles around Cu2: 358.1, sum of angles around Cu3: 357.3, Cu1–Cu2–Cu3: 55.6(1), Cu1–Cu3–Cu2: 56.3(1), Cu2–Cu1–Cu3: 68.1(1), P1–Cu1–Cu2: 74.2(1), P1–Cu1–Cu3: 70.9(1), C1–P1–C9: 101.6(1), C1–P1–C17: 100.8(1), C9–P1–C17: 100.9(1).

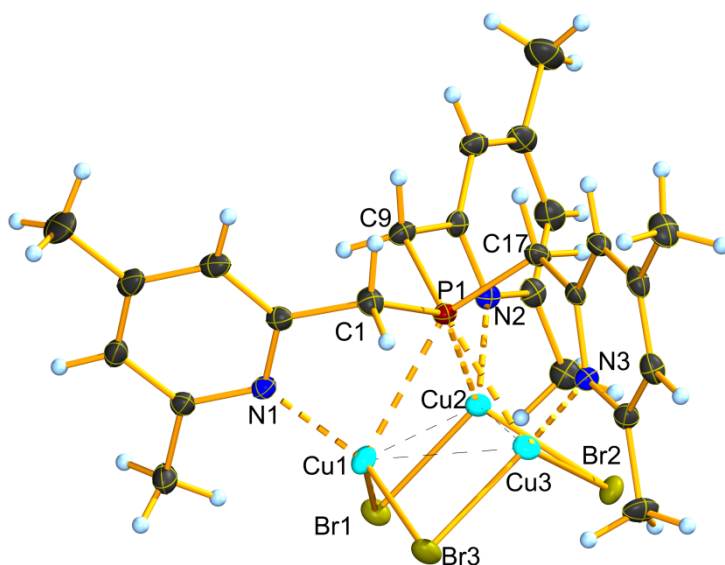


Figure 23: Asymmetric unit of **5-18**. Thermal ellipsoids are drawn at 50% probability level. Selected bond lengths [Å] and angles [°]: Cu1–P1: 2.645(1), Cu1–N1: 2.013(2), Cu1–Br1: 2.472(1), Cu1–Br3: 2.414(1), Cu2–P1: 2.406(1), Cu2–N2: 2.025(2), Cu2–Br1: 2.448(1), Cu2–Br2: 2.512(1), Cu3–P1: 2.501(1), Cu3–N3: 2.020(2), Cu3–Br2: 2.443(1), Cu3–Br3: 2.452(1), Cu1...Cu2: 2.535(1), Cu1...Cu3: 2.670(1), Cu2...Cu3: 2.515(1), P1–C1: 1.846(2), P1–C9: 1.853(2), P1–C17: 1.843(2), P1–Cu1–N1: 81.6(1), P1–Cu1–Br1: 110.8(1), P1–Cu1–Br3: 104.1(1), N1–Cu1–Br1: 120.1(1), N1–Cu1–Br3: 117.9(1), Br1–Cu1–Br3: 115.0(1), P1–Cu2–N2: 85.8(1), P1–Cu2–Br1: 120.5(1), P1–Cu2–Br2: 112.6(1), N2–Cu2–Br1: 117.5(1), N2–Cu2–Br2: 117.6(1), Br1–Cu2–Br2: 103.2(1), P1–Cu3–N3: 85.2(1), P1–Cu3–Br2: 111.7(1), P1–Cu3–Br3: 107.4(1), N3–Cu3–Br2: 116.5(1), N3–Cu3–Br3: 112.9(1), Br2–Cu3–Br3: 118.0(1), Cu1–Cu2–Cu3: 63.8(1), Cu1–Cu3–Cu2: 58.4(1), Cu2–Cu1–Cu3: 57.7(1), P1–Cu1–Cu2: 55.3(1), P1–Cu1–Cu3: 56.1(1), P1–Cu2–Cu1: 64.7(1), P1–Cu2–Cu3: 61.0(1), P1–Cu3–Cu1: 61.4(1), P1–Cu3–Cu2: 57.3(1), Cu1–P1–Cu2: 60.0(1), Cu1–P1–Cu3: 62.4(1), Cu2–P1–Cu3: 61.6(1), C1–P1–C9: 100.7(1), C1–P1–C17: 100.5(1), C9–P1–C17: 99.4(1).

The Cu–P distances of **5-14** are between 2.418(1) Å and 2.593(1) Å, while the Cu–P distances of **5-18** cover a wider range from 2.406(1) Å to 2.645(1) Å. In both cases the Cu–P distances are longer than the mean distance found for literature known copper complexes with triphenylphosphine (2.252 Å),^[13] but within the range of Cu–P distances found in copper complexes with bridging phosphines (2.230(3)–2.728(3) Å).^[18] The Cu1–P1 distance (2.245(1) Å) in the structure of **5-17** is comparable to the mean atom distance of triphenylphosphine copper complexes (2.252 Å),^[13] while the other two Cu–P distances (2.819(1) Å and 2.947(1) Å) are significantly longer and probably the phosphorus does not interact with these two copper atoms. This means that in complexes **5-14** and **5-18** a coordination of the phosphorus atom to all three copper atoms is present, while in complex **5-17** the phosphorus coordinates to only one of the copper atoms.

The Cu–N distances of complexes **5-14** and **5-18** (2.013(2)–2.031(2) Å) are similar to the mean distance between pyridine nitrogen atoms and four-coordinate copper atoms (2.024 Å).^[13] The Cu1–N1 distance of **5-17** (2.067(2) Å) is slightly longer than the Cu–N distances of **5-14** and **5-18**. The Cu2–N2 (1.989(2) Å) and Cu3–N3 (1.995(2) Å) distances of complex **5-17** are comparable to the Cu–N distances of complexes with NCuX₂ coordination (1.9553(16) Å–1.993(5) Å).^[12]

The Cu–Cl distances in complex **5-14** (2.286(1)–2.357(1) Å) are slightly shorter than the mean distance between four-coordinate copper(I) atoms and μ_2 -chlorine atoms (2.364 Å).^[13] The Cu1–Cl1 distance in complex **5-17** (2.337(1) Å) is slightly shorter than the mean Cu–Cl distance for this type of interaction (2.364 Å),^[13] while the distance between Cu1 and Cl2 (2.416(1) Å) is longer. The Cu–Cl distances at Cu2 and Cu3 vary from 2.239(1) Å to 2.397(1) Å around the mean distance between three-coordinate copper(I) atoms and μ_2 -chlorine atoms (2.275 Å).^[13]

The Cu–Br distances in complex **5-18** (2.414(1)–2.512(1) Å) correspond with the mean Cu–Br distance between copper(I) and μ_2 -bromine atoms (2.483 Å).^[13]

All Cu...Cu distances are between 2.515(1) Å and 2.670(1) Å, except for the distance between Cu2 and Cu3 in complex **5-17** (2.918(1) Å). These short Cu...Cu distances might indicate the presence of weak Cu...Cu interactions in the clusters.

The P–C bond lengths of all three complexes are 1.841(3)–1.853(2) Å, which is in the typical range of mean P–C_{Alk} bond lengths in tertiary phosphine complexes (1.825–1.863 Å).^[13]

The angles around the copper atoms of complexes **5-14** and **5-18** vary over a wide range from 81.6(1) ° to 121.0(1) ° around the tetrahedral angle. As observed for the bis(picoly)phosphine based complexes (see 5.2.3.1–5.2.3.4) the P–Cu–N angles are small (81.6(1)–86.0(1) °). The P–Cu–X angles vary around the tetrahedral angle in which the range covered in complex **5-18** is larger than for complex **5-14** (**5-14**: 106.7(1)–113.7(1) °, **5-18**: 104.1(1)–120.5(1) °). All N–Cu–X angles of complexes **5-14** and **5-18** are larger than the tetrahedral angle (**5-14**: 114.8(1)–121.0(1) °, **5-18**: 112.9(1)–120.1(1) °). All Cl–Cu–Cl angles (111.5(1)–114.6(1) °) of **5-14** are larger than the tetrahedral angle, but in complex **5-18** the Br1–Cu2–Br2 angle (103.2(1) °) is smaller than the tetrahedral angle, while the other two Br–Cu–Br angles (115.0(1) ° and 118.0(1) °) are larger.

The angles around Cu1 of complex **5-17** range from 88.3(1) ° to 126.0(1) °. As for complexes **5-14** and **5-18** the P–Cu–N angle (88.3(1) °) is quite small. The P–Cu–Cl (111.9(1) ° and 126.0(1) °) and N–Cu–Cl (110.4(1) ° and 112.9(1) °) angles are larger than the tetrahedral angle, while the Cl–Cu–Cl angle (106.0(1) °) is smaller. The angles around Cu2 and Cu3 vary from 107.6(1) ° to 135.8(1) ° and sum up to 358.1 ° (Cu2) and 357.3 ° (Cu3) respectively. This means the coordination at these two copper atoms is very close to planar.

In complexes **5-14** and **5-18** the three copper atoms and the phosphorus atom form slightly distorted tetrahedrons. The angles within these tetrahedrons vary over a slightly wider range in complex **5-18** (55.3(1)–64.7(1) °) than in complex **5-14** (55.8(1)–62.9(1) °).

The C–P–C angles in complexes **5-14**, **5-17** and **5-18** vary in a small range from 99.4(1) ° to 101.6(1) °.

In the crystal structures of **5-14**, **5-17** and **5-18** the molecules are arranged in layers in an AB pattern (Figure 24).

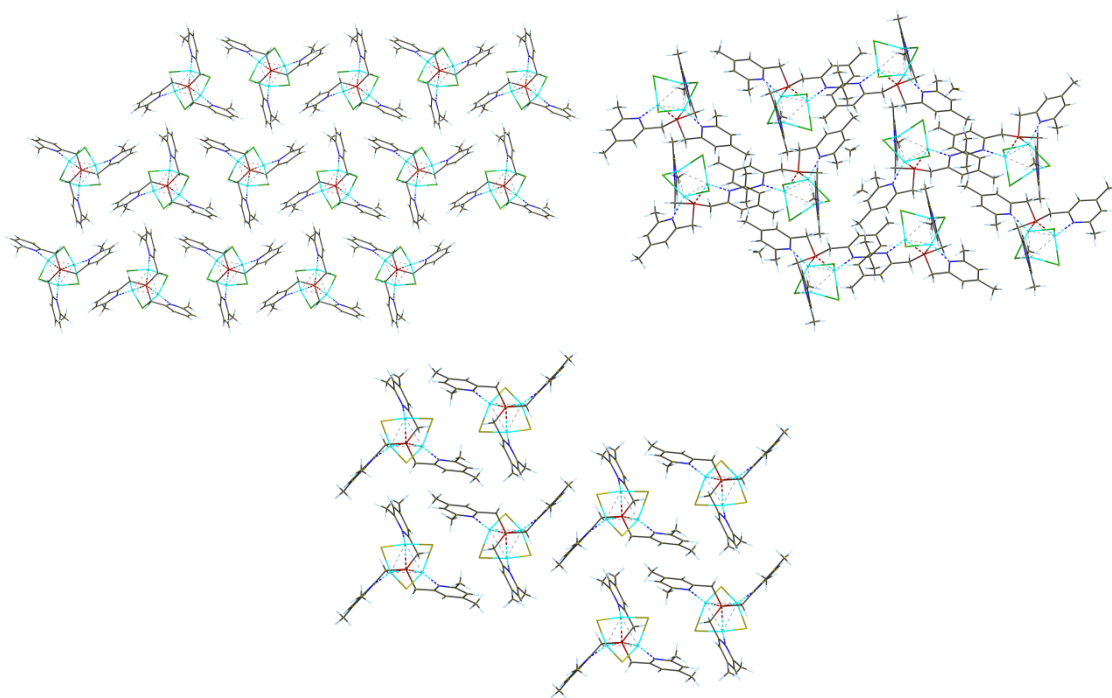


Figure 24: Crystal structures of **5-14** (top left, view along the *b* axis), **5-17** (top right, view along the *a* axis) and **5-18** (bottom, view along the *a* axis).

The crystal structures of the CuCl and CuBr complexes **5-17** and **5-18** of ligand **2-25** are quite similar, but slightly different. In the structure of **5-18** no solvent molecules are included, while one molecule of MeCN is present in the structure of **5-17**. In both complexes the three copper atoms form six-membered rings with the three halide atoms and are coordinated by each one of the nitrogen atoms of the ligand. But the Cu–P distances indicate that in complex **5-17** phosphorus is coordinated to only one of the copper atoms, while in complex **5-18** interactions of the phosphorus atom with all three copper atoms might be present.

5.2.3.6 Crystal structures of **5-20** and **5-21**

Attempts to crystallise the CuCl and CuBr complexes of **2-13** failed, but from solutions in MeCN crystal suitable for X-ray crystallography were obtained. These crystals appeared to be of the corresponding complexes **5-20** (CuCl) and **5-21** (CuBr) of the phosphine oxide of **2-13**. Probably the phosphine ligand was oxidised due to the presence of oxygen during crystallisation.

Both complexes crystallise in the triclinic space group *P*–1 with one formula unit in the unit cell. The asymmetric unit contains one molecule of the solvent MeCN (Figure 25, left). Despite the reaction was performed in a metal to ligand ratio of 3:1, in the phosphine oxide complexes a ratio of 1:1 is found. The complexes are isostructural and display the typical structure motif of the rhomboid dimer (Figure 25, right). The copper atoms in both structures are coordinated distorted tetrahedrally by the two nitrogen atoms of the ligand and two halide atoms. The oxygen atoms do not participate in the coordination to copper.

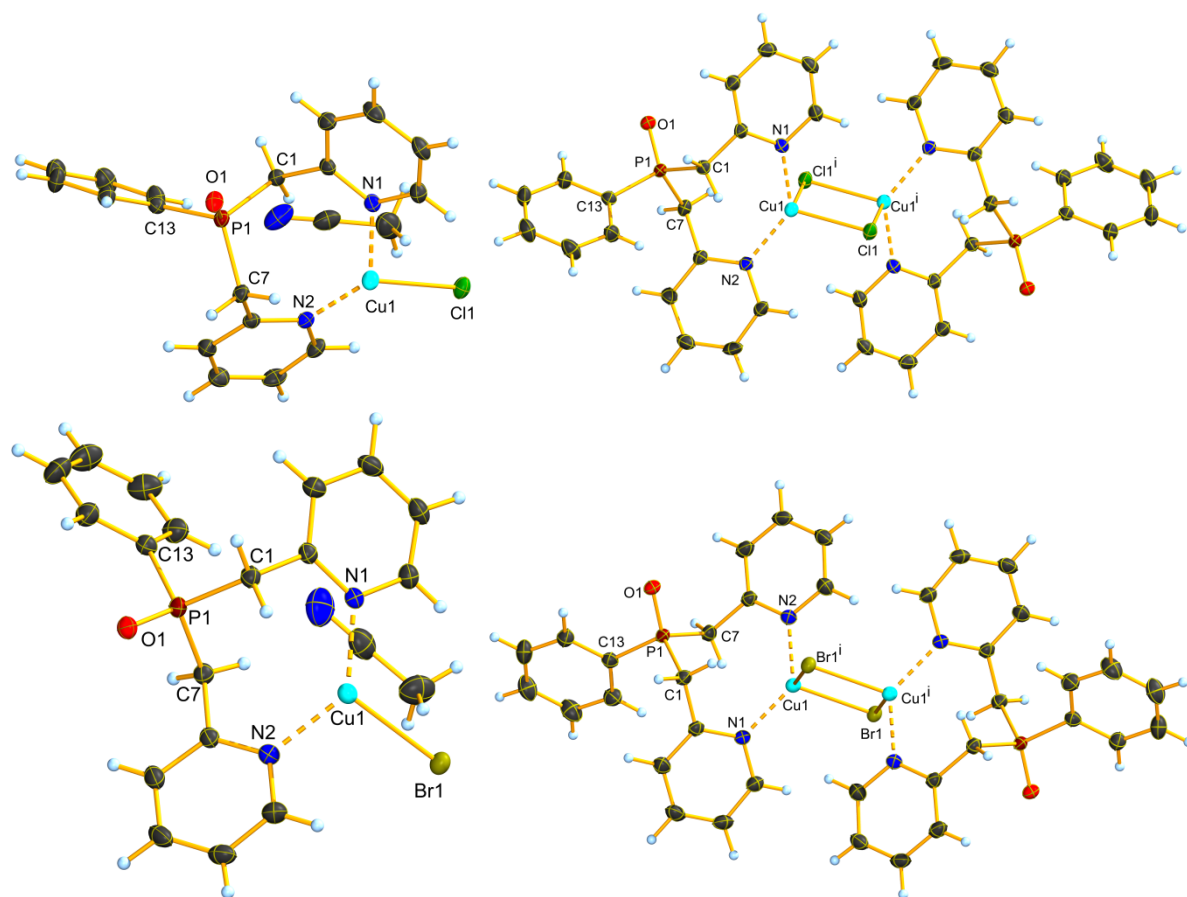


Figure 25: Asymmetric unit (left) and dimeric molecular structure (right) of **5-20** (top) and **5-21** (bottom). Thermal ellipsoids are drawn at 50% probability level. Solvent molecules are omitted for clarity in the pictures of the dimeric structures. Selected bond lengths [Å] and angles [°] of **5-20**: Cu1–N1: 2.019(2), Cu1–N2: 2.005(2), Cu1–Cl1: 2.380(1), Cu1–Cl1ⁱ: 2.533(1), Cu1···Cu1ⁱ: 3.147(1), P1–C1: 1.821(2), P1–C7: 1.809(2), P1–C13: 1.806(2), P1–O1: 1.489(2), N1–Cu1–N2: 130.0(1), N1–Cu1–Cl1: 104.3(1), N1–Cu1–Cl1ⁱ: 97.4(1), N2–Cu1–Cl1: 115.3(1), N2–Cu1–Cl1ⁱ: 103.8(1), Cl1–Cu1–Cl1ⁱ: 100.4(1), C1–P1–C7: 107.8(1), C1–P1–C13: 104.5(1), C1–P1–O1: 113.2(1), C7–P1–C13: 110.4(1), C7–P1–O1: 109.6(1), C13–P1–O1: 111.1(1). i: 2–x, 1–y, 1–z. Selected bond lengths [Å] and angles [°] of **5-21**: Cu1–N1: 2.009(2), Cu1–N2: 2.019(2), Cu1–Br1: 2.496(1), Cu1–Br1ⁱ: 2.647(1), Cu1···Cu1ⁱ: 3.198(1), P1–C1: 1.814(2), P1–C7: 1.819(2), P1–C13: 1.802(2), P1–O1: 1.489(1), N1–Cu1–N2: 129.6(1), N1–Cu1–Br1: 114.5(1), N1–Cu1–Br1ⁱ: 102.3(1), N2–Cu1–Br1: 103.5(1), N2–Cu1–Br1ⁱ: 99.8(1), Br1–Cu1–Br1ⁱ: 103.2(1), C1–P1–C7: 107.5(1), C1–P1–C13: 110.0(1), C1–P1–O1: 110.2(1), C7–P1–C13: 104.6(1), C7–P1–O1: 112.9(1), C13–P1–O1: 111.5(1). i: 1–x, 1–y, –z.

The Cu–N distances of complexes **5-20** and **5-21** (2.005(2)–2.019(2) Å) are in the same range as the Cu–N distances found in various complexes with Cu₂X₂ rhomboids with additional pyridine derived ligands coordinating to the copper atoms (2.00(2)–2.104(5) Å).^[5c]

The Cu1–Cl1 distance (2.380(1) Å) and the Cu1–Cl1ⁱ distance (2.533(1) Å) in **5-20** differ strongly from each other, but both distances are within the range found in the literature for other (py)₄Cu₂Cl₂ complexes (2.357(1)–2.675(6) Å).^[5c] The Cu–Br distances of **5-21** (2.496(1) Å and 2.647(1) Å) also are very diverse, but within the range covered by known complexes of the type (py)₄Cu₂Br₂ (2.493(3)–2.680(3) Å).^[5c]

The distances between the copper atoms in the four-membered rings Cu1 and Cu1ⁱ (3.147(1) Å (**5-20**) and 3.198(1) Å (**5-21**)) are comparable to the literature values of other (py)₄Cu₂X₂ complexes (2.609(1)–3.418(2) Å, X = Cl, Br, I).^[5c] The distances are significantly longer than the sum of the *van der Waals* radii, which indicates that there are no interactions between the copper atoms.

The P–C_{Alk} bond lengths of **5-20** and **5-21** are between 1.809(2) Å and 1.821(2) Å, which is close to the mean bond length of P–C_{sp3} bonds in phosphine oxides (1.813 Å).^[13] The lengths of the P1–C13

bonds (1.806(2) Å and 1.802(2) Å) are comparable to the mean P–C_{Ar} bond length of phosphine oxides (1.801 Å).^[13]

The P–O bond lengths of **5-20** and **5-21** (1.489(2) Å and 1.489(1) Å) correspond with the mean P–O bond length of phosphine oxides (1.489 Å).^[13]

The angles around the copper atoms of **5-20** and **5-21** vary in the range from 97.4(1) ° to 130.0(1) ° around the ideal tetrahedral angle of 109.5 °. The N–Cu–N angles (130.0(1) ° and 129.6(1) °) are larger than the tetrahedral angle, while the X–Cu–X angles (100.4(1) ° and 103.2(1) °) are smaller. The N–Cu–X angles vary around the tetrahedral angle in a range from 97.4(1) ° to 115.3(1) °.

The angles around the phosphorus atoms of **5-20** and **5-21** range from 104.5(1) ° to 113.2(1) °, which is close to the tetrahedral angle. All C–P–O angles (109.6(1)–113.2(1) °) are slightly larger than the tetrahedral angle, while the C–P–C angles (104.5(1)–110.4(1) °) vary around the tetrahedral angle.

In the crystal the dimers are arranged in layers in an AB pattern (Figure 26, left).

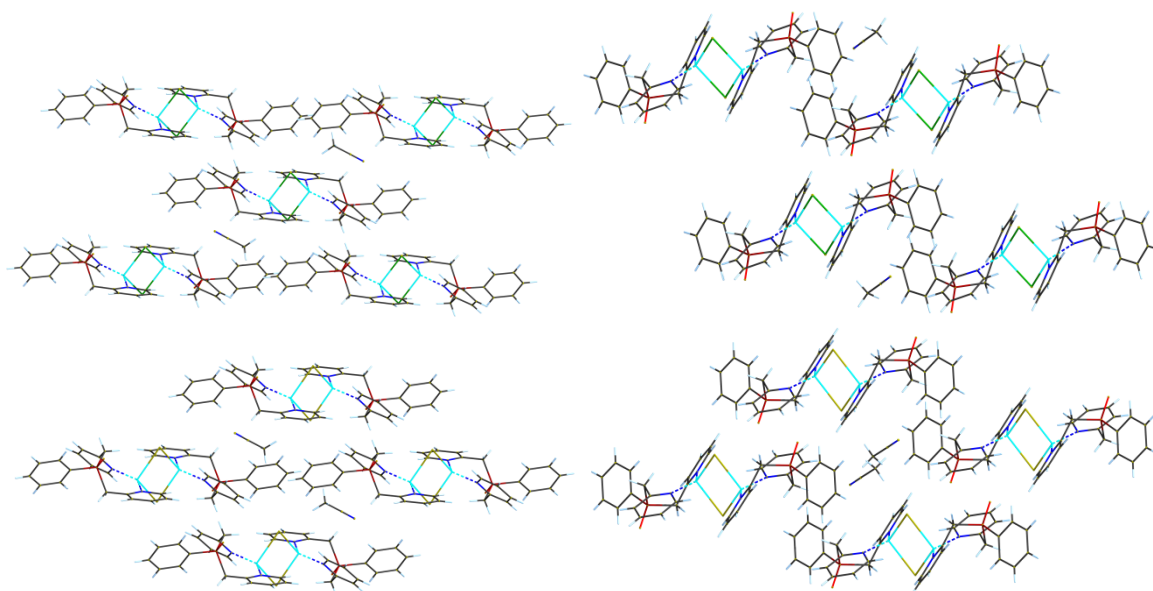
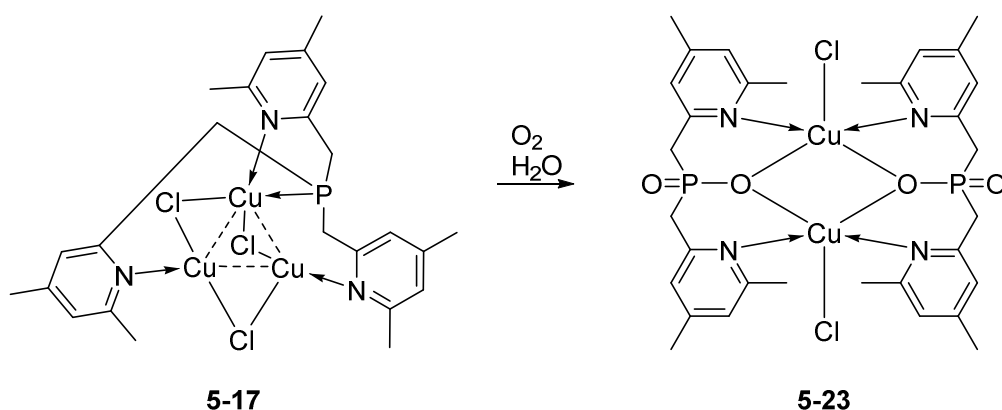


Figure 26: Crystal structure of **5-20** (top) and **5-21** (bottom). View along the *a* axis (left) and *b* axis (right).

5.2.3.7 Formation and crystal structures of hydrolysis products Col₂PO₂[−] Cu(II)Cl **5-23** and PhLutPO₂[−] 6-methylpicolinate Cu(II) **5-24**

From attempts to crystallise **5-17** by slow diffusion of pentane in a solution in MeCN blue single crystals suitable for X-ray crystallography were obtained. From the crystal structure it was evident that the complex was hydrolysed and oxidised by moisture and air, which entered into the vessel with time. Obviously one of the P–C bonds was cleaved and the phosphine was oxidised to the phosphinate Col₂PO₂[−]. Also Cu(I) was oxidised to Cu(II) (Scheme 5).



Scheme 5: Hydrolysis and oxidation of **5-17** yielding **5-23**.

The hydrolysis product **5-23** was the copper(II) complex of the corresponding phosphinate $\text{Col}_2\text{PO}_2^-$ of ligand **2-25** and one chloride anion. The complex crystallises in the monoclinic space group $P2_1/n$ with two formula units in the unit cell. The complex forms a dimeric structure in which the copper atoms are coordinated distorted trigonal bipyramidal by one nitrogen atom and one oxygen atom of each phosphinate ligand and one chloride atom (Figure 27). In the trigonal bipyramid the nitrogen atoms are at the axial positions, while the oxygen and chlorine atoms occupy the equatorial positions. The Cu1 and O2 atoms of the dimer form a four-membered ring.

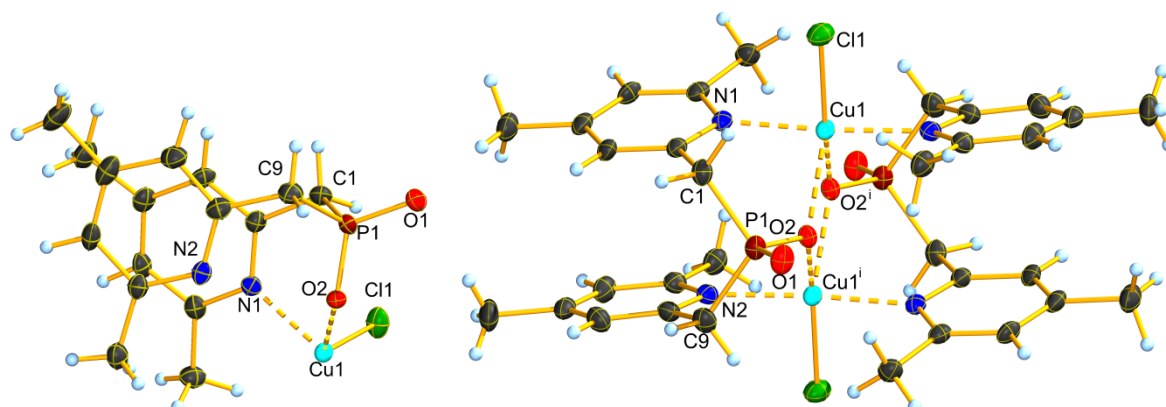


Figure 27: Asymmetric unit (left) and dimeric molecular structure (right) of **5-23**. Thermal ellipsoids are drawn at 50% probability level. Selected bond lengths [Å] and angles [°]: Cu1–N1: 2.046(3), Cu1–N2ⁱ: 2.067(3), Cu1–O2ⁱ: 2.012(2), Cu1–Cl1: 2.260(1), Cu1...Cu1ⁱ: 3.351(1), P1–C1: 1.802(4), P1–C9: 1.816(3), P1–O1: 1.488(3), P1–O2: 1.534(2), N1–Cu1–N2ⁱ: 174.6(1), N1–Cu1–O2ⁱ: 88.7(1), N1–Cu1–O2ⁱ: 88.8(1), N1–Cu1–Cl1: 88.4(1), N2ⁱ–Cu1–O2: 96.4(1), N2ⁱ–Cu1–O2ⁱ: 90.6(1), N2ⁱ–Cu1–Cl1: 90.3(1), O2–Cu1–O2ⁱ: 77.1(1), O2–Cu1–Cl1: 123.2(1), O2ⁱ–Cu1–Cl1: 159.5(1), C1–P1–C9: 108.4(2), C1–P1–O1: 110.2(2), C1–P1–O2: 105.0(2), C9–P1–O1: 110.2(2), C9–P1–O2: 104.8(2), O1–P1–O2: 117.8(1). i: 1–x, –y, 1–z.

The Cu–N distances of **5-23** (2.046(3) Å and 2.067(3) Å) are much shorter than the mean distance between pyridine nitrogen atoms and five-coordinate copper atoms (2.113 Å).^[13] The Cu–N_{py} distances of copper(II) complexes with $\text{N}_2(\mu_2\text{-O})_2\text{CuCl}$ coordination described in the literature vary over a wide range from 1.9294(16) Å to 2.270(9) Å.^[24] The Cu–N distances of **5-23** are within the shorter part this range.

The Cu–O distances (2.012(2) Å and 2.268(2) Å) are longer than the mean atom distance of copper(II) and μ_2 -oxygen atoms of dialkylphosphinates (1.919 Å),^[13] but comparable to the shorter Cu–O distances of known complexes with $\text{N}_2(\mu_2\text{-O})_2\text{CuCl}$ coordination (1.912(2)–2.750(4) Å).^[24a, 24b, 25]

The Cu–Cl distance of **5-23** is comparable to the short (<2.4 Å) mean atom distance between five-coordinate copper(II) atoms and terminal chlorine atoms (2.269 Å).^[13] For the $\text{N}_2(\mu_2\text{-O})_2\text{CuCl}$

complexes reported in the literature Cu–Cl distances of 2.2063(6)–2.6020 Å have been found.^[24a-c, 25c, 26]

The Cu···Cu distance (3.351(1) Å) is slightly longer than those of comparable N₂(μ₂-O)₂CuCl complexes (2.9512(8)–3.333(1) Å).^[24b, 25a, 25b, 26b, 27]

The P–C bond lengths (1.802(4) Å and 1.816(3) Å) are comparable to the P–C bond lengths found in copper complexes of other phosphinates (1.776(3)–1.833(20) Å).^[28]

The P–O bond lengths (1.488(3) Å and 1.534(2) Å) are in the same range as those of literature known phosphinate copper complexes (1.467(16)–1.533(14) Å).^[28]

The N–Cu–N angle (174.6(1) °) is slightly bent, but close to linear. The N–Cu–O angles (88.7(1)–96.4(1) °) and the N–Cu–Cl angles (88.4(1) ° and 90.3(1) °) are close to 90 °, which means that the nitrogen atoms are orthogonal to the oxygen and chlorine atoms.

The O–Cu–O angle (77.1(1) °) and the O–Cu–Cl angles (123.2(1) ° and 159.5(1) °) sum up to 359.8 °, meaning these three atoms are arranged in an almost perfectly planar conformation around the copper atom. Although the equatorial atoms at the copper atom are arranged planar the angles are very different. The O–Cu–O angle is much smaller than the O–Cu–Cl angles and the O²–Cu–Cl angle (159.5(1) °) is much larger than the O¹–Cu–Cl angle (123.2(1) °).

The angles around the phosphorus atom range from 104.8(2) ° to 117.8(1) °. The C–P–C angle (108.4(2) °) is slightly smaller than the ideal tetrahedral angle, while the O–P–O angle (117.8(1) °) is significantly larger than the tetrahedral angle of 109.5 °. The C–P–O angles (104.8(2)–110.2(2) °) vary in a small range around the tetrahedral angle.

In the crystal the dimers are arranged in layers in an AB pattern (Figure 28).

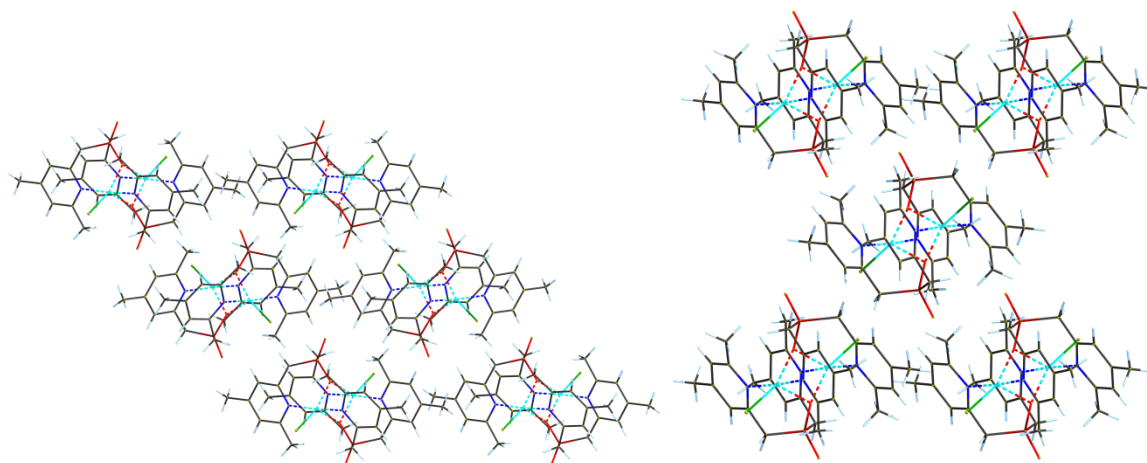
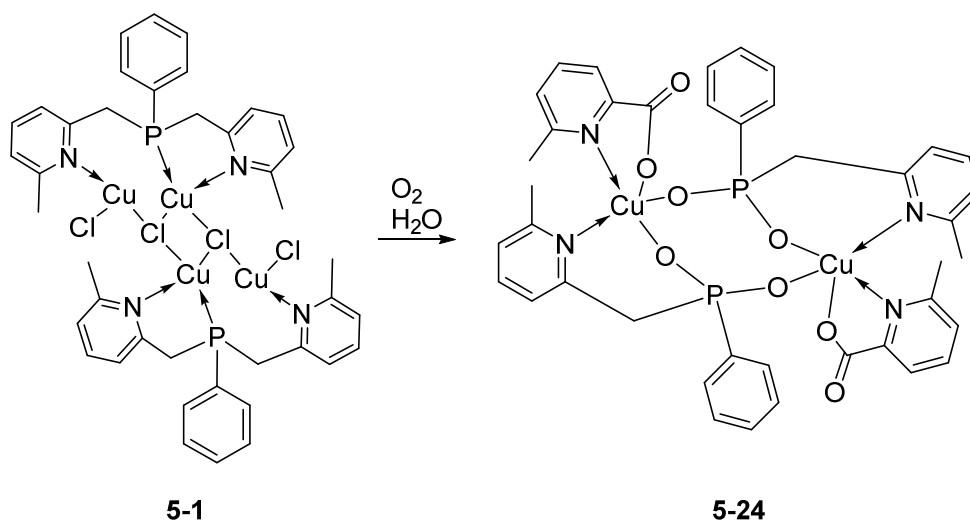


Figure 28: Crystal structure of **5-23**. View along the *a* axis (left) and *b* axis (right).

From a NMR sample of **5-1** in MeCN blue single crystals suitable for X-ray crystallography formed after several weeks. The crystal structure revealed, that the compound was hydrolysed and oxidised by moisture and air, which entered the NMR tube with time.

The P–C bond of one of the lutidinyl substituents was cleaved and the phosphine was oxidised to the corresponding phosphinate PhLutPO₂[−]. Also Cu(I) was oxidised to Cu(II) as observed for **5-23** (Scheme 6). While the disposition of the cleaved collidinyl substituent in the formation of **5-23** is unclear, in the case of **5-24** the cleaved lutidinyl substituent is oxidised to 6-methylpicolinate and coordinates to copper.



Scheme 6: Hydrolysis and oxidation of **5-1** yielding **5-24**.

The hydrolysis product **5-24** was the copper(II) complex of the corresponding phosphinate PhLutPO₂[−] of ligand **2-14** and 6-methylpicolinate. The complex crystallises in the monoclinic space group *P2₁/c* with two formula units in the unit cell. The complex forms a dimeric structure in which the copper atoms are coordinated distorted trigonal bipyramidal by one of the oxygen atoms of each phosphinate ligand, one nitrogen atom of one of the phosphinate ligands and an oxygen atom and the nitrogen atom of one of the 6-methylpicolinate anions (Figure 29). The axial positions are occupied by O1 and N2, while N1, O2 and O4 are at the equatorial positions. The Cu1, O1, O4 and P1 atoms of the dimer form an eight-membered ring.

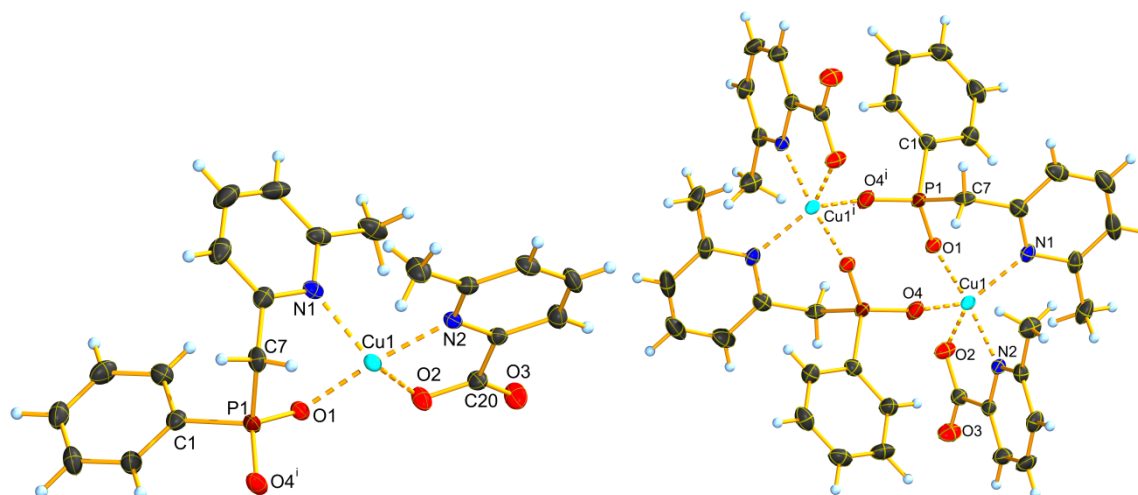


Figure 29: Asymmetric unit (left) and dimeric molecular structure (right) of **5-24**. Thermal ellipsoids are drawn at 50% probability level. Selected bond lengths [Å] and angles [°]: Cu1–N1: 2.050(2), Cu1–N2: 2.010(2), Cu1–O1: 1.946(2), Cu1–O2: 1.975(2), Cu1–O4: 2.135(2), P1–C1: 1.809(3), P1–C7: 1.829(3), P1–O1: 1.515(2), P1–O4ⁱ: 1.490(2), N1–Cu1–N2: 99.4(1), N1–Cu1–O1: 86.3(1), N1–Cu1–O2: 137.5(1), N1–Cu1–O4: 116.4(1), N2–Cu1–O1: 174.1(1), N2–Cu1–O2: 83.0(1), N2–Cu1–O4: 83.3(1), O1–Cu1–O2: 91.8(1), O1–Cu1–O4: 95.5(1), O2–Cu1–O4: 106.1(1), C1–P1–C7: 107.2(1), C1–P1–O1: 108.3(1), C1–P1–O4ⁱ: 108.0(1), C7–P1–O1: 106.0(1), C7–P1–O4ⁱ: 109.6(1), O1–P1–O4ⁱ: 117.4(1). i: 1–x, –y, 2–z.

The Cu–N distances of 2.050(2) Å and 2.010(2) Å are shorter than the mean atom distance of five-coordinate copper atoms to pyridine nitrogen atoms (2.113 Å).^[13] In the literature several copper complexes with N₂CuO₃ coordination and (Cu–O–P–O)₂ eight-membered rings are described. In these complexes the Cu–N distances mostly vary between 1.95(1) Å and 2.0757(18) Å,^[29] with one

exception, in which a very long Cu–N distance of 2.273(3) Å was found.^[30] The Cu–N distances of **5-24** correspond with the literature values of complexes with similar coordination.

The Cu–O4 distance (2.135(2) Å) is significantly longer than the other Cu–O distances of **5-24** (1.946(2) Å and 1.975(2) Å). The same was observed for most of the complexes described in the literature.^[29–31] The Cu–O distances of **5-24** are within the range covered by the known complexes (1.8340(13)–2.472(6) Å).^[29–31]

The P–C bond lengths (1.809(3) Å and 1.829(3) Å) correspond with the bond lengths of P–C bonds of copper complexes of other phosphinates (1.776(3)–1.833(20) Å).^[28]

The P–O bond lengths (1.490(2) Å and 1.515(2) Å) are comparable to those of known phosphinate copper complexes (1.467(16)–1.533(14) Å).^[28]

The N2–Cu1–O1 angle of 174.1(1) ° is almost linear. The N_{ax}–Cu–O_{eq} angles (83.0(1) ° and 83.3(1) °) and the O_{ax}–Cu–N_{eq} angle (86.3(1) °) are smaller than 90 °, while the N_{ax}–Cu–N_{eq} angle (99.4(1) °) and the O_{ax}–Cu–O_{eq} angles (91.8(1) ° and 95.5(1) °) are larger than 90 °.

The O_{eq}–Cu–O_{eq} angle (106.1(1) °) and the O_{eq}–Cu–N_{eq} angles (116.4(1) ° and 137.5(1) °) sum up to 360.0 °, which proves that the atoms in the equatorial positions around the copper atom are in plane.

The angles around P1 vary between 106.0(1) ° and 117.4(1) °. The C–P–C angle (107.2(1) °) is slightly smaller than the ideal tetrahedral angle (109.5 °), while the O–P–O angle (117.4(1) °) is larger than the tetrahedral angle. The C–P–O angles (106.0(1)–109.6(1) °) vary around the tetrahedral angle.

In the crystal the dimers are arranged in layers in an AB pattern (Figure 30, left).

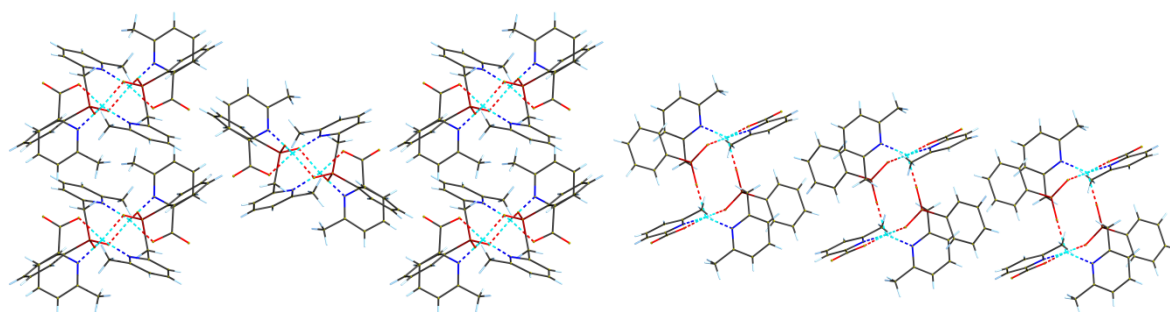


Figure 30: Crystal structure of **5-24**. View along the *a* axis (left) and *b* axis (right).

In the crystal structures of both hydrolysis products no noteworthy interactions between the dimers can be observed. This indicates that the dimers probably are very compact and stable.

5.2.4 DFT calculations

DFT calculations of complexes **5-7a**, **5-14**, **5-17** and **5-18** have been performed with the Gaussian 16 package with the B3LYP functional and 6-31G+(d,p) basis set.^[32] After the optimum geometry of the complexes were determined the distribution and energies of the highest occupied and the lowest unoccupied molecular orbitals were calculated (Figures 31–34).

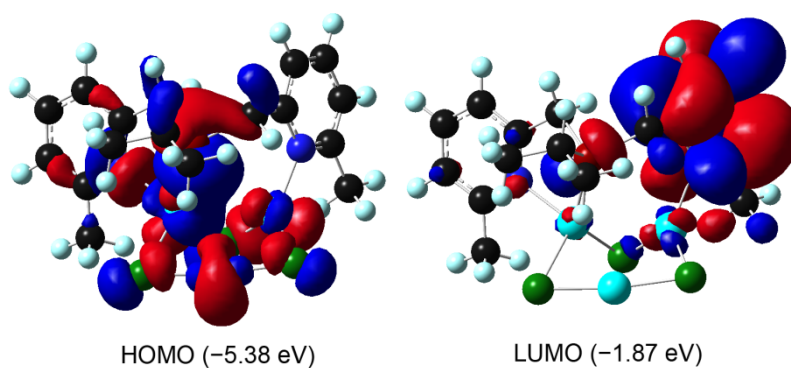


Figure 31: Frontier orbitals of **5-7a**.

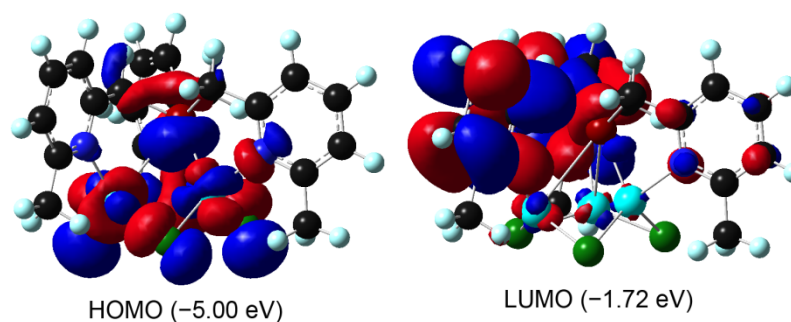


Figure 32: Frontier orbitals of **5-14**.

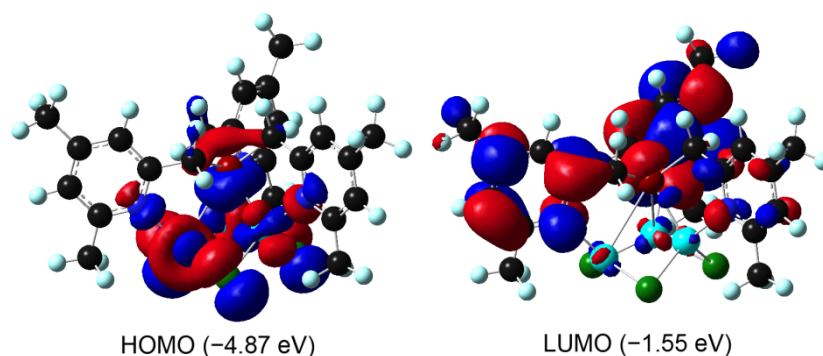


Figure 33: Frontier orbitals of **5-17**.

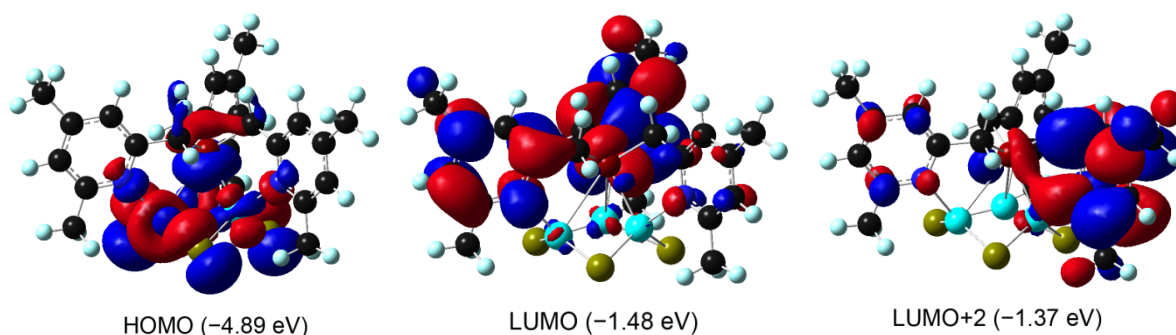


Figure 34: Frontier orbitals and LUMO+2 of **5-18**.

The HOMOs are mostly centred at the Cu_3X_3 clusters with contributions of the phosphorus atom, while the LUMOs are centred at the pyridine rings of the ligands (Figures 31–34). In case of **5-7a** the LUMO is centred at only one of the pyridine rings (Figure 31), but for the tris(picolyl)phosphine

based copper complexes two of the pyridine rings are involved in the shape of the LUMOs (Figures 32–34).

The energy gaps between HOMO and LUMO of **5-7a**, **5-14**, **5-17** and **5-18** are in the range from 3.28 eV (378 nm) to 3.51 eV (353 nm).

The UV/Vis spectra of **5-7a**, **5-14**, **5-17** and **5-18** were calculated with the TD-DFT method at the B3LYP/6-31G+(d,p) level of theory (Figure 35).^[32]

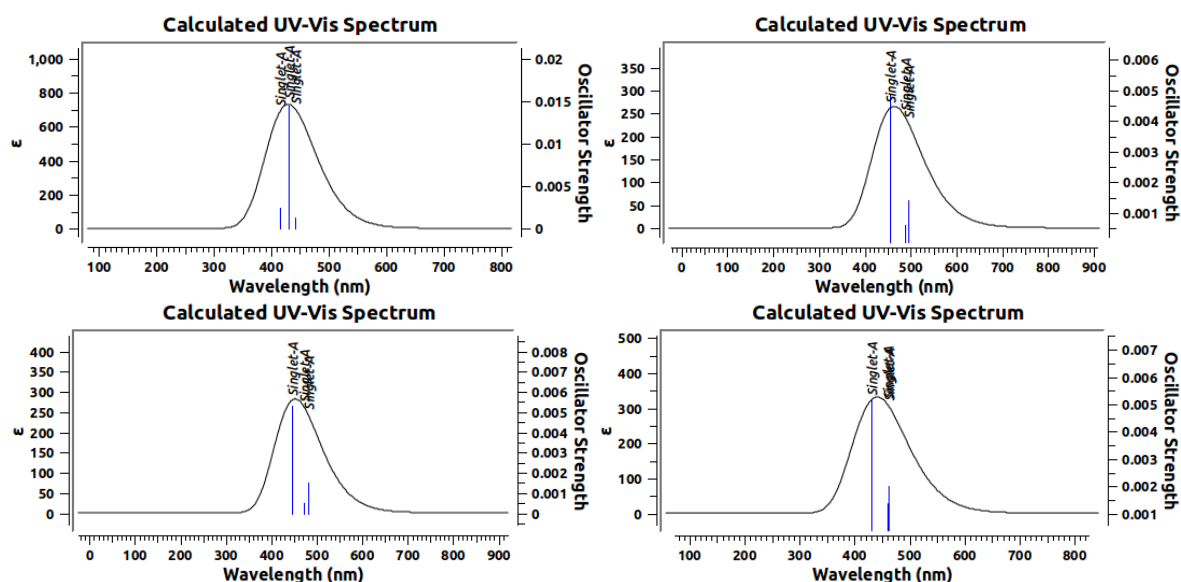


Figure 35: Calculated UV/Vis spectra of **5-7a** (top left), **5-14** (top right), **5-17** (bottom left) and **5-18** (bottom right).

The maxima of the calculated absorption spectra are between 429.0 nm (**5-7a**) and 464.4 nm (**5-14**) (**5-17**: 451.8 nm, **5-18**: 440.2 nm). The main contribution to the absorption is caused by transitions at 431.0 nm (**5-7a**), 454.6 nm (**5-14**), 444.3 nm (**5-17**) and 429.9 nm (**5-18**). In the cases of the copper(I) chloride complexes **5-7a**, **5-14** and **5-17** these absorptions are dominated by a transition from the HOMO to the LUMO, which means that the excitation of these complexes is a MLCT. For the copper(I) bromide complex **5-18** the main contribution to the absorption is caused by a transition from the HOMO to the LUMO+2. As LUMO+2 is centred at one of the pyridine rings (Figure 32) of the ligand in **5-18** this means that for **5-18** the excitation also is a MLCT.

5.3 Summary

The copper(I) chloride, bromide and iodide complexes of four bis(picoly)phosphine based ligands and two tris(picoly)phosphine based ligands have been synthesised, as well as the copper(I) thiocyanate complex of **2-16**. From attempts to synthesise the copper(I) halide complexes of **2-13** the complexes of the corresponding phosphine oxide were obtained.

The crystal structures of nine complexes could be determined by X-ray crystallography. The crystal structures revealed that the phenylbis(picoly)phosphine related ligands react in a ligand to metal ratio of 1:2 with the copper(I) salts used, while the *isopropylbis(picoly)phosphine* based compounds and the tris(picoly)phosphine based compounds react in a ligand to metal ratio of 1:3 with the copper(I) salts. In the crystal structures of the phosphine oxide complexes **5-20** and **5-21** a ligand to metal ratio of 1:1 was observed.

The structures of the complexes showed a great variety in how the bis- and tris(picoly)phosphine related ligands coordinate to the copper atoms (Figure 36). In the case of **5-7** it was even possible to isolate two structural isomers.

The most frequently observed structural motif found in the copper(I) halide complexes of the bis- and tris(picoly)phosphine based ligands was the six-membered ring of Cu_3X_3 , but also other structural motifs could be found, such as the infinite CuCl -chains in complexes **5-7b** and **5-11**. In many of the complexes described above copper atoms in different coordination modes and with different coordination numbers were present. The structure of **5-7a** even contains three completely different coordinated copper atoms in one molecule. In all structures except from **5-7a** and **5-11** at least one of the copper atoms is coordinated by both the phosphorus atom and one of the nitrogen atoms of the ligand, while the other nitrogen atoms coordinate other copper atoms.

In some of the complexes the phosphorus acts as a bridging ligand, which coordinates to two or in case of **5-14** and **5-18** even three copper atoms.

While the complexation of the bis- and tris(picoly)phosphine based ligands to the copper(I) salts led to rather unusual structures, the crystal structures of the phosphine oxide complexes **5-20** and **5-21** revealed the typical Cu_2X_2 rhomboid structure with N,N coordination to the copper atoms.

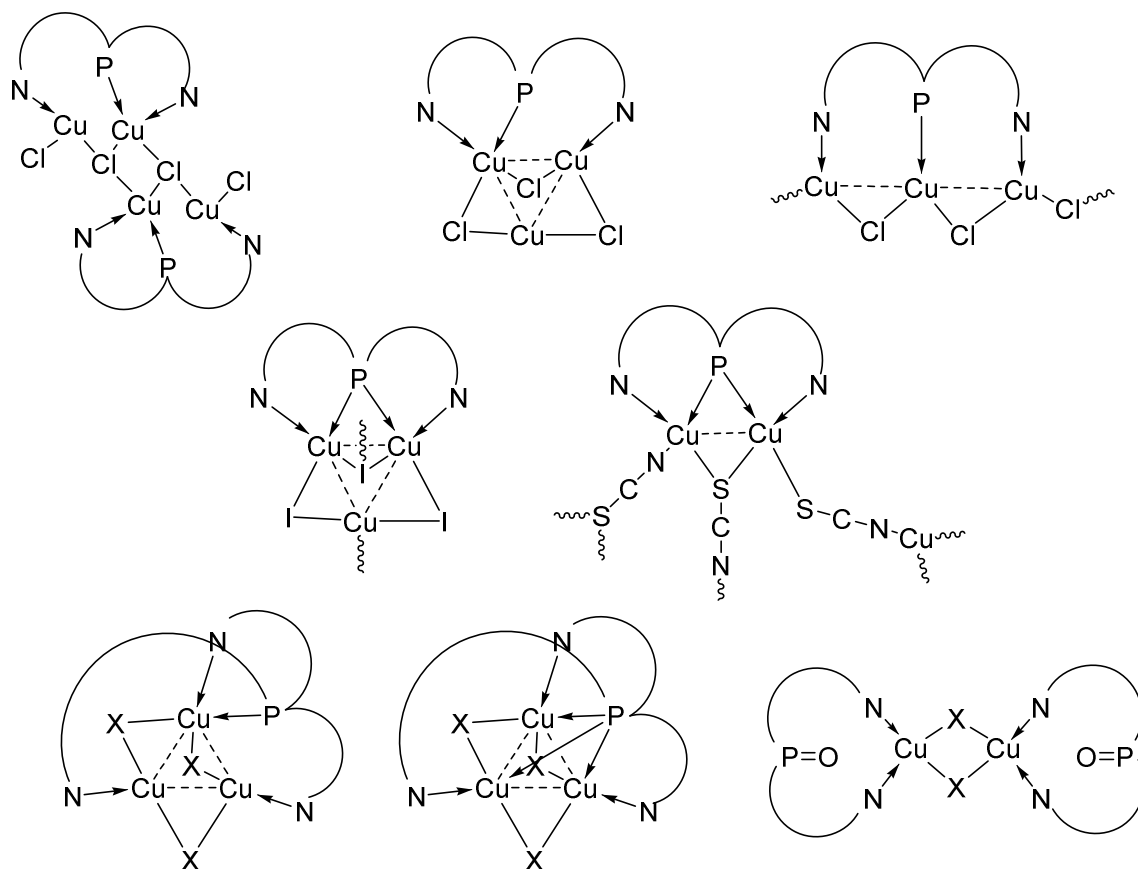


Figure 36: Coordination modes of copper(I) found in complexes **5-4**, **5-7**, **5-9**, **5-10**, **5-11**, **5-13**, **5-14**, **5-17**, **5-18**, **5-20** and **5-21**.

Complexes **5-1** and **5-2** and the phosphine oxide complexes **5-20**, **5-21** and **5-22** showed intense green to blue-green luminescence under UV light, while complexes **5-8**, **5-14**, **5-18** and **5-19** showed only weak luminescence. The emission maximum is blue-shifted upon change from chloride to bromide and iodide.

DFT calculations of **5-7a**, **5-14**, **5-17** and **5-18** indicated that MLCT is the excitation mechanism of the complexes.

Through crystal structures of the hydrolysis products of **5-1** and **5-17** (**5-23** and **5-24**) it was possible to find out that hydrolysis of the complexes leads to cleavage of one of the P–C bonds of the ligands and one of the picolyl based substituents is eliminated. In the presence of oxygen the fragments are oxidised to a phosphinate and a carboxylic acid.

5.4 Experimental

For general information about methods and analytical instruments used see 2.4.1. For details about the DFT calculations see 4.4.1.

Due to the low solubility of the copper(I) complexes the compounds could not be purified. Therefore no yields and no analytics like melting points, NMR or IR data are reported. Listed data from elemental analysis were obtained from single crystals. The compounds were identified *via* HRMS of precipitates obtained from reactions.

5.4.1 Phenyl-bis(6-methylpyridin-2-ylmethyl)phosphine copper(I) chloride complex **5-1**

CuCl (236 mg, 2.4 mmol, 2 eq) was dissolved in 5 mL dry MeCN. To the yellow solution **2-14** (2.4 mL, 0.5 M in MeCN, 1.2 mmol, 1 eq) was added dropwise and the reaction was stirred overnight. The precipitate was filtered off and dried *in vacuo*. A pale yellow solid was obtained (375 mg).

m/z (ESI) [%]: 482.97102 (16), 383.07427 (100), 321.15250 (2), 214.07851 (2).

m/z (FAB⁺) [%]: 383.0755 (100).

m/z(FAB⁻) [%]: 35 (2).

5.4.2 Phenyl-bis(6-methylpyridin-2-ylmethyl)phosphine copper(I) bromide complex **5-2**

CuBr (359 mg, 2.5 mmol, 2 eq) was suspended in 5 mL dry MeCN. To the pale blue-green suspension **2-14** (2.5 mL, 0.5 M in MeCN, 1.3 mmol, 1 eq) was added dropwise and the reaction was stirred overnight. The solid was filtered off and dried *in vacuo*. A pale blue-green solid was obtained (477 mg).

m/z (ESI) [%]: 526.92072 (40), 383.07399 (100), 321.15257 (4), 214.07854 (2).

5.4.3 Phenyl-bis(6-methylpyridin-2-ylmethyl)phosphine copper(I) iodide complex **5-3**

CuI (556 mg, 2.9 mmol, 2 eq) was suspended in 5 mL dry MeCN. To the colourless suspension **2-14** (2.9 mL, 0.5 M in MeCN, 1.5 mmol, 1 eq) was added dropwise and the reaction was stirred overnight. The solid was filtered off and dried *in vacuo*. A colourless solid was obtained (682 mg).

m/z (ESI) [%]: 572.90784 (7), 383.07340 (100), 321.15176 (15), 214.07821 (2).

5.4.4 Phenyl-bis(4,6-dimethylpyridin-2-ylmethyl)phosphine copper(I) chloride complex 5-4

Reaction 1: CuCl (99 mg, 1.0 mmol, 1 eq) was dissolved in 2 mL dry MeCN. To the yellow solution **2-15** (1.0 mL, 1 M in THF, 1.0 mmol, 1 eq) was added dropwise and the reaction was stirred overnight. The precipitate was filtered off and dried *in vacuo*. A yellow-green solid was obtained (119 mg).

Reaction 2: CuCl (250 mg, 2.5 mmol, 2 eq) was dissolved in 5 mL dry MeCN. To the yellow solution **2-15** (2.5 mL, 0.5 M in MeCN, 1.3 mmol, 1 eq) was added dropwise and the reaction was stirred overnight. The precipitate was filtered off and dried *in vacuo*. A pale yellow solid was obtained (120 mg).

m/z (ESI) [%]: 511.00248 (33), 411.10557 (100), 349.08393 (2), 228.09426 (1).

m/z(FAB⁺) [%]: 411.1029 (100).

m/z(FAB⁻) [%]: 35 (4).

5.4.5 Phenyl-bis(4,6-dimethylpyridin-2-ylmethyl)phosphine copper(I) bromide complex 5-5

CuBr (316 mg, 2.2 mmol, 2 eq) was suspended in 5 mL dry MeCN. To the pale blue-green suspension **2-15** (2.2 mL, 0.5 M in MeCN, 1.1 mmol, 1 eq) was added dropwise and the reaction was stirred overnight. The solid was filtered off and dried *in vacuo*. A pale blue-green solid was obtained (175 mg).

m/z (ESI) [%]: 554.95239 (100), 411.10550 (100), 349.18426 (3), 228.09434 (1).

5.4.6 Phenyl-bis(4,6-dimethylpyridin-2-ylmethyl)phosphine copper(I) iodide complex 5-6

CuI (524 mg, 2.8 mmol, 2 eq) was suspended in 5 mL dry MeCN. To the colourless suspension **2-15** (2.8 mL, 0.5 M in MeCN, 1.4 mmol, 1 eq) was added dropwise and the reaction was stirred overnight. The solid was filtered off and dried *in vacuo*. A colourless solid was obtained (536 mg).

m/z (ESI) [%]: 600.93941 (19), 411.10495 (65), 349.18325 (9), 228.09391 (1).

m/z(FAB⁺) [%]: 411.1036 (100).

m/z(FAB⁻) [%]: 127 (15).

5.4.7 *iso*Propyl-bis(6-methylpyridin-2-ylmethyl)phosphine copper(I) chloride complex 5-7

Reaction 1: CuCl (115 mg, 1.2 mmol, 3 eq) was dissolved in 3 mL dry MeCN. **2-16** (0.77 mL, 0.5 M in MeCN, 0.39 mmol, 1 eq) was added dropwise to the yellow solution and after stirring for 30 min the solvent was removed *in vacuo*. A greenish solid was obtained (167 mg).

Reaction 2: CuCl (386 mg, 3.9 mmol, 3 eq) was dissolved in 5 mL dry MeCN. To the yellow solution **2-16** (2.6 mL, 0.5 M in MeCN, 1.3 mmol, 1 eq) was added dropwise and after stirring for 10 min the reaction was left overnight. From the solution crystals of **5-7b** formed. The remaining solution was

removed and the crystals were dried under vacuum. The product was obtained as yellowish crystals (156 mg, 0.27 mmol, 21%).

EA: Found: C, 34.3; H, 3.75; N, 4.7. Calc. for $C_{17}H_{23}Cu_3Cl_3N_2P$: C, 35.0; H, 4.0; N, 4.8%.

m/z (ESI) [%]: 546.88631 (2), 448.98622 (100), 349.08953 (96), 287.16796 (2), 180.09403 (1).

5.4.8 *iso*Propyl-bis(6-methylpyridin-2-ylmethyl)phosphine copper(I) bromide complex 5-8

CuBr (443 mg, 3.1 mmol, 3 eq) was suspended in 5 mL dry MeCN. To the pale blue-green suspension **2-16** (2.1 mL, 0.5 M in MeCN, 1.0 mmol, 1 eq) was added dropwise and the reaction was stirred overnight. The solid was filtered off and dried *in vacuo*. A pale blue-green solid was obtained (134 mg).

m/z (ESI) [%]: 492.93589 (27), 349.08960 (100), 287.16802 (4), 180.09408 (1).

5.4.9 *iso*Propyl-bis(6-methylpyridin-2-ylmethyl)phosphine copper(I) iodide complex 5-9

Reaction 1: CuI (196 mg, 1.0 mmol, 3 eq) was suspended in 3 mL dry MeCN. **2-16** (0.69 mL, 0.5 M in MeCN, 0.34 mmol, 1 eq) was added dropwise to the colourless suspension and after stirring for 5 min the solution was left standing until the product had crystallised. The remaining solution was removed and the product was dried *in vacuo*. The product was obtained as colourless crystals (110 mg, 0.13 mmol, 38%).

Reaction 2: CuI (577 mg, 3.0 mmol, 3 eq) was suspended in 5 mL dry MeCN. To the colourless suspension **2-16** (2.0 mL, 0.5 M in MeCN, 1.0 mmol, 1 eq) was added dropwise and the reaction was stirred overnight. The solid was filtered off and dried *in vacuo*. A colourless solid was obtained (536 mg).

EA: Found: C, 24.1; H, 2.9; N, 3.25. Calc. for $C_{17}H_{23}N_2PCu_3I_3$: C, 23.8; H, 2.7; N, 3.3%.

m/z (ESI) [%]: 538.92397 (9), 349.08949 (100), 287.16744 (4), 180.09376 (0.1).

5.4.10 *iso*Propyl-bis(6-methylpyridin-2-ylmethyl)phosphine copper(I) thiocyanate complex 5-10

CuSCN (159 mg, 1.31 mmol, 3 eq) was suspended in 3 mL dry MeCN. **2-16** (0.87 mL, 0.5 M in MeCN, 0.44 mmol, 1 eq) was added dropwise to the colourless suspension and the reaction was stirred overnight. The solvent was removed *in vacuo* and a colourless solid was obtained (195 mg).

5.4.11 *iso*Propyl-bis(4,6-dimethylpyridin-2-ylmethyl)phosphine copper(I) chloride complex 5-11

Reaction 1: CuCl (121 mg, 1.2 mmol, 1 eq) was dissolved in 2.4 mL dry MeCN. **2-17** (2.4 mL, 0.5 M in MeCN, 1.2 mmol, 1 eq) was added dropwise to the yellow solution and stirred overnight. The precipitate was filtered off and dried *in vacuo*. A yellow-green solid was obtained (314 mg).

Reaction 2: CuCl (308 mg, 3.1 mmol, 3 eq) was dissolved in 5 mL dry MeCN. To the yellow solution **2-17** (2.1 mL, 0.5 M in MeCN, 1.0 mmol, 1 eq) was added dropwise and after stirring for 10 min the reaction was left overnight. From the solution crystals of **5-11** formed. The remaining solution was removed and the crystals were dried under vacuum. The product was obtained as yellowish crystals (120 mg, 0.22 mmol, 17%).

m/z (ESI) [%]: 574.91732 (1), 475.01963 (64), 377.12070 (100), 315.19924 (5), 194.10968 (2).

m/z(FAB⁺) [%]: 377.1195 (100).

m/z(FAB⁻) [%]: 35 (3).

5.4.12 isoPropyl-bis(4,6-dimethylpyridin-2-ylmethyl)phosphine copper(I) bromide complex 5-12

CuBr (420 mg, 2.9 mmol, 3 eq) was suspended in 5 mL dry MeCN. To the pale blue-green suspension **2-17** (2.0 mL, 0.5 M in MeCN, 1.0 mmol, 1 eq) was added dropwise and the reaction was stirred overnight. The solid was filtered off and dried *in vacuo*. A pale blue-green solid was obtained (89 mg).

m/z (ESI) [%]: 662.81719 (1), 520.96736 (31), 377.12109 (100), 315.19952 (4), 194.10982 (1).

m/z(FAB⁺) [%]: 377.1188 (100).

m/z(FAB⁻) [%]: 79 (6).

5.4.13 isoPropyl-bis(4,6-dimethylpyridin-2-ylmethyl)phosphine copper(I) iodide complex 5-13

CuI (579 mg, 3.0 mmol, 3 eq) was suspended in 5 mL dry MeCN. To the colourless suspension **2-17** (2.0 mL, 0.5 M in MeCN, 1.0 mmol, 1 eq) was added dropwise and the reaction was stirred overnight. The solid was filtered off and dried *in vacuo*. A colourless solid was obtained (454 mg).

m/z (ESI) [%]: 566.95512 (23), 377.12032 (100), 315.19863, (30), 194.10939 (3).

m/z (FAB⁺) [%]: 377.1228 (100).

m/z (FAB⁻) [%]: 127 (16).

5.4.14 Tris(6-methylpyridin-2-ylmethyl)phosphine copper(I) chloride complex 5-14

CuCl (306 mg, 3.1 mmol, 3 eq) was dissolved in 5 mL dry MeCN. To the yellow solution **2-24** (2.1 mL, 0.5 M in MeCN, 1.0 mmol, 1 eq) was added dropwise and the reaction was stirred overnight. The precipitate was filtered off and dried *in vacuo*. A pale yellow solid was obtained (391 mg).

m/z (ESI) [%]: 509.99885 (1), 412.10000 (47), 350.17828 (11), 243.10466 (10).

5.4.15 Tris(6-methylpyridin-2-ylmethyl)phosphine copper(I) bromide complex 5-15

CuBr (424 mg, 3.0 mmol, 3 eq) was suspended in 5 mL dry MeCN. To the pale blue-green suspension **2-24** (2.0 mL, 0.5 M in MeCN, 1.0 mmol, 1 eq) was added dropwise and the reaction was stirred overnight. The solid was filtered off and dried *in vacuo*. A pale blue-green solid was obtained (504 mg).

m/z (ESI) [%]: 555.94622 (4), 412.10005 (8), 350.17821 (7), 243.10460 (8).

5.4.16 Tris(6-methylpyridin-2-ylmethyl)phosphine copper(I) iodide complex 5-16

CuI (610 mg, 3.2 mmol, 3 eq) was suspended in 5 mL dry MeCN. To the colourless suspension **2-24** (2.1 mL, 0.5 M in MeCN, 1.1 mmol, 1 eq) was added dropwise and the reaction was stirred overnight. The solid was filtered off and dried *in vacuo*. A colourless solid was obtained (643 mg).
m/z (ESI) [%]: 793.76717 (2), 601.93454 (11), 412.10006 (51), 350.17825 (43), 243.10462 (50).

5.4.17 Tris(4,6-dimethylpyridin-2-ylmethyl)phosphine copper(I) chloride complex 5-17

CuCl (238 mg, 2.4 mmol, 3 eq) was dissolved in 5 mL dry MeCN. To the yellow solution **2-25** (1.6 mL, 0.5 M in MeCN, 0.8 mmol, 1 eq) was added dropwise and the reaction was stirred overnight. The precipitate was filtered off and dried *in vacuo*. A greenish solid was obtained (254 mg).
EA: Found: C, 37.5; H, 3.9; N, 5.4. Calc. for $C_{24}H_{30}Cu_3Cl_3N_3P \cdot CDCl_3$: C, 37.1; H, 4.0; N, 5.2%.
m/z (ESI) [%]: 649.94505 (1), 554.04364 (15), 454.14673 (100), 392.22523 (21), 271.13596 (9).

5.4.18 Tris(4,6-dimethylpyridin-2-ylmethyl)phosphine copper(I) bromide complex 5-18

CuBr (420 mg, 2.9 mmol, 3 eq) was suspended in 5 mL dry MeCN. To the pale blue-green suspension **2-25** (2.0 mL, 0.5 M in MeCN, 1.0 mmol, 1 eq) was added dropwise and the reaction was stirred overnight. The solid was filtered off and dried *in vacuo*. A pale blue-green solid was obtained (466 mg).
m/z (ESI) [%]: 597.99323 (18), 454.14680 (92), 392.22501 (100), 271.13589 (19).

5.4.19 Tris(4,6-dimethylpyridin-2-ylmethyl)phosphine copper(I) iodide complex 5-19

CuI (554 mg, 2.9 mmol, 3 eq) was suspended in 5 mL dry MeCN. To the colourless suspension **2-25** (1.9 mL, 0.5 M in MeCN, 1.0 mmol, 1 eq) was added dropwise and the reaction was stirred overnight. The solid was filtered off and dried *in vacuo*. A colourless solid was obtained (611 mg).
m/z (ESI) [%]: 835.81315 (1), 643.98158 (1), 454.14711 (10), 392.22524 (14), 271.13597 (10).

5.4.20 Phenyl-bis(pyridin-2-ylmethyl)phosphine oxide copper(I) chloride complex 5-20

CuCl (158 mg, 1.6 mmol, 3 eq) was dissolved in 3 mL dry MeCN. **2-13** (1.1 mL, 0.5 M in MeCN, 0.53 mmol, 1 eq) was added dropwise to the yellow solution and stirred overnight. The precipitate was filtered off and dried *in vacuo*. A greenish solid was obtained (96 mg).
³¹P NMR (162 MHz, $CDCl_3$) δ = 36.1 ppm.

5.4.21 Phenyl-bis(pyridin-2-ylmethyl)phosphine oxide copper(I) bromide complex 5-21

CuBr (230 mg, 1.6 mmol, 3 eq) was suspended in 3 mL dry MeCN. **2-13** (1.1 mL, 0.5 M in MeCN, 0.53 mmol, 1 eq) was added dropwise to the pale blue-green suspension and stirred overnight. The solid was filtered off and the solvent was removed *in vacuo*. A yellow solid was obtained (134 mg).

³¹P NMR (162 MHz, CDCl₃) δ = 35.1 ppm.

5.4.22 Phenyl-bis(pyridin-2-ylmethyl)phosphine oxide copper(I) iodide complex 5-22

CuI (305 mg, 1.6 mmol, 3 eq) was suspended in 3 mL dry MeCN. **2-13** (1.1 mL, 0.5 M in MeCN, 0.53 mmol, 1 eq) was added dropwise to the colourless suspension and stirred overnight. The solid was filtered off and the solvent was removed *in vacuo*. A light yellow solid was obtained (116 mg).

³¹P NMR (162 MHz, CDCl₃) δ = 31.1 ppm.

5.4.23 Crystallographic data

Table 1: Crystallographic data of **5-4**, **5-7** and **5-9**.

	5-4	5-7a	5-7b	5-9
Identification code	kx322	mx256	ox353	mx238
Empirical formula	C ₂₂ H ₂₅ Cl ₂ Cu ₂ N ₂ P	C ₁₇ H ₂₃ Cl ₃ Cu ₃ N ₂ P	C ₁₇ H ₂₃ Cl ₃ Cu ₃ N ₂ P	C ₃₄ H ₄₆ Cu ₆ I ₆ N ₄ P ₂
Formula weight [g·mol ⁻¹]	546.39	583.31	583.31	1715.33
Temperature [K]	173(2)	143(2)	123(3)	143(2)
Crystal size [mm ³]	0.10× 0.15× 0.20	0.05× 0.15× 0.35	0.05× 0.40× 0.40	0.02× 0.10× 0.10
Colour, shape	Colourless block	Colourless block	Yellow platelet	Colourless block
Crystal system	Monoclinic	Monoclinic	Orthorhombic	Monoclinic
Space group	<i>P</i> 2 ₁ / <i>c</i>	<i>P</i> 2 ₁ / <i>c</i>	<i>Pba</i> 2	<i>Cc</i>
<i>a</i> [Å]	11.0090(5)	14.1998(6)	16.6410(6)	20.8746(5)
<i>b</i> [Å]	13.0530(5)	7.9080(3)	27.9440(11)	15.9960(3)
<i>c</i> [Å]	16.4000(5)	21.9024(11)	9.0090(4)	14.4722(3)
α [°]	90	90	90	90
β [°]	99.381(4)	105.979(5)	90	110.189(3)
γ [°]	90	90	90	90
<i>V</i> [Å ³]	2325.17(16)	2364.44(19)	4189.3(3)	4535.50(19)
<i>Z</i>	4	4	8	4
ρ_{calc} [g·cm ⁻³]	1.561	1.639	1.850	2.512
Radiation [Å]	MoK α = 0.71073	MoK α = 0.71073	MoK α = 0.71073	MoK α = 0.71073
μ [cm ⁻¹]	2.139	3.085	3.482	6.948
<i>F</i> (000)	1112	1168	2336	3200
Index ranges	-13≤ <i>h</i> ≤13 -16≤ <i>k</i> ≤14 -20≤ <i>l</i> ≤20	-17≤ <i>h</i> ≤16 -9≤ <i>k</i> ≤9 -23≤ <i>l</i> ≤27	-22≤ <i>h</i> ≤22 -37≤ <i>k</i> ≤33 -11≤ <i>l</i> ≤12	-29≤ <i>h</i> ≤29 -22≤ <i>k</i> ≤22 -20≤ <i>l</i> ≤20
θ range [°]	4.165≤ θ ≤ 26.371	4.253≤ θ ≤ 26.368	2.448≤ θ ≤ 28.281	4.106≤ θ ≤ 30.508
Reflections collected	17187	16828	38917	43406
Independent reflections	4728	4733	10111	13773
Observed reflections	3450	3781	8444	12343
Data/restraints/parameters	4728/0/266	4733/0/240	10111/1/479	13773/2/477
<i>R</i> _{int}	0.0487	0.0352	0.0581	0.0307
<i>R</i> ₁ , <i>wR</i> ₂ [I>2σ(I)]	0.0448, 0.0986	0.0443, 0.1128	0.0408, 0.0813	0.0280, 0.0612
<i>R</i> ₁ , <i>wR</i> ₂ [all data]	0.0702, 0.1146	0.0601, 0.1238	0.0556, 0.0887	0.0338, 0.0642
GooF	1.058	1.049	1.046	1.021
$\delta\rho_{\text{max}}$, $\delta\rho_{\text{min}}$ [e·nm ⁻³]	1.180, -0.414	1.908, -0.558	0.744, -0.576	2.756, -0.586

Table 2: Crystallographic data of **5-10**, **5-11**, **5-13** and **5-14**.

	5-10	5-11	5-13	5-14
Identification code	mx177	ox385	xv538	mx131
Empirical formula	C ₂₀ H ₂₃ Cu ₃ N ₅ PS ₃	C ₁₉ H ₂₇ Cl ₃ Cu ₃ N ₂ P	C ₁₉ H ₂₇ Cu ₃ I ₃ N ₂ P	C ₂₁ H ₂₄ Cl ₃ Cu ₃ N ₃ P
Formula weight [g·mol ⁻¹]	651.20	611.36	885.71	646.37
Temperature [K]	173(2)	128(2)	104(2)	173(2)
Crystal size [mm ³]	0.06× 0.17× 0.25	0.05× 0.40× 0.45	0.02× 0.07× 0.08	0.03× 0.15× 0.25
Colour, shape	Colourless block	Yellow platelet	Colourless platelet	Colourless block
Crystal system	Orthorhombic	Orthorhombic	Orthorhombic	Monoclinic
Space group	<i>Pbca</i>	<i>Pna2</i> ₁	<i>Pbca</i>	<i>C2/c</i>
<i>a</i> [Å]	10.8645(2)	16.1620(3)	16.2479(5)	32.5615(13)
<i>b</i> [Å]	20.0628(6)	13.3450(3)	14.4034(4)	7.6042(2)
<i>c</i> [Å]	23.8267(6)	10.6630(2)	20.7144(6)	19.6563(7)
α [°]	90	90	90	90
β [°]	90	90	90	102.019(3)
γ [°]	90	90	90	90
<i>V</i> [Å ³]	5193.6(2)	2299.82(8)	4847.7(2)	4760.3(3)
<i>Z</i>	8	4	8	8
ρ_{calc} [g·cm ⁻³]	1.666	1.766	2.427	1.804
Radiation [Å]	MoK α = 0.71073	MoK α = 0.71073	MoK α = 0.71073	MoK α = 0.71073
μ [cm ⁻¹]	2.755	3.176	6.504	3.075
<i>F</i> (000)	2624	1232	3328	2592
Index ranges	-14≤ <i>h</i> ≤13 -26≤ <i>k</i> ≤26 -30≤ <i>l</i> ≤26	-21≤ <i>h</i> ≤21 -17≤ <i>k</i> ≤ 17 -14≤ <i>l</i> ≤14	-21≤ <i>h</i> ≤21 -19≤ <i>k</i> ≤19 -27≤ <i>l</i> ≤27	-43≤ <i>h</i> ≤40 -10≤ <i>k</i> ≤9 -25≤ <i>l</i> ≤26
θ range [°]	4.152≤ θ ≤ 27.484	2.520≤ θ ≤ 28.274	2.130≤ θ ≤ 28.278	4.106≤ θ ≤ 28.282
Reflections collected	44639	21446	77609	21380
Independent reflections	5927	5554	5965	5872
Observed reflections	3760	5252	5377	4636
Data/restraints/parameters	5927/0/298	5554/1/259	5965/0/268	5872/0/295
<i>R</i> _{int}	0.0944	0.0296	0.0370	0.0395
<i>R</i> ₁ , <i>wR</i> ₂ [<i>I</i> >2 σ (<i>I</i>)]	0.0417, 0.0755	0.0235, 0.0591	0.0163, 0.0357	0.0342, 0.0700
<i>R</i> ₁ , <i>wR</i> ₂ [all data]	0.0852, 0.0900	0.0268, 0.0615	0.0210, 0.0388	0.0496, 0.0773
GooF	1.015	1.054	1.125	1.046
δp_{max} , δp_{min} [e·nm ⁻³]	0.375, -0.364	0.508, -0.348	0.422, -0.806	0.439, -0.554

Table 3: Crystallographic data of **5-17**, **5-18**, **5-20** and **5-21**.

	5-17·MeCN	5-18	5-20 · 2MeCN	5-21 · 2MeCN
Identification code	xv308	xv537	mx405	mx400
Empirical formula	C ₂₆ H ₃₃ Cl ₃ Cu ₃ N ₄ P	C ₂₄ H ₃₀ Br ₃ Cu ₃ N ₃ P	C ₄₀ H ₄₀ Cl ₂ Cu ₂ N ₆ O ₂ P ₂	C ₄₀ H ₄₀ Br ₂ Cu ₂ N ₆ O ₂ P ₂
Formula weight [g·mol ⁻¹]	729.50	821.83	896.70	985.62
Temperature [K]	106(2)	104(2)	138(2)	298(2)
Crystal size [mm ³]	0.02× 0.03× 0.07	0.02× 0.05× 0.10	0.11× 0.19× 0.22	0.24× 0.29× 0.33
Colour, shape	Colourless rod	Colourless platelet	Pale yellow block	Colourless block
Crystal system	Monoclinic	Triclinic	Triclinic	Triclinic
Space group	<i>P</i> 2 ₁ / <i>n</i>	<i>P</i> -1	<i>P</i> -1	<i>P</i> -1
<i>a</i> [Å]	11.7494(5)	8.1750(2)	9.7327(6)	9.8162(2)
<i>b</i> [Å]	17.6960(8)	10.0440(3)	10.0126(6)	10.0591(3)
<i>c</i> [Å]	14.3167(7)	17.6380(4)	11.5320(9)	11.5530(3)
α [°]	90	103.0550(8)	110.922(7)	109.434(2)
β [°]	107.4184(15)	95.1230(9)	100.657(6)	101.523(2)
γ [°]	90	96.6230(9)	102.972(5)	102.891(2)
<i>V</i> [Å ³]	2840.2(4)	1391.41(6)	978.56(12)	1001.00(5)
<i>Z</i>	4	2	1	1
ρ_{calc} [g·cm ⁻³]	1.706	1.962	1.522	1.635
Radiation [Å]	MoK α = 0.71073	MoK α = 0.71073	MoK α = 0.71073	MoK α = 0.71073
μ [cm ⁻¹]	2.589	6.656	1.349	3.182
<i>F</i> (000)	1480	804	460	496
Index ranges	-15≤ <i>h</i> ≤15 -23≤ <i>k</i> ≤23 -19≤ <i>l</i> ≤19	-11≤ <i>h</i> ≤11 -14≤ <i>k</i> ≤14 -25≤ <i>l</i> ≤25	-12≤ <i>h</i> ≤13 -14≤ <i>k</i> ≤13 -16≤ <i>l</i> ≤15	-14≤ <i>h</i> ≤14 -14≤ <i>k</i> ≤14 -16≤ <i>l</i> ≤16
θ range [°]	2.933≤ θ ≤ 28.30	3.053≤ θ ≤ 30.56	4.178≤ θ ≤ 30.507	4.160≤ θ ≤ 30.508
Reflections collected	52593	27130	10322	19609
Independent reflections	7048	8470	5939	6079
Observed reflections	6018	6811	4512	5171
Data/restraints/parameters	7048/0/341	8470/0/313	5939/0/260	6079/0/260
<i>R</i> _{int}	0.0424	0.0351	0.0325	0.0314
<i>R</i> ₁ , <i>wR</i> ₂ [<i>I</i> >2σ(<i>I</i>)]	0.0250, 0.0534	0.0282, 0.0530	0.0408, 0.0795	0.0309, 0.0751
<i>R</i> ₁ , <i>wR</i> ₂ [all data]	0.0346, 0.0581	0.0430, 0.0571	0.0618, 0.0898	0.0397, 0.0801
GooF	1.057	1.041	1.021	1.039
$\delta\rho_{\text{max}}$, $\delta\rho_{\text{min}}$ [e·nm ⁻³]	0.520, -0.679	0.522, -0.647	0.446, -0.507	0.767, -0.685

Table 4: Crystallographic data of **5-23** and **5-24**.

	5-23	5-24
Identification code	mx403	mx289
Empirical formula	C ₃₂ H ₄₀ Cl ₂ Cu ₂ N ₄ O ₄ P ₂	C ₄₀ H ₃₉ Cu ₂ N ₄ O ₈ P ₂
Formula weight [g·mol ⁻¹]	804.60	891.76
Temperature [K]	143(2)	143(2)
Crystal size [mm ³]	0.03× 0.09× 0.38	0.02× 0.08× 0.10
Colour, shape	Blue needle	Pale blue block
Crystal system	Monoclinic	Monoclinic
Space group	<i>P</i> 2 ₁ / <i>n</i>	<i>P</i> 2 ₁ / <i>c</i>
<i>a</i> [Å]	10.2044(6)	10.8407(6)
<i>b</i> [Å]	12.3572(6)	7.8134(4)
<i>c</i> [Å]	13.0525(7)	22.5525(12)
α [°]	90	90
β [°]	91.661(5)	98.684(6)
γ [°]	90	90
<i>V</i> [Å ³]	1645.20(15)	1888.36(18)
<i>Z</i>	2	2
ρ_{calc} [g·cm ⁻³]	1.624	1.568
Radiation [Å]	MoK α = 0.71073	MoK α = 0.71073
μ [cm ⁻¹]	1.597	1.271
<i>F</i> (000)	828	916
Index ranges	-13≤ <i>h</i> ≤11 -16≤ <i>k</i> ≤16 -15≤ <i>l</i> ≤17	-13≤ <i>h</i> ≤14 -10≤ <i>k</i> ≤10 -29≤ <i>l</i> ≤30
θ range [°]	4.323≤ θ ≤ 28.278	4.462≤ θ ≤ 28.280
Reflections collected	13715	17021
Independent reflections	4056	4668
Observed reflections	2707	3323
Data/restraints/parameters	4056/0/217	4668/0/268
<i>R</i> _{int}	0.0712	0.0617
<i>R</i> ₁ , <i>wR</i> ₂ [<i>I</i> >2 σ (<i>I</i>)]	0.0460, 0.0863	0.0432, 0.0813
<i>R</i> ₁ , <i>wR</i> ₂ [all data]	0.0863, 0.1029	0.0742, 0.0919
GooF	1.023	1.023
$\delta\rho_{\text{max}}$, $\delta\rho_{\text{min}}$ [e·nm ⁻³]	0.521, -0.421	0.548, -0.406

5.5 References

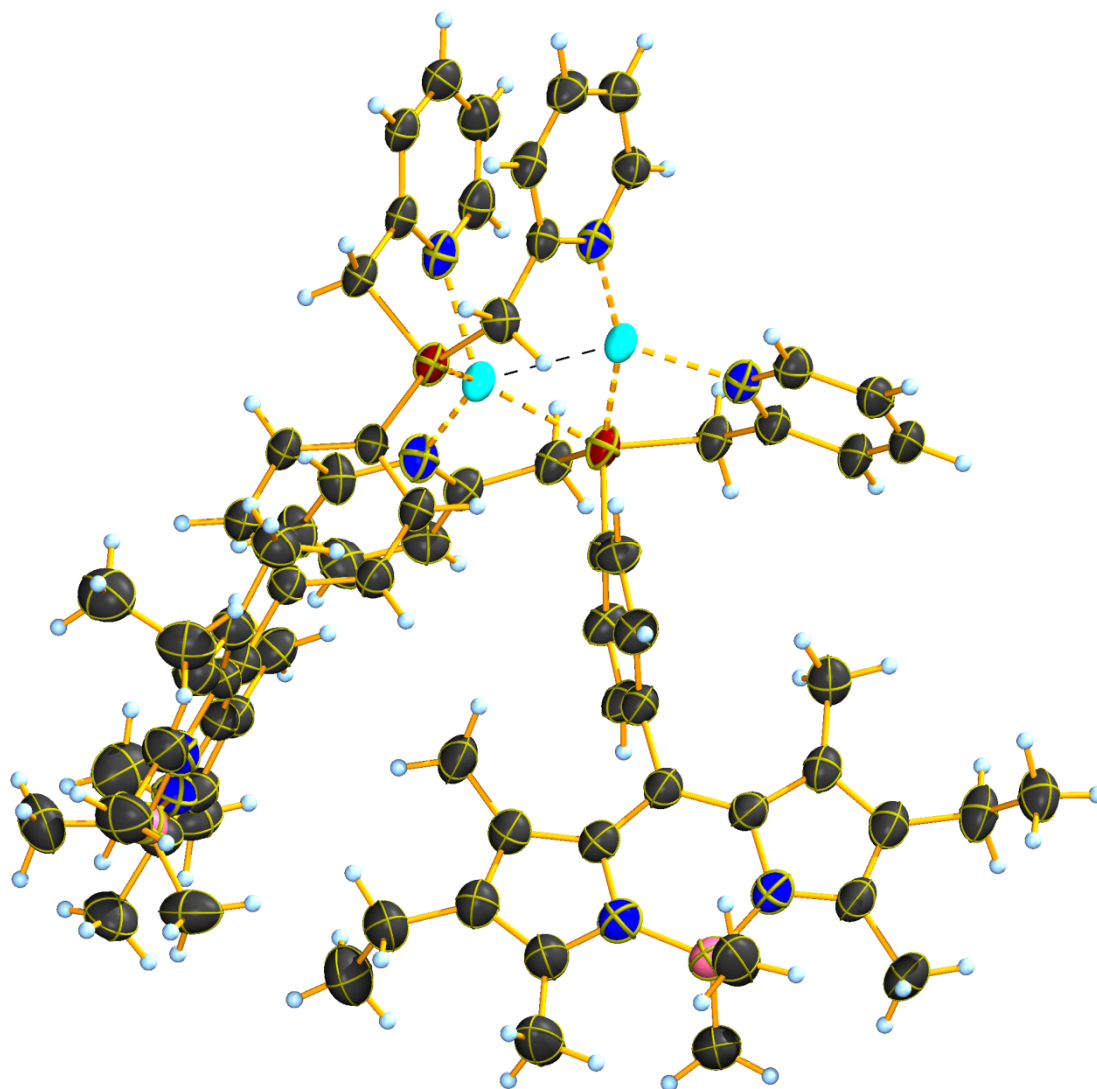
- [1] *Comprehensive Coordination Chemistry*, Vol. 5, 1st ed., Pergamon Books Ltd., Oxford, **1987**.
- [2] a) R. Peng, M. Li, D. Li, *Coord. Chem. Rev.* **2010**, 254, 1-18; b) P. M. Graham, R. D. Pike, M. Sabat, R. D. Bailey, W. T. Pennington, *Inorg. Chem.* **2000**, 39, 5121-5132.
- [3] a) H. L. Hermann, G. Boche, P. Schwerdtfeger, *Chem. Eur. J.* **2001**, 7, 5333-5342; b) W. F. Fu, X. Gan, C. M. Che, Q. Y. Cao, Z. Y. Zhou, N. N. Zhu, *Chem. Eur. J.* **2004**, 10, 2228-2236; c) M.-X. Xie, X. Xu, X.-X. Huang, *Chin. J. Struct. Chem.* **2010**, 29, 668-675; d) P. Pyykkö, *Chem. Rev.* **1997**, 97, 597-636.
- [4] S. Dinda, A. G. Samuelson, *Chem. - Eur. J.* **2012**, 18, 3032-3042.
- [5] a) N. Armaroli, G. Accorsi, F. Cardinali, A. Listorti, in *Photochemistry and Photophysics of Coordination Compounds I* (Eds.: V. Balzani, S. Campagna), Springer Berlin Heidelberg, Berlin, Heidelberg, **2007**, 69-115; b) A. Lavie-Cambot, M. Cantuel, Y. Leydet, G. Jonusauskas, D. Bassani, N. McClenaghan, *Coord. Chem. Rev.* **2008**, 252, 2572-2584; c) K. Tsuge, Y. Chishina, H. Hashiguchi, Y. Sasaki, M. Kato, S. Ishizaka, N. Kitamura, *Coord. Chem. Rev.* **2016**, 306, 636-651; d) V. W.-W. Yam, K. K.-W. Lo, *Comments Inorg. Chem.* **1997**, 19, 209-229; e) P. D. Harvey, M. Knorr, *Macromol. Rapid Commun.* **2010**, 31, 808-826; f) A. A. Karasik, E. I. Musina, I. D. Strelnik, I. R. Dayanova, J. G. Elistratova, A. R. Mustafina, O. G. Sinyashin, *Pure Appl. Chem.* **2019**, 91, 839-849.
- [6] K. Tsuge, *Chem. Lett.* **2013**, 42, 204-208.
- [7] P. D. Harvey, *Macromol. Symp.* **2004**, 209, 81-96.
- [8] A. Kobayashi, M. Kato, *Chem. Lett.* **2017**, 46, 154-162.
- [9] P. C. Ford, E. Cariati, J. Bourassa, *Chem. Rev.* **1999**, 99, 3625-3648.
- [10] B. Valeur, *Molecular Fluorescence: Principles and Applications*, Wiley-VCH, Weinheim, **2002**.
- [11] C. Hettstedt, PhD thesis, Ludwig-Maximilians-Universität München **2015**.
- [12] a) L. Yang, R. P. Houser, *Inorg. Chem.* **2006**, 45, 9416-9422; b) A. Banisafar, R. L. LaDuca, *Inorg. Chim. Acta* **2011**, 373, 295-300; c) J. H. Wang, M. Li, J. Zheng, X. C. Huang, D. Li, *Chem. Commun.* **2014**, 50, 9115-9118; d) Y.-M. Song, Q. Ye, Y.-Z. Tang, Q. Wu, R.-G. Xiong, *Cryst. Growth Des.* **2005**, 5, 1603-1608.
- [13] A. J. C. Wilson, E. Prince, *International Tables for Crystallography, Vol. C Mathematical, physical and chemical tables*, 2nd ed., Kluwer Academic Publishers, Dordrecht/Boston/London, **1999**.
- [14] a) L. Kang, J. Chen, T. Teng, X.-L. Chen, R. Yu, C.-Z. Lu, *Dalton Trans.* **2015**, 44, 11649-11659; b) V. Karthik, V. Gupta, G. Anantharaman, *Organometallics* **2015**, 34, 3713-3720.
- [15] a) J. A. Pino-Chamorro, Y. A. Laricheva, E. Guillaumon, M. J. Fernandez-Trujillo, A. G. Algarra, A. L. Gushchin, P. A. Abramov, E. Bustelo, R. Llusar, M. N. Sokolov, M. G. Basallote, *Inorg. Chem.* **2016**, 55, 9912-9922; b) M. H. Habibi, M. Montazerzohori, K. Barati, R. W. Harrington, W. Clegg, *Acta Crystallogr., Sect. C: Cryst. Struct. Commun.* **2007**, 63, m592-m594; c) D. Aydin-Cantürk, H. Nuss, *Z. Naturforsch. B* **2012**, 67, 759-764; d) L. Kuehn, A. F. Eichhorn, T. B. Marder, U. Radius, *J. Organomet. Chem.* **2019**, 881, 25-33; e) J.-H. Yu, Z.-L. Lü, J.-Q. Xu, H.-Y. Bie, J. Lu, X. Zhang, *New J. Chem.* **2004**, 28, 940-945.
- [16] C. Janiak, *Dalton Trans.* **2000**, 3885-3896.
- [17] a) D. Mendoza-Espinosa, B. Donnadieu, G. Bertrand, *Chem. Asian J.* **2011**, 6, 1099-1103; b) G. A. Bowmaker, J. Wang, R. D. Hart, A. H. White, P. C. Healy, *Dalton Trans.* **1992**, 787-795; c) T. Miyaji, Z. Xi, M. Ogasawara, K. Nakajima, T. Takahashi, *J. Org. Chem.* **2007**, 72, 8737-8740; d) R. J. Davidson, E. W. Ainscough, A. M. Brodie, G. H. Freeman, G. B. Jameson, *Polyhedron* **2016**, 119, 584-589; e) E. W. Ainscough, A. M. Brodie, A. K. Burrell, G. H. Freeman, G. B. Jameson, G. A. Bowmaker, J. V. Hanna, P. C. Healy, *Dalton Trans.* **2001**, 144-151; f) D. H. A. Boom, A. W. Ehlers, M. Nieger, J. C. Slootweg, *Z. Naturforsch. B* **2017**, 72, 781-784; g) M. R. Churchill, F. J. Rotella, *Inorg. Chem.* **2002**, 18, 166-171.

- [18] a) B. Nohra, R. Reau, C. Lescop, *Eur. J. Inorg. Chem.* **2014**, 2014, 1788-1796; b) B. Nohra, E. Rodriguez-Sanz, C. Lescop, R. Reau, *Chem. Eur. J.* **2008**, 14, 3391-3403; c) Y. Yao, W. Shen, B. Nohra, C. Lescop, R. Reau, *Chem. Eur. J.* **2010**, 16, 7143-7163; d) V. Vreshch, B. Nohra, C. Lescop, R. Reau, *Inorg. Chem.* **2013**, 52, 1496-1503; e) V. Vreshch, W. Shen, B. Nohra, S. K. Yip, V. W. Yam, C. Lescop, R. Reau, *Chem. Eur. J.* **2012**, 18, 466-477; f) F. Hung-Low, A. Renz, K. K. Klausmeyer, *Eur. J. Inorg. Chem.* **2009**, 2009, 2994-3002.
- [19] F. Leca, C. Lescop, E. Rodriguez-Sanz, K. Costuas, J. F. Halet, R. Reau, *Angew. Chem. Int. Ed.* **2005**, 44, 4362-4365.
- [20] a) G. A. Bowmaker, J. V. Hanna, S. P. King, F. Marchetti, C. Pettinari, A. Pizzabiocca, B. W. Skelton, A. N. Sobolev, A. Tăbăcaru, A. H. White, *Eur. J. Inorg. Chem.* **2014**, 2014, 6104-6116; b) G. A. Bowmaker, J. V. Hanna, R. D. Hart, P. C. Healy, S. P. King, F. Marchetti, C. Pettinari, B. W. Skelton, A. Tabacaru, A. H. White, *Dalton Trans.* **2012**, 41, 7513-7525; c) C. Pettinari, C. di Nicola, F. Marchetti, R. Pettinari, B. W. Skelton, N. Somers, A. H. White, W. T. Robinson, M. R. Chierotti, R. Gobetto, C. Nervi, *Eur. J. Inorg. Chem.* **2008**, 2008, 1974-1984.
- [21] a) R. Hehl, G. Thiele, *Z. Anorg. Allg. Chem.* **2000**, 626, 2167-2172; b) P. C. Healy, C. Pakawatchai, R. I. Papasergio, V. A. Patrick, A. H. White, *Inorg. Chem.* **1984**, 23, 3769-3776; c) O. A. Babich, V. N. Kokozay, V. A. Pavlenko, *Polyhedron* **1996**, 15, 2727-2731; d) S.-M. Kuang, Z.-Z. Zhang, Q.-G. Wang, T. C. W. Mak, *Dalton Trans.* **1997**, 4477-4478; e) M. Trivedi, G. Singh, A. Kumar, N. P. Rath, *Dalton Trans.* **2013**, 42, 12849-12852; f) L.-L. Li, R.-X. Yuan, L.-L. Liu, Z.-G. Ren, A.-X. Zheng, H.-J. Cheng, H.-X. Li, J.-P. Lang, *Cryst. Growth Des.* **2010**, 10, 1929-1938.
- [22] a) K. M. Miller, S. M. McCullough, E. A. Lepekhina, I. J. Thibau, R. D. Pike, X. Li, J. P. Killarney, H. H. Patterson, *Inorg. Chem.* **2011**, 50, 7239-7249; b) N. W. Aboeella, B. F. Gherman, L. M. R. Hill, J. T. York, N. Holm, V. G. Young, Jr., C. J. Cramer, W. B. Tolman, *J. Am. Chem. Soc.* **2006**, 128, 3445-3458; c) W.-L. Zhang, M. Liu, C.-J. Ma, L.-R. Zhang, Z.-P. Huang, Y.-X. Zai, Q. Yang, Y.-Y. Niu, Y. Liang, *Inorg. Chim. Acta* **2015**, 426, 80-88; d) J. A. Manskaya, V. N. Kokozay, K. V. Domasevitch, *Z. Naturforsch., B: Chem. Sci.* **1997**, 52, 1311-1314; e) S. Pohl, M. Harmjanz, J. Schneider, W. Saak, G. Henkel, *Inorg. Chim. Acta* **2000**, 311, 106-112.
- [23] M. Kabešová, M. Dunaj-jurčo, M. Serator, J. Gažo, J. Garaj, *Inorg. Chim. Acta* **1976**, 17, 161-165.
- [24] a) H. Wang, *Acta Crystallogr., Sect. E: Struct. Rep. Online* **2012**, 68, m95; b) A. M. Prokhorov, P. A. Slepukhin, D. N. Kozhevnikov, *J. Organomet. Chem.* **2008**, 693, 1886-1894; c) L. Lu, *J. Inorg. Biochem.* **2003**, 95, 31-36; d) C. Boldron, S. Özalp-Yaman, P. Gamez, D. M. Tooke, A. L. Spek, J. Reedijk, *Dalton Trans.* **2005**, 3535-3541; e) C. Boldron, P. Gamez, D. M. Tooke, A. L. Spek, J. Reedijk, *Angew. Chem. Int. Ed.* **2005**, 44, 3585-3587.
- [25] a) H. S. Jena, *Inorg. Chim. Acta* **2014**, 410, 156-170; b) A. Biswas, M. G. Drew, C. Diaz, A. Bauza, A. Frontera, A. Ghosh, *Dalton Trans.* **2012**, 41, 12200-12212; c) B. Zheng, H. Liu, J. Feng, J. Zhang, *Appl. Organomet. Chem.* **2014**, 28, 372-378.
- [26] a) J. Suo, *Acta Crystallogr., Sect. E: Struct. Rep. Online* **2008**, 64, m1046; b) C. Chen, Y. Cheng, P. Liu, H. Zhou, Z. Q. Pan, *Acta Crystallogr., Sect. E: Struct. Rep. Online* **2009**, 65, m162.
- [27] S. K. Gupta, C. Anjana, R. J. Butcher, N. Sen, *Acta Crystallogr., Sect. E: Struct. Rep. Online* **2010**, 66, m1531-1532.
- [28] a) J. S. Haynes, K. W. Oliver, S. J. Rettig, R. C. Thompson, J. Trotter, *Can. J. Chem.* **1984**, 62, 891-898; b) K. W. Oliver, S. J. Rettig, R. C. Thompson, J. Trotter, *Can. J. Chem.* **1982**, 60, 2017-2022; c) K. W. Oliver, S. J. Rettig, R. C. Thompson, J. Trotter, S. Xia, *Inorg. Chem.* **1997**, 36, 2465-2468; d) J. Rohovec, I. Lukes, P. Vojtisek, I. Cisarova, P. Hermann, *Dalton Trans.* **1996**, 2685-2691.
- [29] a) B. E. Fischer, R. Bau, *Inorg. Chem.* **2002**, 17, 27-34; b) Q.-H. Zhao, L. Du, R.-B. Fang, *Acta Crystallogr., Sect. E: Struct. Rep. Online* **2006**, 62, m219-m221; c) K. Aoki, *J. Am. Chem. Soc.* **1978**, 100, 7106-7108; d) K. Aoki, *Chem. Commun.* **1979**, 589-591; e) M. Kato, A. K. Sah, T. Tanase, M. Mikuriya, *Eur. J. Inorg. Chem.* **2006**, 2006, 2504-2513; f) R. Murugavel, S.

- Kuppuswamy, A. N. Maity, M. P. Singh, *Inorg. Chem.* **2009**, *48*, 183-192; g) V. Chandrasekhar, T. Senapati, R. Clérac, *Eur. J. Inorg. Chem.* **2009**, *2009*, 1640-1646.
- [30] E. Kövári, R. Krämer, *J. Am. Chem. Soc.* **1996**, *118*, 12704-12709.
- [31] C.-Y. Wei, B. E. Fischer, R. Bau, *Chem. Commun.* **1978**, 1053-1055.
- [32] M. J. Frisch, G. W. Trucks, H. B. Schlegel, G. E. Scuseria, M. A. Robb, J. R. Cheeseman, G. Scalmani, V. Barone, G. A. Petersson, H. Nakatsuji, X. Li, M. Caricato, A. V. Marenich, J. Bloino, B. G. Janesko, R. Gomperts, B. Mennucci, H. P. Hratchian, J. V. Ortiz, A. F. Izmaylov, J. L. Sonnenberg, D. Williams-Young, F. Ding, F. Lipparini, F. Egidi, J. Goings, B. Peng, A. Petrone, T. Henderson, D. Ranasinghe, V. G. Zakrzewski, J. Gao, N. Rega, G. Zheng, W. Liang, M. Hada, M. Ehara, K. Toyota, R. Fukuda, J. Hasegawa, M. Ishida, T. Nakajima, Y. Honda, O. Kitao, H. Nakai, T. Vreven, K. Throssell, J. Montgomery, J. A., J. E. Peralta, F. Ogliaro, M. J. Bearpark, J. J. Heyd, E. N. Brothers, K. N. Kudin, V. N. Staroverov, T. A. Keith, R. Kobayashi, J. Normand, K. Raghavachari, A. P. Rendell, J. C. Burant, S. S. Iyengar, J. Tomasi, M. Cossi, J. M. Millam, M. Klene, C. Adamo, R. Cammi, J. W. Ochterski, R. L. Martin, K. Morokuma, O. Farkas, J. B. Foresman, D. J. Fox, Gaussian 16, Revision A.03 ed., Gaussian, Inc., Wallingford CT, **2016**.

Chapter 6

Transition metal complexes of fluorescent P,N ligands based on Bodipy



Parts of this chapter have been published in
S. Linert, S. Wagner, P. Schmidt, L. Higham, C. Hepples, P. Waddell, K. Karaghiosoff
Phosphorus Sulfur, **2019**, 194, 565–568.

6.1 Introduction

6.1.1 Bodipy

Bodipy (4,4-difluoro-4-bora-3a,4a-diaza-s-indacene) dyes are some of the most versatile fluorophores available (Figure 1).^[1] This is due to a number of desirable properties of these compounds, including (i) a strong UV absorption profile, (ii) a sharp fluorescence emission peak, (iii) high quantum yields, (iv) negligible triplet state formation, (v) high thermal and photochemical stability, (vi) chemical robustness and (vii) good solubility.^[2]

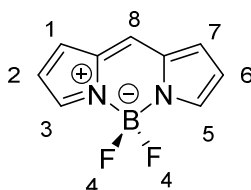
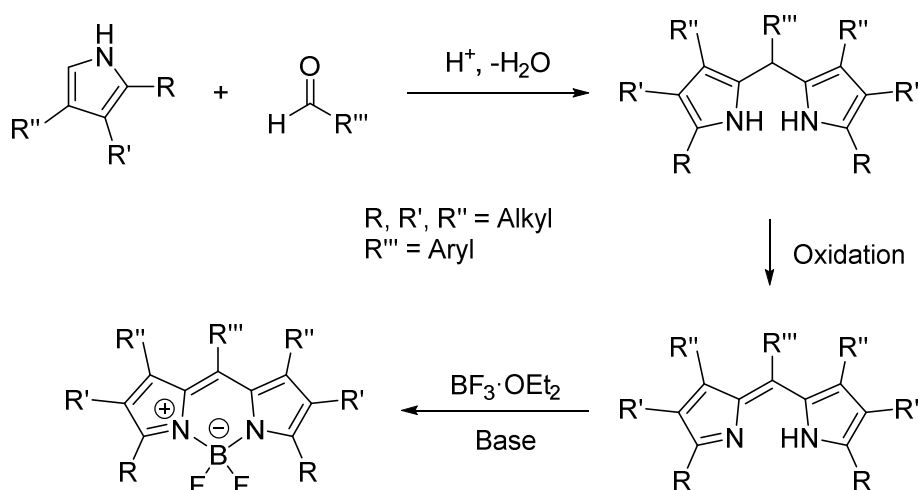


Figure 1: Bodipy: 4,4-difluoro-4-bora-3a,4a-diaza-s-indacene.

Bodipy dyes were first discovered by A. Treibs and F. Kreuzer in 1968^[3] and since then they have been investigated for different applications, such as biomolecular labels, drug delivery agents, cation sensors, fluorescent switches, laser dyes, electroluminescent films and sensitizers for solar cells.^[2] The properties of Bodipy dyes can strongly be influenced by minor changes to the structure of Bodipy.^[4]

Symmetrical Bodipy derivatives are usually synthesised by a condensation reaction, starting from a pyrrole compound and an electrophilic carbonyl derivative. Subsequently the compound is oxidised and finally the structure is closed by addition of boron trifluoride diethyl etherate (Scheme 1).^[1]



Scheme 1: General synthesis of symmetrical Bodipy derivatives.

Commonly additional substituents are attached to C8, which is also called the *meso* position. Using the synthetic route described above it is very easy to introduce aryl or alkyl substituents at the *meso* position. Modifications at this position have very little effect on the absorption and emission wavelengths.^[4-5] On the contrary substitution at the positions 1 and 7 has a large effect on the quantum yield, because this prevents free rotation of the *meso* substituent.^[5]

The fluorine atoms at boron can be substituted with aryl or alkyl groups by use of organolithium or *Grignard* reagents.^[1]

6.1.2 Metal complexes of Bodipy derivatives

In the literature many Bodipy derivatives are described, which have substituents with additional heteroatoms that are able to coordinate metals.

A possible application of complexes of Bodipy derivatives is in catalysis. Complex **B1** (Figure 2) can be used as a redox switchable catalyst for hydroborations of alkenes.^[6] Another example of a catalytically active complex based on Bodipy is compound **B2** (Figure 3), which can be applied for *Sonogashira* C–C cross-coupling reactions.^[7]

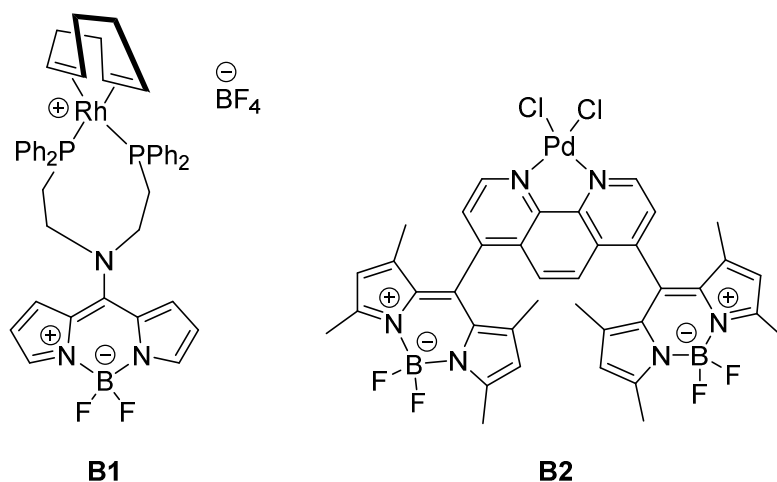


Figure 2: Complexes **B1** and **B2** used as catalysts.^[6-7]

Due to their fluorescent properties complexes of Bodipy derivatives also are of interest for applications in bioimaging.^[8] A number of complexes also shows cytotoxic properties, which makes them of interest not only for cell imaging, but also as potential anti-cancer agents.^[8a, 9]

In many cases the coordination of the substituents has a strong influence on the fluorescence properties of the Bodipy moiety. Therefore some Bodipy derivatives can be used as fluorescent sensors for the detection of metal ions, such as Yb,^[10] Zn,^[11] Cu,^[12] Hg,^[12-13] and Ag.^[14] The antimony complex **B3** (Figure 3) can bind anions, such as fluoride, cyanide and azide, in organic solvents and the binding is accompanied by a change of fluorescence.^[15] This makes the complex suitable for application as an anion sensor.^[15] Other complexes can be used to detect small molecules, such as CO (**B4**)^[16] or ethylene (**B5**) (Figure 3).^[17] The mechanism of the detection of these molecules is based on the fact that the complexes show weak or no fluorescence due to heavy atom quenching. After reaction with the molecule to detect the ligand is no longer coordinated to the metal and therefore the fluorescence significantly increases.^[16-17]

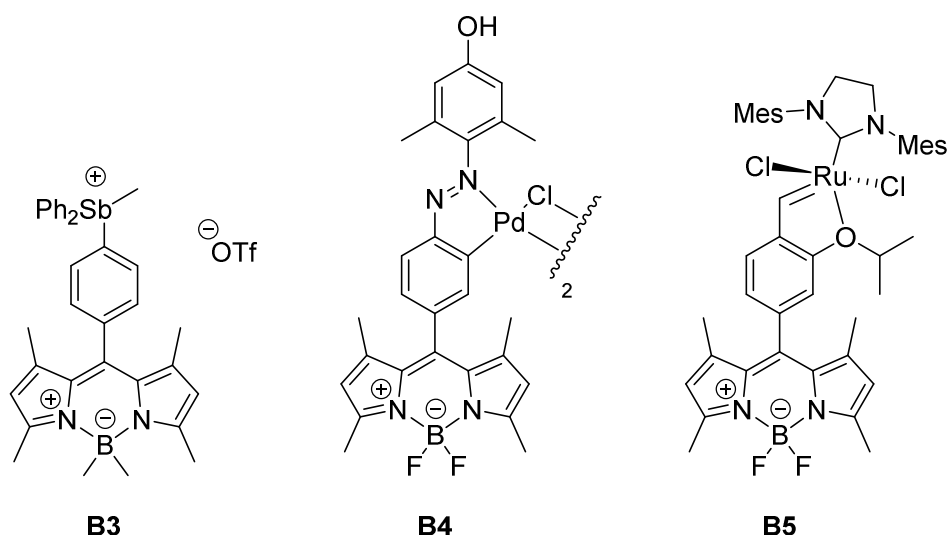


Figure 3: Complexes **B3**, **B4** and **B5** used as sensors for anions or small molecules.^[15-17]

Also it is possible in some cases to monitor ligand exchange reactions via fluorescence changes upon changes of electron density at the metal centre.^[18]

As the fluorescence of the Bodipy moiety is influenced by the coordination situation of the attached complex, this raises the question, which luminescent properties a compound containing both the Bodipy moiety and a luminescent complex would have.

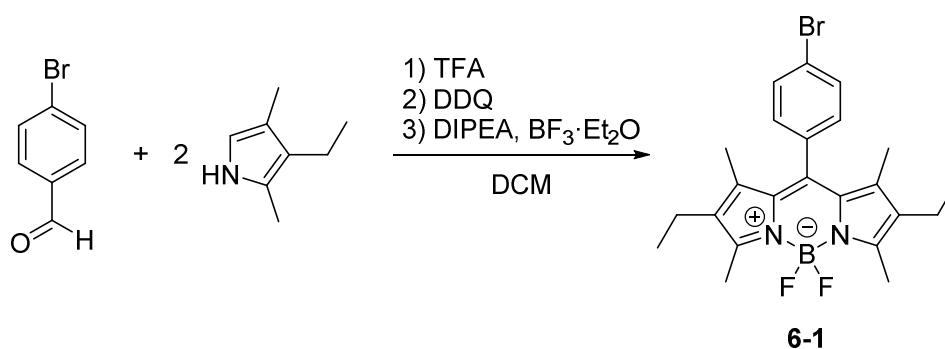
6.2 Results and discussion

6.2.1 Synthesis of primary phosphine 6-5

The air-stable primary phosphine 2,8-diethyl-1,3,5,5,7,9-hexamethyl-10-(4-phosphanylphenyl)-5*H*-4λ⁴,5λ⁴-dipyrrolo[1,2-*c*:2',1'-*f*][1,3,2]diazaborinine **6-5** was first synthesised in the research group of *L. Higham*.^[19] By substitution of the hydrogen atoms at phosphorus a variety of organic moieties can be introduced to the molecule.

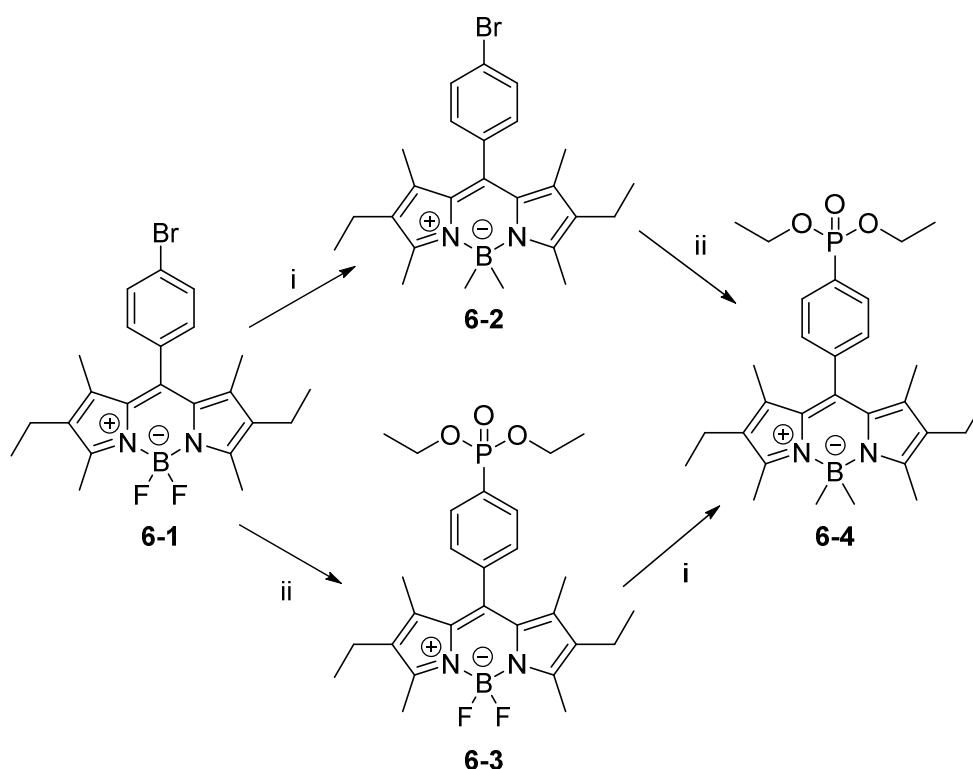
6-5 was used as a precursor for the synthesis of the desired ligands **6-6** and **6-9**. The synthesis was carried out in four steps according to the procedures described by *L. H. Davies et al.*, starting from 4-bromobenzaldehyde and 2,4-dimethyl-3-ethylpyrrole.^[20]

The first step was the condensation of 4-bromobenzaldehyde with 2,4-dimethyl-3-ethylpyrrole, followed by oxidation of the product with 2,3-Dicyano-5,6-dichloroparabenzoquinone (DDQ). Afterwards BF₃·Et₂O was added to form the Bodipy moiety of 10-(4-bromophenyl)-2,8-diethyl-5,5-difluoro-1,3,7,9-tetramethyl-5*H*-4λ⁴,5λ⁴-dipyrrolo[1,2-*c*:2',1'-*f*][1,3,2]diazaborinine **6-1** (Scheme 2).



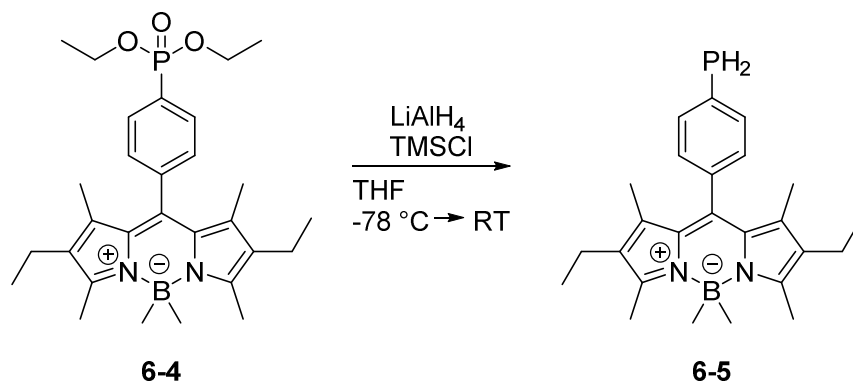
Scheme 2: Synthesis of 10-(4-bromophenyl)-2,8-diethyl-5,5-difluoro-1,3,7,9-tetramethyl-5H-4 λ^4 ,5 λ^4 -dipyrrolo[1,2-c:2',1'-f][1,3,2]diazaborinine **6-1**.

In the next two steps the fluorine substituents on the boron were replaced with methyl groups and the bromine on the phenyl ring was substituted with a diethoxy phosphonate group to obtain diethyl (4-(2,8-diethyl-1,3,5,5,7,9-hexamethyl-5H-4 λ^4 ,5 λ^4 -dipyrrolo[1,2-c:2',1'-f][1,3,2]diazaborinin-10-yl)phenyl)phosphonate **6-4**. The methylation was carried out by a *Grignard* reaction with methyl magnesium bromide and for the phosphonylation a palladium catalysed cross coupling reaction with diethyl phosphite was used. These two steps can be performed in both orders: first the methylation and afterwards the phosphonylation or *vice versa* round (Scheme 3). Both sequences have been described by *L. H. Davies et al.* and they have found, that higher yields can be obtained when compound **6-1** is phosphonylated first and diethyl (4-(2,8-diethyl-5,5-difluoro-1,3,7,9-tetramethyl-5H-4 λ^4 ,5 λ^4 -dipyrrolo[1,2-c:2',1'-f][1,3,2]diazaborinin-10-yl)phenyl)phosphonate **6-3** methylated afterwards.^[20] Both reaction pathways were tested and the previous results were confirmed.



Scheme 3: Synthesis of diethyl (4-(2,8-diethyl-1,3,5,5,7,9-hexamethyl-5H-4 λ^4 ,5 λ^4 -dipyrrolo[1,2-c:2',1'-f][1,3,2]diazaborinin-10-yl)phenyl)phosphonate **6-4**. i: MeLi, THF, RT. ii: HP(O)OEt₂, Pd(OAc)₂, DPPB, DMSO, 90°C.

Finally the phosphonate was reduced with LiAlH_4 to obtain the primary phosphine **6-5**. Therefore lithium aluminium hydride was activated with TMSCl and subsequently a solution of **6-4** in THF was added at -78°C (Scheme 4).



Scheme 4: Synthesis of 2,8-diethyl-1,3,5,5,7,9-hexamethyl-10-(4-phosphanylphenyl)-5*H*-4 λ^4 ,5 λ^4 -dipyrrolo[1,2-*c*:2',1'-*f*][1,3,2]diazaborinine **6-5**.

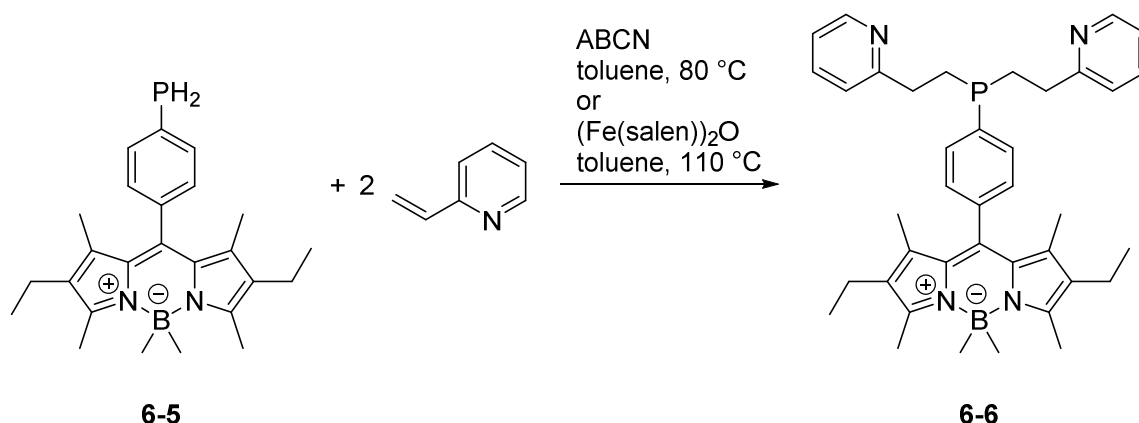
Primary phosphine **6-5** was obtained as an orange solid with an overall yield of 18%.

6.2.2 Synthesis of the P,N ligands

10-(4-(bis(2-(pyridin-2-yl)ethyl)phosphanyl)phenyl)-2,8-diethyl-1,3,5,5,7,9-hexamethyl-5*H*-4 λ^4 ,5 λ^4 -dipyrrolo[1,2-*c*:2',1'-*f*][1,3,2]diazaborinine **6-6** was synthesised via hydrophosphination of 2-vinylpyridine with **6-5**. This reaction has been performed in the research group of *L. Higham* before applying different methods. Experiments were performed as a radical reaction with 1,1'-azobis(cyclohexane-carbonitrile) (ABCN) and with a Pt catalyst, but both reaction pathways afforded only moderate yields and needed reaction times of several days.^[21]

First the reaction was performed according to the procedure described before in the research group of *L. Higham*.^[21] Primary phosphine **6-5** was allowed to react with 2-vinyl pyridine in a radical reaction, using ABCN as radical starter. After three days the ^{31}P NMR showed that no starting material was present in the reaction mixture. The solvent was removed and the crude product was purified by column chromatography. From this reaction the desired product was obtained in a low yield of 28%.

Therefore an iron catalyst for this reaction was tested. The reaction was performed according to the procedure described by *K. Gallagher et al.* who used the catalyst $(\text{Fe}(\text{salen}))_2\text{O}$ for similar reactions (Scheme 5).^[22]



Scheme 5: Synthesis of 10-(4-(bis(2-(pyridin-2-yl)ethyl)phosphanyl)phenyl)-2,8-diethyl-1,3,5,5,7,9-hexamethyl-5*H*-4 λ^4 ,5 λ^4 -dipyrrolo[1,2-*c*:2',1'-*f*][1,3,2]diazaborinine **6-6**.

The reaction was first tested in THF at 40°C, but no conversion of the starting material was observed in the ^{31}P NMR spectrum of the reaction solution. Increase of the reaction temperature to 60°C led to a slow reaction, but after four days only 9% of the used primary phosphine had reacted to the intermediate secondary phosphine, in which one of the hydrogen atoms is replaced by the $(\text{CH}_2)_2\text{py}$ group. Therefore the solvent was changed to toluene and the reaction was heated to 110°C.

The progress of the reaction was monitored with ^{31}P NMR spectroscopy. After one day the NMR spectrum showed a large signal at -124 ppm, which is caused by unreacted starting material **6-5** and a small signal at -51 ppm, which can be assigned to the corresponding secondary phosphine (Figure 4). After a reaction time of four days the ^{31}P NMR spectrum showed, that no **6-5** was left in the reaction mixture, but a mixture of the secondary phosphine and the desired product **6-6** was present. After an overall reaction time of eleven days the ^{31}P NMR spectrum of the reaction mixture showed complete conversion of the primary phosphine and the intermediate secondary phosphine to **6-6**.

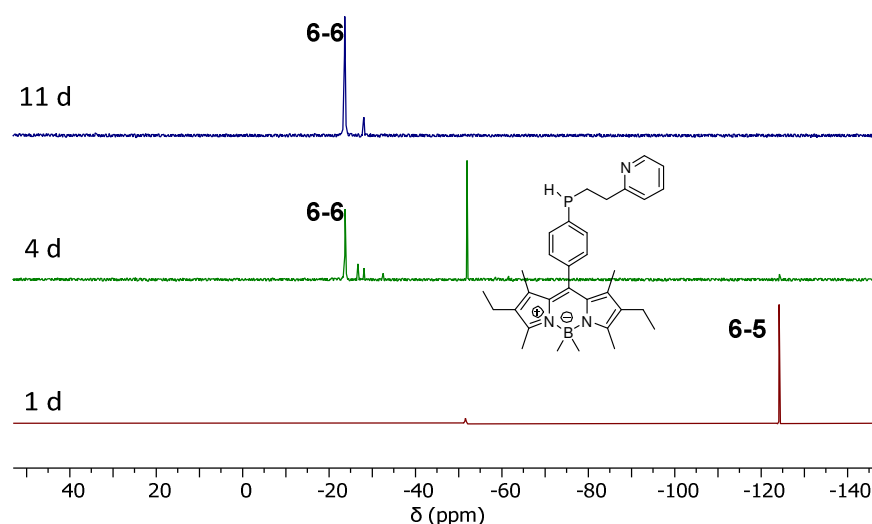


Figure 4: ^{31}P NMR spectra of the reaction to form **6-6** with iron catalyst $(\text{Fe}(\text{salen}))_2\text{O}$ in toluene.

After removal of the solvent under vacuum and column chromatography the product was obtained in 66% yield. Ligand **6-6** is air-sensitive and easily oxidised to the corresponding phosphine oxide **6-7** (Figure 5).

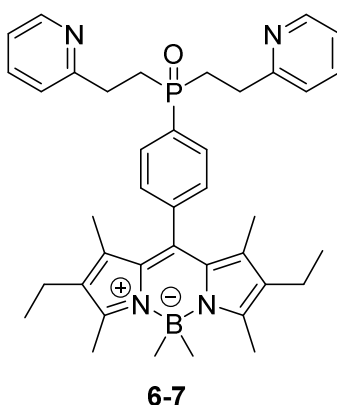
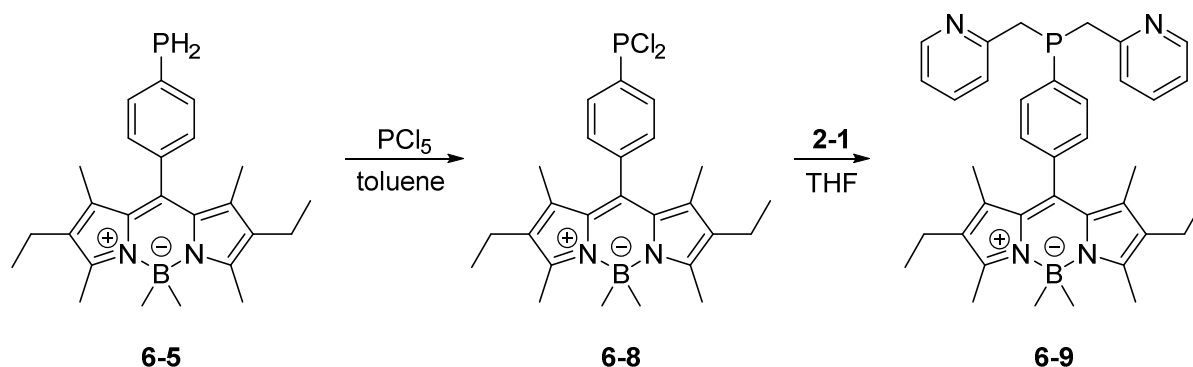


Figure 5: Oxide of ligand **6-6** (4-(2,8-diethyl-1,3,5,5,7,9-hexamethyl-5*H*-4 λ^4 ,5 λ^4 -dipyrrolo[1,2-*c*:2',1'-*f*][1,3,2]diazaborinin-10-yl)phenyl)bis(2-(pyridin-2-yl)ethyl)phosphine oxide **6-7**.

10-(4-(bis(pyridin-2-ylmethyl)phosphanyl)phenyl)-2,8-diethyl-1,3,5,5,7,9-hexamethyl-5*H*-4 λ^4 ,5 λ^4 -dipyrrolo[1,2-*c*:2',1'-*f*][1,3,2]diazaborinine **6-9** was synthesised from **6-5** in a two-step reaction. First the primary phosphine was allowed to react with PCl_5 in toluene to obtain the corresponding dichlorophosphine **6-8** according to the procedure described by *J. Wallis*.^[23] After the solvent was removed *in vacuo* THF was added and **6-8** was allowed to react with two equivalents of **2-1** as described by *C. Hettstedt* to afford ligand **6-9** (Scheme 6).^[24]



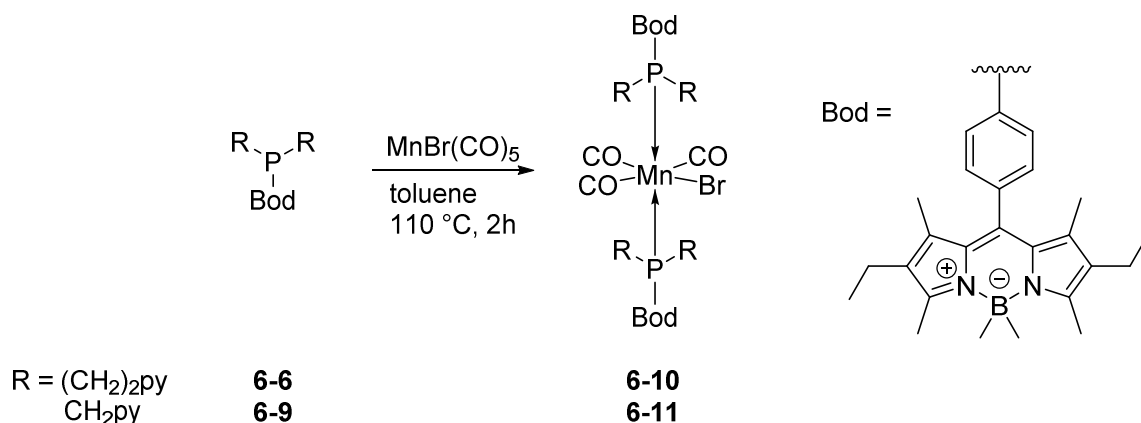
Scheme 6: Synthesis of 10-(4-(bis(pyridin-2-ylmethyl)phosphanyl)phenyl)-2,8-diethyl-1,3,5,5,7,9-hexamethyl-5*H*-4 λ^4 ,5 λ^4 -dipyrrolo[1,2-*c*:2',1'-*f*][1,3,2]diazaborinine **6-9**.

After removal of the solvent under vacuum the product was purified by column chromatography on silica gel. This procedure afforded the desired product in good yields of 69% to 87%.

6.2.3 Transition metal complexes

6.2.3.1 Manganese complexes

To form the manganese complexes **6-10** and **6-11** the corresponding P,N ligands were allowed to react with $\text{MnBr}(\text{CO})_5$ for 2 h at 110°C in toluene (Scheme 7) according to a procedure developed in the research group of *L. Higham*.^[25]



Scheme 7: Synthetic route towards complexes **6-10** and **6-11**.

Previous experiments in the research group of *L. Higham* to synthesise a P,N coordinated manganese complex of **6-6** have shown, that in the resulting complex two molecules of CO coordinating to the manganese atom are replaced with the phosphorus atoms of two molecules of **6-6** to form **6-10**.^[25a] Therefore the reaction of **6-6** with $\text{MnBr}(\text{CO})_5$ was performed in a metal to ligand ratio of 1:2.

The product that was obtained from this reaction was analysed by NMR and IR spectroscopy. The chemical shift of the signal in the ^{31}P NMR spectrum is 34.2 ppm, which corresponds with the signal of the phosphine oxide of the ligand **6-7**. Due to the presence of the paramagnetic manganese the ^1H NMR spectrum showed only a few broad signals, which could not be assigned.

Single crystals suitable for X-ray structure analysis were obtained. Although the crystals were of very poor quality their identity was determined as the phosphine oxide **6-7**.

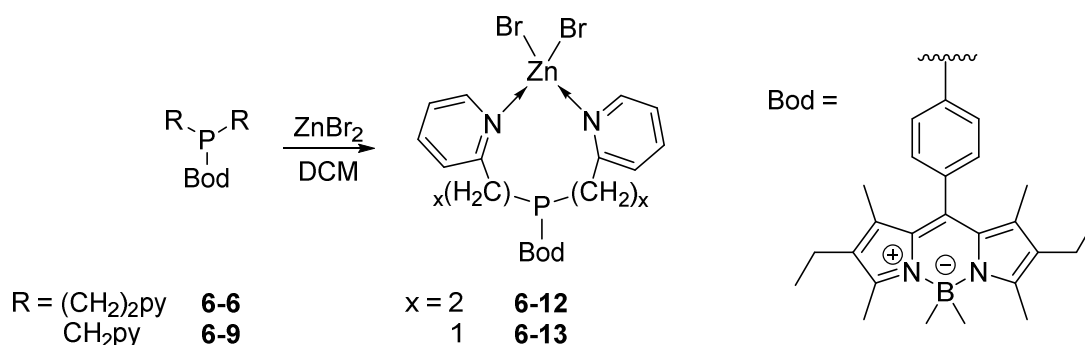
As no previous results of the coordination behaviour of **6-9** to $\text{MnBr}(\text{CO})_5$ were available these two compounds were allowed to react in a 1:1 ratio. Due to the shorter spacer between the phosphorus atom and the pyridine ring in **6-9** compared to **6-6** in complex **6-11** P,N coordination of the ligand to the manganese might also be possible. To find out in which way the metal is coordinated by **6-9** it would be necessary to determine the crystal structure. Unfortunately no single crystals suitable for X-ray crystallography of **6-11** could be obtained.

In the ^{31}P NMR spectrum of the product a signal at 72.0 ppm was observed, which indicates that most probably phosphorus is coordinating to manganese. The ^1H NMR spectrum again showed only broad signals, which could not be assigned.

In the IR spectrum absorption bands at 1930.5 cm^{-1} and 2027.6 cm^{-1} confirm the presence of a coordinated CO molecule in the sample.

6.2.3.2 Zinc complexes

To form the zinc bromide complexes **6-12** and **6-13** the corresponding P,N ligands were allowed to react with ZnBr_2 in DCM at room temperature (Scheme 8).



Scheme 8: Synthetic route towards complexes **6-12** and **6-13**.

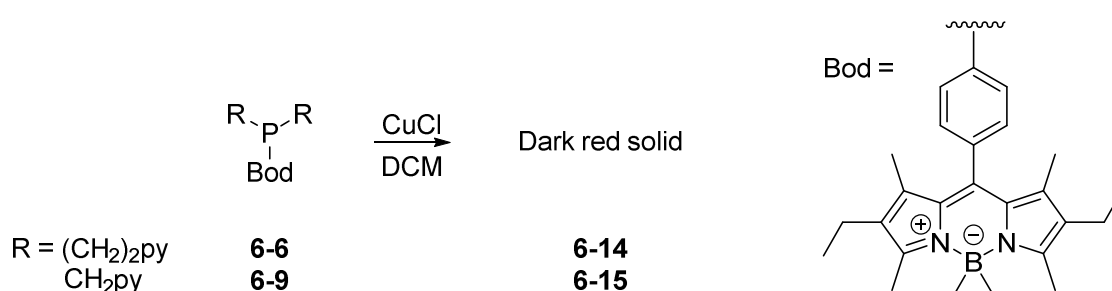
The ^{31}P NMR signals of **6-12** and **6-13** are shifted 3.6 ppm and 0.1 ppm respectively towards lower field compared to the signal of the free ligand.

Ligand **6-9** has a very similar structure to **2-13**. The only difference is the Bodipy moiety in *para* position at the phenyl ring that is present in **6-9**. Therefore similar coordination behaviour as of **2-13** might be expected for **6-9**. Upon coordination of **2-13** to zinc chloride a low field shift of the ^{31}P NMR signal compared to the signal of the free ligand of 3.4 ppm was observed (see 4.2.2), which is very similar to the shift of the signal found for **6-13**. This indicates that in complex **6-13** the zinc is probably coordinated by the nitrogen atoms of the pyridine rings, without any interaction with the phosphorus atom. This was confirmed by single crystal X-ray diffraction (see 6.2.5.1).

As the effect of the reaction of **6-6** with zinc bromide on the chemical shift of the ^{31}P NMR signal is very small, it can be assumed that in compound **6-12** also no coordination of phosphorus to zinc is present.

6.2.3.3 Copper complexes

To form the copper chloride complexes **6-14** and **6-15** the corresponding P,N ligands were allowed to react with CuCl in DCM at room temperature (Scheme 9).



Scheme 9: Synthetic route towards complexes **6-14** and **6-15**.

From both reactions dark red solids were obtained. In solution both compounds showed green luminescence, but had lower quantum yields than the pure phosphine ligands.

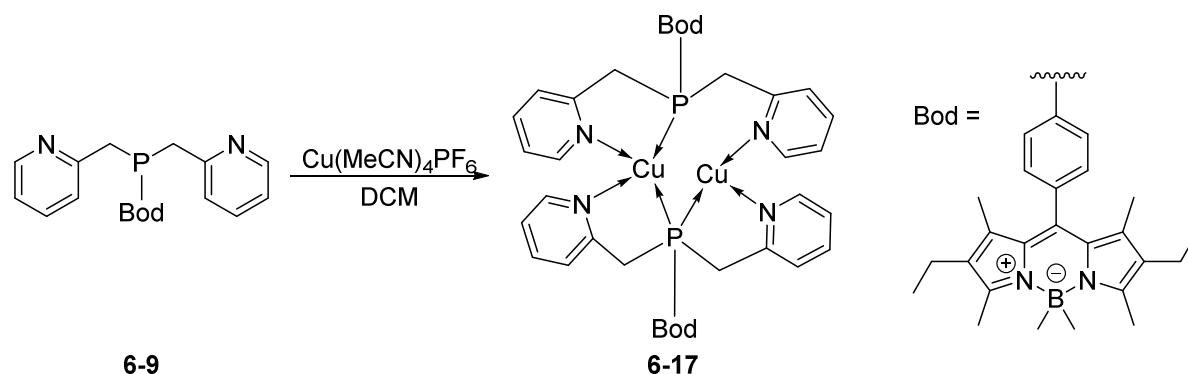
In the ^{31}P NMR spectrum of the product of the reaction to produce **6-14** a large signal at 41.0 ppm could be observed, which indicates oxidation of the ligand.

From a NMR sample of the product of the reaction to form **6-15** single crystals suitable for X-ray diffraction were obtained. The crystals were of very poor quality, but it was possible to identify the compound as the oxide of the phosphine ligand **6-9**. The ^{31}P NMR spectrum of this NMR sample showed a large, broad signal at -10.8 ppm and a small signal at 34.6 ppm. The large signal is

probably caused either by non-oxidised ligand that did not react with the copper chloride or by complex **6-15**, while the small signal is caused by the phosphine oxide.

No crystals suitable for X-ray single crystal structure analysis of the desired complexes **6-14** and **6-15** could be obtained.

To form the copper hexafluorophosphate complexes **6-16** and **6-17** the corresponding P,N ligands were allowed to react with $\text{Cu}(\text{MeCN})_4\text{PF}_6$ in DCM at room temperature (Scheme 10).



Scheme 10: Synthetic route towards complex **6-17**.

The ^{31}P NMR spectrum of the product of the reaction to obtain **6-16** showed a septet at -144.5 ppm, which is caused by the hexafluorophosphate anion and a broad signal at 40.5 ppm, which can be assigned to phosphine oxide **6-7**. This means that again during the reaction the ligand was oxidised.

The ^{31}P NMR spectrum of the product of the reaction to synthesise **6-17** showed the signal of the anion, two signals at 36.9 ppm and 39.5 ppm that might be caused by the oxidised ligand and its copper complex and a signal at -16.6 ppm that is probably caused by the desired complex **6-17**.

No statements about the coordination behaviour of **6-6** towards $\text{Cu}(\text{I})$ can be made. However, X-ray diffraction on single crystals of **6-17** showed the coordination depicted in Scheme 10 (see 6.2.5.2). a similar coordination of the ligand might be assumed in **6-16**.

6.2.4 Photophysical data

Due to the Bodipy moiety the literature known compounds **6-1–6-5** show green fluorescence under UV light.^[20, 26]

The Bodipy based ligands **6-6** and **6-9** and all synthesised complexes of these two ligands also show green fluorescence under UV light in solution. In the solid state no luminescence could be observed for these compounds. In Table 1 the photophysical data of compounds **6-5–6-7**, **6-9**, **6-13** and **6-17** are listed.

Table 1: Maximum absorption and fluorescence emission wavelengths and fluorescence quantum yields of compounds **6-5–6-7**, **6-9**, **6-13** and **6-17** in THF at room temperature.

Compound	λ_{abs}	λ_{em}	Φ_{F}
6-5	512.5	527.5	0.28
6-6	513 ^[25]	527 ^[25]	0.35 ^[25]
6-7	513	529	0.29
6-9	513	528.5	0.33
6-13	513	530.5	0.30
6-17	513.5	529	0.20

The absorption maxima of all compounds are at 512.5–513.5 nm, which is typical for Bodipy based fluorescent materials. The emission maxima are also in the range of Bodipy caused luminescence between 527 nm and 530.5 nm.

The quantum yields of the P,N ligands **6-6** (0.35) and **6-9** (0.33) are slightly higher than that of primary phosphine **6-5** (0.28). Phosphine oxide **6-7** (0.29) has a quantum yield, which is comparable to the quantum yield of **6-5**.

Complexation of ligand **6-9** decreases the quantum yields. The quantum yield of zinc complex **6-13** (0.30) is only slightly lower than the quantum yield of **6-9**, while the quantum yield of **6-17** (0.20) is significantly lower.

The absorption and emission spectra of **6-9**, **6-13** and **6-17** are shown in Figure 6.

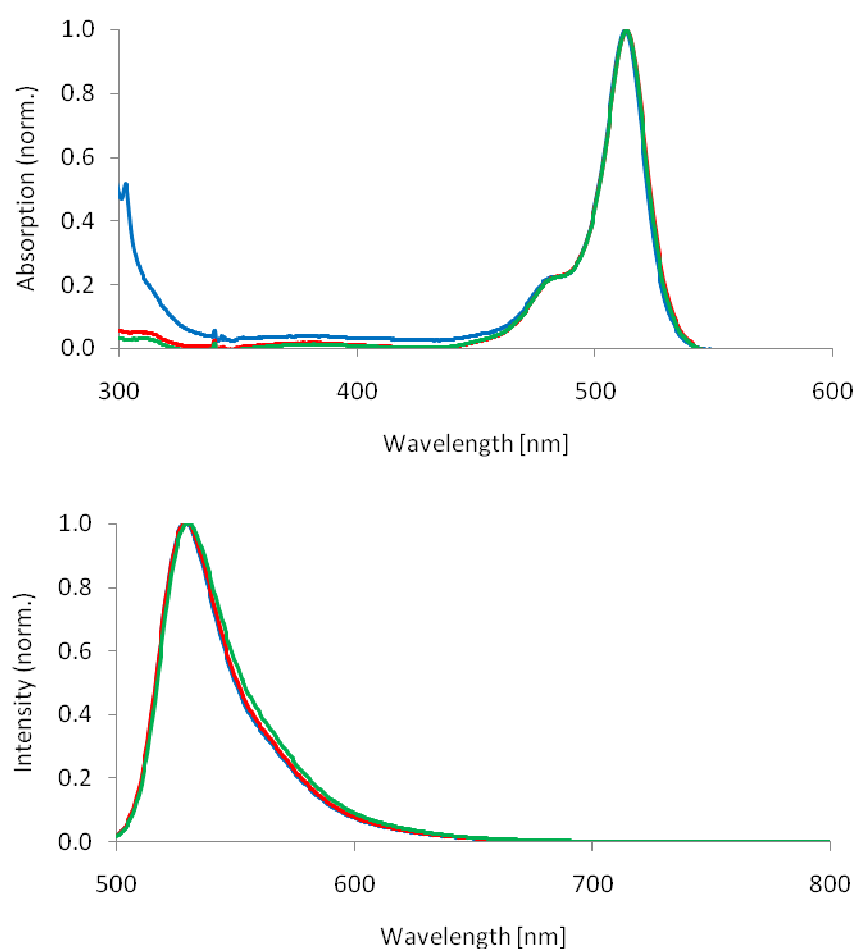


Figure 6: Absorption (top) and fluorescence emission (bottom) spectra of **6-9** (blue), **6-13** (green) and **6-17** (red) in THF at RT.

6.2.5 Crystal structures

6.2.5.1 Crystal structure of **6-13**

Single crystals of **6-13** suitable for X-ray crystallography were obtained by slow diffusion of Et₂O in a solution in DCM.

The complex crystallises in the triclinic space group $P\bar{1}$ with four formula units in the unit cell. The asymmetric unit comprises two molecules of **6-13** and three molecules of DCM. The molecular structure is shown in Figure 7.

The zinc atoms are coordinated tetrahedrally by the nitrogen atoms of the two picolyl groups of the ligand and two bromide anions. The bromine atoms Br3 and Br4 at Zn2 are disordered.

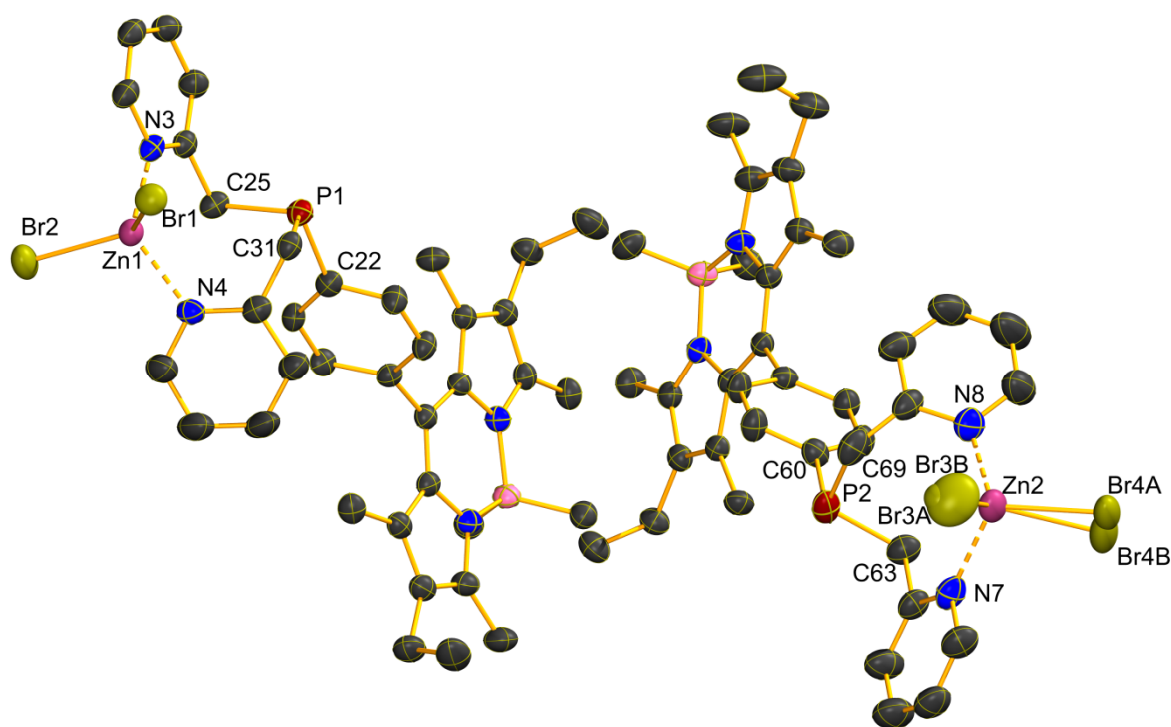


Figure 7: Asymmetric unit of **6-13**. Thermal ellipsoids are drawn at 50% probability level. H atoms and solvent molecules have been omitted for clarity. Selected bond lengths [Å] and angles [°]: Zn1–N3: 2.064(4), Zn1–N4: 2.054(4), Zn1–Br1: 2.390(1), Zn1–Br2: 2.351(1), Zn2–N7: 2.081(5), Zn2–N8: 2.065(5), Zn2–Br3A: 2.417(3), Zn2–Br3B: 2.281(7), Zn2–Br4A: 2.347(3), Zn2–Br4B: 2.390(4), P1–C22: 1.835(5), P1–C25: 1.856(5), P1–C31: 1.864(5), P2–C60: 1.837(5), P2–C63: 1.859(6), P2–C69: 1.871(7), Br1–Zn1–Br2: 119.1(1), Br1–Zn1–N3: 101.9(1), Br1–Zn1–N4: 105.0(1), Br2–Zn1–N3: 105.6(1), Br2–Zn1–N4: 107.9(1), N3–Zn1–N4: 117.9(2), Br3A–Zn2–Br4A: 114.8(1), Br3A–Zn2–Br4B: 127.6(1), Br3A–Zn2–N7: 98.4(2), Br3A–Zn2–N8: 110.2(2), Br3B–Zn2–Br4A: 109.8(2), Br3B–Zn2–Br4B: 122.7(2), Br3B–Zn2–N7: 101.0(2), Br3B–Zn2–N8: 112.5(3), Br4A–Zn2–N7: 111.5(1), Br4A–Zn2–N8: 106.8(2), Br4B–Zn2–N7: 97.7(2), Br4B–Zn2–N8: 107.1(2), N7–Zn2–N8: 115.1(2), C22–P1–C25: 102.3(2), C22–P1–C31: 102.7(2), C25–P1–C31: 102.4(2), C60–P2–C63: 102.3(2), C60–P2–C69: 101.5(3), C63–P2–C69: 102.0(3).

There are no zinc bromide complexes of bis(picolyl)phosphines described in the literature, but the coordination of **6-9** to zinc is the same as found in **4-1** (see 4.2.4) and the bis(picolyl)phosphine zinc chloride complexes of *C. Hettstedt*.^[27]

The Zn–N distances of 2.054(4)–2.082(1) Å are close to the average Zn–N distance of 2.064 Å of pyridine ligands in complexes with four-coordinate zinc atoms.^[28] The Zn–N distances of **6-13** are also in the same range as those of the known bis(picolyl)phosphine zinc chloride complexes.^[27]

The average Zn–Br distance in complexes with four-coordinate zinc atoms is 2.386 Å.^[28] The Zn1–Br2 distance (2.351(1) Å) and the average Zn2–Br distances (2.369 Å for Br3 and 2.349 Å for Br4) are slightly shorter than this value, while the Zn1–Br1 distance (2.390(1) Å) is slightly longer. This means that the Zn–Br distances found in the structure of **6-13** are in a range, which is typical for the involved atoms.

The P–C_{Ar} distances (1.835(5) Å and 1.837(5) Å) are slightly longer than those found in the structure of triphenylphosphine (1.822(5)–1.831(5) Å),^[29] and the P–C_{Alk} distances (1.856(5)–1.871(7) Å) are slightly longer than those of tribenzylphosphine (1.855(2)–1.858(2) Å).^[30]

The angles around Zn1 range from 101.9(1) ° to 119.1(1) °. The N–Zn1–N angle (117.9(2) °) and Br–Zn1–Br angle (119.1(1) °) are larger than the ideal tetrahedral angle of 109.5 °, while the N–Zn1–Br angles 101.9(1)–107.9(1) ° are smaller. This is in analogy to the angles around zinc found in complex **4-1**.

The C–P–C angles range from 101.5(3) ° to 102.7(2) °, which is slightly smaller than the ideal tetrahedral angle of 109.5 °. The angles sum up to 307.4 ° and 305.8 ° respectively, meaning that the conformation around the phosphorus atoms is rather pyramidal than planar.

In the crystal the complex forms layers along the *c* axis in an ABCD pattern (Figure 8).

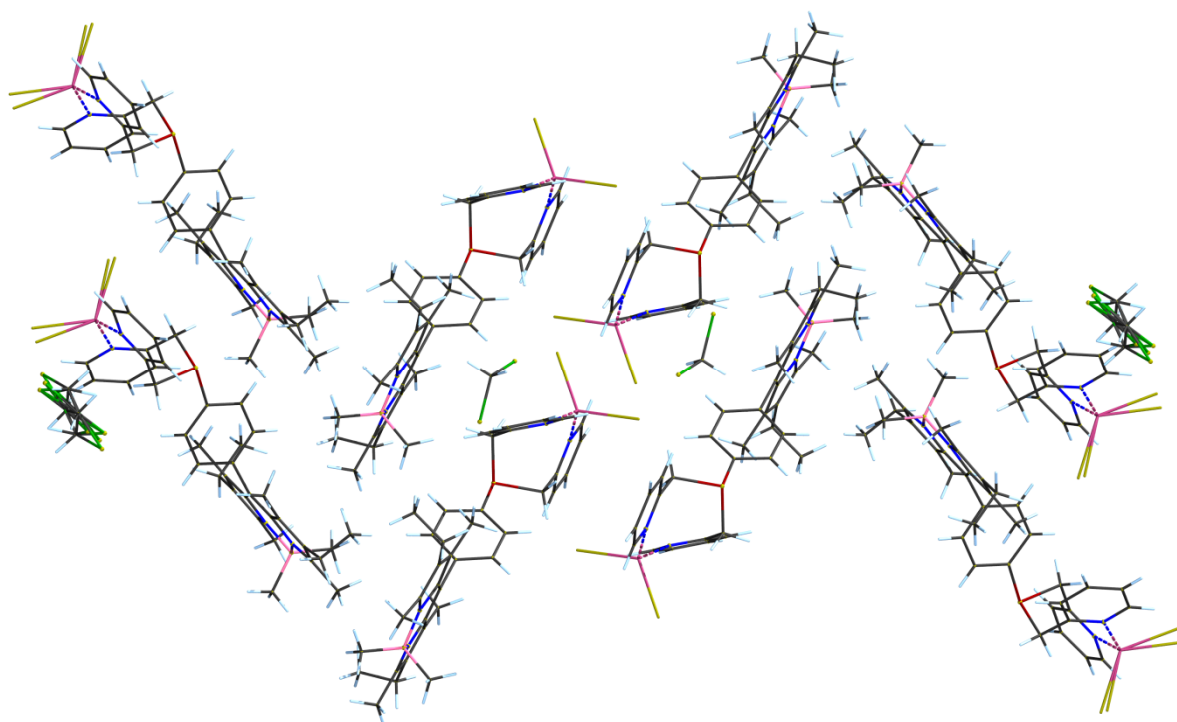


Figure 8: Crystal structure of **6-13**. View along the *b* axis.

6.2.5.2 Crystal structure of **6-17**

Single crystals of **6-17** suitable for X-ray crystallography were obtained by slow diffusion of Et₂O in a solution in DCM.

The complex crystallises in the orthorhombic space group *P*2₁2₁2₁ with four formula units in the unit cell. The asymmetric unit comprises one molecule of **6-17** and two molecules of Et₂O. The molecular structure is shown in Figure 9.

The complex forms an asymmetric dimer, in which each copper atom is coordinated by one of the pyridine nitrogen atoms of each ligand. Additionally Cu1 is coordinated by both phosphorus atoms, while Cu2 is only coordinated by P2. Therefore the coordination of Cu1 is distorted tetrahedral and the coordination of Cu2 is trigonal planar. The same coordination as in **6-17** can be found in the literature known copper hexafluorophosphate complex of **2-13**.^[31]

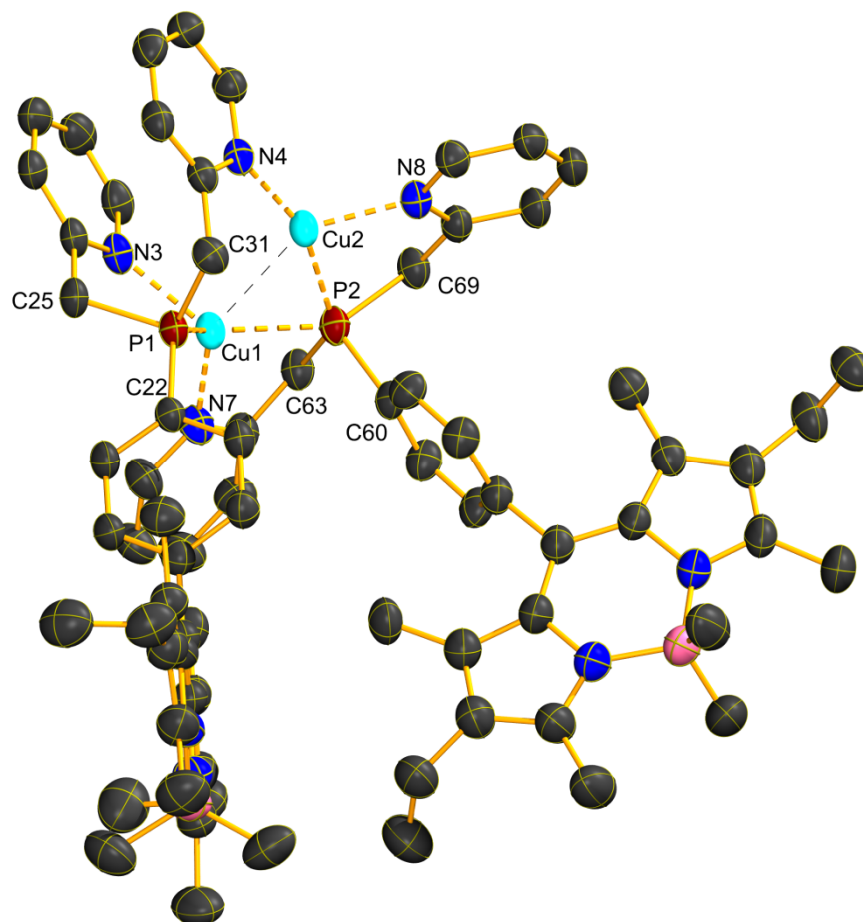


Figure 9: Molecular structure of **6-17**. Thermal ellipsoids are drawn at 50% probability level. H atoms, PF_6^- anions and solvent molecules have been omitted for clarity. Selected bond lengths [Å] and angles [°]: Cu1–P1: 2.245(1), Cu1–P2: 2.355(1), Cu1–N3: 2.116(3), Cu1–N7: 2.009(3), Cu2–P1: 3.282(1), Cu2–P2: 2.309(1), Cu2–N4: 1.993(3), Cu2–N8: 2.018(3), Cu1...Cu2: 2.464(1), P1–C22: 1.815(3); P1–C25: 1.834(3), P1–C31: 1.844(3), P2–C60: 1.817(3), P2–C63: 1.849(3), P2–C69: 1.852(3), P1–Cu1–P2: 130.0(1), P1–Cu1–N3: 85.7(1), P1–Cu1–N7: 121.2(1), P2–Cu1–N3: 127.6(1), P2–Cu1–N7: 84.8(1), N3–Cu1–N7: 110.1(1), P2–Cu2–N4: 159.0(1), P2–Cu2–N8: 85.5(1), N4–Cu2–N8: 114.9(1), Cu1–P2–Cu2: 63.8(1), C22–P1–C25: 107.8(2), C22–P1–C31: 102.5(2), C25–P1–C31: 102.5(2), C60–P2–C63: 106.1(2), C60–P2–C69: 100.1(2), C63–P2–C69: 98.2(2).

In the literature only a small number of copper(I) complexes with bridging phosphine ligands are described.^[31–32] The first examples were reported in 2005 by *F. Leca et al.* with a ligand based on 2,5-bis(2-pyridyl)phosphole.^[33]

The Cu–P distances of P2 (2.355(1) Å (Cu1) and 2.309(1) Å (Cu2)) are slightly different, but closer to each other than the corresponding distances in the complex of **2-13** (2.497(2) Å and 2.235(2) Å respectively).^[31] The Cu1–P1 distance (2.245(1) Å) is slightly shorter than the corresponding distance in the literature known complex (2.254(2) Å).^[31] The distance between Cu2 and P1 (3.282(1) Å) is significantly longer than the other Cu–P distances and too long to assume bonding interactions between these two atoms.

The Cu–N distances involving the nitrogen atoms of the ligand containing P2 (N7 and N8) are very similar (2.009(3) Å and 2.018(3) Å respectively), while the other two Cu–N distances (1.993(3) Å and 2.116(3) Å) are quite different. The same can be observed for the complex of **2-13**.^[31]

The Cu...Cu distance found in the structure of **6-17** (2.464(1) Å) is slightly shorter than that of the literature known complex,^[31] meaning that it is one of the shortest, if not the shortest, Cu...Cu distances in complexes with bridging phosphine ligands.

The P–C distances in **6-17** are in the range of 1.815(3)–1.853(4) Å, whereby the P–C_{Ar} bonds (1.815(3) Å and 1.817(4) Å) are slightly shorter than in triphenylphosphine^[29] and the P–C_{Alk} bonds (1.834(3)–1.853(4) Å) are slightly shorter than those of tribenzylphosphine.^[30]

The angles around Cu1 (N/P–Cu1–N/P) vary over a wide range from 84.8(1)° to 130.0(1)°. Only the angle N3–Cu1–N7 of 110.1(1)° is quite close to the ideal tetrahedral angle of 109.5°. A similar distribution of the corresponding angles was observed in the copper hexafluorophosphate complex of **2-13**.^[31]

The N/P–Cu2–N angles (85.5(1)–159.0(1)°) sum up to 359.4°, which confirms that Cu2 is coordinated trigonal planar by P2, N4 and N8. Usually in a trigonal planar configuration all three angles should be 120°, but only the angle N4–Cu2–N8 (114.9(1)°) is close to 120°. The angle P2–Cu2–N8 (85.5(1)°) is much smaller, because the pyridine ring containing N8 is bonded to P2 *via* the methylene group. These findings are analogous to those described in the literature.^[31]

The Cu–P–Cu angle (63.8(1)°) is slightly larger, but comparable to the angle found in the literature known complex (63.2(1)°).^[31]

All C–P–C angles are smaller than the ideal tetrahedral angle and range from 98.2(2)° to 107.8(2)°.

In the crystal the molecules are arranged in layers along the *c* axis in an ABAB pattern (Figure 10).

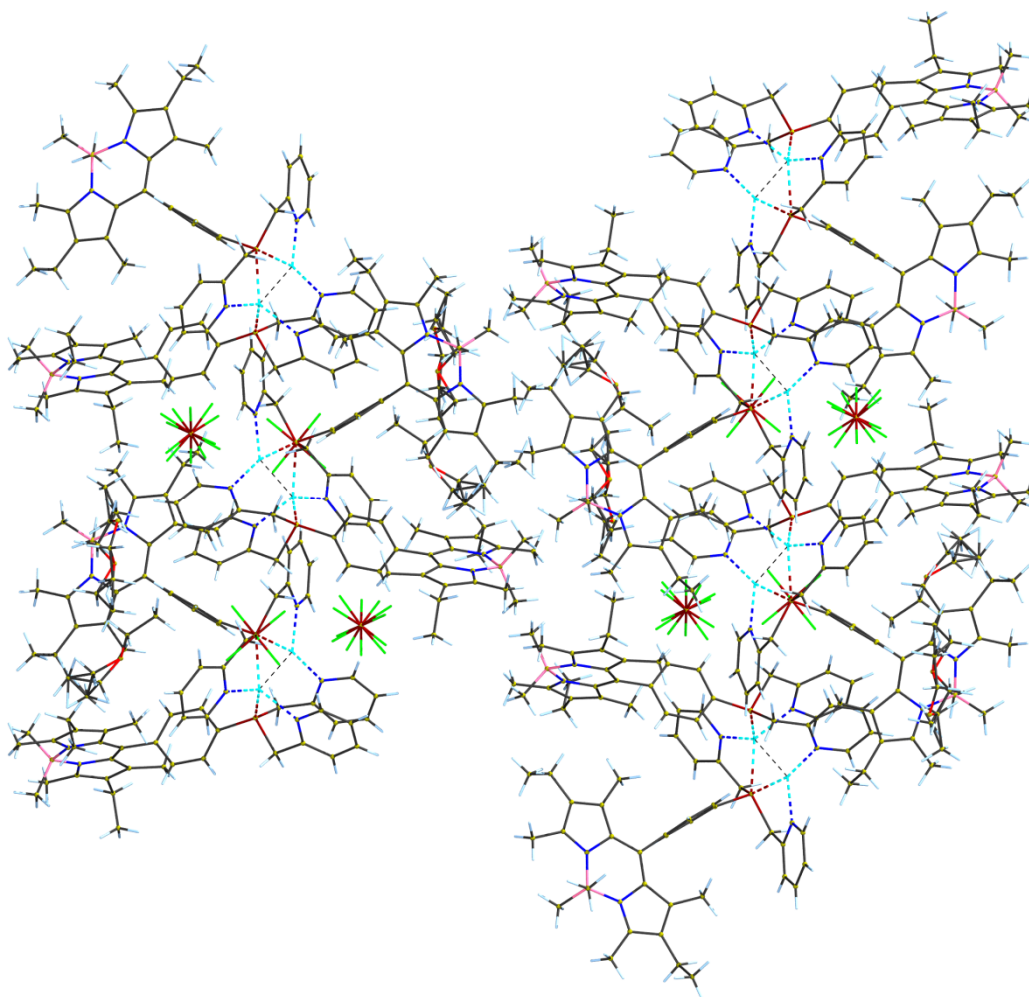


Figure 10: Crystal structure of **6-17**. View along the *a* axis.

6.3 Summary

Two P,N ligands (known compound **6-6** and new compound **6-9**) with the fluorescent Bodipy moiety in one of the substituents bonded to phosphorus have been synthesised successfully. The only difference between ligands **6-6** and **6-9** is the length of the carbon chains between the phosphorus atom and the pyridine rings, which is shorter by one carbon atom in ligand **6-9**.

For the synthesis of **6-6** a new synthetic procedure was tested, which led to higher yields, but needed longer reaction times. Ligand **6-9** could be synthesised in good yield by replacing the hydrogen atoms at the phosphorus atom in primary phosphine **6-5** with chlorine and subsequent reaction of dichlorophosphine **6-8** with **2-1** in analogy to the synthesis of the bis(picolyl)phosphine related compounds described in Chapter 2.

The P,N ligands were allowed to react with salts of manganese, zinc and copper(I) to obtain the corresponding complexes. Ligand **6-6** is very sensitive towards oxidation and was easily oxidised to give phosphine oxide **6-7** by even small amounts of oxygen.

The ligands as well as the complexes showed green fluorescence under UV light in solution. The absorption and emission spectra of the ligands **6-6** and **6-9**, phosphine oxide **6-7** and the complexes **6-13** and **6-17** all correspond with the spectra that are typical for Bodipy based fluorescent dyes. The highest fluorescence quantum yields of 0.35 and 0.33 respectively were measured for the free ligands. Upon coordination of **6-9** to metals a decrease of the quantum yields was observed.

Of complexes **6-13** and **6-17** crystals suitable for single crystal X-ray diffraction could be obtained. From the crystal structures it is obvious that the Bodipy moiety in *para* position at the phenyl ring does not have great influence on the coordination behaviour of the bis(picolyl)phosphine to zinc and copper(I). In the structure of complex **6-13** the zinc bromide is coordinated by the ligand in the same way as the zinc chloride in the structure of **4-1** (see 4.2.4) and the same coordination of **6-9** to the copper atoms in complex **6-17** was found in the copper(I) complex of **2-13** described in the literature.^[31]

6.4 Experimental

6.4.1 General

6.4.1.1 Schlenk technique

All air- and/or moisture sensitive reactions were performed under a nitrogen atmosphere using standard Schlenk line techniques.

6.4.1.2 Solvents

THF and toluene were dried over sodium/benzophenone and sodium respectively, dichloromethane was dried over calcium hydride; all solvents were distilled prior to use. Dimethyl sulfoxide and pentane were purchased in an anhydrous state.

6.4.1.3 Chemicals

All starting materials were purchased from Aldrich, Acros Organics, Alfa Aesar or Strem and used as received.

Flash chromatography was performed on silica gel from Fluorochem (40–63 μ , 60 Å). Thin-layer chromatography was carried out on Fisher aluminium-based plates with silica gel and fluorescent indicator (254 nm).

6.4.1.4 NMR

^1H , ^{13}C , ^{31}P , ^{19}F and ^{11}B NMR spectra were recorded on a Bruker 300 MHz, Bruker 400 MHz or Bruker 500 MHz spectrometer at room temperature (21°C); ^1H and ^{13}C shifts are reported relative to tetramethylsilane, ^{31}P relative to 80% H_3PO_4 , ^{11}B relative to $\text{BF}_3\cdot\text{Et}_2\text{O}$ and ^{19}F relative to CFCl_3 .

6.4.1.5 IR spectroscopy

Infrared spectra were recorded on a Varian 800 FT-IR spectrometer.

6.4.1.6 X-ray diffraction of single crystals

X-ray crystal structures were determined by *Dr. Paul Waddell*. For **6-13** a Xcalibur Atlas Gemini Ultra diffractometer equipped with a fine-focus sealed X-ray tube ($\lambda_{\text{CuK}\alpha} = 1.54184 \text{ \AA}$), an Oxford Cryosystems CryostreamPlus open-flow N_2 cooling device and an Atlas CCD plate detector was used. For **6-17** a Fluid Film Devices synchrotron with an Undulator, I19, DLS, RAL ($\lambda = 0.6889 \text{ \AA}$) and a photon counting pixel array detector was used.

6.4.1.7 Data collection from the diffractometer and crystal structure solution

Cell refinement, data collection and data reduction were performed with the CrysAlisPro 1.171.38.42b software.^[34] Intensities were corrected for absorption using the CrysAlisPro 1.171.38.42b software.^[34] Analytical numeric absorption correction was performed using a multifaceted crystal model based on expressions. Empirical absorption correction used spherical harmonics, implemented in SCALE3 ABSPACK scaling algorithm.^[35] Using Olex2,^[36] the structures were solved with the ShelXT^[37] structure solution program using Direct Methods and refined with the XL refinement package using Least Squares minimisation.^[38]

6.4.1.8 Absorption and Emission Spectroscopy

Absorption spectra were recorded with a Hitachi Model U-3310 spectrophotometer while fluorescence studies were recorded with a Hitachi F-4500 fluorescence spectrophotometer. Solvents used for spectroscopic experiments were of spectrophotometric grade. Absorption and emission spectra were recorded for all compounds in dry degassed tetrahydrofuran solution at room temperature. Fluorescence quantum yields were measured with respect to 4,4-difluoro-8-phenyl-1,3,5,7-tetramethyl-2,6-diethyl-4-bora-3a,4a-diaza-s-indacene ($\Phi_{\text{F}} = 0.76$, $\lambda_{\text{abs}} = 524 \text{ nm}$, $\lambda_{\text{em}} =$

537 nm, $\epsilon = 86,000 \text{ M}^{-1} \text{ cm}^{-1}$, THF). Dyes were excited at 485 nm and excitation and emission slits were both set to 5 nm.

6.4.1.9 Quantum Yield Method

The fluorescence quantum yield (Φ_F) can be defined as the ratio of emitted photons relative to the number of absorbed photons.^[39] All quantum yields were determined in solution at room temperature. An appropriate reference compound to determine the fluorescence quantum yield was selected, which absorbs and emits over ranges comparable to those of the studied samples. The excitation wavelength, slit widths and the emission range were kept constant for the reference and the sample. Optically dilute solutions were prepared to possess the same absorbance at the excitation wavelength ($A < 0.09$ at the excitation wavelength, with an error limit of ± 0.005 between the reference and sample). The following formulae were used to correct the relative emission areas for minor differences in absorbance:

$$A = \log \left(\frac{I_0}{I_T} \right)$$

$$I_a + I_T = I_0 = 1$$

$$QY_{REL} = \frac{area}{I_a}$$

A is the absorbance, I_0 is the intensity of incident light, I_T is the intensity of the transmitted light, I_a is the intensity of absorbed light and QY_{REL} is the relative quantum yield.^[40]

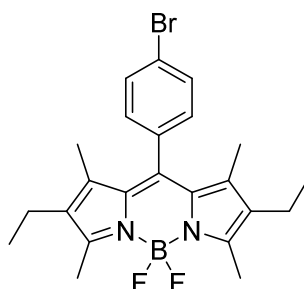
The quantum yield of the sample was determined using the following equation:

$$QY^{Sl} = \left(\frac{QY_{REL}^{Sl}}{QY_{REL}^{Ref}} \right) QY^{Ref}$$

Superscript Sl and Ref denote sample and reference respectively.^[40]

6.4.2 Syntheses

6.4.2.1 10-(4-Bromophenyl)-2,8-diethyl-5,5-difluoro-1,3,7,9-tetramethyl-5H-4 λ^4 ,5 λ^4 -dipyrrolo[1,2-c:2',1'-f][1,3,2]diazaborinine 6-1



4-Bromobenzaldehyde (10.0 g, 54.0 mmol, 1 eq) and 3-ethyl-2,4-dimethyl-1H-pyrrole (14.6 mL, 108 mmol, 2 eq) were dissolved in DCM (600 mL). TFA (10 drops) was added and the remaining red solution was stirred overnight in the dark. DDQ (12.3 g, 54.0 mmol, 1 eq) was added and the mixture was stirred for 2.5 h. After addition of N,N-diethylpropan-2-amine (56.4 mL, 324 mmol, 6 eq) the mixture turned yellow-brown. Addition of trifluoroboron etherate (53.3 mL, 432 mmol, 8 eq) yielded a purple solution. The reaction mixture was stirred overnight in the dark. 500 mL of water were added, the organic fraction was separated and the aqueous layer was extracted with DCM (2 x 100 mL). The combined organic fractions were dried over magnesium sulphate and the solvent was removed. The product was purified by column chromatography (silica; toluene). After removal of the solvent the product was obtained as a dark purple solid (11.3 g, 24.6 mmol, 46%).

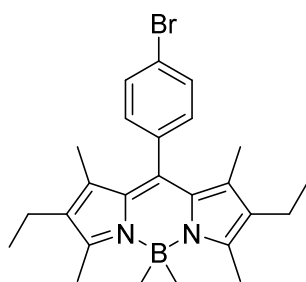
¹H NMR (300 MHz, CDCl₃) δ = 7.63 (d, ³J_{HH} = 8.3 Hz, 2H), 7.18 (d, ³J_{HH} = 8.4 Hz, 2H), 2.53 (s, 6H), 2.30 (q, ³J_{HH} = 7.6 Hz, 4H), 1.31 (s, 6H), 0.98 (t, ³J_{HH} = 7.5 Hz, 6H).

¹¹B NMR (96 MHz, CDCl₃) δ = 0.8 (t, ¹J_{BF} = 33.0 Hz).

¹³C NMR (75 MHz, CDCl₃) δ = 154.3, 138.6, 138.3, 134.9, 133.2, 132.5, 130.7, 130.3, 123.2, 17.2, 14.8, 12.7, 12.1.

¹⁹F NMR (282 MHz, CDCl₃) δ = -145.8 (q (equal intensity), ¹J_{FB} = 33.2 Hz).

6.4.2.2 10-(4-Bromophenyl)-2,8-diethyl-1,3,5,5,7,9-hexamethyl-5H-4λ⁴,5λ⁴-dipyrrolo[1,2-c:2',1'-f][1,3,2]diazaborinine 6-2



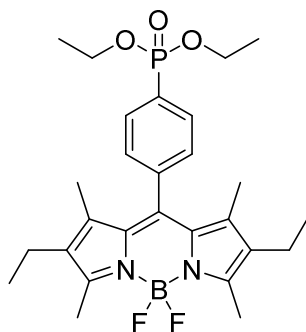
6-1 (3.7 g, 8.0 mmol, 1 eq) was dissolved in THF (150 mL) and a solution of methyl magnesium bromide (3.0 M in Et₂O, 5.6 mL, 16.7 mmol, 2.1 eq) was added. The dark orange reaction mixture was stirred overnight. The remaining methyl magnesium bromide was quenched with MeOH and the solvent was removed under vacuum. The crude product was purified by column chromatography (silica; petrol ether). After removal of the solvent the product was obtained as an orange solid (2.1 g, 4.6 mmol, 58%).

¹H NMR (300 MHz, CDCl₃) δ = 7.61 (d, ³J_{HH} = 8.4 Hz, 2H), 7.21 (d, ³J_{HH} = 8.4 Hz, 2H), 2.45 (s, 6H), 2.32 (q, ³J_{HH} = 7.5 Hz, 4H), 1.30 (s, 6H), 0.99 (t, ³J_{HH} = 7.6 Hz, 6H), 0.27 (s, 6H).

¹¹B NMR (96 MHz, CDCl₃) δ = -1.0.

¹³C NMR (75 MHz, CDCl₃) δ = 151.1, 139.0, 136.4, 133.7, 132.8, 132.1, 130.8, 129.0, 122.6, 17.6, 14.8, 14.5, 12.3. Broad signal of Me-B at 10.4 ppm is not visible in the noise of the spectrum.

6.4.2.3 Diethyl (4-(2,8-diethyl-5,5-difluoro-1,3,7,9-tetramethyl-5H-4λ⁴,5λ⁴-dipyrrolo[1,2-c:2',1'-f][1,3,2]diazaborinin-10-yl)phenyl)phosphonate 6-3



6-1 (3.9 g, 8.4 mmol, 1 eq), DPPB (358 mg, 0.84 mmol, 0.1 eq) and Pd(OAc)₂ (188 mg, 0.84 mmol, 0.1 eq) were dissolved in DMSO (150 mL). DIPEA (4.4 mL, 25.2 mmol, 3 eq) and diethyl phosphite (1.2 mL, 9.2 mmol, 1.1 eq) were added and the reaction mixture was stirred at 90°C for 3 d. After cooling the reaction mixture down to room temperature 350 mL of DCM were added. The organic layer was washed with water (5 × 200 mL), dried over magnesium sulphate and the solvent was removed. The product was purified by column chromatography (silica; EtOAc/petrol ether, 3:1). After removal of the solvent the product was obtained as a dark purple solid (3.3 g, 6.4 mmol, 76%).

¹H NMR (300 MHz, CDCl₃) δ = 7.94 (dd, ³J_{HP} = 13.1 Hz, ³J_{HH} = 8.4 Hz, 2H), 7.43 (dd, ³J_{HH} = 8.4 Hz, ⁴J_{HP} = 3.9 Hz, 2H), 4.16 (m, 4H), 2.53 (s, 6H), 2.29 (q, ³J_{HH} = 7.5 Hz, 4H), 1.35 (td, ³J_{HH} = 7.1 Hz, ⁴J_{HP} = 0.5 Hz, 4H), 1.25 (s, 6H), 0.98 (t, ³J_{HH} = 7.5 Hz, 6H).

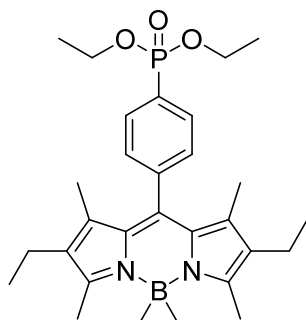
¹¹B NMR (96 MHz, CDCl₃) δ = 0.8 (t, ¹J_{BF} = 33.0 Hz).

¹³C NMR (75 MHz, CDCl₃) δ = 154.5, 140.3 (d, ²J_{PC} = 3.2 Hz), 138.1, 133.3, 132.6, 132.4, 130.5, 128.8 (d, ¹J_{PC} = 15.2 Hz), 128.3, 62.5 (d, ²J_{PC} = 5.5 Hz), 17.2, 16.5 (d, ³J_{PC} = 6.2 Hz), 14.7, 12.7, 11.9.

¹⁹F NMR (282 MHz, CDCl₃) δ = -145.8 (q (equal intensity), ¹J_{FB} = 33.0 Hz).

³¹P NMR (121 MHz, CDCl₃) δ = 17.6.

6.4.2.4 Diethyl (4-(2,8-diethyl-1,3,5,5,7,9-hexamethyl-5H-4λ⁴,5λ⁴-dipyrrolo[1,2-c:2',1'-f][1,3,2]diazaborinin-10-yl)phenyl)phosphonate 6-4



Method A: **6-2** (2.1 g, 4.6 mmol, 1 eq), DPPB (196 mg, 0.46 mmol, 0.1 eq) and Pd(OAc)₂ (103 mg, 0.46 mmol, 0.1 eq) were dissolved in DMSO (100 mL). DIPEA (2.4 mL, 13.8 mmol, 3 eq) and diethyl phosphite (0.71 mL, 5.5 mmol, 1.2 eq) were added and the reaction mixture was stirred at 90°C for 2 d. After cooling the reaction mixture down to RT 150 mL of DCM were added. The organic layer was washed with water (5 × 100 mL), dried over magnesium sulphate and the solvent was removed.

The product was purified by column chromatography (silica; EtOAc/petrol ether, 3:1). After removal of the solvent the product was obtained as an orange solid (1.9 g, 3.8 mmol, 83%).

Method B: **6-3** (3.3 g, 6.4 mmol, 1 eq) was dissolved in THF (100 mL) and a solution of methyl magnesium bromide (3.0 M in Et₂O, 4.5 mL, 13.4 mmol, 2.1 eq) was added. The dark orange reaction mixture was stirred overnight. The remaining methyl magnesium bromide was quenched with MeOH and the solvent was removed under vacuum. The crude product was purified by column chromatography (silica; EtOAc/petrol ether, 3:1). After removal of the solvent the product was obtained as an orange solid (2.3 g, 4.5 mmol, 70%).

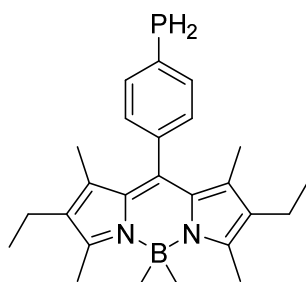
¹H NMR (300 MHz, CDCl₃) δ = 7.92 (dd, ³J_{HP} = 13.1 Hz, ³J_{HH} = 8.2 Hz, 2H), 7.47 (dd, ³J_{HH} = 8.2 Hz, ³J_{HP} = 3.9 Hz, 2H), 4.16 (m, 4H), 2.46 (s, 6H), 2.31 (q, ³J_{HH} = 7.5 Hz, 4H), 1.35 (td, ³J_{HH} = 7.1 Hz, ⁴J_{HP} 0.5 Hz, 6H), 1.22 (s, 6H), 0.98 (t, ³J_{HH} = 7.5 Hz, 6H), 0.28 (s, 6H).

¹¹B NMR (96 MHz, CDCl₃) δ = -0.5.

¹³C NMR (75 MHz, CDCl₃) δ = 151.2, 138.9, 133.6, 132.9, 132.3 (d, ¹J_{CP} = 10.2 Hz), 129.4, 129.2, 128.7, 62.4, 17.6, 16.5 (d, ³J_{CP} = 6.1 Hz), 14.8, 14.5, 12.0. Signals at 141.5 ppm and 10.2 ppm are not visible in the noise of the spectrum.

³¹P NMR (121 MHz, CDCl₃) δ = 18.1.

6.4.2.5 2,8-Diethyl-1,3,5,5,7,9-hexamethyl-10-(4-phosphanylphenyl)-5H-4 λ^4 ,5 λ^4 -dipyrrolo[1,2-c:2',1'-f][1,3,2]diazaborinine **6-5**



LiAlH₄ (202 mg, 5.3 mmol, 2 eq) was suspended in THF (10 mL) and cooled down to -78°C. TMSCl (0.67 mL, 5.3 mmol, 2 eq) was added and the reaction mixture was warmed up to RT. The suspension was cooled down to -78°C and a solution of **6-4** (1.4 g, 2.7 mmol, 1 eq) in THF (110 mL) was added. The reaction mixture was allowed to warm to RT and stirred overnight. The reaction was quenched with water and the solvent was removed under vacuum. The remaining solid was dissolved in Et₂O (150 mL) and washed with water (250 mL). The aqueous layer was extracted with Et₂O (4 × 150 mL). The combined organic fractions were dried over magnesium sulphate and the solvent was removed. The crude product was purified by column chromatography (silica; chloroform/petrol ether, 1:4). After removal of the solvent the product was obtained as an orange solid (0.81 g, 2.0 mmol, 75%).

¹H NMR (300 MHz, CDCl₃) δ = 7.59 (m, 2H), 7.23 (m, 2H), 4.10 (d, ¹J_{HP} = 202.6 Hz, 2H), 2.45 (s, 6H), 2.31 (q, ³J_{HH} = 7.6 Hz, 4H), 1.27 (s, 6H), 0.98 (t, ³J_{HH} = 7.6 Hz, 6H), 0.27 (s, 6H).

¹¹B NMR (96 MHz, CDCl₃) δ = -1.0.

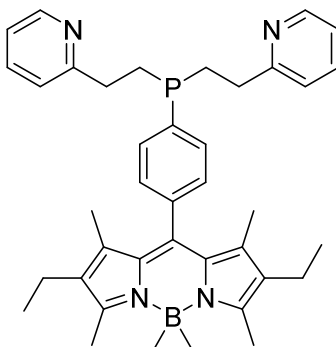
¹³C NMR (75 MHz, CDCl₃) δ = 150.9, 137.4, 135.2, 135.0, 133.9, 132.6, 129.1, 129.0 (d, ²J_{PC} = 6.1 Hz), 128.8, 17.6, 14.8, 14.5, 12.1. Broad signal of Me-B at 10.4 ppm is not visible in the noise of the spectrum.

³¹P NMR (¹H coupled) (121 MHz, CDCl₃) δ = -122.3 (tt, ¹J_{PH} = 202.7 Hz, ³J_{PH} = 7.0 Hz).

IR (neat) $\tilde{\nu}$ = 2958 (m), 2926(w), 2290 (w), 1546(s), 1532 (s), 1471 (m), 1450 (m), 1385 (m), 1371 (m), 1359 (m), 1314 (s), 1300 (m), 1289 (m), 1262 (w), 1167 (s), 1143 (s), 1110 (m), 1070 (m), 1024 (m),

978 (s), 942 (s), 907 (s), 823 (w), 785 (s), 722 (m), 690 (w), 669 (m), 609 (w), 559 (w), 518 (s), 506 (m), 468 (w) cm^{-1} .

6.4.2.6 10-(4-(Bis(2-(pyridin-2-yl)ethyl)phosphanyl)phenyl)-2,8-diethyl-1,3,5,5,7,9-hexamethyl-5H-4 λ^4 ,5 λ^4 -dipyrrolo[1,2-c:2',1'-f][1,3,2]diazaborinine 6-6



Method A: **6-5** (100 mg, 0.25 mmol, 1 eq) was dissolved in toluene (10 mL). 2-vinylpyridine (0.11 mL, 0.99 mmol, 4 eq) and ABCN (18 mg, 0.07 mmol, 0.3 eq) were added and the reaction mixture was stirred at 80°C for 3 d. The solvent was removed under vacuum and the crude product was purified by column chromatography (silica; EtOAc (MeOH 3–10%)). After removal of the solvent the product was obtained as an orange red solid (43 mg, 0.07 mmol, 28%).

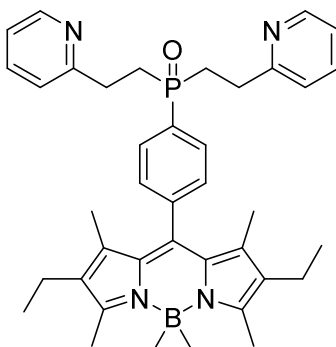
Method B: **6-5** (100 mg, 0.25 mmol, 1 eq) and $(\text{Fe}(\text{salen}))_2\text{O}$ (2 mg, 0.003 mmol, 0.01 eq) were dissolved in toluene (10 mL). 2-vinylpyridine (0.11 mL, 1.0 mmol, 4 eq) was added and the reaction mixture was stirred at 110°C for 11 d. The solvent was removed under vacuum and the crude product was purified by column chromatography (silica; EtOAc (MeOH 7.5%)). After removal of the solvent the product was obtained as an orange red solid (100 mg, 0.16 mmol, 66%).

^1H NMR (300 MHz, CDCl_3) δ = 8.54 (ddd, $^3J_{\text{HH}}$ = 4.9 Hz, $^4J_{\text{HH}}$ = 1.9 Hz, $^5J_{\text{HH}}$ = 0.9 Hz, 2H), 7.69 (t, $^3J_{\text{HH}}$ = 7.7 Hz, 2H), 7.58 (td, $^3J_{\text{HH}}$ = 7.7 Hz, $^4J_{\text{HH}}$ = 1.9 Hz, 2H), 7.35 (dd, $^3J_{\text{HH}}$ = 8.2 Hz, $^4J_{\text{PH}}$ = 0.7 Hz, 2H), 7.11 (m, 4H), 2.86 (m, 4H), 2.45 (s, 6H), 2.28 (m, 8H), 1.27 (s, 6H), 0.98 (t, $^3J_{\text{HH}}$ = 7.5 Hz, 6H), 0.28 (s, 6H).

^{11}B NMR (96 MHz, CDCl_3) δ = -1.0.

^{31}P NMR (^1H coupled) (121 MHz, CDCl_3) δ = -23.1 (p, $^2J_{\text{PH}}$ = 8.0 Hz).

6.4.2.7 (4-(2,8-Diethyl-1,3,5,5,7,9-hexamethyl-5H-4 λ^4 ,5 λ^4 -dipyrrolo[1,2-c:2',1'-f][1,3,2]diazaborinin-10-yl)phenyl)bis(2-(pyridin-2-yl)ethyl)phosphine oxide 6-7



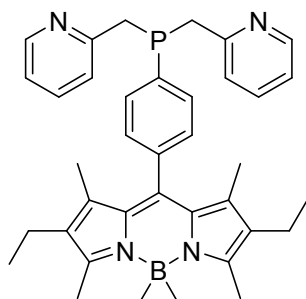
¹H NMR (300 MHz, CDCl₃) δ = 8.52 (ddd, ³J_{HH} = 4.9 Hz, ⁴J_{HH} = 1.9 Hz, ⁵J_{HH} = 1.0 Hz, 2H), 7.92 (dd, ³J_{PH} = 10.7 Hz, ³J_{HH} = 8.0 Hz, 2H), 7.59 (td, ³J_{HH} = 7.7 Hz, ⁴J_{HH} = 1.9 Hz, 2H), 7.51 (dd, ³J_{HH} = 8.2 Hz, ⁴J_{PH} = 2.5 Hz, 2H), 7.15 (m, 2H), 7.11 (m, 2H), 3.18 (m, 2H), 2.95 (m, 2H), 2.55 (m, 4H), 2.45 (s, 6H), 2.29 (q, ³J_{HH} = 7.5 Hz, 4H), 1.20 (s, 6H), 0.97 (t, ³J_{HH} = 7.5 Hz, 6H), 0.28 (s, 6H).

¹¹B NMR (96 MHz, CDCl₃) δ = -0.3.

³¹P NMR (121 MHz, CDCl₃) δ = 40.4.

IR (neat) $\tilde{\nu}$ = 2962 (w), 2926 (w), 2867 (w), 1655 (w), 1590 (w), 1545 (m), 1472 (w), 1435 (m), 1360 (w), 1322 (m), 1260 (m), 1172 (s), 1145 (s), 1110 (s), 1020 (s), 981 (m), 945 (s), 910 (w), 855 (w), 786 (s), 747 (s), 728 (s), 672 (m), 644 (m), 630 (m), 605 (m), 535 (m), 517 (m), 457 (m), 402 (s) cm⁻¹.

6.4.2.8 10-(4-(Bis(pyridin-2-ylmethyl)phosphanyl)phenyl)-2,8-diethyl-1,3,5,5,7,9-hexamethyl-5H-4λ⁴,5λ⁴-dipyrrolo[1,2-c:2',1'-f][1,3,2]diazaborinine 6-9



6-5 (100 mg, 0.25 mmol, 1 eq) and PCl₅ (113 mg, 0.55 mmol, 2.2 eq) were dissolved in toluene (3 mL) and stirred at ambient temperature for 1 h. The solvent was removed under vacuum and the remaining solid was dissolved in THF (3 mL). **2-1** (0.10 mL, 0.54 mmol, 2.2 eq) was added and the reaction mixture was stirred overnight. The solvent was removed under vacuum and the crude product was purified by column chromatography (silica; EtOAc (MeOH 8%)). After removal of the solvent the product was obtained as an orange red solid (126 mg, 0.21 mmol, 87%).

¹H NMR (300 MHz, CDCl₃) δ = 8.48 (ddd, ³J_{HH} = 4.9 Hz, ⁴J_{HH} = 1.9 Hz, ⁵J_{HH} = 1.0 Hz, 2H), 7.48 (m, 4H), 7.23 (m, 2H), 7.04 (m, 4H), 3.50 (dd, ²J_{HH} = 13.2 Hz, ²J_{PH} = 3.0 Hz, 2H), 3.39 (d, ²J_{HH} = 13.2 Hz, 2H), 2.45 (s, 6H), 2.31 (q, ³J_{HH} = 7.5 Hz, 4H), 1.19 (s, 6H), 0.99 (t, ³J_{HH} = 7.5 Hz, 6H), 0.27 (s, 6H).

¹¹B NMR (96 MHz, CDCl₃) δ = -0.8.

¹³C NMR (75 MHz, CDCl₃) δ = 158.1 (d, *J*_{PC} = 5.0 Hz), 150.8, 149.5 (d, *J*_{PC} = 0.8 Hz), 139.9, 138.4 (d, *J*_{PC} = 0.7 Hz), 136.7 (d, *J*_{PC} = 19.6 Hz), 136.2 (d, *J*_{PC} = 0.5 Hz), 133.7, 133.5 (d, *J*_{PC} = 20.5 Hz), 132.6, 129.0, 128.8 (d, *J*_{PC} = 7.3 Hz), 123.8 (d, *J*_{PC} = 4.9 Hz), 121.1 (d, *J*_{PC} = 2.0 Hz), 37.8 (d, ¹*J*_{PC} = 19.0 Hz), 17.6, 14.9, 14.5, 12.1.

³¹P NMR (121 MHz, CDCl₃) δ = -13.8.

IR (neat) $\tilde{\nu}$ = 2970 (w), 1589 (w), 1538 (s), 1469 (m), 1455 (m), 1430 (m), 1387 (m), 1361 (m), 1320 (s), 1299 (m), 1290 (m), 1258 (w), 1172 (s), 1146 (s), 1112 (m), 1065 (m), 1038 (m), 979 (s), 944 (s), 908 (m), 864 (w), 828 (w), 801 (s), 790 (s), 781 (s), 745 (s), 701 (w), 672 (m), 626 (w), 593 (m), 558 (w), 517 (m), 498 (m), 471 (w), 436 (w), 405 (m) cm⁻¹.

6.4.2.9 Reaction of 6-6 with MnBr(CO)₅ 6-10

MnBr(CO)₅ (14 mg, 0.05 mmol, 1 eq) and **6-6** (62 mg, 0.1 mmol, 2 eq) were dissolved in anhydrous toluene (5 mL) and stirred at 110°C for 2 h. The solvent was removed under vacuum and the crude product was dissolved in chloroform. After filtration through celite a dark red solid was obtained by slow diffusion of pentane (61 mg).

³¹P NMR and IR data indicated that the product was the oxide of the ligand **6-7**.

6.4.2.10 Reaction of 6-9 with MnBr(CO)₅ 6-11

MnBr(CO)₅ (59 mg, 0.21 mmol, 1 eq) and **6-9** (126 mg, 0.21 mmol, 1 eq) were dissolved in anhydrous toluene (7 mL) and stirred at 110°C for 2 h. The solvent was removed under vacuum and the crude product was dissolved in DCM. After filtration through celite the product a dark red solid was obtained by slow diffusion of pentane (95 mg).

¹¹B NMR (96 MHz, CDCl₃) δ = -1.6.

³¹P NMR (202 MHz, CDCl₃) δ = 72.0.

IR (neat) $\tilde{\nu}$ = 2981 (m), 2028 (w), 1931 (w), 1548 (m), 1435 (m), 1386 (m), 1360 (m), 1319 (m), 1260 (m), 1171 (s), 1145 (s), 1111 (m), 980 (m), 945 (s), 910 (w), 799 (s), 672 (m), 639 (m), 492 (m) cm⁻¹.

6.4.2.11 Reaction of 6-6 with ZnBr₂ 6-12

ZnBr₂ (23 mg, 0.10 mmol, 1 eq) and **6-6** (62 mg, 0.10 mmol, 1 eq) were dissolved in anhydrous DCM (3 mL) and stirred at room temperature overnight. The solvent was removed under vacuum and a dark red solid was obtained (48 mg).

¹H NMR (300 MHz, CDCl₃) δ = 8.84 (d, ³J_{HH} = 4.4 Hz, 2H), 8.03 (dd, ³J_{PH} = 10.6 Hz, ³J_{HH} = 8.1 Hz, 2H), 7.75 (t, ³J_{HH} = 7.8 Hz, 2H), 7.47 (dd, ³J_{HH} = 8.2 Hz, ⁴J_{PH} 1.9 Hz, 2H), 7.32 (t, ³J_{HH} = 6.1 Hz, 4H), 3.23 (m, 4H), 2.61 (s, 2H), 2.48 (s, 2H), 2.44 (s, 6H), 2.28 (q, ³J_{HH} = 7.6 Hz, 4H), 1.17 (s, 6H), 0.96 (t, ³J_{HH} = 7.5 Hz, 6H), 0.27 (s, 6H).

¹¹B NMR (96 MHz, CDCl₃) δ = -0.9.

³¹P NMR (121 MHz, CDCl₃) δ = -23.1.

6.4.2.12 Reaction of 6-9 with ZnBr₂ 6-13

ZnBr₂ (30 mg, 0.13 mmol, 1 eq) and **6-9** (77 mg, 0.13 mmol, 1 eq) were dissolved in anhydrous DCM (3 mL) and stirred at room temperature overnight. The solvent was removed under vacuum and a dark red solid was obtained (52 mg).

¹H NMR (300 MHz, CDCl₃) δ = 9.24 (d, ³J_{HH} = 4.5 Hz, 2H), 7.50 (t, ³J_{HH} = 6.3 Hz, 2H), 7.43 (dd, ³J_{HH} = 7.7 Hz, ⁴J_{PH} = 3.0 Hz, 2H), 7.28 (m, 4H), 7.10 (t, ³J_{HH} = 7.6 Hz, 2H), 3.46 (br, 4H), 2.46 (s, 6H), 2.33 (q, ³J_{HH} = 7.7 Hz, 4H), 1.25 (s, 6H), 1.01 (t, ³J_{HH} = 7.8 Hz, 6H), 0.27 (s, 6H).

¹¹B NMR (96 MHz, CDCl₃) δ = -0.8.

³¹P NMR (121 MHz, CDCl₃) δ = -10.2.

IR (neat) $\tilde{\nu}$ = 2961 (w), 2925 (w), 2867 (w), 1606 (w), 1549 (s), 1439 (m), 1360 (m), 1318 (s), 1172 (s), 1145 (s), 1112 (m), 1022 (m), 981 (s), 944 (s), 909 (m), 800 (s), 672 (m), 646 (m), 516 (m), 422 (m) cm⁻¹.

6.4.2.13 Reaction of 6-6 with CuCl 6-14

CuCl (13 mg, 0.14 mmol, 1 eq) and **6-6** (83 mg, 0.14 mmol, 1 eq) were dissolved in anhydrous DCM (3 mL) and stirred at ambient temperature for 3 h. The solvent was removed under vacuum and a dark red solid was obtained (59 mg).

IR (neat) $\tilde{\nu}$ = 2970 (m), 2924 (w), 1549 (m), 1435 (w), 1386 (m), 1361 (w), 1320 (m), 1261 (m), 1172 (s), 1145 (s), 1097 (s), 1020 (s), 980 (m), 801 (s), 673 (w), 516 (m) cm^{-1} .

6.4.2.14 Reaction of 6-9 with CuCl 6-15

CuCl (11 mg, 0.11 mmol, 1 eq) and **6-9** (63 mg, 0.11 mmol, 1 eq) were dissolved in anhydrous DCM (3 mL) and stirred at ambient temperature for 2 h. The solvent was removed under vacuum and a dark red solid was obtained (55 mg).

^{31}P NMR (121 MHz, DCM) δ = -10.8.

IR (neat) $\tilde{\nu}$ = 2963 (w), 2925 (w), 1597 (w), 1548 (m), 1471 (m), 1435 (m), 1387 (m), 1360 (m), 1320 (m), 1260 (m), 1172 (s), 1146 (s), 1111 (s), 1019 (s), 981 (s), 910 (m), 797 (s), 750 (m), 703 (m), 672 (m), 596 (w), 557 (w), 516 (m), 491 (m) cm^{-1} .

6.4.2.15 Reaction of 6-6 with Cu(MeCN)₄PF₆ 6-16

Cu(MeCN)₄PF₆ (29 mg, 0.08 mmol, 1 eq) and **6-6** (47 mg, 0.08 mmol, 1 eq) were dissolved in anhydrous DCM (3 mL) and stirred at ambient temperature for 3 h. The solvent was removed under vacuum and a dark red solid was obtained (45 mg).

IR (neat) $\tilde{\nu}$ = 2962 (w), 2923 (w), 2853 (w), 1549 (m), 1440 (w), 1404 (w), 1360 (w), 1320 (m), 1260 (s), 1172 (m), 1144 (m), 1093 (s), 1017 (s), 982 (m), 946 (m), 911 (w), 835 (s), 798 (s), 734 (m), 702 (m), 673 (m), 557 (s), 517 (m), 478 (m), 439 (m) cm^{-1} .

6.4.2.16 Reaction of 6-9 with Cu(MeCN)₄PF₆ 6-17

Cu(MeCN)₄PF₆ (40 mg, 0.11 mmol, 1 eq) and **6-9** (63 mg, 0.11 mmol, 1 eq) were dissolved in anhydrous DCM (3 mL) and stirred at ambient temperature for 2 h. The solvent was removed under vacuum and a dark red solid was obtained (57 mg).

^{11}B NMR (96 MHz, CDCl₃) δ = 0.4.

^{31}P NMR (202 MHz, CDCl₃) δ = -16.6, -145.0 (hept, $^1J_{\text{PF}} = 707.4$ Hz).

IR (neat) $\tilde{\nu}$ = 2981 (w), 1550 (w), 1387 (w), 1320 (w), 1173 (m), 1145 (m), 946 (m), 839 (s), 798 (m), 557 (m) cm^{-1} .

6.4.3 Crystallographic data

Table 2: Crystallographic data of **6-13** and **6-17**.

	6-13· 0.75DCM	6-17· 2Et₂O
Identification code	ljh180019	ljh180013
Empirical formula	C _{37.75} H _{45.5} BBr ₂ Cl _{1.5} N ₄ PZn	C ₈₂ H ₁₀₈ B ₂ Cu ₂ F ₁₂ N ₈ O ₂ P ₄
Formula weight [g·mol ⁻¹]	875.42	1738.34
Temperature [K]	150.0(2)	100.0(2)
Crystal size [mm ³]	0.02× 0.11× 0.15	0.03× 0.06× 0.18
Colour, shape	Orange plate	Red plate
Crystal system	Triclinic	Orthorhombic
Space group	<i>P</i> -1	<i>P</i> 2 ₁ 2 ₁ 2 ₁
<i>a</i> [Å]	8.7567(3)	12.6351(4)
<i>b</i> [Å]	11.5823(4)	16.3845(5)
<i>c</i> [Å]	38.9805(13)	41.97940(10)
α [°]	92.578(3)	90
β [°]	90.424(3)	90
γ [°]	95.971(3)	90
<i>V</i> [Å ³]	3927.8(2)	8690.6(4)
<i>Z</i>	4	4
ρ_{calc} [g·cm ⁻³]	1.480	1.329
Radiation [Å]	CuK α = 1.54184	Synchrotron = 0.6889
μ [cm ⁻¹]	4.816	0.635
<i>F</i> (000)	1782	3632
Index ranges	-10≤ <i>h</i> ≤10 -13≤ <i>k</i> ≤13 -46≤ <i>l</i> ≤45	-16≤ <i>h</i> ≤16 -21≤ <i>k</i> ≤21 -54≤ <i>l</i> ≤54
θ range [°]	3.841≤ θ ≤ 66.968	1.293≤ θ ≤ 26.571
Reflections collected	51259	123841
Independent reflections	13866	19930
Observed reflections	8900	18371
Data/restraints/parameters	13866/934/944	19930/1357/1130
<i>R</i> _{int}	0.1049	0.0573
<i>R</i> ₁ , <i>wR</i> ₂ [<i>I</i> >2 σ (<i>I</i>)]	0.0552, 0.1133	0.0412, 0.1195
<i>R</i> ₁ , <i>wR</i> ₂ [all data]	0.0956, 0.1314	0.0441, 0.1216
GooF	1.007	1.054
$\delta\rho_{\text{max}}$, $\delta\rho_{\text{min}}$ [e·nm ⁻³]	0.620, -0.526	0.797, -0.319

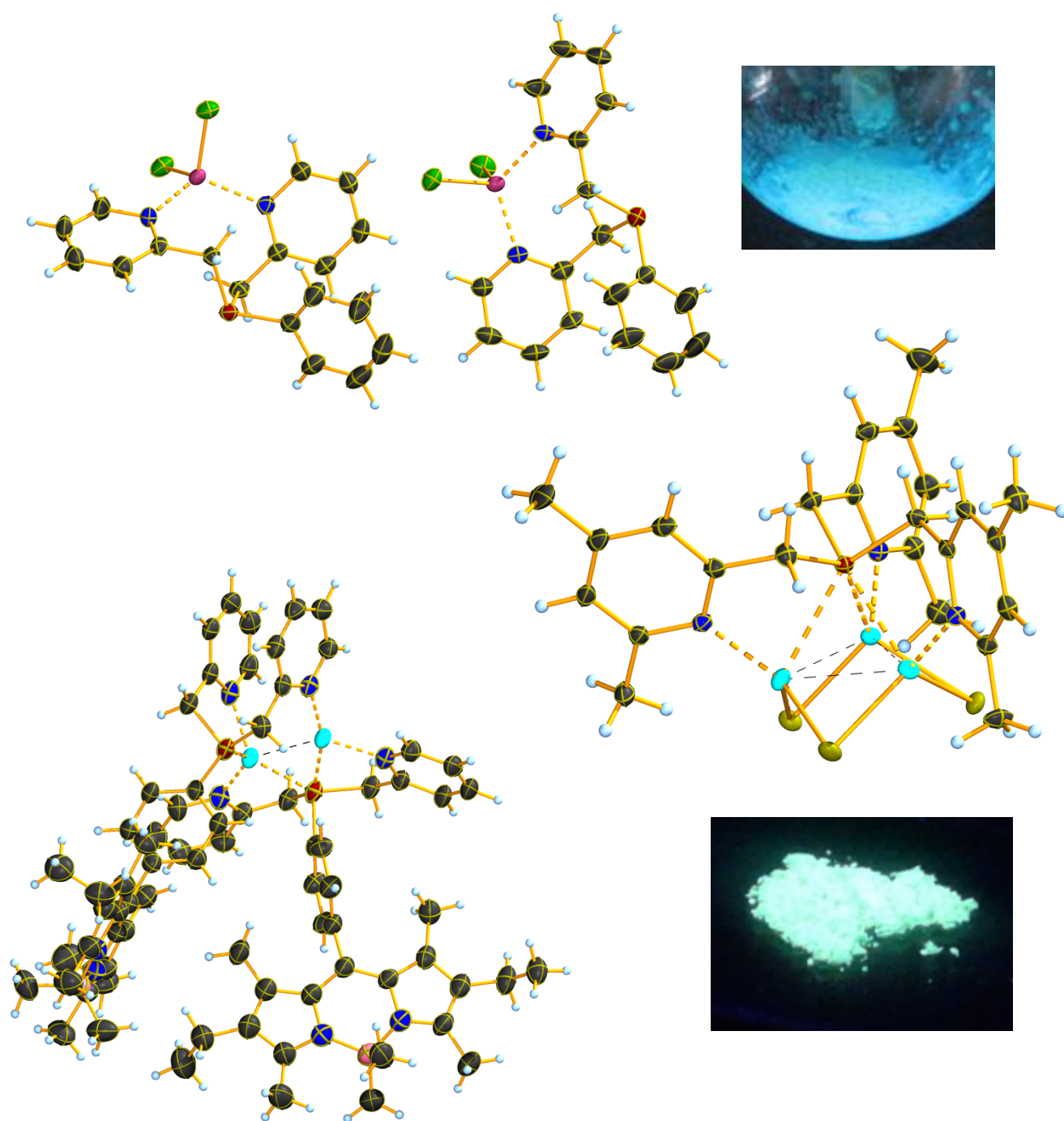
6.5 References

- [1] G. Ulrich, R. Ziessel, A. Harriman, *Angew. Chem. Int. Ed.* **2008**, *47*, 1184-1201.
- [2] R. Ziessel, G. Ulrich, A. Harriman, *New J. Chem.* **2007**, *31*, 496-501.
- [3] A. Treibs, F. H. Kreuzer, *Justus Liebigs Ann. Chem.* **1968**, *718*, 208-223.
- [4] M. Liu, S. Ma, M. She, J. Chen, Z. Wang, P. Liu, S. Zhang, J. Li, *Chin. Chem. Lett.* **2019**, *30*, 1815-1824.
- [5] A. Loudet, K. Burgess, *Chem. Rev.* **2007**, *107*, 4891-4932.
- [6] B. L. Thompson, C. R. Simons, Z. M. Heiden, *Chem. Commun.* **2019**, *55*, 11430-11433.
- [7] K. C. Dissanayake, P. O. Ebukuyo, Y. J. Dhahir, K. Wheeler, H. He, *Chem. Commun.* **2019**, *55*, 4973-4976.
- [8] a) N. Mukherjee, S. Podder, K. Mitra, S. Majumdar, D. Nandi, A. R. Chakravarty, *Dalton Trans.* **2018**, *47*, 823-835; b) L. H. Davies, R. W. Harrington, W. Clegg, L. J. Higham, *Dalton Trans.* **2014**, *43*, 13485-13499; c) L. H. Davies, B. B. Kasten, P. D. Benny, R. L. Arrowsmith, H. Ge, S. I. Pascu, S. W. Botchway, W. Clegg, R. W. Harrington, L. J. Higham, *Chem. Commun.* **2014**, *50*, 15503-15505.
- [9] a) M. Ucuncu, E. Karakus, E. Kurulgan Demirci, M. Sayar, S. Dartar, M. Emrullahoglu, *Org. Lett.* **2017**, *19*, 2522-2525; b) E. Palao, R. Sola-Llano, A. Tabero, H. Manzano, A. R. Agarrabeitia, A. Villanueva, I. Lopez-Arbeloa, V. Martinez-Martinez, M. J. Ortiz, *Chem. Eur. J.* **2017**, *23*, 10139-10147; c) D. Boison, W. L. Lu, Q. M. Xu, H. Yang, T. Huang, Q. Y. Chen, J. Gao, Y. Zhao, *Colloids Surf. B* **2016**, *147*, 387-396; d) A. Trommenschlager, F. Chotard, B. Bertrand, S. Amor, L. Dondaine, M. Picquet, P. Richard, A. Bettaieb, P. Le Gendre, C. Paul, C. Goze, E. Bodio, *Dalton Trans.* **2017**, *46*, 8051-8056; e) A. Garai, A. Gandhi, V. Ramu, M. K. Raza, P. Kondaiah, A. R. Chakravarty, *ACS Omega* **2018**, *3*, 9333-9338.
- [10] A. Kukoyi, E. A. Micheli, B. Liu, H. He, P. S. May, *Dalton Trans.* **2019**, *48*, 13880-13887.
- [11] A. Harriman, L. J. Mallon, B. Stewart, G. Ulrich, R. Ziessel, *Eur. J. Org. Chem.* **2007**, *2007*, 3191-3198.
- [12] K. Kim, S. H. Choi, J. Jeon, H. Lee, J. O. Huh, J. Yoo, J. T. Kim, C. H. Lee, Y. S. Lee, D. G. Churchill, *Inorg. Chem.* **2011**, *50*, 5351-5360.
- [13] H. Agarwalla, P. S. Mahajan, D. Sahu, N. Taye, B. Ganguly, S. B. Mhaske, S. Chattopadhyay, A. Das, *Inorg. Chem.* **2016**, *55*, 12052-12060.
- [14] M. N. Pinto, I. Chakraborty, W. Schultz-Simonton, M. Rojas-Andrade, R. Braslau, P. K. Mascharak, *Chem. Commun.* **2017**, *53*, 1459-1462.
- [15] A. M. Christianson, F. P. Gabbai, *Chem. Commun.* **2017**, *53*, 2471-2474.
- [16] Y. Li, X. Wang, J. Yang, X. Xie, M. Li, J. Niu, L. Tong, B. Tang, *Anal. Chem.* **2016**, *88*, 11154-11159.
- [17] S. N. W. Toussaint, R. T. Calkins, S. Lee, B. W. Michel, *J. Am. Chem. Soc.* **2018**, *140*, 13151-13155.
- [18] a) M. Navarro, S. Wang, H. Müller-Bunz, G. Redmond, P. Farràs, M. Albrecht, *Organometallics* **2017**, *36*, 1469-1478; b) O. Halter, R. Vasiuta, I. Fernandez, H. Plenio, *Chem. Eur. J.* **2016**, *22*, 18066-18072; c) O. Halter, J. Spielmann, Y. Kanai, H. Plenio, *Organometallics* **2019**, *38*, 2138-2149.
- [19] L. H. Davies, B. Stewart, R. W. Harrington, W. Clegg, L. J. Higham, *Angew. Chem. Int. Ed.* **2012**, *51*, 4921-4924.
- [20] L. Davies, J. Wallis, M. Probert, L. Higham, *Synthesis* **2014**, *46*, 2622-2628.
- [21] J. G. Felber, Master thesis, Ludwig-Maximilians-Universität München/Newcastle University, **2017**.
- [22] a) K. J. Gallagher, M. Espinal-Viguri, M. F. Mahon, R. L. Webster, *Adv. Synth. Catal.* **2016**, *358*, 2460-2468; b) K. J. Gallagher, R. L. Webster, *Chem. Commun.* **2014**, *50*, 12109-12111.
- [23] J. F. Wallis, PhD thesis, Newcastle University, **2017**.

- [24] C. Hettstedt, M. Unglert, R. J. Mayer, A. Frank, K. Karaghiosoff, *Eur. J. Inorg. Chem.* **2016**, 2016, 1405-1414.
- [25] a) T. Backhouse, Master thesis, Newcastle University, **2015**; b) S. Ghambir, Master thesis, Newcastle University, **2016**.
- [26] L. H. Davies, B. Stewart, R. W. Harrington, W. Clegg, L. J. Higham, *Angew. Chem.* **2012**, 51, 4921-4924.
- [27] C. Hettstedt, PhD thesis, Ludwig-Maximilians-Universität München, **2015**.
- [28] A. J. C. Wilson, E. Prince, *International Tables for Crystallography, Vol. C Mathematical, physical and chemical tables*, 2nd ed., Kluwer Academic Publishers, Dordrecht/Boston/London, **1999**.
- [29] J. J. Daly, *J. Chem. Soc.* **1964**, 3799-3810.
- [30] W. Levason, D. Pugh, G. Reid, *Acta Crystallogr. C* **2013**, 69, 560-564.
- [31] F. Hung-Low, A. Renz, K. K. Klausmeyer, *Eur. J. Inorg. Chem.* **2009**, 2009, 2994-3002.
- [32] S. Linert, S. Wagner, P. Schmidt, L. Higham, C. Hepples, P. Waddell, K. Karaghiosoff, *Phosphorus Sulfur Relat. Elem.* **2019**, 194, 565-568.
- [33] F. Leca, C. Lescop, E. Rodriguez-Sanz, K. Costuas, J. F. Halet, R. Reau, *Angew. Chem.* **2005**, 44, 4362-4365.
- [34] CrysAlisPro 1.171.138.142b, **2015**, Rigaku, Oxford Diffraction.
- [35] SCALE3 ABSPACK - An Oxford Diffraction program (v. 1.0.4, gui:1.0.3), **2005**, Oxford Diffraction Ltd., Oxfordshire, UK.
- [36] O. V. Dolomanov, L. J. Bourhis, R. J. Gildea, J. A. K. Howard, H. Puschmann, *J. Appl. Crystallogr.* **2009**, 42, 339-341.
- [37] G. Sheldrick, *Acta Crystallogr. A* **2015**, 71, 3-8.
- [38] G. Sheldrick, *Acta Crystallogr. A* **2008**, 64, 112-122.
- [39] B. Valeur, *Molecular Fluorescence: Principles and Applications*, Wiley-VCH, Weinheim, **2002**.
- [40] J. R. Lakowicz, *Principles of Fluorescence Spectroscopy*, 3rd ed., Springer, New York, **2006**.

Chapter 7

Summary



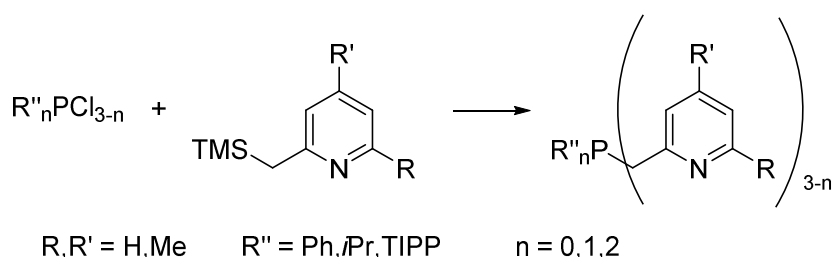
This thesis describes the synthesis of novel mono-, bis- and tris(picoly)phosphine based compounds. The new polydentate phosphines contain one or more pyridine rings and the methylene group between phosphorus and the pyridine rings provides additional flexibility and makes them interesting ligands for transition metals. First structural information on the conformation of the substituents at phosphorus is provided by the crystal structures of mono(picoly)phosphine related compounds. The versatile coordination properties of the new phosphines towards Zn(II) and Cu(I) were investigated by the synthesis and structural characterisation of a series of complexes. The complexes displayed fascinating structures and interesting luminescent properties in the solid state. The influence of the ligands and an additional fluorescent moiety in the ligand on the luminescent properties of the complexes was investigated.

Picolyphosphine based phosphines – novel polydentate ligands

Starting from a chlorophosphine compound by reaction with silyl compounds of picoline, lutidine or collidine the corresponding mono-, bis- and tris(picoly)phosphine based compounds could easily be synthesised according to the *Braunstein* route (Scheme 1). Reactions of PhPCl_2 , $i\text{PrPCl}_2$ and TIPPPCl_2 with the silyl compounds yielded the corresponding bis(picoly)phosphine based compounds, while the reaction of $t\text{BuPCl}_2$ with the silyl compounds stopped after the substitution of one of the chlorine atoms with a Lut or Col substituent.

Using the same synthetic strategy tris((2-methylen)benzoxazol)phosphine could also be produced and the crystal structure of the corresponding phosphine oxide was determined.

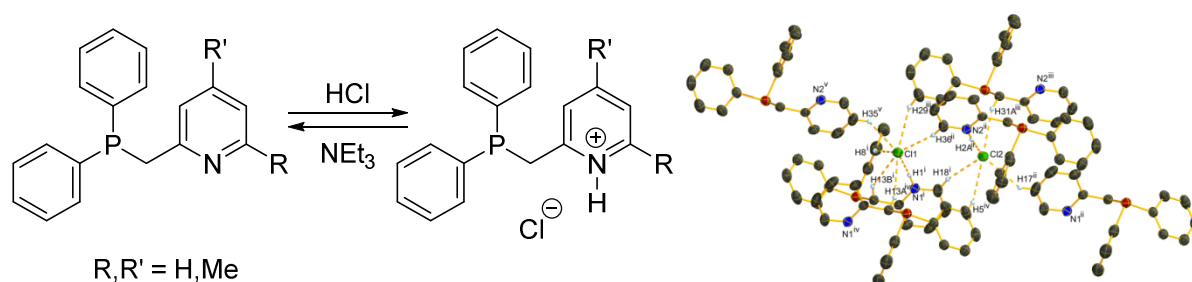
These phosphines are of interest as hemilabile, multidentate ligands with one phosphorus atom and one, two or three nitrogen atoms respectively to coordinate to transition metals. In the case of tris((2-methylen)benzoxazol)phosphine also three oxygen atoms are present, which are able to coordinate.



Scheme 1: Synthesis of picolyphosphine based ligands in this thesis.

Picolyphosphine based hydrochlorides – A convenient source of the phosphines

The hydrochlorides of three mono(picoly)phosphine based compounds were formed by protonation with HCl. The crystal structures of the obtained hydrochlorides were determined and it was found that the most important factor in these structures is the hydrogen bonding including the chloride ions. The hydrochlorides can easily be deprotonated to recover the phosphines (Scheme 2).



Scheme 2: Protonation and deprotonation reaction of mono(picolyl)phosphine based compounds and the corresponding hydrochlorides (left). Hydrogen bonding in the crystal structure of **3-1** (right). Thermal ellipsoids are drawn at 50 % probability level. H atoms not interacting with the shown Cl atoms have been omitted for clarity. i: -x, 1-y, 1-z, ii: x, 1+y, -1+z, iii: 1-x, 1-y, 1-z, iv: x, y, -1+z, v: 1-x, -y, 1-z.

Also PicPCl₂, which tends to dismutation, was stabilised by protonation at nitrogen and could be isolated and structurally characterised for the first time as the corresponding hydrochloride (Figure 1).

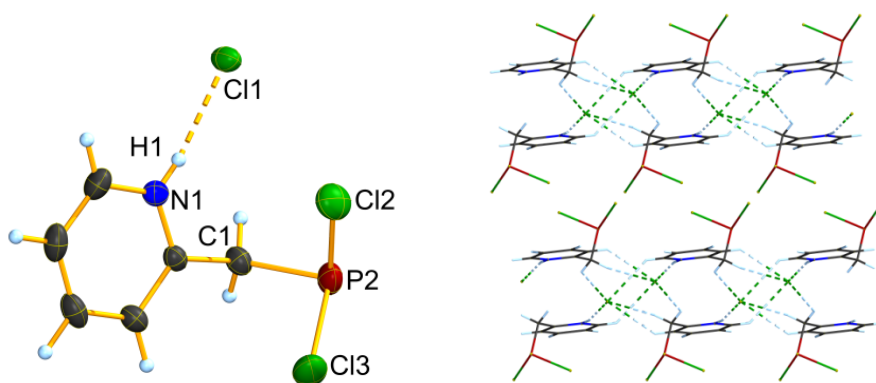


Figure 1: Molecular (left) and crystal structure (right, view along the *b* axis) of **3-5**. Thermal ellipsoids are drawn at 50% probability level.

Novel zinc complexes with blue luminescence

The zinc chloride complexes of five bis- and two tris(picolyl)phosphine based ligands have been synthesised. Single crystal X-ray analysis revealed that in the complex of phenylbis(picolyl)phosphine the zinc atom is coordinated by the two nitrogen atoms (Figure 2), while the ³¹P NMR data indicate that in the other complexes the coordination situation is more difficult.

The synthesised zinc chloride complexes showed blue luminescence under UV light (Figure 2). Although the relaxation times indicate that these compounds are singlet emitters, they might be of interest for application in OLEDs, due to their facile synthesis and low costs compared to the currently used emitters.

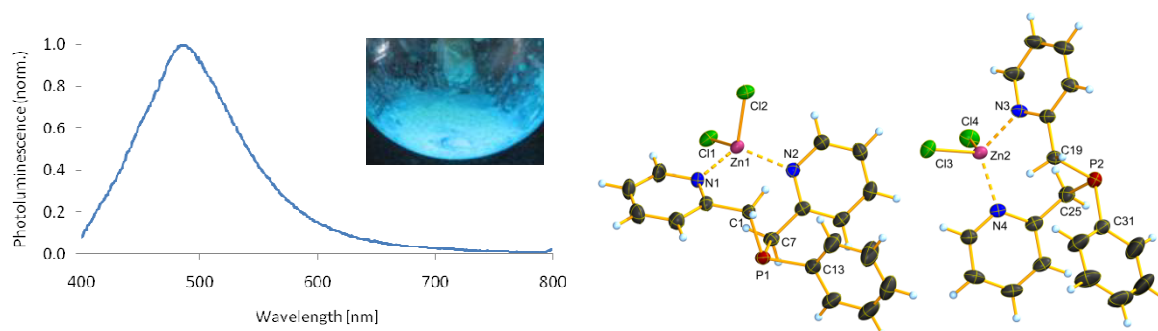


Figure 2: Emission spectrum and luminescence under UV light of **4-1** in the solid state (left). Asymmetric unit of **4-1** (right). Thermal ellipsoids are drawn at 50% probability level.

Unexpected Cu(I) complexes with fascinating structures

Eighteen copper(I) halide complexes and one copper(I) thiocyanate complex of bis- and tris(picoly)phosphine based ligands have been synthesised. Structural characterisations by X-ray crystallography revealed ligand to metal ratios of 1:2 for the phenylbis(picoly)phosphine related complexes and 1:3 for the *isopropylbis(picoly)phosphine* and tris(picoly)phosphine based complexes. In the crystal structures a great variety of coordination modes of the ligands to the copper atoms was observed (Figure 3).

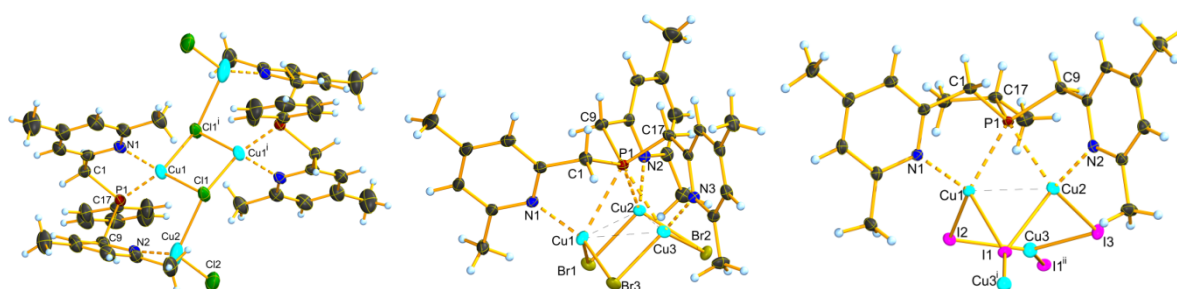


Figure 3: Dimeric molecular structure of **5-4** (left), molecular structure of **5-18** (middle) and asymmetric unit of **5-13** (right). Thermal ellipsoids are drawn at 50% probability level.

Particularly interesting is the CuSCN complex **5-10** of **2-16**, which forms a polymeric structure in the crystal. This structure contains parts with copper atoms, which interact with the ligand, and CuSCN chains, which do not show any interactions with the ligand (Figure 4).

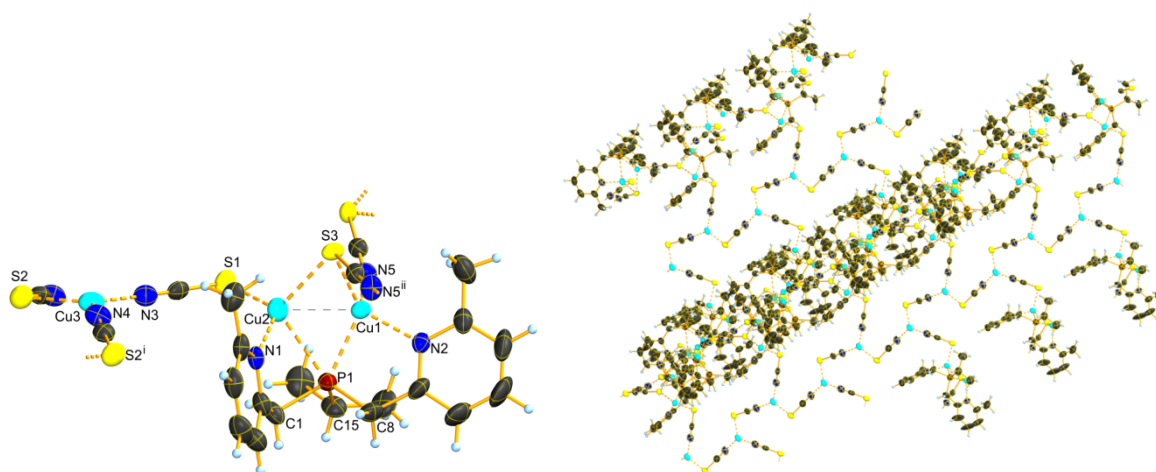


Figure 4: Asymmetric unit (left) and crystal structure of **5-10** (right). Thermal ellipsoids are drawn at 50% probability level.

Some of the copper(I) complexes showed green to blue-green luminescence under UV light and the relaxation times indicated that the luminescence of the complexes might be based on a TADF mechanism (Figure 5). The most promising candidates for potential application as emitters are the copper(I) halide complexes **5-1**, **5-2** and **5-20–5-22**.

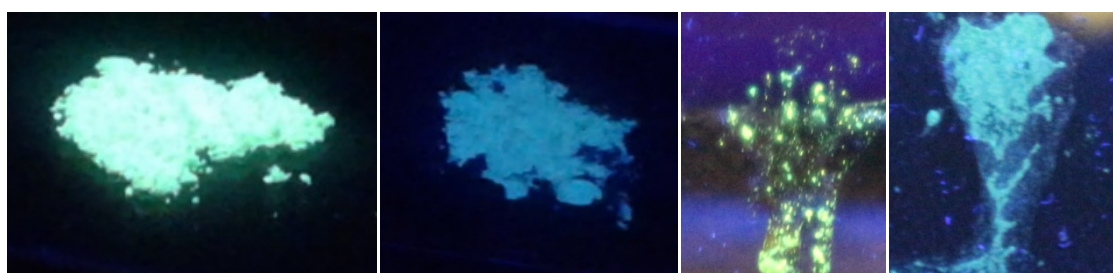


Figure 5: Luminescence of Cu(I) complexes under UV light. From left to right: **5-1**, **5-2**, **5-20**, **5-21**.

Flexible P,N ligands meet Bodipy

Two tridentate P,N ligands **6-6** and **6-9** with substituents containing the fluorescent Bodipy moiety in the third substituent at the phosphorus atom have been synthesised (Figure 6).

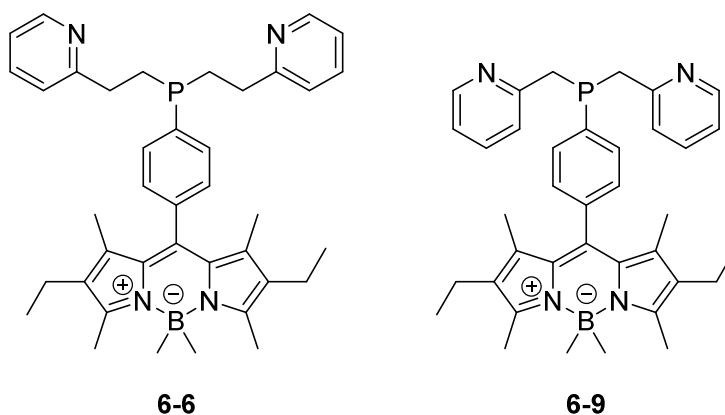


Figure 6: Tridentate ligands **6-6** and **6-9** with fluorescent moiety synthesis in this thesis.

The effect of the complexation with transition metals on the fluorescent properties of the ligand was investigated. The absorption and emission spectra of the complexes were very similar to those of the

free ligands, but a decrease of the fluorescence quantum yield was observed after complexation. The single crystal X-ray structures of complexes **6-13** and **6-17** could be determined (Figure 7). The coordination behaviour of ligand **6-9** is not influenced by the Bodipy moiety attached to the phenyl ring, but the same coordination towards zinc and copper(I) as found for complexes of PhPPic₂ **2-13** was observed in **6-13** and **6-17**.

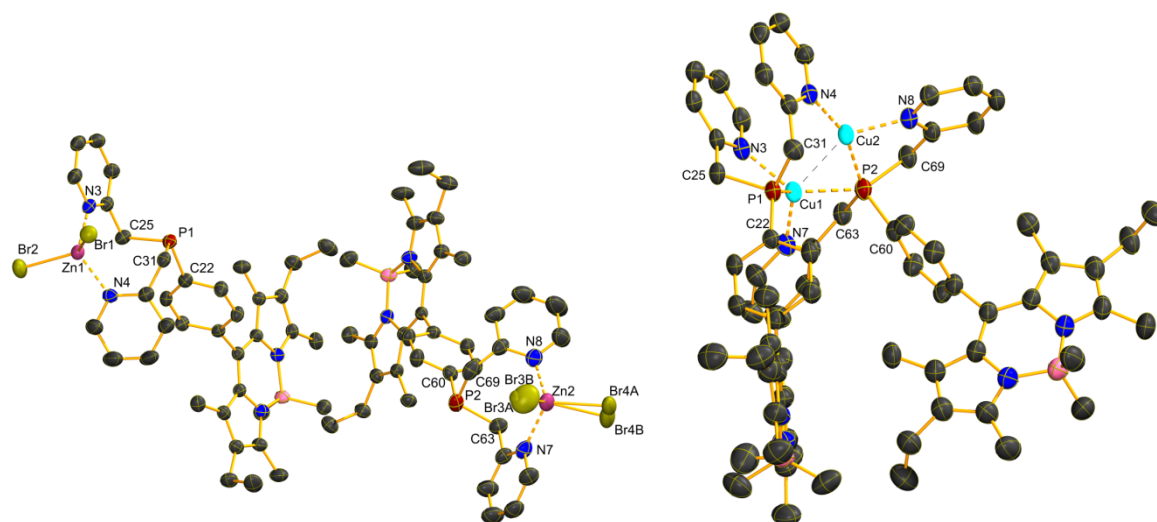
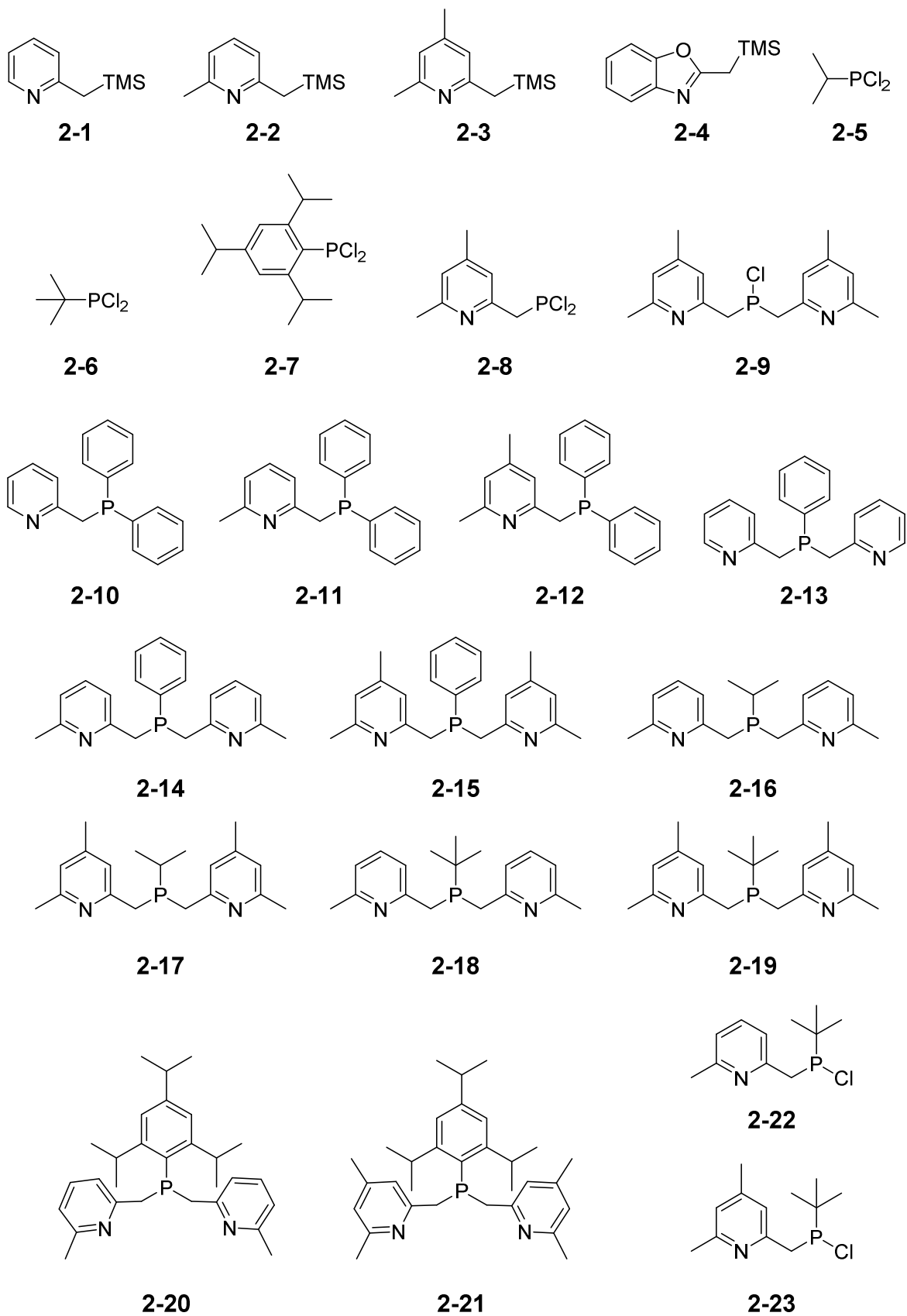
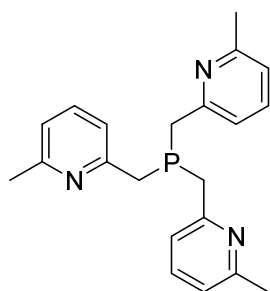


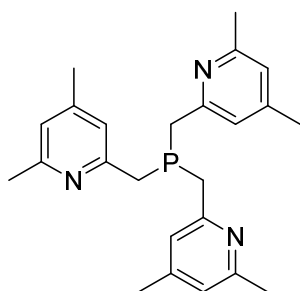
Figure 7: Asymmetric unit of **6-13** (left) and molecular structure of **6-17** (right). Thermal ellipsoids are drawn at 50% probability level. H atoms, PF₆⁻ anions of **6-17** and solvent molecules have been omitted for clarity.

List of compounds

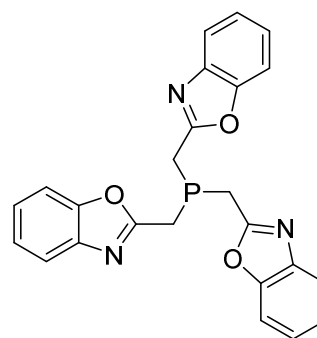




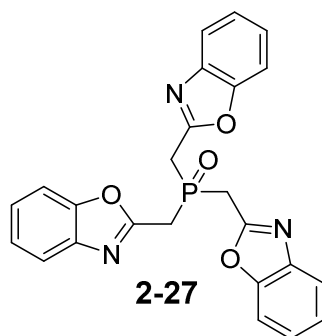
2-24



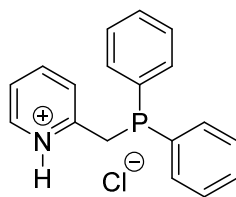
2-25



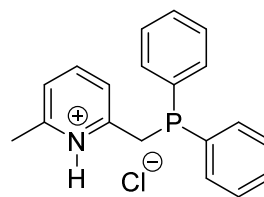
2-26



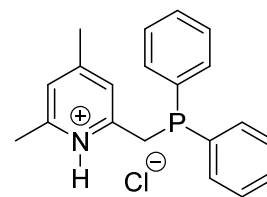
2-27



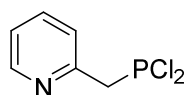
3-1



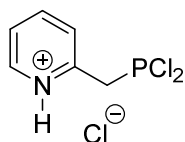
3-2



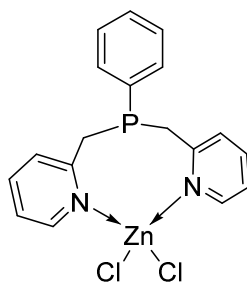
3-3



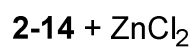
3-4



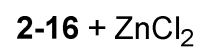
3-5



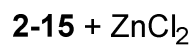
4-1



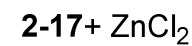
4-2



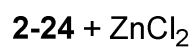
4-4



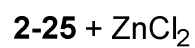
4-3



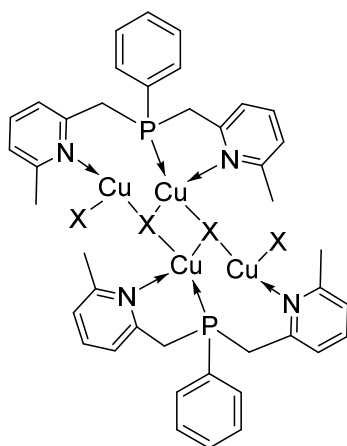
4-5



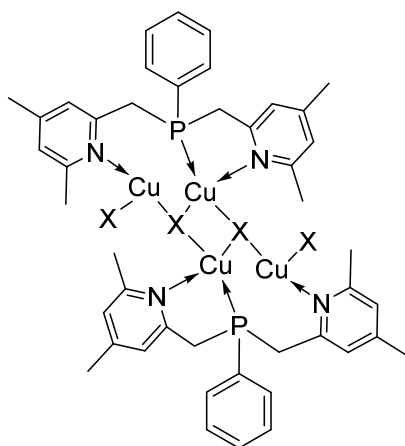
4-6



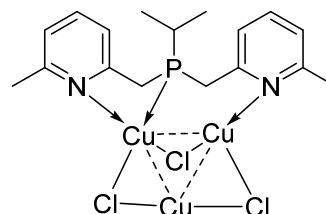
4-7



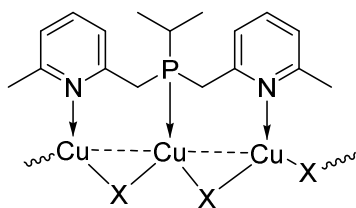
X = Cl **5-1**
 Br **5-2**
 I **5-3**



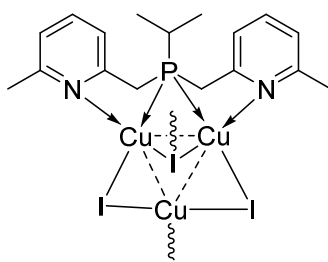
X = Cl **5-4**
 Br **5-5**
 I **5-6**



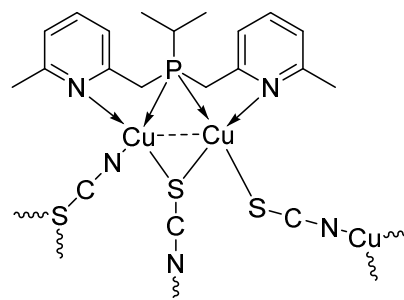
5-7a



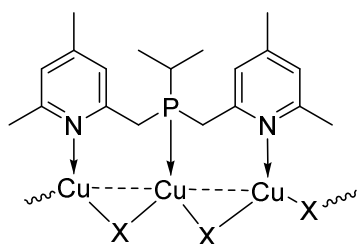
X = Cl **5-7b**
 Br **5-8**



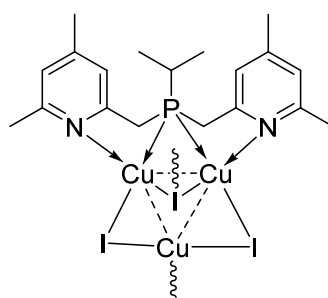
5-9



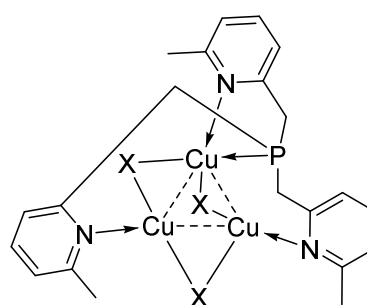
5-10



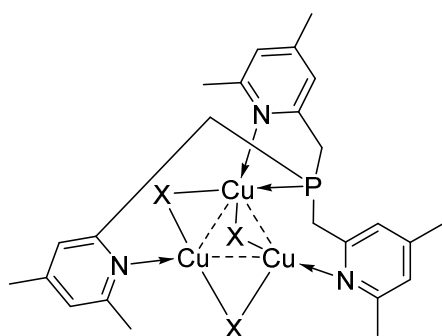
X = Cl **5-11**
 Br **5-12**



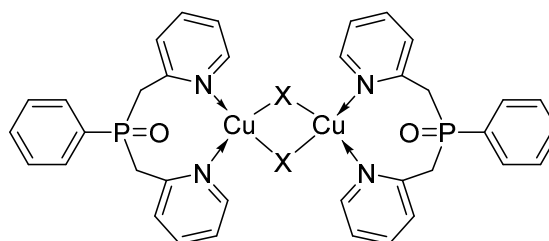
5-13



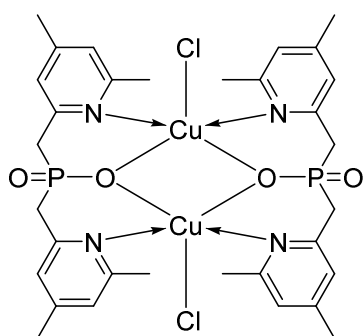
X = Cl **5-14**
 Br **5-15**
 I **5-16**



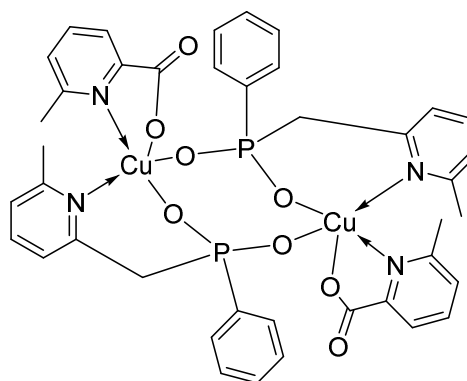
X = Cl **5-17**
 Br **5-18**
 I **5-19**



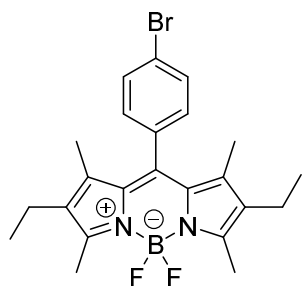
X = Cl **5-20**
 Br **5-21**
 I **5-22**



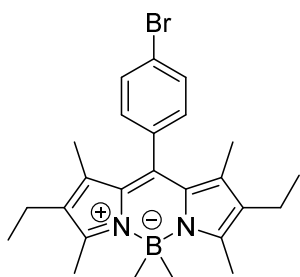
5-23



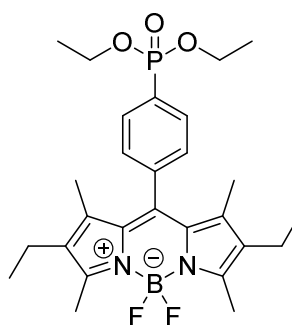
5-24



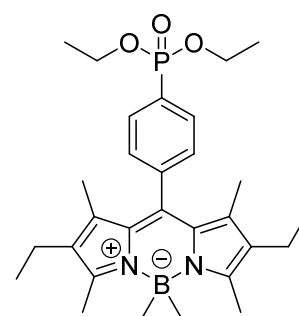
6-1



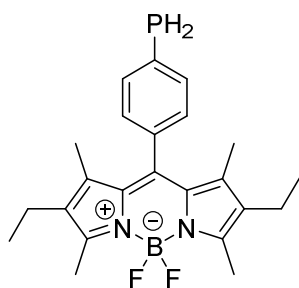
6-2



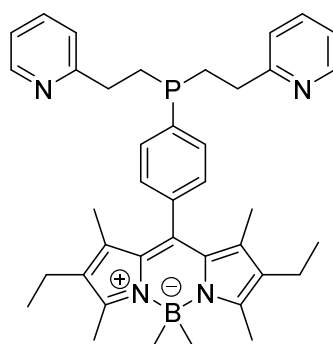
6-3



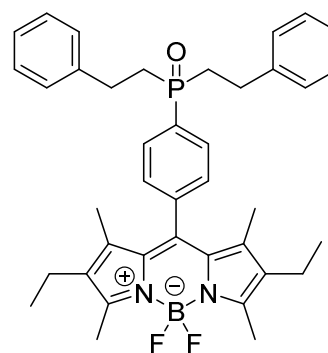
6-4



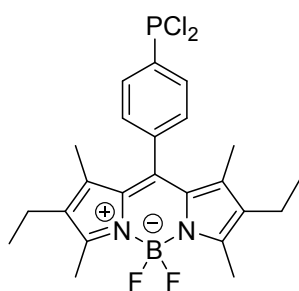
6-5



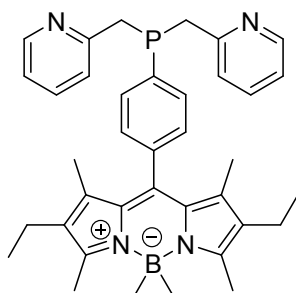
6-6



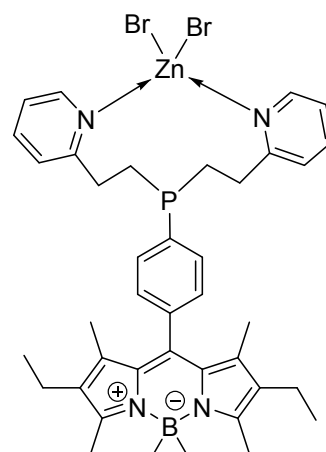
6-7



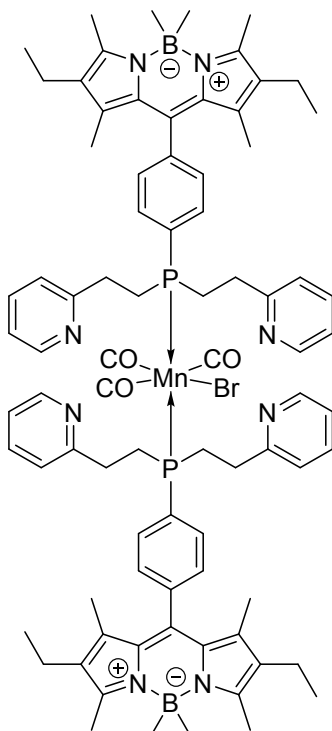
6-8



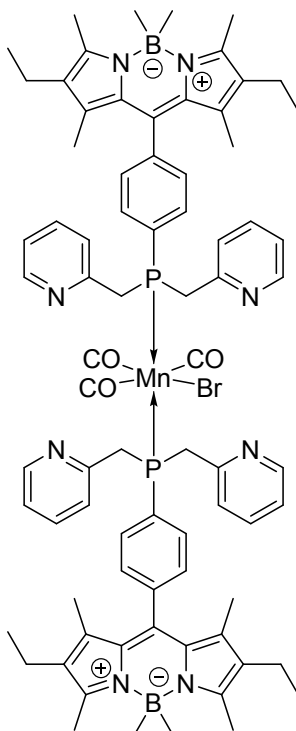
6-9



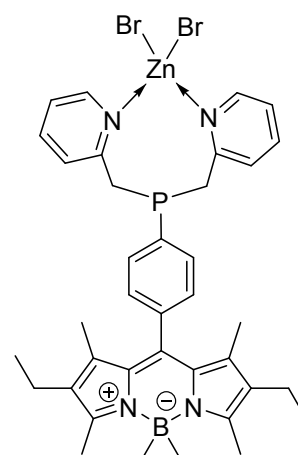
6-12



6-10



6-11



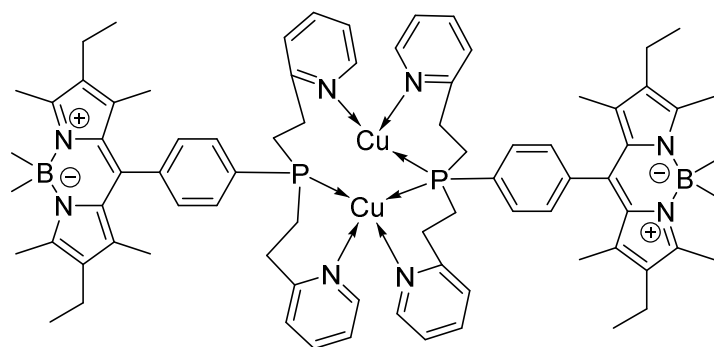
6-13

6-6 + CuCl

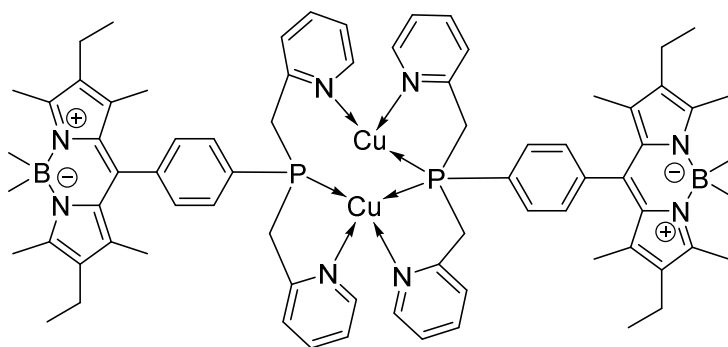
6-14

6-9 + CuCl

6-15



6-16



6-17